Densité des arrangements de disques et de sphères : aspects théoriques et computationnels de l'approche de densité locale

Daria Pchelina

Université Sorbonne Paris Nord
Laboratoire d'Informatique de Paris Nord - LIPN
Équipe: Combinatoire, ALgorithmique et INteractions - CALIN
École Doctorale Galilée

Density of Disc and Sphere Packings

Theoretical and Computational Aspects of Local Density Approach

Thèse de doctorat

présentée par

Daria Pchelina

pour obtenir le grade de

Docteur en Informatique

soutenue le 26 octobre 2023

devant le jury composé de :

Sandor Fekete	Professeur, Université de Braunschweig	Rapporteur
Thomas Fernique	Chargé de Recherche, Université Sorbonne Paris Nord	Directeur
Xavier Goaoc	Professeur, Université de Lorraine	Examinateur
Nabil Mustafa	Professeur, Université Sorbonne Paris Nord	Examinateur
Michaël Rao	Directeur de Recherche, ENS de Lyon	Rapporteur
Nathalie Revol	Chargée de Recherche, ENS de Lyon	Examinatrice
Guillaume Theyssier	Chargé de Recherche, Université d'Aix-Marseille	Examinateur

Abstract

How to stack an infinite number of oranges to maximize the proportion of the covered space? Kepler conjectured that the "cannonball" packing is an optimal way to do it. This conjecture took almost 400 years to prove, and the proof of Hales and Ferguson consists of 6 papers and tens of thousands of lines of computer code.

Given an infinite number of coins of 3 fixed radii, how to place them on an infinite table to maximize the proportion of the covered surface? *Triangulated* disc packings are those where each "hole" is bounded by three pairwise tangent discs. Connelly conjectured that for the sets of disc radii where triangulated packings exist, one of them maximizes the proportion of the covered surface; this holds for unary and binary disc packings.

In this thesis, we study various techniques used in the proof of the Kepler conjecture and other crucial results of the domain of disc and sphere packings, such as local density redistribution based on computer search and interval arithmetic. This allows us to prove the statement of the Connelly conjecture for 32 triangulated triplets of disc radii and disprove it for 45 other triplets. Besides that, we obtain tight upper bounds on the local density of simplicial cells in 2-sphere packings in 3D.

Résumé

Comment empiler un nombre infini d'oranges pour maximiser la proportion de l'espace couvert ? Kepler a conjecturé que l'empilement des "balles de canon" est optimal. 400 ans se sont écoulés avant que cette conjecture soit démontrée par Hales et Ferguson dont la preuve comporte 6 papiers et des dizaines de milliers de lignes de code informatique.

Comment arranger un nombre infini de pièces de monnaie de 3 rayons différents sur une table infinie pour maximiser la proportion de la surface couverte ? Un arrangement de disques est dit *triangulé* si chacun de ses "trous" est borné par trois disques mutuellement tangents. Connelly a conjecturé que si de tels arrangements existent, l'un d'eux maximise la proportion de la surface couverte; cela est vrai pour les arrangement unaires et binaires.

Dans cette thèse, nous étudions diverses techniques utilisées dans la preuve de la conjecture de Kepler ainsi que dans d'autres résultats importants de le domaine des arrangements de disques et de sphères, tels que la redistribution de la densité locale basée sur la recherche par l'ordinateur et l'arithmétique d'intervalles. Cela nous permet de prouver l'assertion de la conjecture de Connelly pour 32 triplets de rayons de disques triangulés et de la réfuter pour 45 autres triplets. En outre, nous obtenons des bornes précises sur la densité locale des cellules simpliciales dans les empilements à 2 sphères en 3D.

Acknowledgements, Remerciements, Благодарности

In this Section, I would like to thank all those who contributed, in one way or another, to the creation of this manuscript.

First things first, I have to thank Thomas for being patient, for motivating me every time I needed it, for giving valuable advice every time I needed one, and for being present the best possible in the given context.

I thank Sandor Fekete and Michaël Rao for accepting to review my thesis, as well as Xavier Goaoc, Nabil Mustafa, Nathalie Revol, and Guillaume Theyssier, for being a part of my jury.

Merci à mes collègues du LIPN qui rendent ce bâtiment ~~moche~~ d'architecture industrielle des années 70s aussi charmant et chaleureux (comme les fleurs de cerisiers de la passerelle). En particulier, je remercie ceux avec qui nous partagions tant de choses et d'activités (patinage, escalade, des pauses de danse avec Britney Spears...), pas seulement le bureau (B103 forever). Ghazy pour être drôle et pour son talent naturel au *rock 4 temps*, Francesco D. pour les lasagnes qui resteront gravées dans mon coeur à jamais, Francesco P. pour des petits gâteaux qui remontaient le moral, Mathieu pour rajouter une goutte de folie dans toutes les situations... Thank you Will for not killing yourself when you jumped from the second floor into a 1 meter deep swimming pool (I want to emphasize that Will spent 4 hours in a hospital after falling halfway from some 2 meter rock in Fontainebleau). Un énorme merci à Victor et Théo, avec qui nous rédigions en même temps, pour votre soutien et pour la semaine de rédaction au bord de mer qui restera mon plus beau souvenir en rapport avec ce manuscrit.

Merci à mes collègues hors du LIPN que j'ai eu la chance d'avoir rencontrer pendant des conférences, des journées SDA2, et des séminaires, pour former une communauté accueillante et pour s'être intéressés à mes travaux.

Merci à mes amis qui m'entouraient au début de ma thèse, qui sont, en grande partie, partis, plus ou moins loin, mais qui resteront toujours proches de mon coeur. Merci à Coline et Karina pour notre confinement paradisiaque et pour tout le reste, vous êtes les plus belles fleurs de ma vie. Léo et Thibault qui suivent le même chemin que moi dans des domaines différents (j'attends avec impatience d'être invitée à vos soutenances), merci pour tous les bons moments qu'on a passés ensemble.

Merci à Jordi d'avoir été un MJ de qualité exceptionnelle du JdR qui fut ma seule activité sociale pendant les longs mois de la rédaction. Ces missions effectuées au service du Castel Drachenfels me tiraient de ce pauvre monde tangible. Il est bien vrai que la descente des dieux du chaos sur terre est un problème autrement plus angoissant que l'incertitude dans sa carrière scientifique. Merci à toi Celio pour avoir apporté cette ambiance bon vivant dans les nombreuses activités que l'on a partagé (et surtout d'avoir fait la cuisine pendant tout le séjour au ski), Fanriel je suis votre plus grande fan.

Merci à mes colocataires humains, Nil et Violette, pour ces deux années du bonheur dans notre coloc du bonheur, merci de m'avoir supportée et soutenue dans tous mes états. J'espère que vous ne m'oublierez pas dans vos remerciements pour un (juste un) des Césars, Oscars et Palmes d'or... Merci à mes colocataires félins, Duchesse et Otto, pour être des choupinous d'amour et pour avoir rendu un peu plus supportables des nombreuses heures de rédaction de ce manuscrit. En plus, ils ont chassé toutes les souris de la maison pour que je puisse dormir tranquillement.

Спасибо моим учителям. Сергею Александровичу Дориченко за наш маткласс и за то, что он научил нас восхищаться математикой. Николаю Константиновичу Верещагину, моему научному руководителю на мехмате, который познакомил

меня с замощениями (и, впоследствии, с Томой — моим нынешним научным руководителем), и чьи спецкурсы сформировали моё понимание области теоретической информатики.

Спасибо моим далёким (но близким) друзьям, с которыми мы провели вместе юность, и с которыми нас со временем разбрасывало дальше и дальше. Нике: расстояние и время не имеют над нами никакой силы, не так ли? Анечке и Жанне, с которыми мы одновременно проходили непростой и переломный этап в жизни, и с которыми нас, надеюсь, связывают не только воспоминания. Отдельное спасибо Тане, с которой мы, к тому же, одновременно и похоже переживали наши диссертации, и которая перечитала моё вступление, не только исправляя ошибки и неточности, но и подтягивая стиль.

Спасибо всей моей семье. Особенно, бабушке, Татьяне Фёдоровне Болдыревой, которая научила меня любопытству, терпению и любви к чтению – трём главным качествам учёного, решала со мной задачки с самого раннего возраста и показывала мне созвездия на даче. Наконец, спасибо маме, которая всегда поддерживала меня во всех ситуациях, и без которой этой диссертации бы не существовало.

Enfin, merci Alex.

Contents

Chapter 1




Introduction

C'est ce que je fais qui m'apprend ce que je cherche.

Pierre Soulages

László Fejes Tóth used the term "intuitive geometry" to describe the fields of geometry featuring problems which are simple to state and extremely hard to resolve, such as the Kepler conjecture and the four color theorem.

Problems with straightforward statements that still remain open tend to have difficult proofs. "Difficult" nowadays often implies requiring computer assistance, as it happened with both the proof of the Kepler conjecture [HF06] and of the four color theorem [AH89]. Both proofs share similar ideas of "localizing": the local density redistribution in the Kepler conjecture proof and the discharging method in the proof of the four color theorem. Such problems lie at the edge of the continuous and discrete; to resolve them, one should combine theoretical tools (continuous) and computer calculations (discrete). They are both essential: a strong theoretical basis should be built to make computer calculations feasible in terms of time and memory costs.

The domain of the optimal packings of simple bodies is a shining example of intuitive geometry. A *packing* is a collection of bodies with disjoint interiors in an Euclidean space. Typical questions of interest of this area often concern regular (for various definitions of regularity) patterns which are often optimal (in various senses). See the book of Lázló Fejes Tóth to find out more on the connections of regularity and optimality [FT64]. The notion of pattern can also be defined in different ways: this manuscript is dedicated to packings (i.e., the bodies can not intersect), while another possibility is to consider coverings (i.e., the union of the bodies shall cover the entire space).

In this manuscript, we study the maximal density of disc and sphere packings. A brief description of the domain is given in Section 1.1. Before diving into our main subject, Section 1.2 gives a survey on various adjacent areas of research, all concerning optimal packings. To conclude this introduction chapter, Section 1.3 provides a detailed plan of the remaining manuscript.

1.1 Density of disc and sphere packings

In middle school, one of my math teachers once posed an intriguing problem during the break: Is it better to grind coffee or to keep it in whole beans to fit the most

of it in a jar?[1] Although approximating coffee grains and grounds as spheres is way too optimistic, this question captures the essence of research on the density of sphere packings. Back then, I would never have imagined that about 13 years later, I would be writing a PhD thesis on the subject of this amusing coffee problem.

The study of two-dimensional and three-dimensional packings holds great interest because they represent real-life phenomena and practical challenges, such as the aforementioned coffee packing scenario. Even smaller-scale problems, which are by no means simpler, arise in the realm of nano-materials. Chemists are particularly interested in disc and sphere packings that maximize density, to eventually design compact materials using spherical nanoparticles of specific sizes [PDKM15] (see Fig. 1.1).

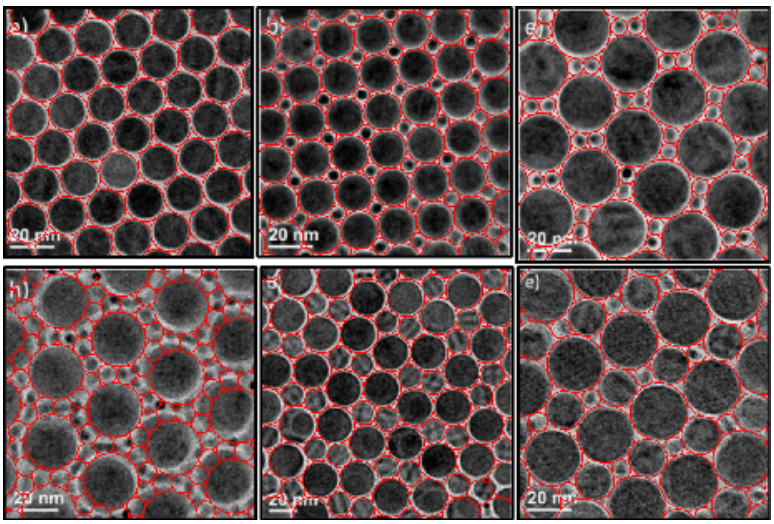

Figure 1.1: Disc packings self-assembled from colloidal nanodiscs and nanorods in [PDKM15].

In this manuscript, our focus is on infinite packings of the entire plane (or space), even though many industrial problems are about packings within finite containers (such problems are discussed in Section 1.2.1). However, when dealing with nano-particles, the container's size can be considered infinite as a good approximation.

To measure the "optimality" of a packing, we introduce the concept of *density* which represents the proportion of the plane (or space) covered by the packing. Our main goal is to determine, given a set of radii, an arrangement of non-intersecting discs (spheres) of these radii (each can be used infinitely many times) that maximizes the density. When we fail to answer this question, we try to at least provide lower and upper bounds on the maximal density.

The first activity in the area was provoked by the Kepler conjecture in 1611 [Kep11]. Kepler conjectured that the "cannonball packing", depicted in Figure 1.3, maximized the density among packings of congruent spheres. This conjecture was only resolved 400 years later by Hales and Ferguson [HF06].

In 1942, Fejes Tóth published the first complete proof that the *hexagonal packing*, represented in Figure 1.2, maximizes the density among packings of congruent discs [FT42].

[1] This question is a trick: the best way is to mix whole bean *and* ground coffee so that the grounds fill the empty space between the beans. Let computing the optimal ratio of beans to grounds be an exercise to the reader.

Various upper and lower bounds on the optimal density were obtained for multi-size disc and sphere packings [Bli69, Fer22, DLDOFV14, OH11]. The precise values of the optimal density is only known for several pairs and triplets of disc radii proportions [BF22, Hep03, Ken05, FP23a].

Figure 1.2: Hexagonal packing of "coins" generated by DALL·E AI.

Figure 1.3: The "cannonball packing" representation in art: Roelof Louw, "Soul City (Pyramid of Oranges)", 1967.

1.2 Alternative densities, packings, and dimensions

The domain of optimal packings is very wide, the abstract problems vary in function of the dimension (2D and 3D correspond to real-life objects, higher dimensions — to error-correcting codes (Section 1.2.3)) and shape of the object to be packed (spheres, other centrally-symmetric bodies or platonic solids (Section 1.2.4)). One can study specific classes of packing as congruent, lattice or translative packings (Section 1.2.2). Finally, the precise definition of optimality varies: in this manuscript, we consider the proportion of the covered space, but one may also study the maximal number of objects that fits into a container of a certain shape or the most compact local configurations (this approach is discussed in Section 1.2.1).

This section is dedicated to a few cases of packing problems which are not covered by the research described in the manuscript but which are scientifically close. The field of optimal packings is incredibly expansive but the techniques used to resolve different questions are often similar. The problems described below, besides being a subject of curiosity, have quite a few links with the results we are going to discuss later. Most of them, however, will not appear outside this section.

1.2.1 Finite density approach

Instead of computing the maximal density of infinite packings of the whole space, one can take a finite approach. Given a solid S, we can consider the smallest container of a given shape fitting a given number of copies of S (*bin packings*) or the minimal volume of the convex hull of a configuration of a finite number of copies of S. Besides that, to find a locally optimal way to pack copies of S around S, one can look for the configuration maximizing the density "locally around S". Another measure of optimality

of a local configuration around a solid is the number of its non-intersecting copies all tangent to S (so-called *kissing number*).

Packings in containers

The bin packing problem for discs is formulated as follows: given k unit discs (or spheres) and the shape of the container, we are looking for the container of a minimal size where k discs (spheres) can be fit without intersection. The shapes of the containers vary, the most studied being circular, rectangular (with the simplest specific case of a square), and triangular shapes.

Optimal bin packings for small numbers of discs rarely match the optimal solution on the entire plane or in the space, see Figures. 1.4, 1.5.

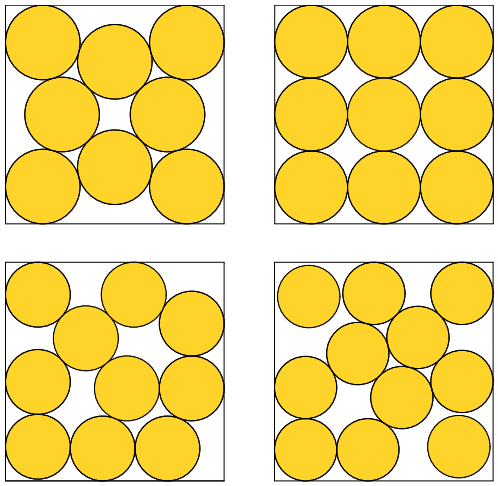

Figure 1.4: The optimal packing of 8, 9, 10 and 11 discs in a square [SM65, Sch65, PWMG92].

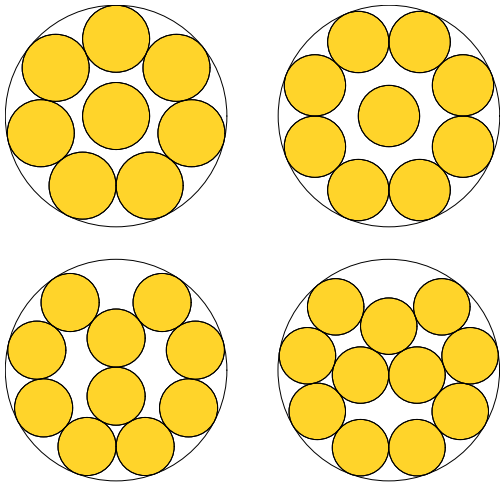

Figure 1.5: The optimal packing of 8, 9, 10, and 11 discs in a circle [Pir69, GDJJ98, Mel94].

For packings in square containers, the configuration of discs minimizing the size of the square were found for k up to 30, as well as $k = 36$ (Figure 1.4 depicts the optimal configurations of 8, 9, 10, and 11 discs). Most of the proofs, as [PWMG92, NO99, MC05], use computer assistance and consist in combining the *branch-and-bound method* with *interval arithmetic* (where intervals represent disc coordinates). Some other values of k feature configurations conjectured to be optimal without any proof being currently provided. There are also results proving the optimality up to a relatively small tolerance value.

The optimal container circles for $k = 1, \ldots, 4$ unit discs are pretty straightforward. The radii of optimal circles were found for $k = 1, \ldots, 13$, as well as for $k = 19$ discs [Pir69, Mel94, Fod99, Fod03]; Figure 1.5 depicts the optimal configurations of 8, 9, 10, and 11 discs in a circle. In contrast to the results on square containers, the results mentioned above do not require computer assistance and are based uniquely on combinatorial and geometric arguments. For the large values of k, various results propose candidates for the optimal solution, which are obtained using heuristic optimization algorithms; these results, also interesting from the algorithmic point of view, give lower bounds on the optimal density [SYR$^+$20, LHY$^+$21].

As for the case of multi-size disc packings, there are numerous optimization algorithms allowing to efficiently pack unequal discs into circular and square contain-

ers [ALS08, MSS09, LB13]. Another direction of bin packings studies concerns the *worst-case density* which equal to the largest value A such that any set of (not necessary equal) discs of total combined area A can be packed in the container of unit area. For square containers, this value equals $\frac{\pi}{3+2\sqrt{2}}$ [Mor17]. The worst-case density of a triangle equals to the area of its incircle [FMS17]. For the circular containers the worst-case density was proved to be $\frac{1}{2}$ in [FKS23].

The optimal packings of spheres in a cube were found for $k = 1, \ldots, 10$, as well as for $k = 14$ [Sch66, Sch94, Joó09]. For the spherical container, the author is not aware of any proof of optimality for $k > 3$. The densest known configurations for $k = 1, \ldots, 14$ and $k = 25$ coincide with the solutions of the Tammes problem mentioned below. For both cubic and spherical containers, new packings for high values of k of higher and higher density are being discovered each year by state-of-the art optimization algorithms [Tat15, ZRH$^+$23].

For up-to-date information on the best optimal containers of various shapes for congruent and non-congruent discs and spheres, take a look at the Packomania website[2] maintained by Eckard Specht.

Dodecahedral conjecture

To obtain an upper bound on the density of a congruent sphere packing, one can find the densest possible *Voronoi cell* of a sphere. The Voronoi cell of a sphere S in a packing is the polyhedron consisting of all points closer to the center of S than to the center of any other sphere of the packing (Figure 1.6 depicts a packing around the red central sphere to the left and its Voronoi cell to the right). Since the density of a packing in a Voronoi cell is the volume of the unit sphere divided by the volume of the cell, this problem is equivalent to finding the Voronoi cell of the minimal volume.

The maximal density of a Voronoi cell provides an upper bound on the density of the packings of the plane. Fejes Tóth used this fact in his proof of the optimality of the hexagonal disc packing (in that case, this upper bound was tight) and suggested to apply it to the 3-dimensional case; he conjectured that the volume of the Voronoi cell of a unit sphere is minimized by a regular dodecahedral circumscribed to the sphere [FT42] (see Fig. 1.6). This assertion is known by the name of *dodecahedral conjecture* and got a lot of attention together with the Kepler conjecture.

Years later, Fejes Tóth proved that the dodecahedral conjecture holds for the Voronoi cells with at most twelve faces [FT64]. However, the complete proof was only given in 1998 (and published in 2010), by Hales and McLaughlin [HM10], at the same time as the proof of the Kepler conjecture. Even though these conjectures are independent from the logical point of view, their proofs are strongly related. Indeed, since the problems share the same nature, similar methods were used in both demonstrations, such as interval arithmetic and linear programming. Both results are strongly computer assisted, and, moreover, share some parts of the code.

Tammes problem and kissing number

Dutch botanist Tammes in his study of equidistribution of pores on pollen grains, published in 1930 [Tam30], asked the following question: What is the maximum number of circular caps of a given angular diameter that can be placed without overlap on a unit sphere? This question, known under the name of *Tammes problem*, plays an important

[2] `http://www.packomania.com` (accessed on 15 July, 2023)

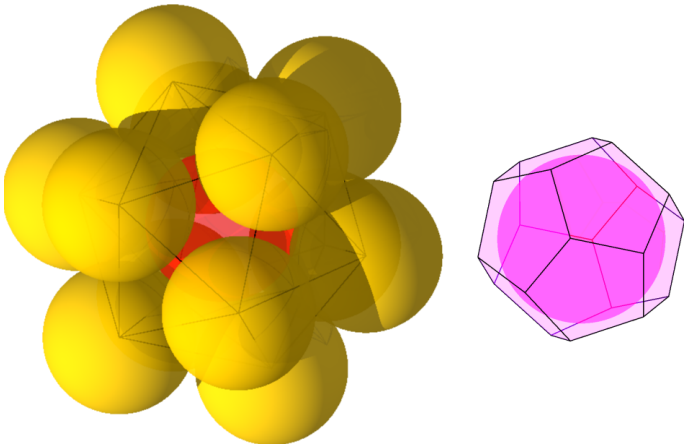

Figure 1.6: Spheres tangent to the red sphere are centered in the vertices of the regular icosahedron, the Voronoi cell of the central sphere (to the right) is a regular dodecahedron.

role in the domain of sphere packings. It is equivalent to finding the minimum radius $R(k)$ of a central sphere possible for k non-intersecting unit spheres to touch it. The Tammes problem in 3D was resolved exactly for $k = 1, \ldots, 14$ [FT43, SvdW51, Dan63, MT14] and for $k = 24$ [Rob61] spheres.

To determine how compact an arrangement of congruent spheres can be, one can count the maximal number of spheres that all touch the common central sphere. Given a dimension, such number is called its *kissing number*. Kissing number is a particular case of the Tammes problem. One can easily notice that the kissing number in one dimension is 2, while in 2 dimensions, it equals 6. The optimal kissing arrangement in 2D is given on the left of Figure 1.7, notice that it is rigid and unique up to rotation.

The 3 dimensional kissing number is famous thanks to Newton who conjectured it to be 12 (that is why it is also called "Newton number") and Gregory who believed that 13 sphere could fit. One can place 12 spheres centered in the vertices of a regular icosahedron around the central sphere, as in the dodecahedral conjecture (see Fig. 1.6, 1.7), the gaps between spheres might make you believe that the 13th sphere would fit after some reorganizing. However, Newton was right, the kissing number in 3D is equal to 12. In 1874, Hoppe proposed a proof which, however, contained a flaw (explained in detail by Hales in [Hal94]). The first complete proof was given by Schütte and van der Waerden in 1953 [vdWS52]. Another proof, based on linear programming bounds, is provided in [Ans04].

Both the Tammes and the kissing number problems become even more interesting in higher dimensions (see Section 1.2.3).

Sausage conjecture

A *finite packing* is a packing of a finite number k of unit spheres. In this setting, where the notion of density of infinite packings is not applicable, the optimal packings are those minimizing the volume of the convex hull. This concept was introduced by Thue for disc packings [Thu92]; Henk and Wills recently proposed a way to generalize it using parameterized density [HW21] which established a connection between the finite and infinite approaches.

We call a finite packing of k unit hyperspheres in $\mathbb{R}^n$ a *sausage configuration* if their

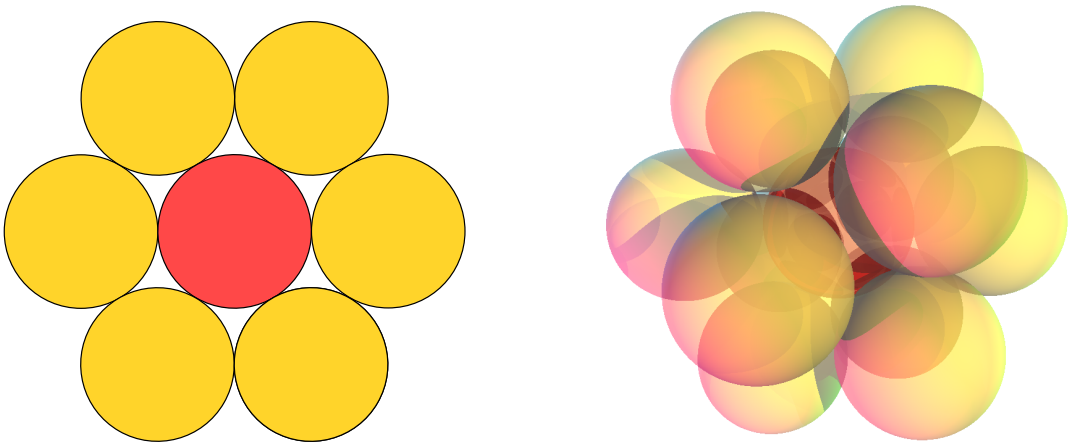

Figure 1.7: On the left, the prefect kissing configuration in two dimensions: 6 discs. On the right, an optimal kissing configuration in three dimensions: 12 spheres centered in the vertices of a regular icosahedron.

centers are collinear and two consecutive spheres are tangent (so their convex hull looks like a "sausage" of length $2k$, see Fig 1.8). Fejes Tóth in 1975 formulated a so-called *sausage conjecture*: an optimal finite packing of any number of unit spheres in $\mathbb{R}^n$ is always a sausage configuration for all $n \geq 5$ [FT75].

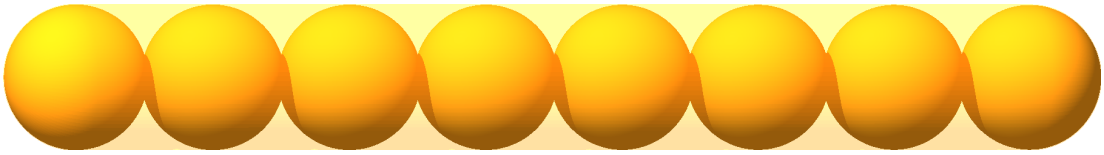

Figure 1.8: A sausage configuration of 8 spheres in 3D.

For now, the conjecture is proved for $n \geq 42$ by Betke, Henk, and Wills [BHW94, BH98]. They used a purely analytical parametric density approach with no computer aid. Besides that, Chun in his talk "Finite sphere packings in low and high dimensions" at the workshop on "Optimal Point Configurations on Manifolds"[3] announced a work in progress with Henk for $n \geq 36$ based on the methods of the previous result and using interval arithmetic.

In low dimensions $n = 2, 3, 4$, the sausage conjecture does not hold. This is due to the presence of infinite lattice packings whose infinite densities are strictly higher than the finite densities of the majority of sausages. On the plane, the sausage is never optimal for the number of spheres $k \geq 3$ [BJ04]. In dimensions $n = 3, 4$, the sausage is always optimal for low numbers of spheres $k < n_n^*$, and starting from a certain value, for $k \geq N_n^*$, the optimum is always a full-dimensional packing. The best-known packings always seem to be either sausages or full-dimensional, this phenomenon being called the *sausage catastrophe* [FT75]. The up-to-date bounds on the sausage thresholds in dimensions 3 and 4 are the following:

$$5 \leq n_3^* \leq 56, \quad 5 \leq n_4^* \leq 338196, \quad 56 \leq N_3^* \leq 58, \quad 5 \leq N_4^* \leq 516964,$$

according to [Wil83, BG84, GZ92, GW92, BJ93, Chu23].

[3] `https://www.esi.ac.at/events/e427/` (accessed on 15 July, 2023)

1.2.2 Congruent, lattice and translative densities

There are different ways to measure how densely copies of a given solid S can be packed. One can consider the optimal density of infinite packings by congruent copies of S or choose the maximal density of a specific class of infinite packings (like translative and lattice densities).

Given a convex body B in $\mathbb{R}^n$, its *congruent packing* (or just *packing*, for simplicity) is a collection of copies of B in $\mathbb{R}^n$ with disjoint interiors. All packings formed by the translated copies of B (i.e. no rotations are allowed) form the class of *translative packings* of B. The subset of translative packings where the centers of B form a lattice are called *lattice packings*. Notice that congruent sphere packings are all translative since spheres are invariant under rotation.

Given a packing P of B, its *density*, $\delta(P)$, is the proportion of $\mathbb{R}^n$ covered by the copies of B from P. The maximal density of a B-packing is called its *congruent density* and is denoted by $\delta^c(B)$. The maximal density of a translative packing of B is called its *tranlative density* and is denoted by $\delta^t(B)$; $\delta^l(B)$ stands for the *lattice density*, the maximal density of a lattice packing. By definition, for any solid B we have

$$\delta^l(B) \leq \delta^t(B) \leq \delta^c(B).$$

It is always easier to obtain the value of the lattice density: indeed, lattice packings are described by a basis matrix of the lattice and the density of a lattice packing is directly derived from the its determinant (see Section 2.1.1 for more details). The lattice density of disc and sphere packings [Lag75, Gau31] were both obtained much earlier than the respective congruent densities.

Fejes Tóth proved that in 2D, for any convex body B, the proportion between the area of B and the minimal area of a hexagon containing B is an upper bound of the congruent density of B [FT64]. Dowker showed that if B is centrally symmetric, then among the hexagons of minimal area, there is a centrally symmetric hexagon [Dow44]. Since any centrally symmetric hexagon can tile the plane to form a lattice tiling, combining the aforementioned results, we get that, for a convex centrally symmetric body, the densest packing is a lattice packing:

$$\delta^c(B) = \delta^l(B). \tag{1.1}$$

More information on the lattice density in higher dimensions is provided in Section 1.2.3. Section 1.2.4 contains some results on translative and lattice densities of the packings of other solids (as regular tetrahedra).

1.2.3 Packings in higher dimensions

In computer science, sphere packings in high dimensions are studied in the context of error-correcting codes [CS98]. There is a correspondence between binary codes and sphere packings, with linear codes being associated to lattice packings. For instance, an extended Hamming $(8, 4)$ code produces the E_8-lattice, while $(24, 12)$ Golay code is used to construct the Leech lattice.

Until recently, the optimal packings of congruent spheres were only known in dimensions up to 3. Thanks to the recent results of Viasovska alone and in collaboration with Cohn, Kumar, Miller, and Radchenko, the problem is now also solved in 8 and 24 dimensions [Via17, CKM$^+$17], in these cases, the optimal packings are lattice packings

generated by respectively E_8 and Leech lattices. To study packings in arbitrary dimensions, one can not rely on geometric properties of low-dimensional spaces and a new kit of techniques is needed. Notably, both results mentioned above are based on the linear programming bound for sphere packings introduced by Cohn an Elkies [CE03], as well as the theory of modular forms.

As we already mentioned, in dimensions $n = 1, 2, 3, 8, 24$, densest lattice packings are also densest among all packings. Besides that, densest lattice packings are known for $n = 4, 5, 6, 7$ thanks to the studies on quadratic forms by Korkin and Zolotarev for $n = 4, 5$ [KZ77] and by Blichfeldt for $n = 6, 7$ [Bli35].

De Laat, de Oliveira Filho, and Vallentin in [DLDOFV14] use semidefinite programming and harmonic analysis to obtain upper bounds on the density of binary sphere packings. They only provide numerical results for $n = 2, \ldots, 5$, but their methods are applicable to any dimension. Their results also improve some upper bounds on the density of 1-sphere packings for $n = 4, \ldots, 36$ provided by Cohn and Elkies [CE03].

Spherical codes and kissing number

The *spherical codes* is a further generalization of the Tammes problem mentioned in Section 1.2.1. Any subset X of unit sphere in $\mathbb{R}^n$ is called a *spherical code*; X is said to have minimal angle ϕ if ϕ is the largest number such that for any pair of points from X, their dot-product is at least $\cos(\phi)$. Therefore, the Tammes problem in dimension n for circular caps of angular diameter ϕ is equivalent to finding the maximal number, denoted $A(n, \phi)$, of points in an n-dimensional spherical code of minimal angle ϕ. The kissing number problem, in turn, consists in finding the maximal n-dimensional spherical code of minimal angle $\frac{\pi}{3}$, i.e., $A(n, \frac{\pi}{3})$.

There are various bounds on the maximal size $A(n, \phi)$ of a spherical code for a given dimension n and minimal angle ϕ. The known kissing numbers in higher dimensions are $A(4, \frac{\pi}{3}) = 24$ [Mus03], $A(8, \frac{\pi}{3}) = 240$ [Lev79], and $A(24, \frac{\pi}{3}) = 196560$ [OS79]. For other dimensions, there exist various lower and upper bounds on kissing numbers and $A(n, \phi)$ in general [ERS98, KKW17, LdL23].

1.2.4 Non-sphere packings

Packings of other bodies than spheres are also studied from various points of view. In 2 dimensions, there are numerous results on bin packings of squares.

The optimal square container is of size $\sqrt{k} \times \sqrt{k}$ for k-square packings if k is a perfect square number, it also turns out to be optimal for packings $k-1$ and $k-2$ squares in this case [Nag05]. Besides these cases close to perfect squares, less-trivial square packings were proved to be optimal for $k = 5, \ldots, 10, 13, 46$ [Fri09, Ben10]. For other k, there are lower and upper bounds: for $k = 11$, for instance, the tightest known packing is rigid and fits into a square of side length ≈ 3.877 (see the leftmost illustration in the comic depicted in Figure 1.9) [Gen05], while the best lower bound is $2 + \frac{4}{\sqrt{5}} \approx 3.789$ [Str03]. The worst-case optimal density of packings of unequal squares is defined in the same way as for discs (see Section 1.2.1, page 5); the worst-case density of squares in a square container equals $\frac{1}{2}$ [MM67].

For square packings of circles, only the trivial cases ($k = 1, 2$) and $k = 3$ [MNMD19] were proved optimal. The worst-case optimal density for packings of unequal squares into a circle equals $\frac{8}{5\pi}$ [FGJ+21].

For up-to-date information on square packings in square and circular containers, see the "Squares in Square" website maintained by David Ellsworth[4] and "Squares in Circles" by Erich Friedman[5].

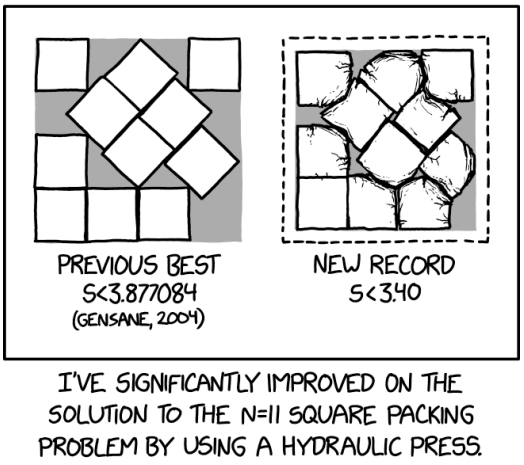

Figure 1.9: Square Packing, xkcd webcomic (`https://xkcd.com/2740/`).

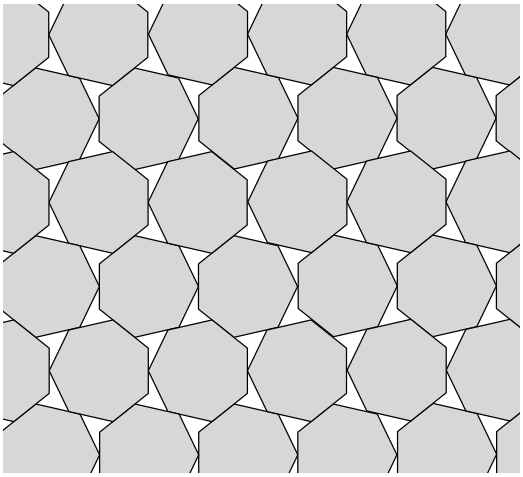

Figure 1.10: Densest known packing of regular heptagons, its density ≈ 0.89269.

Ulam's packing conjecture

The Ulam's conjecture states that the sphere minimizes the optimal density of congruent packings among convex bodies in 3D. This conjecture was attributed to Stanislaw Ulam by Martin Gardner; in his book "New Mathematical Diversions" [Gar95], he wrote:

> Stanislaw Ulam told me in 1972 that he suspected the sphere was the worst case of dense packing of identical convex solids, but that this would be difficult to prove.

Until recently, regular tetrahedra were considered as a possible counterexample to the conjecture since the first tetrahedra packing denser than the densest sphere packing was found only in 2008 [Che08]. As of today, Ulam's conjecture remains unsolved, even though numerous classes of bodies were ruled out, as Johnson and Catalan solids [dGvRD11] and origin-symmetric bodies [Kal14].

In 2 dimensions, the analog of Ulam's conjecture does not hold. The counterexamples are, for instance, the regular octagon for which the optimal packing (see Fig. 1.11)) is of density ≈ 0.906163 and its smoothed version (an octagon rounded at corners by arcs of hyperbola), featuring optimal density ≈ 0.902414 on an infinite family of packings, one of which is depicted in Figure 1.12. These densities are optimal for lattice packings and, since lattice packings are densest for centrally-symmetric convex bodies in two dimensions (see Section 1.2.2 page 8), they are also globally optimal. Reinhardt conjectured that the smoothed octagon has the lowest maximum packing density of all centrally symmetric convex shapes. [Rei34].

Among all convex shapes in 2 dimensions, if central symmetry is not required, the conjecture is that regular heptagons has the lowest maximum density (the densest known packing of regular heptagons is depicted in Figure 1.10) [Kal14].

[4] `https://kingbird.myphotos.cc/packing/squares_in_squares.html` (accessed on 15 July, 2023)
[5] `https://erich-friedman.github.io/packing/squincir/` (accessed on 15 July, 2023)

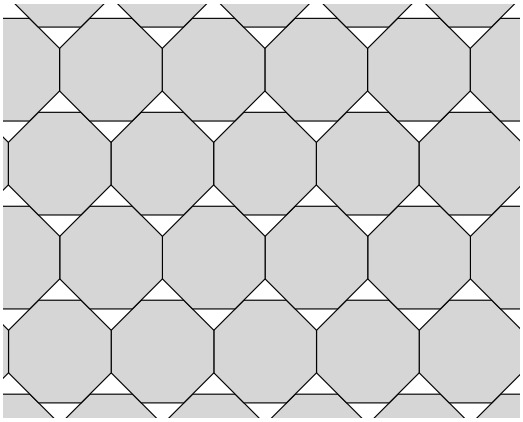

Figure 1.11: Optimal packing of regular octagons, its density ≈ 0.906163.

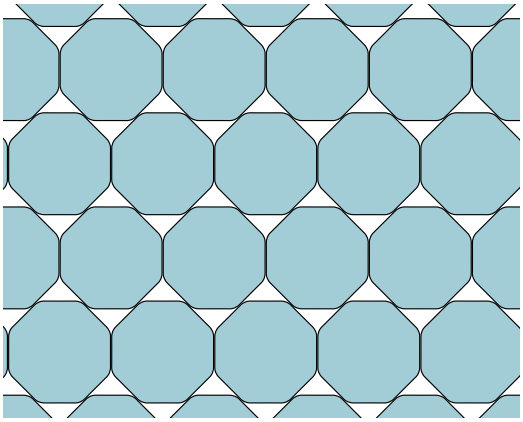

Figure 1.12: Optimal packing of smooth octagons, its density ≈ 0.902414.

For other dimensions the general problem is open, however, Kallus in [Kal14] showed that in dimensions 4, 5, 6, 7, 8, and 24, there are origin-symmetric convex bodies whose lattice density is inferiour to the one of the sphere packings. For non-lattice packings it remains open. Note that for dimensions other than 1, 2, 3, 8, and 24, the densest sphere packings is not yet found (see Section 1.2.3) which also complicates the situation.

Packing tetrahedra

It turns out the Kepler conjecture was not the hardest part of Hilbert's 18th problem [Hil02]: the densest sphere packings are mentioned together with the densest packings of regular tetrahedra (and other solids). Packings by regular tetrahedra got a special attention since Aristotle mistakenly conjectured them to tile the space. It took a long time before Aristotle's conjecture was finally disproved by computing the dihedral angles of regular tetrahedra which can never sum up to 2π. Since the space could not be tiled, a new question arose: what is the maximal density of a packing?

This question is popular even outside mathematical community: researchers in material sciences use tiny tetrahedra to construct nanomaterials and are interested in their density. For example, the the study [HAEK$^+$09] which consisted in simulating a fluid of hard tetrahedra in function of the thermodynamical context emerging into quasicrystalline structures of high densities, was carried out in a chemical engineering lab.

Until 2008, the density of known regular tetrahedra packings has not exceeded $\frac{\pi}{3\sqrt{2}}$, the maximal density of sphere packings [HF06]. Some have even suggested the regular tetrahedron to be a possible counterexample to Ulam's packing conjecture. However, a sequence of results featuring packings with greater and greater densities followed: the first lower bound exceeding the density of sphere packings was given in 2008 [Che08] and the best bound to date, $\frac{4000}{4671} = 0.856347$, was found in 2010 [CEG10]. In contrast, the first upper bound, $1 - 10^{-24}$, was obtained only in 2011 [GEK10] and was not improved yet. There is still a huge gap between the lower and the upper bounds, hence a lot of work to do.

Better progress was made for translative and lattice densities. The optimal lattice density was proved to equal $\frac{18}{49} \approx 0.367$ [Min04]. The maximal translative density whose upper bound, 0.3840610, was given in [Zon14] is conjectured to be equal to the maximal lattice density. In [Zon22], Zong proposes to apply a computer approach to this conjecture reducing the problem to a finite number of optimization problems.

1.3 Structure of the manuscript and main results

Chapter 2 gives a survey of the area of the density of disc packings starting with packings of congruent discs (Section 2.1), where we look at the proof of the optimality of the hexagonal packing among the lattice packings in Section 2.1.1 and in the general case in Section 2.1.2. Section 2.2 provides the definitions and properties needed to work with density of multi-size disc packings (Section 2.2.1) and gives a survey of the most important result of the area (Section 2.2.2); we also introduce the class of triangulated disc packings in Sections 2.2.3, 2.2.4; the only known tight bound on the maximal density were obtained for triangulated packings.

Chapter 3 explains in detail the techniques used to obtain our recent results on the density of triangulated 3-disc packings. We start with the theoretical basis of the proof of optimality of triangulated packings for certain triplet of disc sizes (Sections 3.1–3.4), discuss the details of the implementation of the computer-assisted part of the proof in Section 3.5, and conclude by the explanation of our method to generate dense non-triangulated packings 3.6.

Going in 3D requires more advanced techniques which are given in Chapter 4. Section 4.1 is dedicated to the Kepler conjecture: we discuss the context around the problem, and the main ideas of its eventual proof. In Section 4.2, we combine our tools from 2D and other techniques to investigate the density bounds of 2-sphere packings. Open questions related to these results are provided in Section 5.4.

Chapter 5 is dedicated to the open problems in the area of disc and sphere packings. Sections 5.1–5.3 are dedicated to the problems related to the disc packings from more elaborate density bounds to the computational aspect of the triangulated packings and their connection with tilings. Some open problems on sphere packings are given in Section 5.4.

The main contributions of the author, besides providing alternative proofs for already known results which mostly appear in Chapter 2, comprise the study of the density of triangulated 3-disc packings (Chapter 3) and of 2-sphere packings by spheres of radii 1 and $\sqrt{2}-1$ (Chapter 4). Theorem 3.1 provides the optimal packing densities, which are realized by triangulated packings (16 of them are depicted in Figure 1.13), for 32 triplets of disc sizes, while Theorem 3.2 proves for 45 other triplets that the optimal density is never reached by a triangulated packing[6]. Theorem 4.1 gives detailed tight bounds on the local density inside a cell of a simplicial partition of a 2-sphere packing. The tetrahedral cells maximizing the density among a class of so-called *star* tetrahedra are depicted in Figure 1.14.

[6]The author presented these results at the Symposium of Computational Geometry in 2023 [FP23b], while the journal version appeared in Computational Geometry: Theory and Application [FP23a].

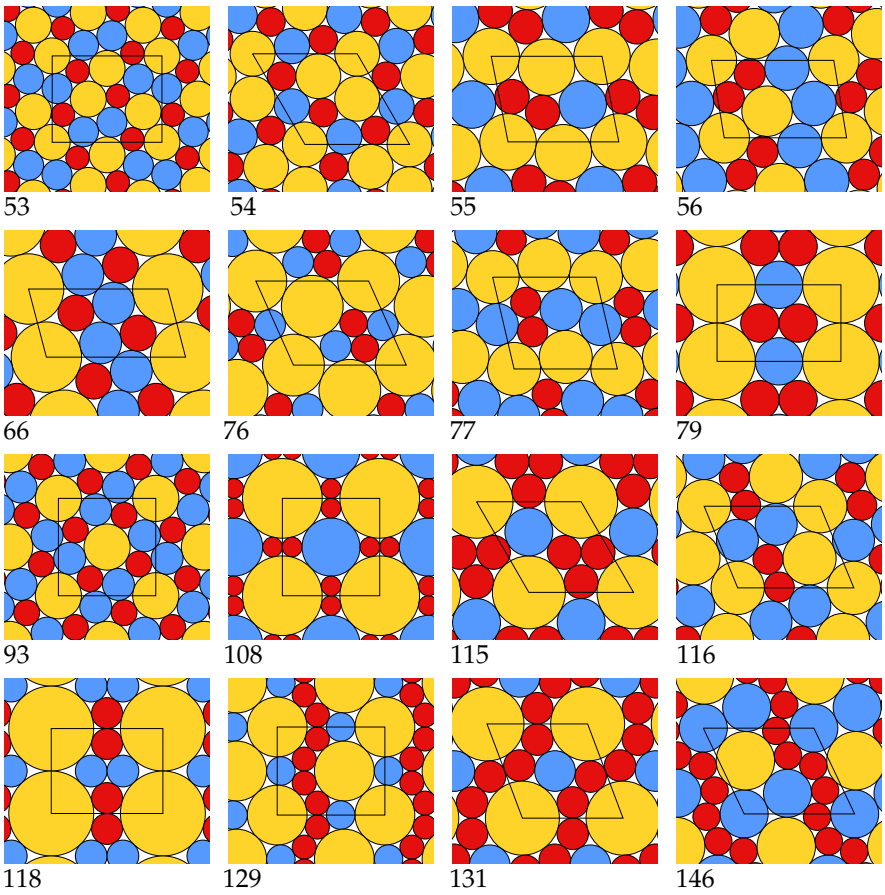

Figure 1.13: The 16 triangulated ternary packings proved to maximize the density (Theorem 3.1.(a)).

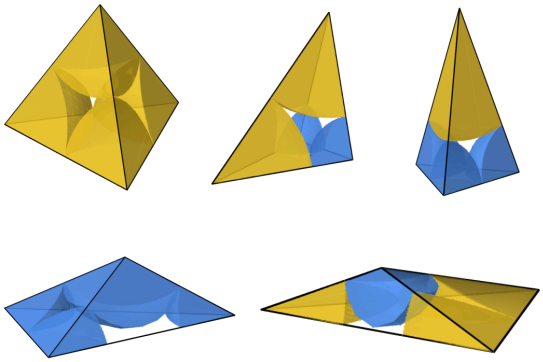

Figure 1.14: The densest tetrahedra for each class of star tetrahedra from Theorem 4.1.

Chapter 2

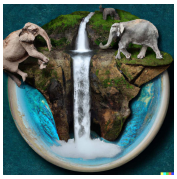

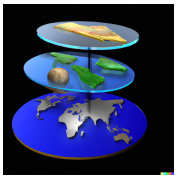


Density of disc packings: survey

> The disc, being flat, has no real horizon. Any adventurous sailor who got funny ideas from staring at eggs and oranges for too long and set out for the antipodes soon learned that the reason why distant ships sometimes looked as though they were disappearing over the edge of the world was that they were disappearing over the edge of the world.
>
> Terry Pratchett, The Light Fantastic

Given a set S of discs, a *packing* of the plane by S is a collection of translated copies of the discs with disjoint interiors. Let $r(D)$ denote the radius of disc D. In this manuscript, for the sake of simplicity, we set the radius of the biggest disc equal to 1 if S is finite. If S is infinite, we assume that $\sup_{D \in S} r(D) = 1$.

Given a packing P and a compact set X, the *density of P inside X* is the proportion of the set covered by the discs from P.

$$\delta(P, X) := \frac{A(X \cap P)}{A(X)},$$

where $A(X)$ denotes the area of X. The *density* of packing P, denoted $\delta(P)$, is the proportion of the plane covered by the discs of the packing.

$$\delta(P) := \limsup_{n \to \infty} \delta(P, B_n),$$

where B_n denotes the disc of radius n centered in the origin.

Our primary problem is the following: given a set of discs S, find the maximal density of a packing of the plane with these discs. We denote this value by δ_S and formally define it as

$$\delta_S := \sup_{P \text{ is a packing by } S} \delta(P).$$

Proposition 2.1. *Given a set of discs S, there is always a packing achieving the maximal density δ_S.*

This proposition follows from a more general result by Groemer [Gro63]. Appendix 2.A provides a detailed proof of this proposition which is omitted here due to its length [1].

The density remains unchanged if a finite portion of a packing is modified, so there is always an infinite number of optimal packings. That is why from now on, we will always talk about "a densest" packing, not "the densest": it is never unique.

Finding optimal packings has a few practical applications. Chemists, for example, are interested in the disc and sphere sizes maximizing the density in order to eventually design compact materials using spherical nanoparticles of given sizes [PDKM15,HST12]. It turns out that self-assembly of spherical and disc-shaped nanoparticles often results into a densest (optimal) disc or sphere packing. Figure 2.1 gives an illustration of experimental results from [PDKM15].

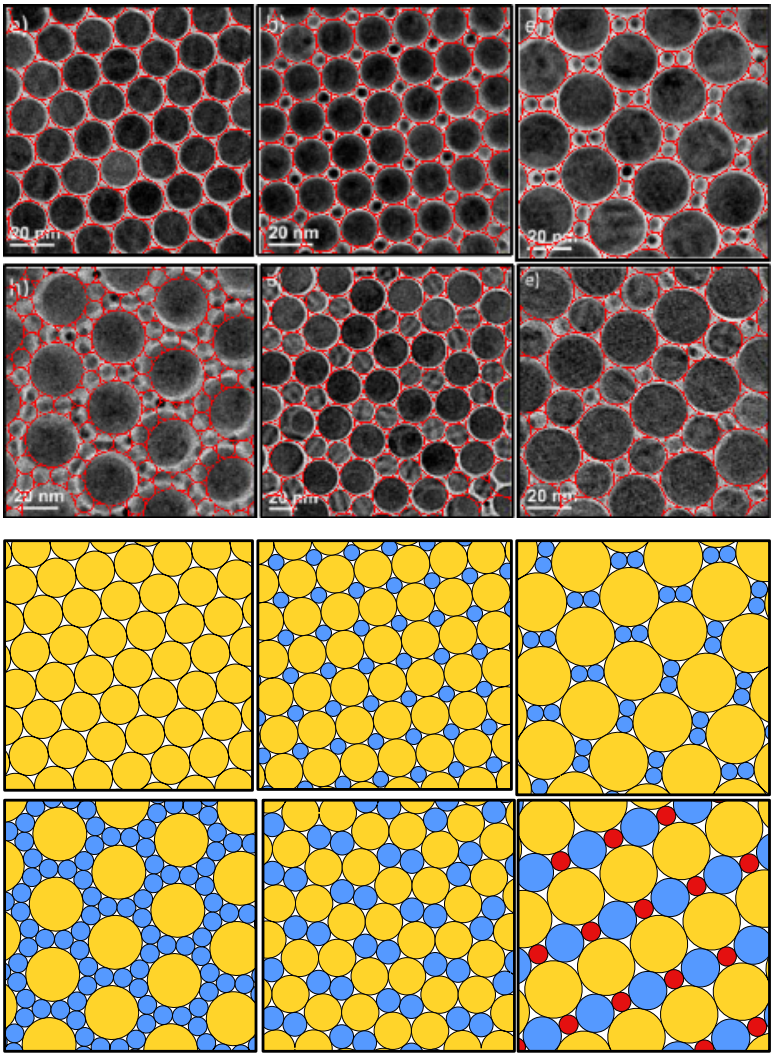

Figure 2.1: Disc packings self-assembled from colloidal nanodiscs and nanorods in [PDKM15] (at the top) which very accurately correspond to triangulated packings (on the bottom).

[1] Even though this fact seems almost immediate after a brief reflection, the length and complexity of the Groemers' proof inspired us to provide an alternative demonstration of Proposition 2.1 which, rather long, remains much lighter than the one in [Gro63].

2.1 1-disc packings

Packings of congruent discs (or *1-disc packings*) are the first non-trivial case of sphere packings. For the sake of simplicity, we consider packings by unit discs. An optimal packing in this case is quite easy to guess: the hexagonal lattice packing maximizes the density of 1-disc packings:

$$\delta_{\text{hex}} := \frac{\pi}{2\sqrt{3}} \approx 0.9069.$$

The hexagonal packing is depicted in Figure 2.2.

Results of Lagrange and Gauss, published respectively in 1773 [Lag75] and 1831 [Gau31], imply that the hexagonal packing is densest among lattice packings. Its optimality among all packings was first shown by Thue in 1910 [Thu10]. His proof was considered incomplete, and the first reliable proof was provided by Fejes Tóth in 1942 [FT42]. The following sections are dedicated to these proofs: Section 2.1.1 treats the case of lattice packings, while Section 2.1.2 explains the general result.

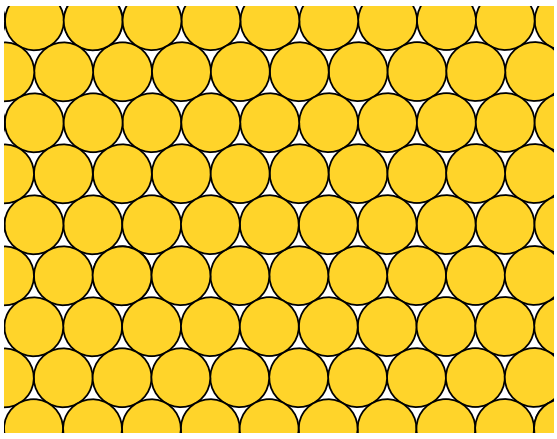

Figure 2.2: The hexagonal disc packing.

2.1.1 Lattice packings

The subclass of lattice packings introduced in Section 1.2.2 is much simpler to work with. Quite a few of results in the domain, as the Kepler conjecture, were first proven for the lattice packings before being demonstrated in the general setting.

Lagrange in 1773 published a work on integer quadratic forms where he separated the binary quadratic forms into equivalence classes, determined that only a finite number of classes have the same value of the discriminant, and introduced reduced quadratic forms (as representatives of the equivalence classes) [Lag75].

Gauss introduced the notion of lattice and found the connection between quadratic forms and lattices, allowing to obtain the area of the domain as a function of the discriminant of the corresponding quadratic form [Gau31]. His result also covers 3-dimensional lattices and implies the lattice version of the Kepler conjecture.

To show that the hexagonal packing is the densest lattice packing, we will combine the Lagrange's results on quadratic forms with the Gauss' work on their connection with lattices.

A *quadratic form* is a polynomial in two variables of the following form:

$$q(x, y) = ax^2 + bxy + cy^2,$$

where a, b, and c are real numbers. The forms with integral coefficients are called *integral quadratic forms*.

The *discriminant* of the form is written as

$$\Delta = b^2 - 4ac.$$

A form with negative discriminant is called *definite*; the coefficients a and c in a definite form are of the same sign. When both coefficients are positive, the form is called *positive definite*.

We say that a form q *represents* an integer N if for some integral values x and y, $q(x, y) = N$. Positive definite forms represent only non-negative numbers. We say that two forms are *equivalent* if they represent the same set of numbers. The discriminant is an invariant of such equivalence classes, and only a finite number of classes can have the same value of the discriminant. To define a representative for each class, we consider the *reduced form*: the form where coefficient b has the smallest absolute value among a, b, c and where $a \leq c$. The reduced form exists and is unique for each equivalence class.

Let $q(x, y) = ax^2 + bxy + cy^2$ be a reduced positive definite quadratic form. Since $|b| \leq |a| \leq |c|$ and a, c are positive, we have

$$\Delta = b^2 - 4ac \leq a^2 - 4ac \leq a^2 - 4a^2 = -3a^2. \tag{2.1}$$

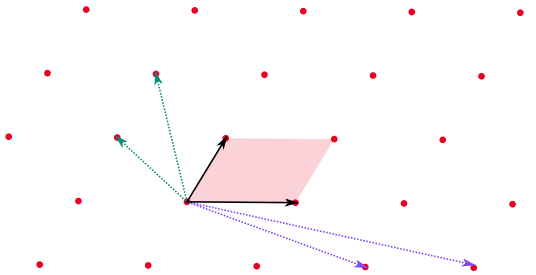

Figure 2.3: A lattice with three pairs of basis vectors indicated in black, green, and violet. A fundamental domain is marked in red.

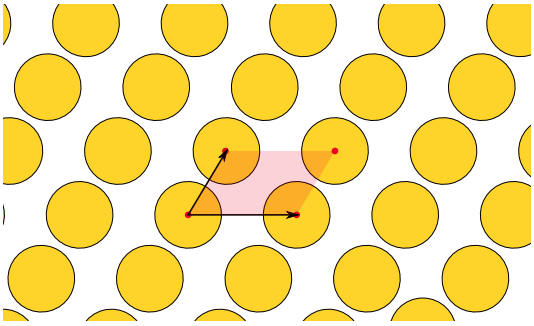

Figure 2.4: A lattice packing, its fundamental domain is marked in red.

Given two non-collinear vectors u, v in $\mathbb{R}^2$, a *lattice* $L(u, v)$ is the set of points obtained by integral linear combinations of these vectors, more formally,

$$L(u, v) := \{xu + yv \,|\, x, y \in \mathbb{Z}\}.$$

The vectors u, v are called *basis vectors* of the lattice. The parallelogram formed by u and v is called a *fundamental domain*, we denote it by D. The lattice can be imagined as a tiling of the plain with its fundamental domain parallelograms. A lattice always has an infinite number of pairs of basis vectors (see Figure 2.3 for a few examples), and thus, fundamental domains. All fundamental domains of a lattice have the same area.

Gauss associated a lattice (up to rotation) to each positive quadratic form in the following way. Given a quadratic form $q(x, y) = ax^2 + bxy + cy^2$, we take a pair of vectors u_q, v_q of lengths $\sqrt{a}$ and $\sqrt{c}$ respectively, separated by angle $\arccos\left(\frac{b}{2\sqrt{ac}}\right)$ (see

Figure 2.5 for an illustration). In this setting, a point of the lattice $xu+yv$ is at distance $\sqrt{q(x,y)}$ of the origin. That means, the numbers represented by the quadratic form correspond to the squares of distances to the origin of the lattice points. Moreover, the area of a fundamental domain D simply depends on the discriminant of the quadratic form:

$$A(D) = \sqrt{\frac{-\Delta}{4}}. \tag{2.2}$$

Let us verify this equation for the fundamental domain defined by u_q, v_q:

$$A(D) = \sqrt{a}\sqrt{c}\,\sin\left(\arccos\left(\frac{b}{2\sqrt{ac}}\right)\right) = \sqrt{a}\sqrt{c}\,\sqrt{1-\left(\frac{b}{2\sqrt{ac}}\right)^2} = \sqrt{\frac{-\Delta}{4}}.$$

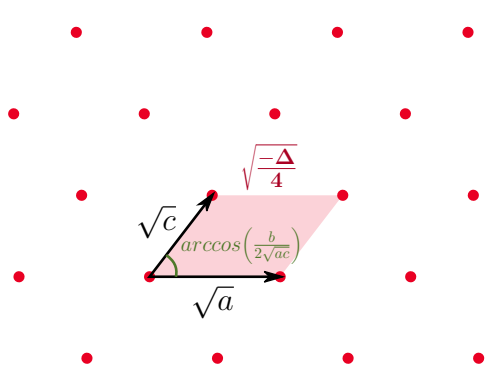

Figure 2.5: The lattice corresponding to a quadratic form $ax^2+bxy+cy^2$, the angle between the basis vectors is given in green, the area of the domain – in red.

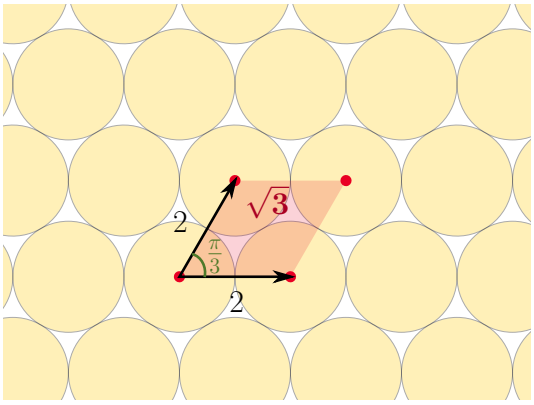

Figure 2.6: The lattice of the hexagonal packing, the angle between the basis vectors is given in green, the area of the domain – in red.

A lattice packing is the one whose disc centers form a lattice (see Figure 2.4). The lengths of the basis vectors of lattices corresponding to lattice packings are at least 2 (otherwise, unit discs would intersect). Notice that given a lattice, the density of its lattice packing P of congruent discs is equal to the proportion of the domain D covered by the discs:

$$\delta(P) = \frac{A(P \cap D)}{A(D)}.$$

Figures 2.3, 2.4 represent a lattice and the corresponding lattice packing, the domain is marked in red.

The domain of a 2-dimensional lattice is a parallelogram, so its intersection with P consists of four disc sectors. The sum of the angles of these sectors, being a sum of angles of a quadrangle, equals 2π. Hence, the part of D covered by P is always equal to the area of a whole unit disc:

$$A(P \cap D) = \pi.$$

A packing maximizing the density, therefore, corresponds to a lattice minimizing the area of its domain.

Equations (2.1),(2.2), imply the following lower bound on the area of the domain:

$$A(D) = \sqrt{\frac{-\Delta}{4}} \geq \sqrt{\frac{3a^2}{4}} = \frac{\sqrt{3}a}{2}.$$

Since the lengths of the basis vectors of a lattice packing are at least 2, $\sqrt{a} \geq 2$ and

$$A(D) \geq 2\sqrt{3}.$$

Applying this to the formula of the density of a lattice packing, we get

$$\delta(P) \leq \frac{\pi}{2\sqrt{3}}\ .$$

The density of the hexagonal packing, δ_{hex}, depicted in Figure 2.6, equals $\frac{\pi}{2\sqrt{3}}$, which means that this packing is indeed optimal.

2.1.2 General result

The proof of the general result, i.e., that the density of a 1-disc packing never exceeds the density of the hexagonal disc packing, was first given by Thue [Thu10], although, his proof was considered incomplete and the first approved version was provided by Fejes Tóth [FT42].

Theorem 2.1 (Thue 1910, Fejes Tóth 1942)**.** *The density of a packing of congruent discs is less or equal to $\delta_{hex} = \frac{\pi}{2\sqrt{3}}$, the density of the hexagonal packing.*

This result is harder than the lattice case since, in general, a packing can not be entirely described by a finite area. It turns out that even a non-lattice packing can be partitioned into finite regions with bounded density. Let us take a look a simplified version of the Tóth's proof provided by Chang and Wang in [CW10].

Delaunay triangulation and Voronoi partition

To proceed with the proof, we shall first partition packings into triangles in a special way. Given a discrete set of points S on the plane, a *Delaunay triangulation* is a triangulation on S where the circumcircle of any triangle contains no points from S other than its vertices.

Delaunay triangulations were introduced by Delaunay in 1934 [Del34], he used them to provide a simplified proof of the Voronoi result on extreme lattices [Vor08]. More precisely, Delaunay showed that if a triangulation satisfies the above condition for each pair of triangles sharing an edge, then it satisfies it for the whole triangulation and is a Delaunay triangulation [2]. This provides us with a somehow more local definition which stands at the origin of numerous algorithms generating Delaunay triangulations [GO04]. The flipping algorithm, for instance, consists in transformation of any triangulation into a Delaunay triangulation by flipping edges not satisfying the Delaunay condition.

In some degenerate cases, a Delaunay triangulation does not exist at all, for example, if all points of the set lie on the same line. If four or more points in the set lie on the same circle, a Delaunay triangulation is not unique (see Figures 2.10, 2.11).

A *Delaunay triangulation of a packing* is a Delaunay triangulation of the disc centers (see Fig. 2.8).

[2] In fact, Delaunay introduced more general n-dimensional Delaunay partitions and proved the result in n dimensions. We, however, are only interested in the two dimensional case in this chapter.

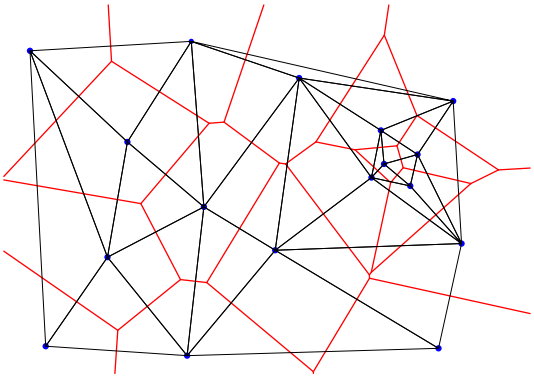

Figure 2.7: Delaunay triangulation and Voronoi partition (in red) of a point set.

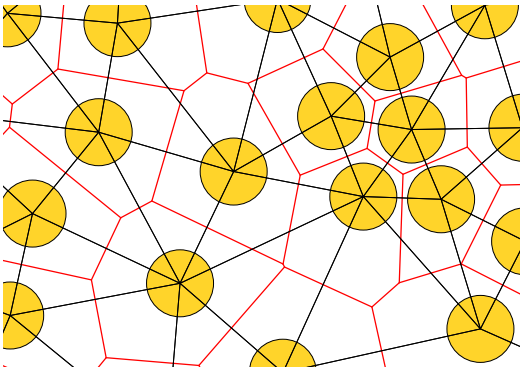

Figure 2.8: Delaunay triangulation and Voronoi partition of a 1-disc packing.

Another way to define a Delaunay triangulation is as a dual of the Voronoi partition. Given a set S of points in the plane, the *Voronoi cell* (also called Thiessen polygon) of a given point p is the set of points on the plane which are closer to p than to any other point in S, this is an intersection of a finite number of half-planes. The *Voronoi partition* of S is the partition of the plane into Voronoi cells associated to the points of S. The Voronoi partition of a 1-disc packing is the Voronoi partition of the disc centers. Notice that, since the discs are all congruent, the Voronoi cell associated to each disc is also the set of points closer to this *disc* than to any other.

The Voronoi partition can be considered as a graph, where the edges are the frontiers between the Voronoi cells, the vertices are points of meeting of three and more Voronoi cells, and the faces are the Voronoi cells themselves. If there are no points of meeting of four or more cells, then the dual of this graph is a Delaunay triangulation. See Figures 2.7, 2.8 for examples of a point set and a packing respectively, their Voronoi partitions (in red) and Delaunay triangulations (in black).

The dual graph of the Voronoi partition is not a triangulation if and only if there is a point shared among more than three cells (see Fig. 2.9). It happens when there are four or more disc centers lying on the same circle (the point of meeting of Voronoi cells is equidistant to their centers), which corresponds to the case, mentioned above, where the Delaunay triangulation is not unique. Anyway, such configuration can always be completed into a triangulation: it is enough to add any maximal triangulation inside the polygon formed by the centers of the discs (Figures 2.10, 2.11 represent two choices of triangulation).

From now on, when we speak of a *triangle* in a Delaunay triangulation associated to a packing, we actually consider the triangle together with the discs centered in its vertices. The *density of a triangle* T in the triangulation is denoted by $\delta(T)$ and is equal to the proportion of the triangle covered by discs from the packing P:

$$\delta(T) := \frac{A(T \cap P)}{A(T)}.$$

By definition, a triangle in a Delaunay triangulation of a packing does not intersect other discs than the ones centered in its vertices.

Proof of Theorem 2.1

A packing P is called *saturated* if no disc can be placed on the plane without intersecting the interiors discs from P. From now on, we only consider saturated packings: indeed,

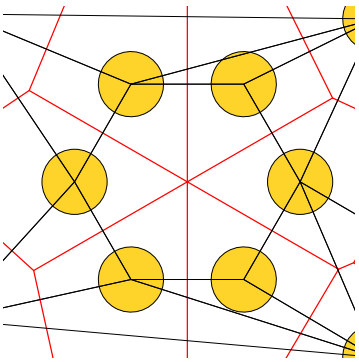

Figure 2.9: Voronoi partition whose dual is not a triangulation.

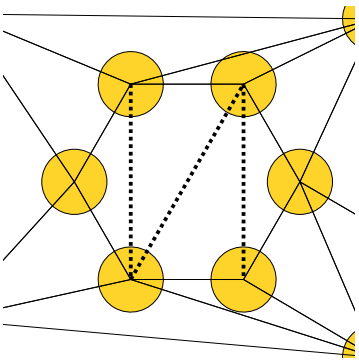

Figure 2.10: A modification of the dual to obtain a Delaunay triangulation.

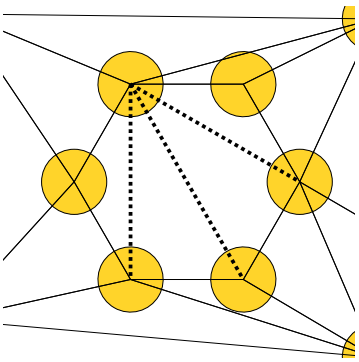

Figure 2.11: Another possible modification.

adding discs does not decrease the density and thus, an upper bound on the density of saturated packings is the upper bound for all packings. A saturated packing always has at least one Delaunay triangulation.

We will now show that the density of a triangle in a Delaunay triangulation of a saturated packing P never exceeds $\frac{\pi}{2\sqrt{3}}$. This directly implies Theorem 2.1 since the density of a union of any finite number of triangles is not greater than the density of the densest of them.

Here and later in this manuscript, given a triangle T formed by points A, B, C, the angle in B is denoted by $\widehat{ABC}$ or simply by $\widehat{B}$ if there is no ambiguity.

Let T be a triangle in a Delaunay triangulation of a saturated 1-disc packing with vertices A, B, C, such that $\widehat{A} \leq \widehat{B} \leq \widehat{C}$. To obtain the bound on the density of T, we will first show the following lemma.

Lemma 2.1. *The value of the largest angle of T is bounded as follows:*

$$\frac{\pi}{3} \leq \widehat{C} \leq \frac{2\pi}{3}.$$

Proof. The lower bound comes from the fact that the sum of the three angles is equal to π, and $\widehat{C}$ is the largest of them.

To obtain the upper bound, let us suppose by contradiction that $\widehat{C} > \frac{2\pi}{3}$. Since $\widehat{A} + \widehat{B} < \frac{\pi}{3}$, the smallest angle $\widehat{A}$ is at most $\frac{\pi}{6}$. This gives a lower bound on the radius R of the circumscribed circle of T:

$$R = \frac{|AB|}{2\sin\widehat{A}} \geq \frac{1}{\sin\widehat{A}} > 2.$$

Nevertheless, by definition of Delaunay triangulations, there are no disc centers inside the circumscribed circle which implies that a supplementary unit disc can be added to P (as illustrated in Fig. 2.12). The last is impossible since the packing is saturated.

□

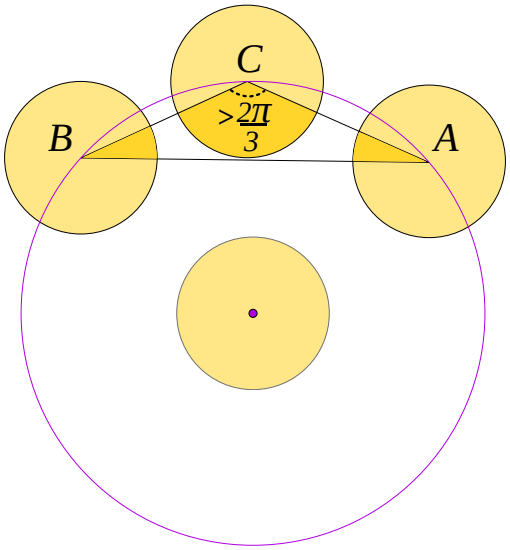

Figure 2.12: Illustration to the proof of Lemma 2.1: a Delaunay triangle with angles $\widehat{A} \leq \widehat{B} \leq \widehat{C}$ and its circumscribed circle (in violet).

By Lemma 2.1 and the fact that the edge lengths of T are at least 2 (discs do not intersect), we have the following lower bound on the area of T:

$$A(T) = \frac{1}{2}|AC|\cdot|BC|\cdot \sin \widehat{C} \geq \frac{1}{2}\cdot 2\cdot 2\cdot \frac{\sqrt{3}}{2} = \sqrt{3}. \tag{2.3}$$

On the other hand, the sum of the circular sectors of the unit discs gives the following upper bound on the area of T covered by the discs:

$$A(T \cap P) \leq \frac{\widehat{A}}{2} + \frac{\widehat{B}}{2} + \frac{\widehat{C}}{2} = \frac{\pi}{2}. \tag{2.4}$$

(This inequality is actually an equality since no disc in a Delaunay triangle can intersect the opposite edge (see Section 2.2.1))

Inequalities (2.3) and (2.4) imply that

$$\delta(T) = \frac{A(T \cap P)}{A(T)} \leq \frac{\pi}{2\sqrt{3}} = \delta_{\text{hex}}$$

which concludes the proof.

2.2 Multi-size disc packings

Let us now consider packings with several disc sizes. Before trying to find bounds on and precise values of the maximal density, let us generalize Delaunay triangulations to packings of unequal discs.

From now on, we write **r-disc** *instead of "disc of radius r".*

2.2.1 FM-triangulation

To work on multi-size disc packings, we first introduce a triangulation adapted for packings using several sizes of discs. Delaunay triangulations do not feature essential

properties if we use several disc sizes. They can, nevertheless, be generalized in order to match our demands.

As mentioned in Section 2.1.2, a Delaunay triangulation of a set of points is a dual graph of the Voronoi partition. An *FM-triangulation* of a packing using several disc sizes was first introduced in [FTM58] and is defined as a dual graph of the Voronoi partition of the packing. This definition is discussed in detail in Chapter VI of the book on regular figures written by Fejes Tóth [FT64].

In Section 2.1.2, we only considered Voronoi partitions of 1-disc packings which coincide with Voronoi partitions of the disc centers. As we saw, the Voronoi cells in that case are convex polygons. On the other hand, in a packings using several disc sizes, the Voronoi cells are not necessarily polygonal: the edges between cells corresponding to discs of different sizes are hyperbolic curves (see Figure 2.13). Indeed, an edge between two Voronoi cells is the set of points equidistant to two non-intersecting circles. Such set is a branch of a hyperbola, with foci in the disc centers, which passes by the midpoint between the disc borders on the segment connecting their centers. Thus, given two discs with centers A and B and of radii r_A and r_B, $r_A \geq r_B$, the border between their Voronoi cells is a branch of a hyperbola of eccentricity $\frac{|AB|}{r_A - r_B}$ with foci A and B.

The Voronoi partition of a disc packing can considered as *additively weighted Voronoi partition* of the disc centers, with weights equal to disc radii. Weighted Voronoi partitions are Voronoi partitions with a modified distance function depending on the weights of the points in the set. Given a point set S and a weight function $\omega : S \to \mathbb{R}^+$, the weighted distance from any point X to a point $Y \in S$ is the Euclidian distance minus the weight of the point:

$$d_\omega(X, Y) := |XY| - \omega(Y).$$

It is enough to use this distance to obtain the additively weighted Voronoi partition. Intuitively, the greater the weight of a point, the larger its modified Voronoi cell.

As for congruent discs, the dual graph of the Voronoi partition might not be a triangulation if there is a point shared among more than three cells (See Fig. 2.9), to obtain a triangulation, the same solution is applied: we add any set of edges triangulating the polygon formed by the cell centers (See Fig. 2.10, 2.11). Certain packings thus feature more than one valid FM-triangulation.

Recall that, as in Section 2.1.2 and in the rest of the manuscrit, given an FM-triangulation of a packing, by a *triangle* we mean a triangle of this triangulation together with the discs centered in its vertices. Also, a triangle that appears in an FM-triangulation of a saturated packing is called an *FM-triangle*.

Definition 2.1. *Given an FM-triangle, its* ***support disc*** *is the smallest disc tangent to the three discs in its vertices without intersecting any of them.*

Support discs are featured in Fig. 2.14.

Aiming to derive several important properties of FM-triangles and their support discs, we start by showing a few facts that seem quite intuitive but still demand formal proofs.

Lemma 2.2. *Given a triangle T with vertices X, Y, Z and with one edge of length less than $2r$, $|XY| < 2r$, any disc of radius greater or equal to r centered in T intersects at least one of the remaining edges, XZ or YZ.*

Proof. Consider a disc D of radius r with center $O \in T$. Suppose by contradiction that D does not intersect XZ nor YZ. Let $X'Y'$ denote the segment parallel to XY passing

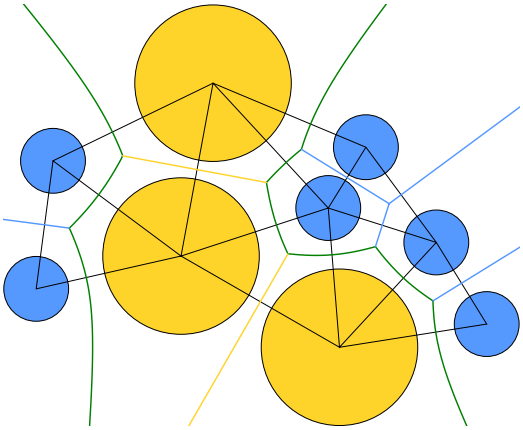

Figure 2.13: Voronoi partition and FM-triangulation of a 2-disc packing. Straight edges of the Voronoi partition between cells of congruent discs are in yellow for 1-discs and blue for r-discs

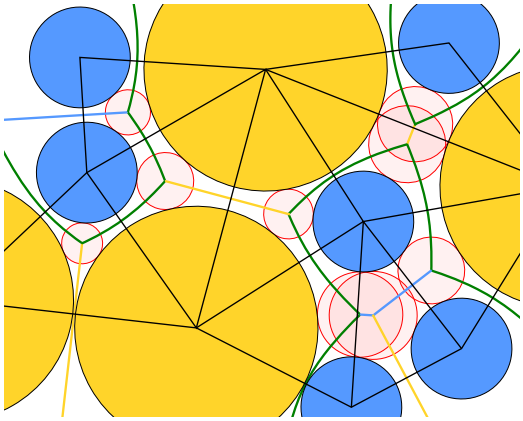

Figure 2.14: Voronoi partition and FM-triangulation of a **saturated** 2-disc packing. support discs are marked in red.

through O such that $X' \in XZ$ and $Y' \in YZ$. On one hand, $X'Y'$ contains a diameter of D, hence $X'Y' \geq 2r$. On the other hand, since it is parallel to XY, $X'Y' \leq |XY| < 2r$ which leads to contradiction (see Fig. 2.15).

□

Lemma 2.3. *Given a quadrilateral $Q = XYZW$ where $|XY| < 2r$ and $|ZW| < 2r$, any disc of radius r centered in Q intersects one of its edges.*

Proof. If $XYZW$ is not convex, suppose without loss of generality that W is in the interior of the convex hull of Q (See Figure 2.16). Therefore, XYZ is a triangle entirely containing Q. Edge XY of triangle XYZ is of length less or equal to $2r$, therefore, by Lemma 2.2, any disc of radius r centered in Q intersects XZ or YZ. If it intersects XY or YZ, we conclude. Otherwise, it intersects XZ and being centered in Q, has a point of intersection with the union of $XW \cup ZW$ which allows us to conclude.

Suppose now that Q is convex and let D be a disc of radius r centered in $O \in Q$. Suppose by contradiction that D has no intersection with edges of Q.

If YZ and XW are parallel, then let us draw a line l passing through O and perpendicular to edges YZ and XW. A segment of intersection of l and Q is of length at least $2r$ and at most $|XY|$, hence, $2r \leq |XY| < 2r$ which leads to contradiction. (see Fig. 2.17)

Otherwise, without loss of generality, $\widehat{YXW} + \widehat{XYZ} < \pi$ and let P denote the point of intersection of the lines containing YZ and XW. Applying Lemma 2.2 to triangle XPY and D, since $|XY| < 2r$, a disc of radius r intersects XP or YP. Since the center of D is inside Q, D also intersects either ZW, or XW or YZ. □

In general, a triangle might have two support discs. However, the following holds.

Property 2.1. *Given an FM-triangle with the smallest disc radius equal to r, there is at most one disc of radius less or equal to r tangent to all three discs.*

Proof. Let T be an FM-triangle with discs D_A, D_B, and D_C of radii r_A, r_B, and r_C, such that $r = r_A \leq r_c \leq r_B = 1$, centered in its vertices denoted by A, B, and C

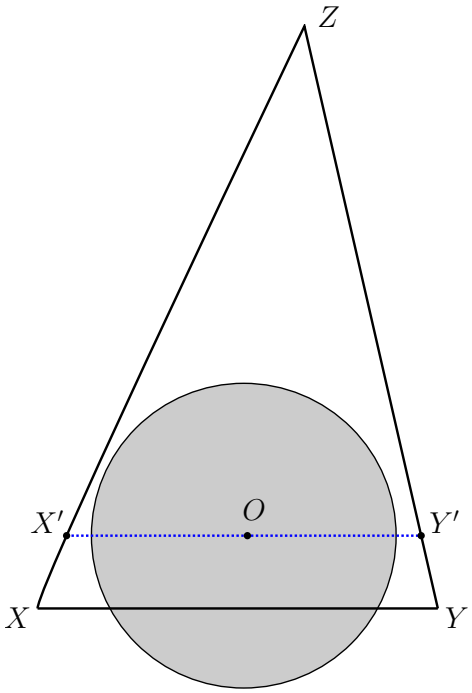

Figure 2.15: Illustration for the proof of Lemma 2.2. $X'Y'$ passes by O and is parallel to XY.

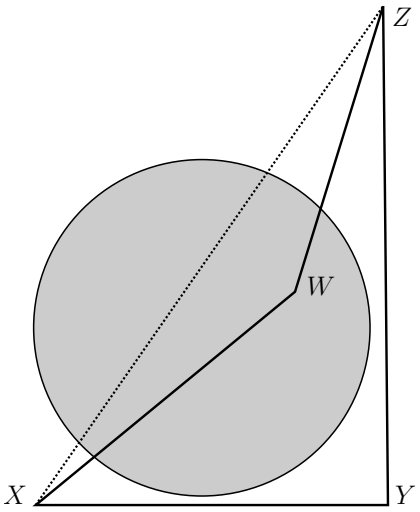

Figure 2.16: Illustration for the proof of Lemma 2.3 for the case where Q is not convex.

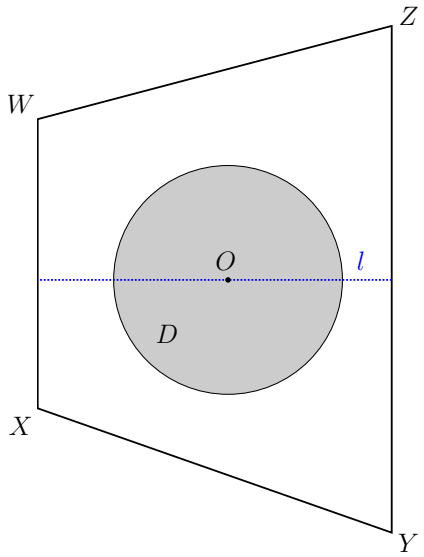

Figure 2.17: Illustration for the proof of Lemma 2.3 in the case where XW is parallel to YZ.

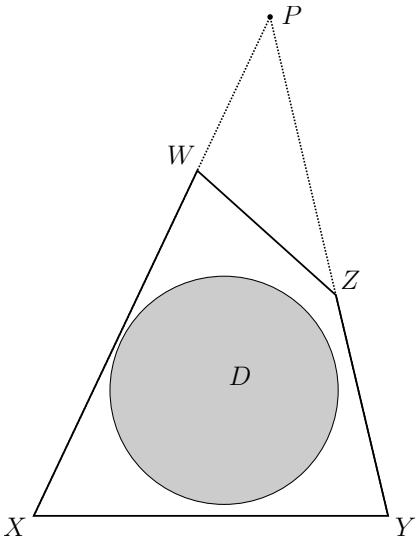

Figure 2.18: Illustration for the proof of Lemma 2.3 in the case where $\widehat{X} + \widehat{Y} < \pi$.

respectively. Suppose T has two support discs D' and D'' centered in O' and O'' of radii r' and r'' both less or equal to r. Discs D' and D'' are tangent both to D_A and D_B, and their centers thus lie on the branch of hyperbola H_{AB} corresponding to the Voronoi partition of D_A and D_B.

Disc D_C does not intersect and is tangent to D', D'', D_A, and D_B, therefore, it belongs to $AO'BO''$ (See Figure 2.19). Let X, Y, Z, and W respectively denote the

points of tangency between D_A and D', D' and D_B, D_B and D'', D'' and D_A. Since D_c does not intersect any of other discs, $C \in XYZW$.

Since $|XY| < 2r$ and $|ZW| < 2r$, by Lemma 2.3, D_C, whose radius is greater or equal to r and which is centered in $XYZW$, intersect one of its edges and, therefore, one of the discs D', D'', D_A, or D_B which leads to contradiction.

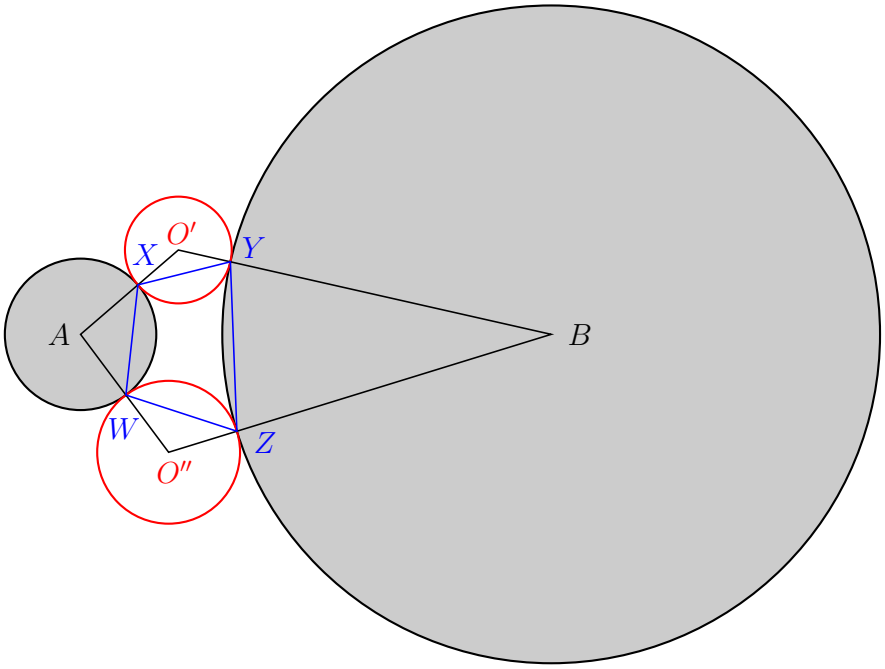

Figure 2.19: Illustration for the proof of Property 2.1, D_A and D_B are marked in grey, the two support discs D' and D'' are marked in red.

□

The main property of the FM-triangulation, partially proved in [FTM58], is the following:

Property 2.2 (support disc)**.** *An FM-triangle in a saturated packing has a unique support disc; the support disc does not intersect the interiors of discs of the packing; the radius of the support disc is smaller than the radius of any disc of the packing.*

Proof. Since the FM-triangulation is the dual of the Voronoi partition, an FM-triangle $T = ABC$ formed by discs D_A, D_B, D_C is the dual of the Voronoi partition of the packing formed by these three discs. Let S denote the point of intersection of the borders of the three Voronoi cells of the discs. This point is equidistant to D_A, D_B, and D_C, let thus D_S denote the disc centered in S tangent to D_A, D_B, and D_C, this disc is marked in red in Figure 2.20.

If D_S intersects the interior of a disc D' of the packing, then S is closer to this disc than to D_A, D_B, and D_C and lies in the interior of the Voronoi cell of D' which leads to contradiction. Therefore, D_S intersects the interior of no disc in the packing.

Let r denote the radius of the smallest of discs D_A, D_B, D_C. If the radius of D_S is strictly greater than the radius of some disc in the packing (including r), then the packings is not saturated since placing the smaller disc inside D_s, no intersection would be created by the previous argument; this contradicts our assumption. Therefore, by

Property 2.1, D_S is the unique disc of radius smaller than r, tangent to all three discs of the FM-triangle. Therefore, D_S is the unique support disc.

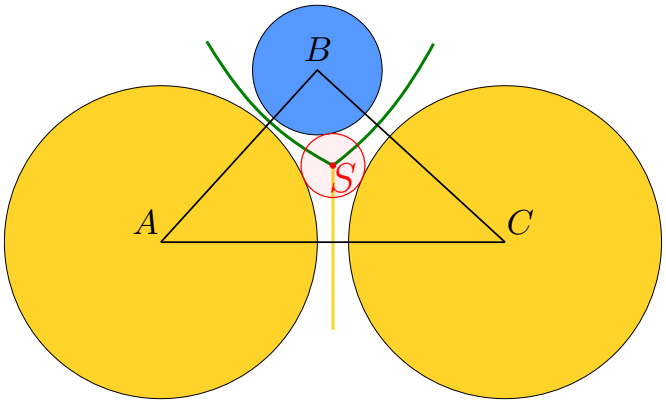

Figure 2.20: Illustration of the proof of Property 2.2: circle D_S is marked in red.

□

Figure 2.20 depicts an FM-triangle, while Figure 2.14 depicts a saturated packing; note that the support discs (in red) are all smaller than the smallest disc of the packing. Another important property of FM-triangles of saturated packings is the following:

Property 2.3. *Given an FM-triangle of a saturated packing, none of its discs can intersect the opposite edge.*

Even though this claim was proved in [FTM58], we give a complete proof here for better understanding.

Proof of Property 2.3. Let T be an FM-triangle of a saturated packing with discs D_A, D_B, and D_C of radii r_A, r_B, and r_C centered in its vertices denoted A, B, and C respectively. Let K_A, K_B, and K_C denote the borders of the discs (which are circles). Let S denote the center of the support disc D_S of T, bounded by circle K_S, of radius r_S.

Let S' denote the point symmetric to S in respect to AC, and $K_{S'}$ – the circle symmetric to K_S. By definition of the support disc, K_S intersects K_A, K_B and K_C by one and unique point each. By symmetry, this also applies to K_S in respect to K_A and K_C. See Figure 2.21 for an illustration.

The union of discs D_A, D_C, D_S, and $D_{S'}$ divides the plane into two connected component: the "hole" between the discs denoted by H (grey area in Figure 2.21) and the rest of the plane (white area in Figure 2.21).

Notice that the interior of D_B is disjoint from the interiors of D_A, D_C, and D_S.

Let us show that disc D_B can not entirely fit into the union $D_{S'} \bigcup H$. Let X denote the tangency between K_A and $K_{S'}$, i.e., $X := K_A \cap K_{S'}$. Let us define in the same manner $Y := K_C \cap K_{S'}$, $Z := K_A \cap K_S$, $W := K_C \cap K_S$ (see Figure 2.21). Suppose the center of D_B lies in $D_{S'} \bigcup H$, let $X'Y'$ denote the diameter of D_B parallel to XY. If $X'Y$ is closer to AC than XY, since $|XY| \leq 2\,r_S \leq 2\,r_B = |X'Y'|$ and XW is parallel to YZ, $X'Y'$ intersects XW or YZ and, therefore, D_B intersects D_A or D_C which leads to contradiction. If $X'Y$ is further from AC than XY, then $X'Y'$ lies entirely in $D_{S'}$ which is impossible since $|X'Y'| = 2\,r_B > 2\,r_S$, which is the diameter of $D_{S'}$.

Therefore, K_B should have points outside $H \cup D_A \cup D_C \cup D_S \cup D_{S'}$, call such a point P. If K_B intersects the part of AC which is not inside D_A nor D_C, then there is a point, denoted Q, which lies in this intersection.

Therefore, K_B is a circle passing through P and Q, having exactly one point of intersection with K_S and not containing D_A nor D_C, nor intersecting their interiors. This implies that K_B has at least 3 points of intersection with $K_{S'}$ which leads to contradiction.

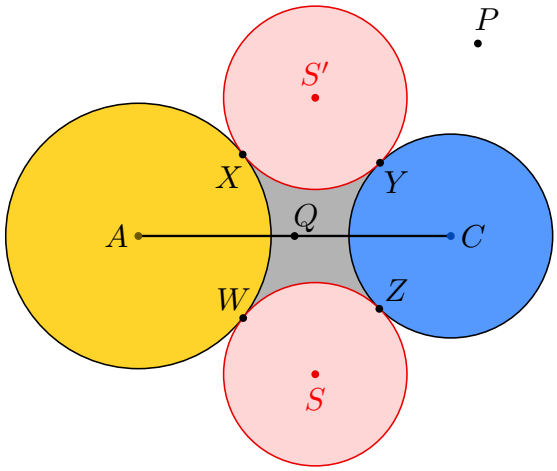

Figure 2.21: An illustration to the proof of Property 2.3.

□

This property allows us, among other, to establish upper bounds on angles of FM-triangles.

Following the notations used in numerous papers on disc packings [Hep92, Hep03, BF22], we call a triangle *tight* if it is formed by three pairwise tangent discs. A triangle with one disc tangent to two others and to the opposite edge is called *stretched*. The support disc of a stretched triangle is symmetric to the disc tangent to the opposite side. By Property 2.2, stretched triangles are not FM-triangles, even though the stretched triangles with the smallest possible disc touching the opposite edge are "almost" FM-triangles: a slight deformation is sufficient to transform them to being FM-triangles.

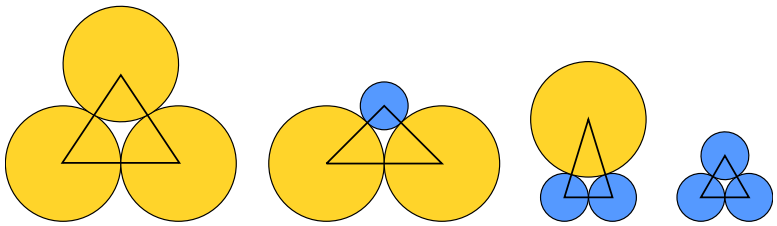

Figure 2.22: Tight triangles for discs of radii 1 and $\sqrt{2}-1$.

Figures 2.22 and 2.23 respectively depict tight and stretched triangles for discs of radii 1 and $\sqrt{2}-1$.

2.2.2 Density bounds

Let us turn to the known bounds on the maximal density of multi-size disc packings. We can always obtain $\delta_{\text{hex}} = \frac{\pi}{2\sqrt{3}}$, the density of the hexagonal packing, by using only one of the discs; this gives us a lower bound on the maximal density.

Using disc of unequal sizes potentially allows us to pack denser than δ_{hex}. For instance, if the small disc fits into the hole between three pairwise tangent big discs,

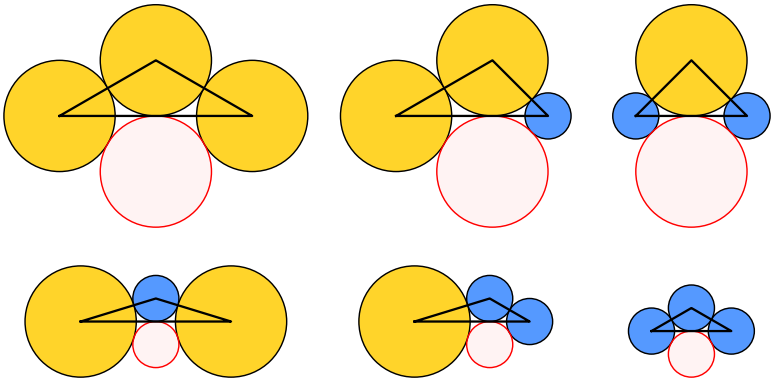

Figure 2.23: Stretched triangles for discs of radii 1 and $\sqrt{2}-1$, their support discs are marked in red. The support discs of the three triangles at the top are of radius 1, while the three at the bottom are of radius $\sqrt{2}-1$.

putting a small disc into each hole of the hexagonal packing strictly increases the density. Moreover, if the size of the small disc tends to 0, we can arrange the small discs in a hexagonal manner inside the holes and obtain the density tending to $\delta_{\text{hex}} + (1 - \delta_{\text{hex}})\delta_{\text{hex}} \approx 0.9913$.

The first upper bounds on the density of multi-size disc packings were found in function of the uniformity of disc radii. Given a finite or infinite set of disc radii $\{r_i\}_{i=1}^{N}$ (or $\{r_i\}_{i=1}^{\infty}$), its *uniformity* q is the smallest ratio between two radii: $q := \inf_{i,j} \frac{r_i}{r_j}$ (notice that this value is always at most 1). After normalization, we define the class of *packings of uniformity* q as the packings whose disc radii are all in $[q, 1]$. The packings of uniformity q, indeed, include all packings of uniformity greater than q. We denote the maximal density of a packing of uniformity q by $\delta_{[q,1]}$, this is a non-increasing function in q.

Florian in 1960 [Flo60] derived an upper bound on the density of packings of uniformity q, which is equal to the density in the triangle formed by two q-discs and a 1-disc, all pairwise tangent. Blind in 1969 [Bli69] showed that if the radius of the smallest disc is too large, using several disc sizes does not improve the maximal density: $\delta_{[q,1]} = \delta_{\text{hex}}$ for $q > q_B$. Moreover, he improved the upper bound for other values of q. Figure 2.30 depicts the Florian and the Blind bounds in function of q.

The following sections are dedicated to the results mentioned above.

Florian bound

The idea behind the Florian density bound [Flo60] is quite similar to the one needed in the proof the optimality of the hexagonal packing explained in Section 2.1.2. Given a value of q, the Florian bound is an upper bound on the density of any FM-triangle of a packing with discs of radii between q and 1. It turns out that this upper bound is the density in the triangle formed by two q-discs and a 1-disc, all pairwise tangent. To show this, we need to make a few intermediate steps.

Let us define the *uniformity of a triangle* as the ratio between the radii of its smallest and its biggest discs. Given a triangle, its number of *contacts* is the number of pairs of tangent discs. For example, a tight triangle has 3 contacts.

First of all, we will prove that given a triangle of uniformity q and of density δ, there is a triangle of uniformity at least q with at least two contacts whose density is at least

δ. This was first shown by Fejes Tóth and Mólnar in [FTM58]; for an English version of this result (the original paper is in German), see Chapter VI of [FT64].

This technique of using a density-increasing transformation to reduce the set of FM-triangles is called *dimension reduction*. This name is easily explained: fixing two contacts between discs, we fix the lengths of two of the edges so the set of triangles is one-dimensional (only one edge is free to change), instead of being three-dimensional. Dimension reduction is widely used to obtain various results on the maximal density of disc packings and in the proof of the Kepler conjecture, so we will encounter it again.

Let us present a sketch of the proof of the Florian bound. We start by the formal statement of the dimension reduction for disc packings:

Lemma 2.4 (Fejes Tóth and Mólnar, 1958)**.** *Given an FM-triangle (of a saturated packing) T of uniformity q and density $\delta(T)$, there is an FM-triangle T_2 of uniformity at least q where one disc is tangent to two others and whose density is at least $\delta(T)$.*

Proof. Let the vertices of T be denoted by A, B, C and the corresponding disc radii — by $r_A, r_B, r_C \in [q, 1]$. By Property 2.3, no disc in T intersects the opposite edge. Suppose no discs in T are tangent and no disc is tangent to the opposite edge; otherwise, we directly proceed to one of two cases of the next step of the proof.

Since homothety is a continuous transformation in function of its ratio h, there is a value $h < 1$ such that the triangle with vertices $A_1 = hA, B_1 = hB, C_1 = hC$ and discs of radii r_A, r_B, r_C is an FM-triangle and there is either exactly one pair of tangent discs or a disc tangent to an edge. This transformation is called *deflation*. Let us denote this triangle by T_1 and notice that its density exceeds the density of T: indeed, the area of the triangle diminished while the area covered by discs did not change since the angles and disc radii are preserved:

$$\delta(T) = \frac{\widehat{A} r_A^2 + \widehat{B} r_B^2 + \widehat{C} r_C^2}{2\ A(T)} \leq \frac{\widehat{A_1} r_A^2 + \widehat{B_1} r_B^2 + \widehat{C_1} r_C^2}{2h^2\ A(T)} = \delta(T_1).$$

First case. Suppose T_1 is an FM-triangle and the discs corresponding to A_1 and B_1 are tangent (Figure 2.24 illustrates the homothety transformation.) Without loss of generality, $r_A \geq r_B$.

If $r_C < r_A$, let us apply a homothety on the r_C-disc until either it becomes tangent with one of the other discs (in this case, we conclude) or its radius is equal to r_A. This transformation does not change the area of the triangle but augments the covered area and, hence, the density (see Fig. 2.25, on the left).

Then we glide the point C_1 along the edge B_1C_1 in the direction of B_1 until the disc corresponding to C becomes tangent to one of the other discs. Let us denote this new point by C_2; we denote by T_2 the triangle $A_1B_1C_2$ with disc radii r_A, r_B, r_A (Fig. 2.25, on the right). This transformation is called *edge reduction* and it does not diminish the density. Indeed, the area of the triangle diminishes while the area covered by the discs stays constant (the disc sector we "gain" from the C_2-disc is "lost" by the A_1-disc). The last is due to the fact that the angle corresponding to B_1 remains constant and the discs corresponding to two other vertices have the same radii:

$$\left(\widehat{B_1A_1C_1} + \widehat{B_1C_1A_1}\right) \cdot r_A^2 + \widehat{A_1B_1C_1} \cdot r_B^2 = \left(\widehat{B_1A_1C_2} + \widehat{B_1C_2A_1}\right) \cdot r_A^2 + \widehat{A_1B_1C_2} \cdot r_B^2.$$

Therefore, T_2 has at least two contacts, its uniformity is at least q and its density is greater than $\delta(T)$.

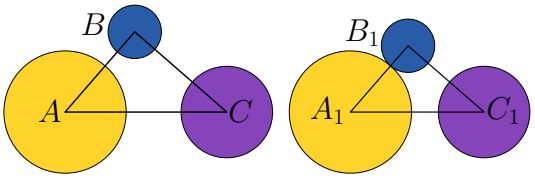

Figure 2.24: *First case:* deflation transformation from T to T_1.

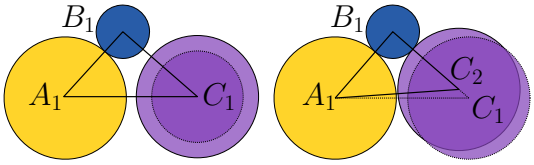

Figure 2.25: *First case:* edge reduction transformation from T_1 to T_2.

Second case. Suppose T_1 is an FM-triangle and the disc corresponding to B_1 is tangent to A_1C_1. Figure 2.26 illustrates of the homothety transformation. Let B_2 be the point symmetric to B_1 in respect to AC, let us place a disc of radius r_B in B_2 (see Fig. 2.27). Without loss of generality, $T_1' := A_1B_1B_2$ is denser than $C_1B_1B_2$. That means, it is also denser than T_1 since the discs do not intersect, $A_1B_1C_1 = A_1B_2C_1$ being symmetric, and

$$A_1B_1C_1 \cup A_1B_2C_1 = A_1B_1B_2 \cup C_1B_1B_2.$$

Let us glide the point A_1 along A_1C_1 until the A_1-disc touches the B_1-disc (and the B_2-disc simultaneously, since they are symmetric); call this new point A_2. Let $T_2 = A_2B_1B_2$, a triangle of uniformity at least q with all three discs pairwise tangent (See Fig. 2.27). The only remaining step is to show that the density of T_2 is greater than the density of T_1'.

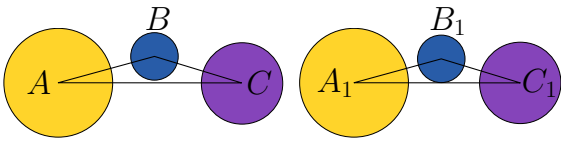

Figure 2.26: *Second case:* deflation transformation from T to T_1.

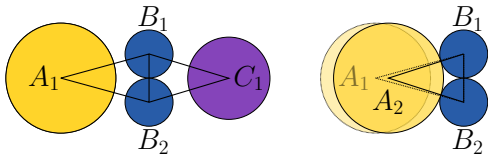

Figure 2.27: *Second case:* transformation from T_1 to T_2.

For the sake of simplicity, let us apply a homothety of ratio $\frac{1}{r_B}$ so that the discs centered in B_1, B_2 are both unit discs. Let $R = \frac{r_A}{r_B}$ denote the radius of the disc once centered in A, then in A_1, and now in A_2.

Let H denote the intersection between A_1C_1 and B_1B_2. Let $A(x)$ denote the point on A_1C_1 at distance x from H. Let $x_1 = |A_1H|$ so $A(x_1) = A_1$, and $x_2 = |A_2H|$ so $A(x_2) = A_2$, as illustrated in Figure 2.28. Our aim is to show that the density of triangle $A(x)B_1B_2$ increases when x goes from x_1 to x_2.

Since B_1B_2 is perpendicular to A_1H, the area of $A(x)B_1B_2$ equals x. Let us compute the area of $A(x)B_1B_2$ covered by the discs:

$$\mathrm{cov}(A(x)B_1B_2) = \frac{\arctan\left(\frac{1}{x}\right)}{2\pi} \cdot R^2 + 2\frac{\arctan(x)}{2\pi}.$$

We need to show that the density of $A(x)B_1B_2$, which is equal to

$$\delta(A(x)B_1B_2) = \frac{\mathrm{cov}(A(x)B_1B_2)}{x},$$

is a decreasing function on $[x_2, x_1]$. Let us simplify the expression multiplying by 2π; we now work with the following function:

$$f(x) := \frac{\arctan\left(\frac{1}{x}\right)}{x} \cdot R^2 + 2\frac{\arctan(x)}{x}.$$

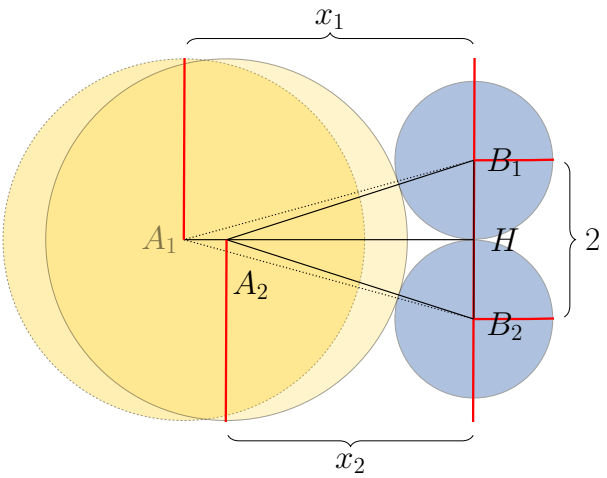

Figure 2.28: Illustration of the proof that the density of the triangle $A(x)B_1B_2$ does not diminish when x goes from x_1 to x_2.

Let us show that its derivative

$$f'(x) = -\frac{2\,R^2 \arctan\left(\frac{1}{x}\right)}{x^2} - \frac{\arctan(x)}{x^2} + \frac{1}{x(1+x^2)} - \frac{2\,R^2}{x(1+x)}$$

is negative for $x > 0$ and any value of R. Since the first and the last terms of this expression are always negative and $x > 0$, it is enough to show that

$$g(x) := (1+x^2)\arctan(x) - x \geq 0.$$

This holds since $g(0) = 0$ and for $x > 0$,

$$g'(x) = 2x\,\arctan(x) > 0.$$

Therefore, $f'(x)$ is negative for $x > 0$, therefore, $\delta(A(x)B_1B_2)$ is a decreasing function which implies

$$\delta(T_2) = \delta\left(A(x_2)B_1B_2\right) \geq \delta(A(x_1)B_1B_2) \geq \delta(T).$$

This allows us to conclude. □

Using the previous lemma, to find the maximal density of an FM-triangle, it is enough to consider only triangles with at least two contacts. The remaining part, proved by Florian in [Flo60], consists in function analysis: given a triplet of disc sizes, after fixing two contacts, i.e., two edges lengths, the density becomes a function on one variable, the third edge length. It turned out that, for a given a triplet of disc sizes, the maximal density is attained either on a tight or on a stretched triangle, and the maximum among all possible triplets of radii was given by a tight triangle formed by one disc of radius 1 and two of radius q:

$$\bar{\delta}_F(q) := \frac{\pi q^2 + 2(1-q^2)\arcsin\left(\frac{q}{1+q}\right)}{2q\sqrt{2q+1}}.$$

Figure 2.29 depicts the density curve of triangles with a 1-disc tangent to two r-discs as a function of the third edge length, for $r = \sqrt{2}-1$. The precise formula of the depicted density function is given below.

$$\delta(r,x) = \frac{2\left(2\,r^2 \arccos\left(\frac{x}{2\,(r+1)}\right) + \arccos\left(\frac{2\,r^2-x^2+4\,r+2}{2\,(r^2+2\,r+1)}\right)\right)}{\sqrt{-x^4+4\,(r^2+2\,r+1)x^2}},$$

where $x = |AC|$.

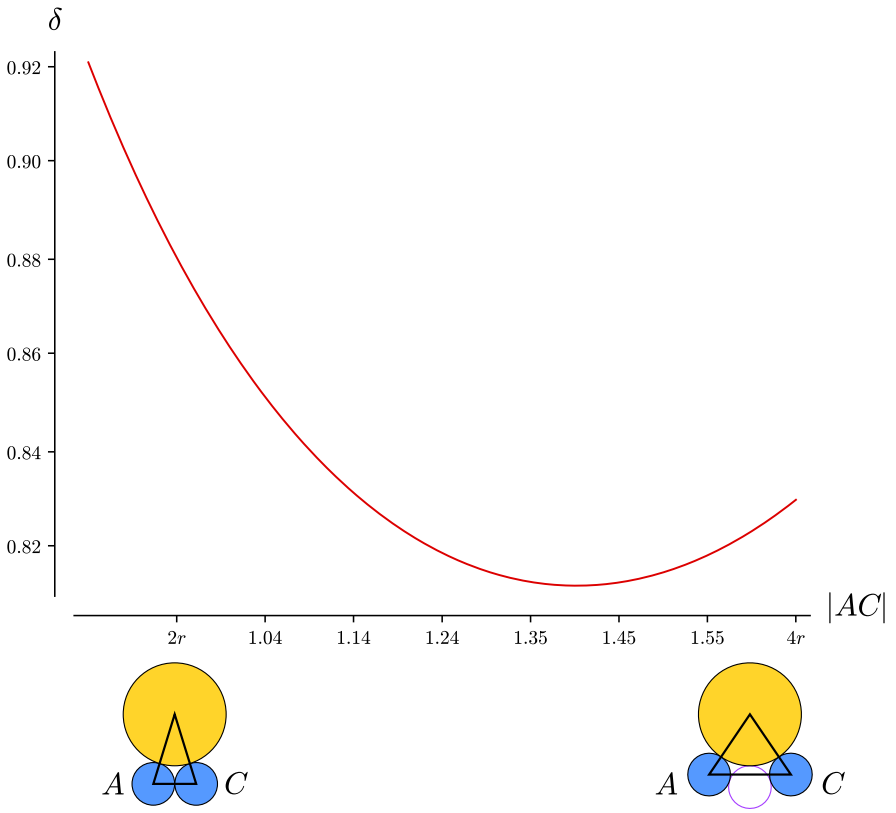

Figure 2.29: Density curve of triangles with a 1-disc tangent to two r-discs as a function of the third edge length for $r = \sqrt{2} - 1$.

Florian in 1963 [Flo63] enhanced his previously mentioned bound by providing an upper bound $q_F = 0.906$ on the *critical uniformity*: the highest uniformity value allowing packings of density greater than the density of the hexagonal packing δ_{hex}. His result implies that for packings of a high enough uniformity ($> q_F$), using several disc sizes does not augment the value of the maximal density which remains equal to δ_{hex}.

Blind bound

Blind in 1969 [Bli69] provided a better upper bound $q_B < q_F$ on the critical uniformity value: he showed that the density of a packing of uniformity greater or equal to $q_B = 0.742990963266321$ never exceeds the density of the hexagonal packing. Moreover, his results imply that for $q \geq 0.612$, the density of a packing never exceeds $\bar{\delta}_B(q)$ which is the density of the union of a regular heptagon around a 1-disc and a regular pentagon around a q-disc:

$$\bar{\delta}_B(q) := \frac{\pi(q^2+1)}{5q^2\tan(\frac{\pi}{5}) + 7\tan(\frac{\pi}{7})}.$$

This enhances the Florian bound for $q \geq 0.6735$. Figure 2.30 depicts the Florian bound (in blue), the Blind bound (in red), the bounds on the critical uniformity value q_F and q_B, and the configurations providing the density bounds: a triangle formed by two q-discs and a 1-disc for the Florian bound and the union of a regular heptagon circumscribed around a 1-disc and a regular pentagon circumscribed around a q-disc for the Blind bound. In this section, we will have a look at the sketch of the Blind's proof, initially given in [Bli69].

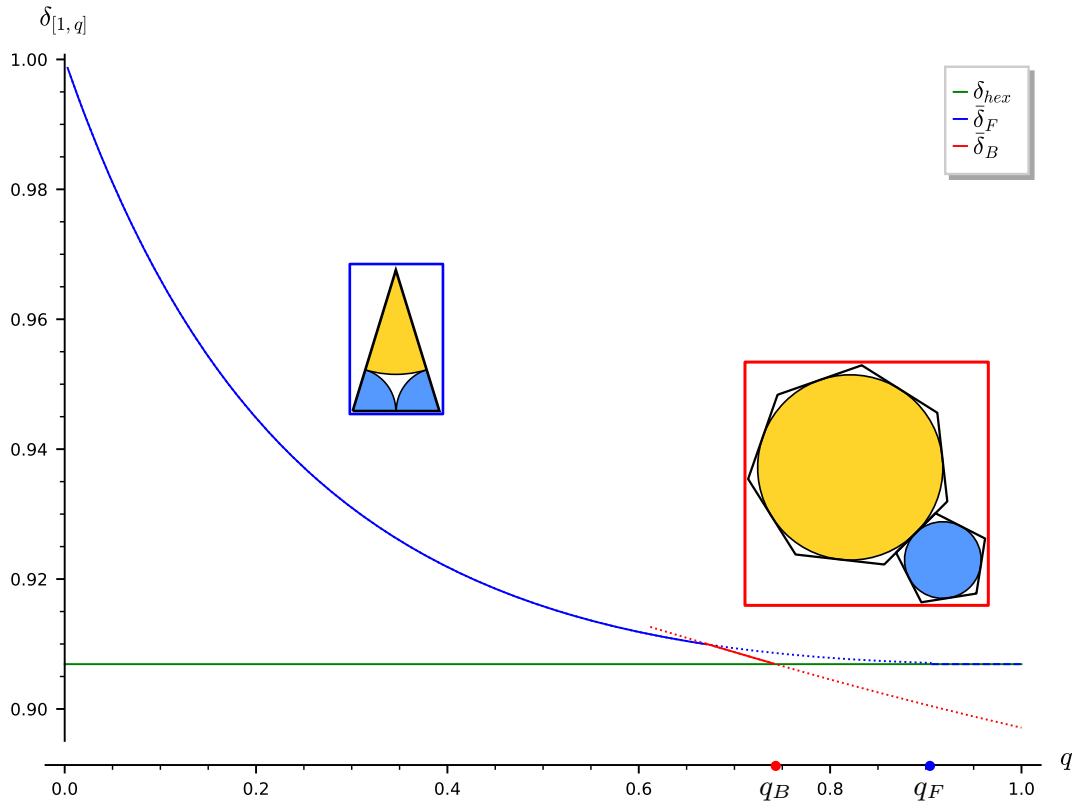

Figure 2.30: Florian bound $\bar{\delta}_F$ (in blue) and Blind bound $\bar{\delta}_B$ (in red), the critical uniformity bounds q_F (•) and q_B (•), and the density of the hexagonal packing (in green).

Blind in his article studies *power diagrams* rather than Voronoi partitions and FM-triangulations commonly used in similar results of the domain. The *power* Π of a point X with respect to a disc D is the square of the distance from X to D, more formally, it is defined as

$$\Pi_D(X) := |OX|^2 - R^2,$$

where O is the center and R the radius of the disc. Given a packing P, its *power diagram* is a partition of the plane into *power cells* associated to the discs; each cell consists of the points whose power distance to a given disc is smaller than to any other disc in P. The cells of the power diagram are all convex and polygonal.

The power diagram of a packing can be considered as a special case of the weighted Voronoi partition. In contrast to the additively weighted case discussed in Section 2.2.1, the modified distance of the power diagram is obtained by substracting the *square* of the disc radius from the *squared* Euclidian distance. Note that the power diagram of

a 1-disc packing coincides with the Voronoi partition. Figures 2.31,and 2.32 depict respectively the Voronoi partition and the power diagram of a disc packing.

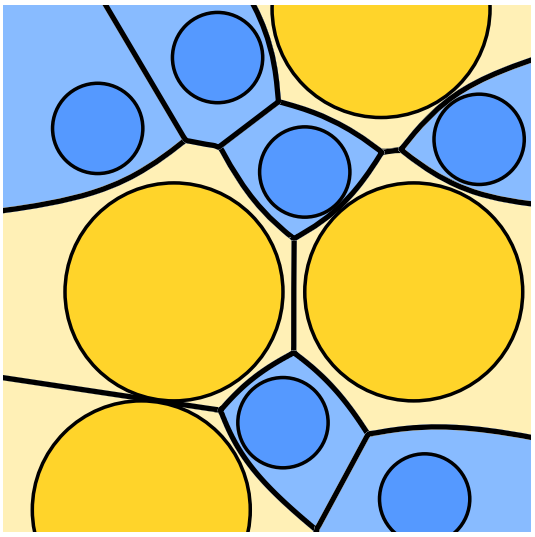

Figure 2.31: The Voronoi partition of a packing.

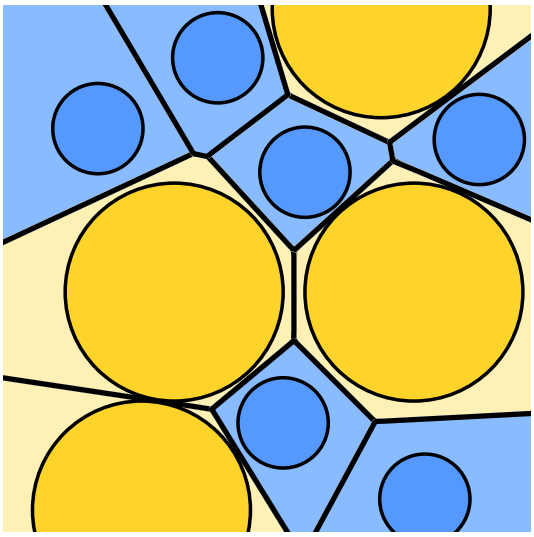

Figure 2.32: The power diagram of a packing.

Given a packing P of uniformity q, let us denote its power diagram graph by $\overline{M}$ and its FM-triangulation by T (we preserve the Blind's original notation). Let us first state a few properties on $\overline{M}$, which are all proved in [Bli69].

Lemma 2.5. *The number of edges in the power diagram $\overline{M}$ does not exceed the number of edges in the FM-triangulation T.*

Let B_R denote the disc of radius $R > 0$ centered in the origin, and let $C_R := \{C_i\}_{i \in I_R}$ denote the cells of $\overline{M}$ entirely lying in B_R. Let $\{D_i\}_{i \in I_R}$ denote the discs of the packing corresponding to these cells. The value of the density of the whole packing can be written as follows:

$$\delta(P) = \lim_{R \to \infty} \frac{\sum\limits_{i \in I_R} A(D_i)}{\sum\limits_{I \in I_R} A(C_i)},$$

where $A(F)$ denotes the area of F (either a disc or a polygon).

Lemma 2.6. *Let e_C denote the number of edges of cell C in the power diagram, then the mean number of edges of cells in a packing is less or equal to 6:*

$$\lim_{R \to \infty} \frac{\sum\limits_{C \in C_R} e_C}{|C_R|} \leq 6.$$

That means, among the polygons of $\overline{M}$, the majority have at most 6 edges. From now on, our aim is to bound the density inside the cells by the density of regular polygons circumscribed to discs.

Let $a(e)$ denote the area of a regular polygon with e edges circumbscribed to a unit disc:

$$a(e) = e \tan\left(\frac{\pi}{e}\right).$$

This function is decreasing and concave for $e \geq 3$.

The following lemma is the technical key to the final result:

Lemma 2.7. *Given* $3 \leq x \leq 5$, $y \geq 7$, *and* $\lambda \in R$,

$$\frac{\lambda x + y}{\lambda + 1} \leq 6$$

implies for all $q \in [0.612, 1]$

$$\frac{\lambda q^2 + 1}{\lambda q^2 a(x) + a(y)} \leq \frac{q^2 + 1}{q^2 a(5) + a(7)}.$$

Given a cell C from C_R corresponding to a disc D, its *regular version*, denoted C', is a regular polygon with the same number of edges circumscribed to D. Indeed, $A(C') \leq A(C)$. Let ${C'}_R$ denote the set of the regular versions of polygons from C_R (see Figures 2.33, 2.34). We thus have the following bound:

$$\delta(P) \leq \lim_{R \to \infty} \frac{\sum_{i \in I_R} A(D_i)}{\sum_{i \in I_R} A(C'_i)}. \tag{2.5}$$

Let us separate the cells from C'_R into three groups: the set of hexagons denoted by ${C'}^6_R := \{C_i\}_{i \in I^6_R}$, the set of cells with at most 5 edges denoted by ${C'}^<_R$, and the set of cells with at least 7 edges ${C'}^>_R$. The same notations hold to the corresponding disc sets.

Given a cell C' with a disc of radius r from ${C'}^<_R$, its *q-version* is a regular polygon with the same number of edges circumscribed to a q-disc (it is actually a homothety of ratio $\frac{q}{r} \leq 1$). Let $\widetilde{C}^<_R := \{C_i\}_{i \in I^<_R}$ denote the q-versions of cells from ${C'}^<_R$ and $\widetilde{D}^<_R$ denote the set of corresponding q-discs.

Similarly, given a cell C' with a disc of radius r from ${C'}^>_R$, its *1-version* is a regular polygon with the same number of edges circumscribed to a unit disc (it is actually a homothety of ratio $\frac{1}{r} \geq 1$). Let $\widetilde{C}^>_R := \{C_i\}_{i \in I^>_R}$ denote the 1-versions of cells from ${C'}^>_R$ and $\widetilde{D}^>_R$ denote the set of corresponding unit discs.

Figure 2.33 depicts a packing of uniformity $q = \sqrt{2} - 1$ (disc color varies in function of its radius r from **blue** for $r = q$ to **yellow** for $r = 1$) and the cells of its power diagram: $C_<$ is a quadrangular cell and $C_>$ is an heptagonal cell. Figure 2.34 depicts their regular versions $C'_< \in {C'}^<_R$ and $C'_> \in {C'}^>_R$, which are respectively a square and a regular heptagon. Finally, Figure 2.35 depicts the cells $\widetilde{C}_<$ and $\widetilde{C}_>$ together with the discs $\widetilde{D}_<$ and $\widetilde{D}_>$ of radii q and 1 respectively.

Lemma 2.8.

$$\frac{\sum_{i \in I^<_R} a(\widetilde{D}_i) + \sum_{j \in I^>_R} a(\widetilde{D}_j)}{\sum_{i \in I^<_R} a(\widetilde{C}_i) + \sum_{j \in I^>_R} a(\widetilde{C}_j)} \leq \frac{\pi(\lambda q^2 + 1)}{\lambda q^2 a(x) + a(y)}.$$

The author chose not to provide proofs of Lemmas 2.5–2.8 due to the high volume of calculations and little interest. However, the remaining part of the proof is given below in its entirety.

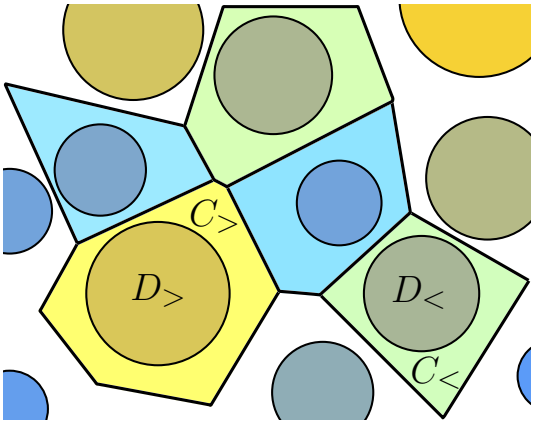

Figure 2.33: Discs D_i of packing P and their power cells C_i; $C_>$ denotes an heptagonal cell, $C_<$ denotes a quadrangular cell.

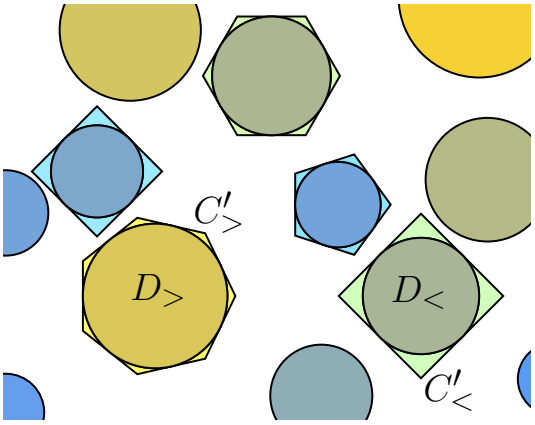

Figure 2.34: Discs D_i and the regular versions C'_i of their power cells.

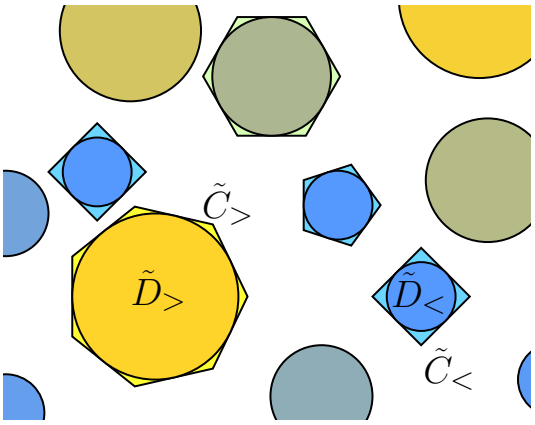

Figure 2.35: Discs $\widetilde{D}_i$ and cells $\widetilde{C}_i$.

Lemma 2.9. *For any value* $\delta \in [\frac{\pi}{a(6)}, \frac{\pi}{a(7)}]$,

$$\frac{\sum\limits_{i\in I_R^<} a(\widetilde{D}_i) + \sum\limits_{j\in I_R^>} a(\widetilde{D}_j)}{\sum\limits_{i\in I_R^<} a(\widetilde{C}_i) + \sum\limits_{j\in I_R^>} a(\widetilde{C}_j)} \leq \delta$$

implies that

$$\frac{\sum\limits_{i\in I_R} A(D_i)}{\sum\limits_{i\in I_R} A(C'_i)} \leq \delta.$$

Proof. Notice that

$$\sum_{i\in I_R^6} a(D_i) = \frac{\pi}{a(6)} \sum_{i\in I_R^6} a(C'_i) \leq \delta \sum_{i\in I_R^6} a(C'_i) \tag{2.6}$$

and since A is a decreasing function, for all $i \in I_R^<$,

$$\frac{a(\widetilde{D}_i)}{a(\widetilde{C}_i)} \leq \frac{\pi}{a(5)} \leq \delta \tag{2.7}$$

and for all $i \in I_R^{>}$,

$$\frac{a(\widetilde{D}_i)}{a(\widetilde{C}_i)} \geq \frac{\pi}{a(7)} \geq \delta. \tag{2.8}$$

By definition, for $i \in I_R^{\leq}$,

$$\widetilde{C}_i = h_i\, C_i' \text{ and } \widetilde{D}_i = h_i\, D_i, h_i \leq 1$$

and for $i \in I_R^{>}$,

$$\widetilde{C}_i = H_i\, C_i' \text{ and } \widetilde{D}_i = H_i\, D_i, H_i \geq 1.$$

Therefore, inequalities (2.7), (2.8) imply

$$\sum_{i \in I_R^{\leq}} (1 - h_i)\, a(D_i) \leq \delta \sum_{i \in I_R^{\leq}} (1 - h_i)\, a(C'_i) \tag{2.9}$$

and

$$\sum_{i \in I_R^{>}} (1 - H_i)\, a(D_i) \leq \delta \sum_{i \in I_R^{>}} (1 - H_i) a(C'_i). \tag{2.10}$$

By the assumption,

$$\sum_{i \in I_R^{\leq}} h_i\, a(D_i) + \sum_{i \in I_R^{>}} H_i\, a(D_i) \leq \delta \left(\sum_{i \in I_R^{\leq}} h_i\, a(C'_i) + \sum_{i \in I_R^{>}} H_i\, a(C'_i) \right). \tag{2.11}$$

Summing up the inequalities (2.6),(2.9), (2.10), and (2.11), we obtain

$$\sum_{i \in I_R} A(D_i) \leq \delta \sum_{i \in I_R} A(C_i'),$$

which allows us to conclude. □

Let us define the Blind density bound as

$$\delta_B(q) := \frac{\pi(q^2+1)}{q^2 a(5) + a(7)}.$$

For $q \in [0.612, 0.74]$,

$$\frac{\pi}{a(5)} \leq \frac{\pi}{a(6)} \leq \delta_B(q) \leq \frac{\pi}{a(7)}.$$

By Lemmas 2.7 and 2.8,

$$\lim_{R \to \infty} \frac{\sum\limits_{i \in I_R^{\leq}} a(\widetilde{D}_i) + \sum\limits_{j \in I_R^{>}} a(\widetilde{D}_j)}{\sum\limits_{i \in I_R^{\leq}} a(\widetilde{C}_i) + \sum\limits_{j \in I_R^{>}} a(\widetilde{C}_j)} \leq \delta_B(q),$$

therefore, using Lemma 2.9, for $q \in [0.612, 0.74]$, we get

$$\delta(P) = \lim_{R \to \infty} \frac{\sum\limits_{i \in I_R} A(D_i)}{\sum\limits_{i \in I_R} A(C_i)} \leq \lim_{R \to \infty} \frac{\sum\limits_{i \in I_R} A(D_i)}{\sum\limits_{i \in I_R} A(C_i)} \leq \delta_B(q)$$

and for $q > 0.74$,

$$\delta(P) \leq \frac{\pi}{a(6)} = \delta_{\text{hex}}.$$

2.2.3 2-disc triangulated packings

Let us now consider *2-disc packings* (also called *binary packings*), those which use 2 sizes of discs. The maximal density of 2-disc packings with the large disc of radius 1 and the small disc of radius $r < 1$ is denoted by δ_r.

Here and later in this chapter, speaking of 2-disc packings, we set the radius of the largest disc equal to 1 *and the radius of the small disc to* $r < 1$.

Indeed, the Florian bound and the Blind bound apply to the 2-disc packings since a packing by discs of radii 1 and r has uniformity r:

$$\delta_r \leq \delta_{[r,1]}.$$

These bounds are, however, relatively far from the precise values of the maximal density in this case.

Getting a tight density bound for all possible disc radii is hard. Let us start from the other end: which packings do look dense? For 1-disc packings, the hexagonal packing is optimal and our proof of optimality was based on the fact that the triangulation of the hexagonal packing consists of tight triangles. Let us generalize this property.

First, let us define a *contact graph* of a packing as a graph whose vertices are disc centers and each edge corresponds to a pair of tangent discs (Figure 2.36 gives four examples of packings with their contact graphs in). Let us call a packing *triangulated* if its contact graph is a triangulation (two examples of triangulated packings with their contact graphs are given in Figures 2.36c, 2.36d). An informal definition is that each of the "holes" of a triangulated packing is bounded by three pairwise tangent discs.

Recall that a packing is called *saturated* if no discs can be added to the packing without intersecting interiors of already placed discs (two examples of saturated packings with their contact graphs are given in Figures 2.36b, 2.36d). In our setup, we always assume packings to be saturated since we are interested in the upper bounds on the density.

As illustrated by Figure 2.36, the properties of being triangulated or saturated are orthogonal.

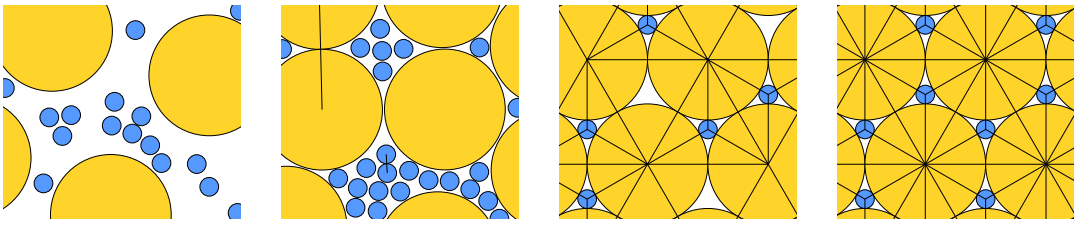

(a) Non-saturated non-triangulated. (b) Saturated non-triangulated. (c) Non-saturated triangulated (d) Saturated triangulated.

Figure 2.36: Examples of packing with indicated edges of their contact graphs.

Fejes Tóth in [FT84] called triangulated packings "compact": since they have no "huge holes", they intuitively look the most compact. Moreover, around each disc, its neighbors form a *corona* of tangent discs which seem to be a locally "optimal" way to pack. For these reasons, triangulated saturated packings appear to be the best candidates to maximize the density on the whole plane.

We call the values of r *triangulated* if it allows triangulated packings featuring both 1-discs and r-discs. Not all values of r are triangulated, to understand this, it is enough to try to assemble together on a table a few coins of two sizes in a triangulated matter.

How to find triangulated radii

In 2006, Kennedy showed that there are exactly 9 values of r allowing triangulated binary packings where both disc sizes are present [Ken06].

Any disc D in a triangulated packing has a so-called *corona*: a sequence of discs all tangent to D and such that two consecutive discs are tangent, as well as the first and the last one. A corona around 1-disc is called *1-corona*, a corona around r-disc is called *r-corona*; examples of 1-corona and r-corona are given is Figure 3.5. If r is triangulated, then there is a 1-corona and an r-corona, both featuring both disc sizes.

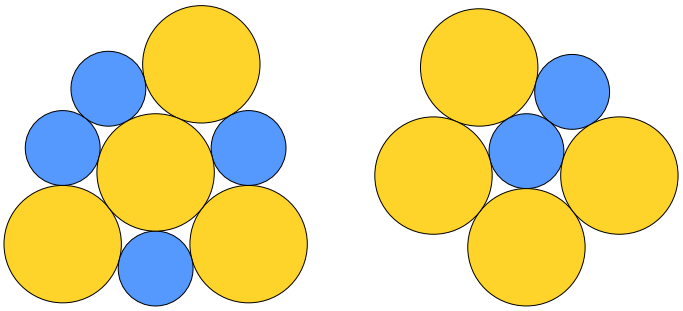

Figure 2.37: The 1-corona (left) and r-corona (right) for $r = r_1$.

Notice that only tight triangles can be a part of a corona and there are only four possible tight triangles for a fixed radius r. There are thus only three possible values of angles corresponding to the center of the central disc of triangles in a 1-corona. The same holds for an r-corona. The sum of these angles equal to 2π in both cases. These angles are either equal $\frac{\pi}{3}$ (in equilateral triangles) or depend on r.

A study of this dependency performed by Kennedy [Ken06] showed that only nine values of r allow 1- and r-coronas featuring both disc sizes. We denote these values $r_1, \ldots, r_9$; Fig. 2.38 depicts corresponding triangulated packings.

Each of the packings in Fig. 2.38 is *periodic*, i.e., if P is a packing in question, there are two non-collinear vectors u and v, called periods, such that $P + u = P + v = P$. In this manuscript, we always consider packings of the whole plane, and since the triangulated packings we show here and below are all periodic, it is enough to represent their fundamental domain (a parallelogram formed by the period vectors, marked in black in Fig. 2.38) to see how the whole plane is packed.

These packings are not the only triangulated packings corresponding to the triangulated radii r. There is an infinite number of triangulated packings for each case, which are described in [Ken06].

A pair of discs with radii $1, r_i$, $i \in \{1, \ldots, 9\}$ is called a *binary case*. The binary cases are denoted by $b_1, \ldots, b_9$.

Optimal packings for binary triangulated cases

It turns out that for each of nine binary cases, the density is maximized by a triangulated binary packing – namely, one of those which are shown in Figure 2.38 [Hep00, Hep03, Ken05, BF22].

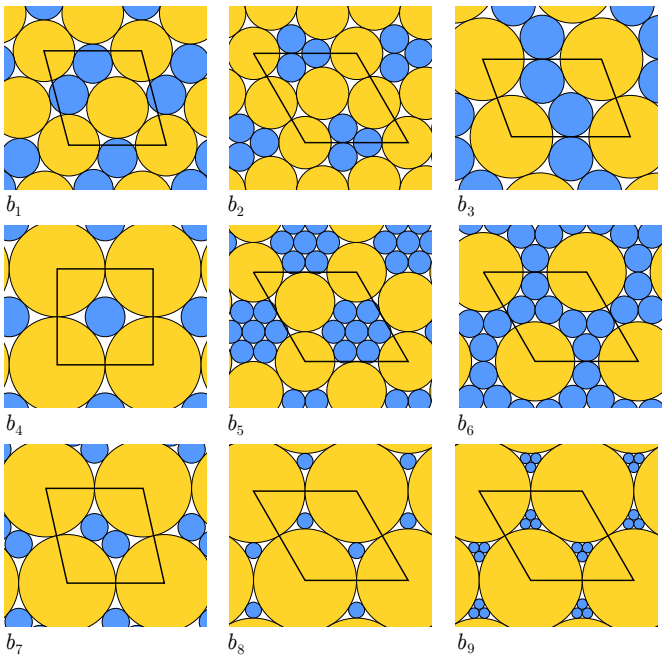

Figure 2.38: Triangulated periodic binary packings corresponding to the cases $b_1, \ldots, b_9$.

The method used in results on the optimality of a class of packings was called "cell balancing" by Heppes [Hep03] and it perfectly matches this title. It consists of two steps: first, we locally "redistribute" the density among some well-defined cells (triangles of the triangulation in for 2-disc packings and a mixture of Delaunay simplices and Voronoi cells, both encoded in so-called decomposition stars, for congruent sphere packings [HF11]) preserving the global density value. Then we prove that the redistributed density of any cell of the packing never exceeds the target density.

Heppes in [Hep00] showed that the triangulated packing of b_4 (depicted in Fig. 2.38), where $r_4 = \sqrt{2}-1$, maximizes the density among all 2-disc packings with discs of radii 1 and r_4. Three years later, Heppes generalized his method to show the same result for 5 more cases: b_1, b_3, b_6, b_7, and b_8 [Hep03]. To obtain the results listed above, Heppes used the aforementioned "cell balancing" approach. More precisely, for each of the listed b_i, he proposes a rule to cut each triangle of the FM-triangulation of a saturated packing into three pieces corresponding to its vertices. The cutting rule is chosen in a way that the density of the cell obtained by gluing together all such pieces around a vertex in the triangulation never exceeds δ^*. Despite being well written, this proof is difficult to understand due to the complex case analysis made by hand; this is the reason why the following results in the domain have been computer assisted. Indeed, separating the demonstration into the human-readable general line of ideas and the computer code treating the case enumeration allows for both better comprehension and reliability.

The next advancement was made by Kennedy who introduced the method of *localizing potentials*, inspired by "m-potentials" from classical statistical mechanics. This new approach allowed him to treat b_2 [Ken05]. His strategy is similar to Heppes' "cell balancing", except that instead of appealing to the shapes of the cells, he distributes the density among the vertices and edges of triangles in the Delaunay triangulation of disc centers. More precisely, Kennedy uses the localizing potential function which is locally less than density but never exceeds δ^* on the whole packing. His proof is computer assisted and, notably, uses *interval arithmetic* (we discuss it in detail in Section 3.5.1).

Finally, the technique necessary to treat the 2 remaining triangulated cases was provided by Bedaride and Fernique, along with the self-contained proof for all 9 cases [BF22]. Their proof is a generalization of the methods used by Heppes and Kennedy.

For cases $b_{5,6,9}$, the Delaunay triangulation of the triangulated packing does not correspond to its contact graph. Thus, instead of using the Delaunay triangulation of disc centers, as Kennedy, Bedaride and Fernique turned to the FM-triangulation (as Heppes).

The reasons the previous results did not include case b_2 is likely due to the fact that it was not known before Kennedy published his characterization of the 9 triangulated cases in 2006 [Ken06]. Case b_5, was not treated before for a different reason: the small disc appears with two different neighborhoods in the triangulated packing, so Bedaride and Fernique needed to use a more complex, less local technique to deal with this specific case. Finally, b_9 features the smallest value of r among all the 9 cases which makes the computations harder due to the high number of possible neighborhoods around a big disc, so the running time of the computer code completing their proof is more than 3 hours for b_9 against 25 minutes for b_8 and a few dozens of seconds for the remaining cases (see Section 9 of [BF22]), let alone trying to deal with it by hand.

Fernique bounds

It turns out that the tight bounds on the density of packings for the 9 triangulated cases allow to get tighter density bounds for other values of r. Fernique in 2022 [Fer22] gave new lower and upper bounds of maximal density of 2-disc packings of the plane, using a fine computer-assisted approach (see Figure 2.39).

To obtain a lower bound on the maximal density, it is enough to find a packing which seems quite dense. Fernique did it using the *flip-and-flow* method explained in detail in Section 3.6. In short, it consists in deforming a triangulated packings continuously, breaking a few contacts and maintaining a high density value, while changing the value of r. This method, applied to the triangulated packings of $b_1, \dots, b_9$ and a few others allowed him to obtain the lower bound marked in green in Fig. 2.39.

To get the upper bound, he used the techniques similar to those from the proof of the tight density bound for the triangulated cases [BF22] on sufficiently small intervals of values of r.

His results, yield four intervals of values of r for which the density of binary packings never exceeds the density of the hexagonal packing $\delta_{\text{hex}} = \frac{\pi}{2\sqrt{3}}$ (marked $I_1, I_2, I_3,$ and I_4 in Fig. 2.39). This is an analogue of the Blind's critical uniformity value in the case of 2-disc packings. These intervals of r are, in addition to $r_1, \dots, r_9$, the radii having a tight bound on the maximal density of binary packings.

2.2.4 3-disc packings

Using more sizes of discs potentially allows to increase the density but complicates the study.

Previously mentioned results suggest the following conjecture formulated by Connelly at the *conference for the 60th birthday of Thomas C. Hales* in 2018 [CGSY18].

Conjecture 2.1 (Connelly, 2018)**.** *If a finite set of discs allows a triangulated saturated packing, then the density of packings by these discs is maximized on a triangulated packing.*

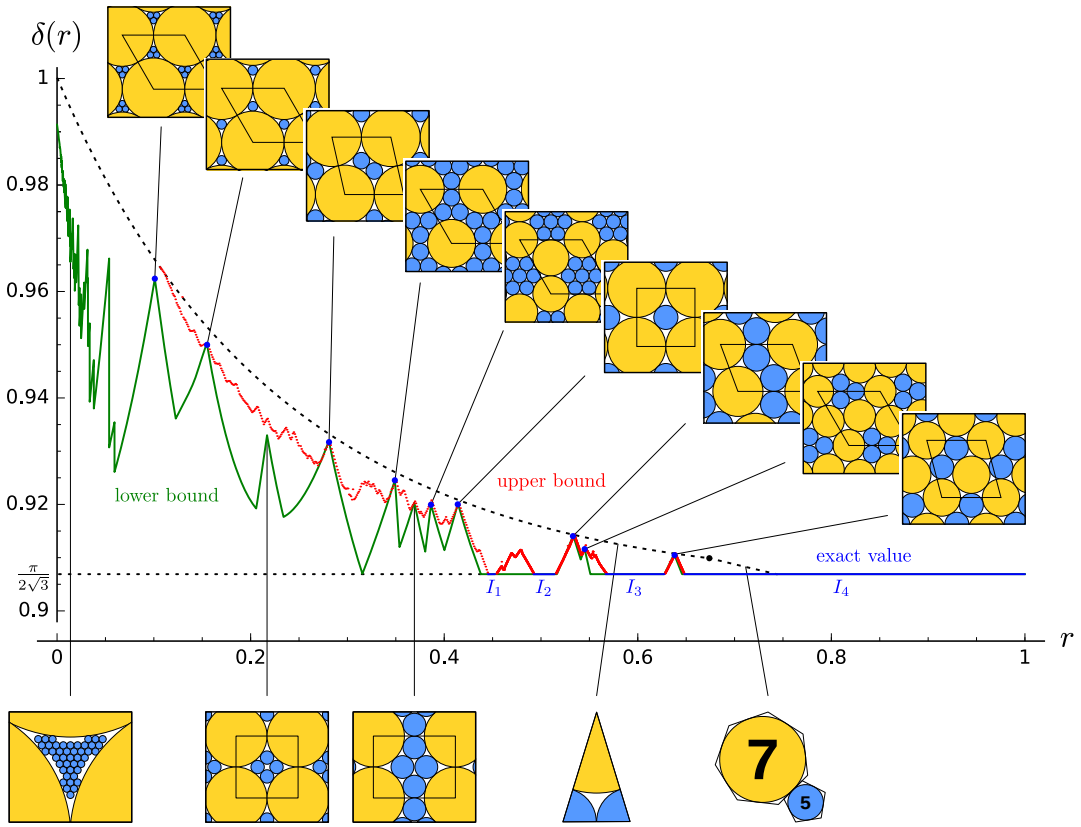

Figure 2.39: Fernique lower and upper bounds together with the Florian and Blind upper bounds and the density of the hexagonal packing (dashed lines) (figure from [Fer22]).

As we saw in the previous sections, the above statement holds for 1-disc packings and 2-disc packings. To study this conjecture, the next step is to verify it for *3-disc* (or *ternary*) *packings* .

To begin with, we need to find the sizes of discs allowing triangulated ternary packings. This problem was solved in 2021 by Fernique, Hashemi, and Sizova: there are 164 pairs (r, s) featuring triangulated packings with discs of radii $1, r, s$ [FHS21].

Here and later, the triplet of discs with radii associated to each of such pairs is called a *ternary case* (or just a *case*). The ternary cases are indexed by positive integers from 1 to 164, like in [FHS21]. They were found by the same method as 2-disc triangulated packings.

The next chapter is dedicated to the study of densest 3-disc packings for the ternary cases: more precisely, we aim to find out whether triangulated packings are densest.

2.A Proof of Proposition 2.1

Proposition 2.1. *Given a set of discs S, there is always a packing achieving the maximal density δ_S.*

The idea of the proof is to construct a packing of optimal density δ_S using a sequence of packings $\{P_n\}$ whose density tends to δ_S. We partition the plane into a sequence of "rings" $\{A_n\}$ of greater and greater radii (as illustrated by Fig. 2.42) and then fill each ring A_n with the discs of packing P_n lying entirely in the ring. The hint to attain the maximal density consists in both choosing a fast enough density convergence of the

sequence of packings and in the fact that the area of the ring A_{n+1} largely dominates the area of the union of all previous rings. Let us proceed to the detailed proof.

Proof. By definition of the maximal density δ_S, there exists a sequence of packings $\{P_n\}_{n=1}^{\infty}$ such that

$$\delta(P_n) = \delta_S - o(1).$$

By definition of the density of a packing, there is a sequence of real numbers $\{R_n\}_{n=0}^{\infty}$ such that $R_1 := 2$ and

$$\frac{A(B_{R_n} \cap P_n)}{A(B_{R_n})} = \delta(P_n) - o(1) \text{ and } R_n > n\, R_{n-1},$$

when $n \to \infty$. By definition, $R_n > n!$ and $\frac{R_{n-1}}{R_n} = o\,(1)$.

Let $A_1 := B_{R_1}$ an for $n > 1$, let A_n denote a ring of inner radius R_{n-1} and outer radius R_n, i.e.,

$$A_n := B_{R_n} \setminus B_{R_{n-1}}.$$

The rings $\{A_n\}_{n=0}^{\infty}$ form a partition of the plane. Let us derive the area of a ring.

$$A(A_n) = A(B_{R_n}) - A(B_{R_{n-1}}) = \pi(R_n^2 - R_{n-1}^2) > \pi\,(n-1)!^2\,(n^2-1).$$

Using the definition of R_n, we bound the density of P_n inside A_n.

$$\begin{aligned} \frac{A(A_n \cap P_n)}{A(A_n)} &= \frac{A(B_{R_n} \cap P_n)}{A(B_{R_n})} - \frac{A(B_{R_{n-1}} \cap P_n)}{A(B_{R_n})} \\ &= \delta(P_n) - o(1) - O\left(\frac{A(B_{R_{n-1}})}{A(B_{R_n})}\right) = \delta(P_n) - o\,(1) - o\,(1) \\ &= \delta_S - o(1). \end{aligned} \tag{2.12}$$

Let A_n^- denote the smallest ring of width 2 in A_n and A_n^+ its biggest ring of width 2:

$$A_n^- := B_{R_{n-1}+2} \setminus B_{R_{n-1}} \text{ and } A_n^+ := B_{R_n} \setminus B_{R_n-2}.$$

Figure 2.40 illustrates, among other, rings A_n, A_n^-, and A_n^+. Let us write their areas,

$$A(A_n^-) = \pi(R_{n-1}+2)^2 - \pi R_{n-1}^2 = \pi(2R_{n-1}+2).$$

$$A(A_n^+) = \pi R_n^2 - \pi(R_n-2)^2 = \pi(2R_n-2).$$

Let $P_n|_{A_n}$ denote the sub-packing of P_n consisting of discs entirely lying in A_n.

$$P_n|_{A_n} := \bigcup\{D \mid D \in P_n, D \subset A_n\}.$$

Using (2.12), we write the density of $P_n|_{A_n}$ inside A_n as

$$\begin{aligned} \frac{A(A_n \cap P_n|_{A_n})}{A(A_n)} &= \frac{A(A_n \cap P_n)}{A(A_n)} - \frac{A(A_n \cap P_n) - A(A_n \cap P_n|_{A_n})}{A(A_n)} \\ &= \delta_S - o\,(1) - \frac{A(A_n \cap (P_n \setminus P_n|_{A_n}))}{A(A_n)} \\ &= \delta_S - o\,(1) - \frac{A\left(\bigcup\{A_n \cap D \mid D \setminus A_n \neq \emptyset\}\right)}{A(A_n)}. \end{aligned} \tag{2.13}$$

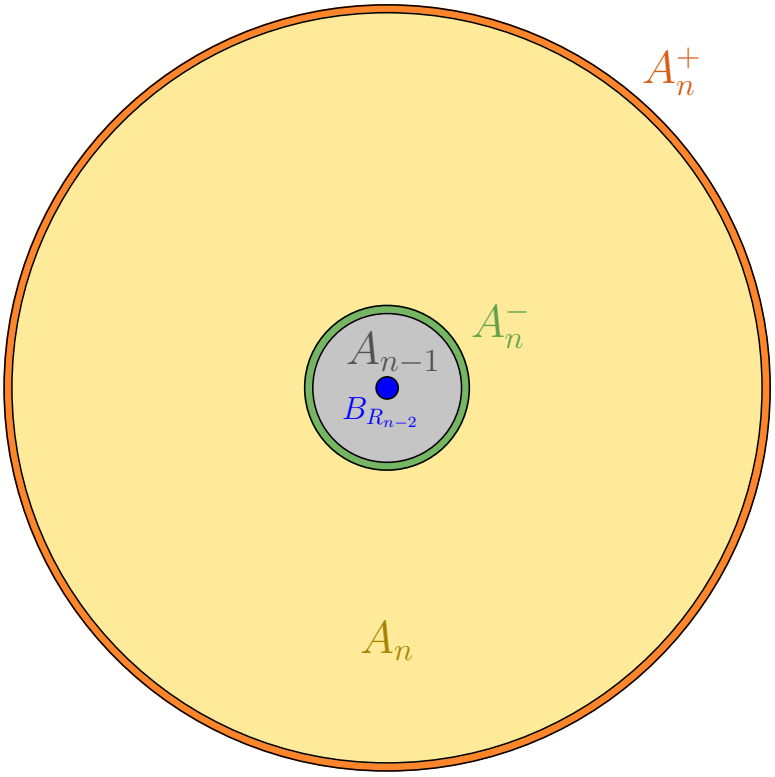

Figure 2.40: Illustration of the proof of Proposition 2.1: ring A_n (in green, yellow, and orange), ring A_n^- (in green), ring A_n^+ (in orange), ring A_{n-1} (in grey), and disc $B_{R_{n-2}}$ (in blue).

Since a disc radius is at most 1, if disc D has points inside A_n and outside A_n, its intersection with A_n either belongs to A_n^- or to A_n^+ (see Fig. 2.41).
Therefore, for $n > 2$, the last part of (2.13) can be bounded from above as follows

$$\begin{aligned} \frac{A\left(\bigcup\{A_n \cap D \mid D \setminus A_n \neq \emptyset\}\right)}{A(A_n)} &\leq \frac{A(A_n^-) + A(A_n^+)}{A(A_n)} \\ &= \frac{2\pi(R_{n-1} + R_n)}{\pi(R_n^2 - R_{n-1}^2)} = \frac{2}{R_n + R_{n-1}} \\ &= o\left(\frac{1}{n}\right), \end{aligned} \tag{2.14}$$

which implies that

$$\frac{A(A_n \cap P_n|_{A_n})}{A(A_n)} = \delta_S - o(1) - o\left(\frac{1}{n}\right) = \delta_S - o(1). \tag{2.15}$$

Let us define a packing P^* as the union of reductions of packings P_n on rings A_n.

$$P^* := \bigcup_{n=1}^{\infty} P_n|_{A_n}.$$

P^* is a valid packing since the rings A_n do not intersect and hence packings $P_n|_{A_n}$ are all pairwise disjoint. Figure 2.42 illustrates the union of the first three packings $P_n|_{A_1}$, $P_n|_{A_2}$, and $P_n|_{A_3}$.

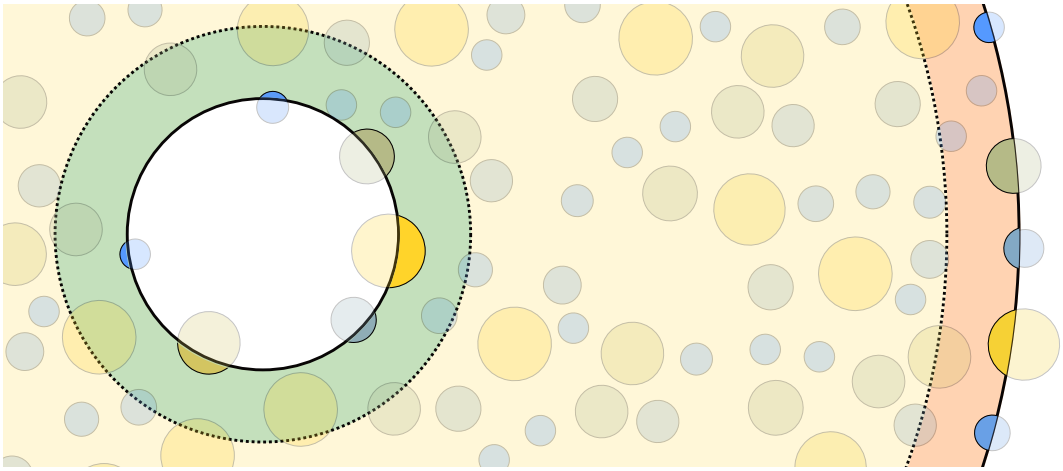

Figure 2.41: Ring A_n (in green, yellow, and orange) and discs from P_n intersecting it. Ring A_n^- is marked green, ring A_n^+ is marked in orange. The set $\bigcup\{A_n \cap D \mid D \setminus A_n \neq \emptyset\}$ is formed by the non-transparent parts of discs.

Let us derive a lower bound on the density of P^*. By definition,

$$\delta(P^*) \geq \lim_{n\to\infty} \frac{A(B_{R_n} \cap P^*)}{A(B_{R_n})}.$$

By definitions of A_n and R_n and by (2.15), for all $n > 2$,

$$\begin{aligned}\frac{A(B_{R_n} \cap P^*)}{A(B_{R_n})} &= \frac{\sum_{i=0}^{n} A(A_i \cap P_i|_{A_i})}{A(B_{R_n})} \geq \frac{A(A_n \cap P_n|_{A_n})}{A(B_{R_n})} \\ &= \frac{A(A_n)}{A(B_{R_n})}\left(\delta_S - o\left(1\right)\right) = \left(1 - \frac{A(B_{R_{n-1}})}{A(B_{R_n})}\right)\left(\delta_S - o\left(1\right)\right) \\ &= \left(1 - o\left(\frac{1}{n}\right)\right)\left(\delta_S - o\left(1\right)\right) = \delta_S - o\left(1\right).\end{aligned}$$

Therefore, we get

$$\delta(P^*) \geq \lim_{n\to\infty} \left(\delta_S - o\left(1\right)\right) = \delta_S$$

which concludes our demonstration.

□

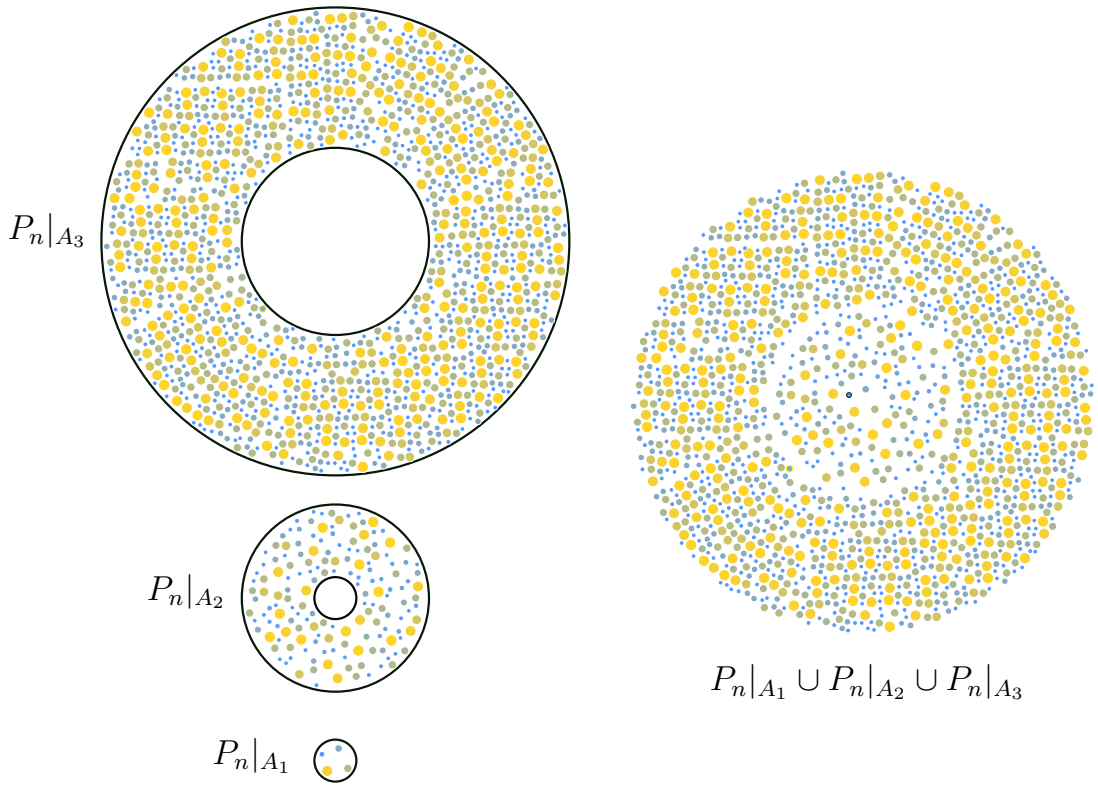

Figure 2.42: The union of the first three partial packings in the construction of P^* (the width of ring A_3 is diminished for clarity).

Chapter 3

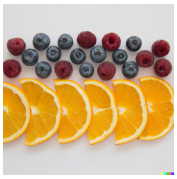


Density of 3-disc triangulated packings

> Then thou must count to three. Three shall be the number of the counting and the number of the counting shall be three. Four shalt thou not count, neither shalt thou count two, excepting that thou then proceedeth to three. Five is right out.
>
> Monty Python and the Holy Grail

When we work with 3-disc packings, the disc radii are, as usually, normalized: the disc radii are denoted by $1, r$, and s, where $1 > r > s$. A triplet $(1, r, s)$ of disc radii allowing a triangulated packing using all three sizes of discs is called a *case*. The cases are indexed by positive integers from 1 to 164, like in [FHS21].

The Connelly conjecture (Conjecture 2.1) is applicable only to the cases having triangulated *saturated* packings. This eliminates 15 cases where no triangulated packing is saturated and leaves us with 149 cases.

Our main contribution is a classification of 77 cases formulated in the following theorems:

Theorem 3.1 (Densest triangulated packings)**.**

(a) For each of the 16 following cases: 53, 54, 55, 56, 66, 76, 77, 79, 93, 108, 115, 116, 118, 129, 131, 146, the density is maximized by a triangulated ternary packing.

(b) For each of the cases 1–15 and 19, the density is maximized by a triangulated binary packing. For cases 1–5, it is the triangulated packing of b_8; for case 6 — b_4; for cases 7–9 — b_7; for cases 10–16 — b_9, for case 19 — b_6.

Theorem 3.2 (Counterexamples)**.** *For each of the 45 following cases: 20, 25, 47, 51, 60, 63, 64, 70, 73, 80, 81, 84, 92, 95, 96, 97, 98, 99, 100, 104,106, 110, 111, 117, 119, 126, 132, 133, 135, 136, 137, 138, 139, 141, 142, 151, 152, 153, 154, 159, 160, 161, 162, 163, 164, there exists a non-triangulated packing denser than any triangulated one.*

Appendix 3.A contains the approximate values of disc radii and optimal density for the cases from Theorem 3.1.(a). Appendix 3.B provides detailed information for the cases from Theorem 3.2. More information on the cases from Theorems 3.1, 3.2 are given in [FHS21].

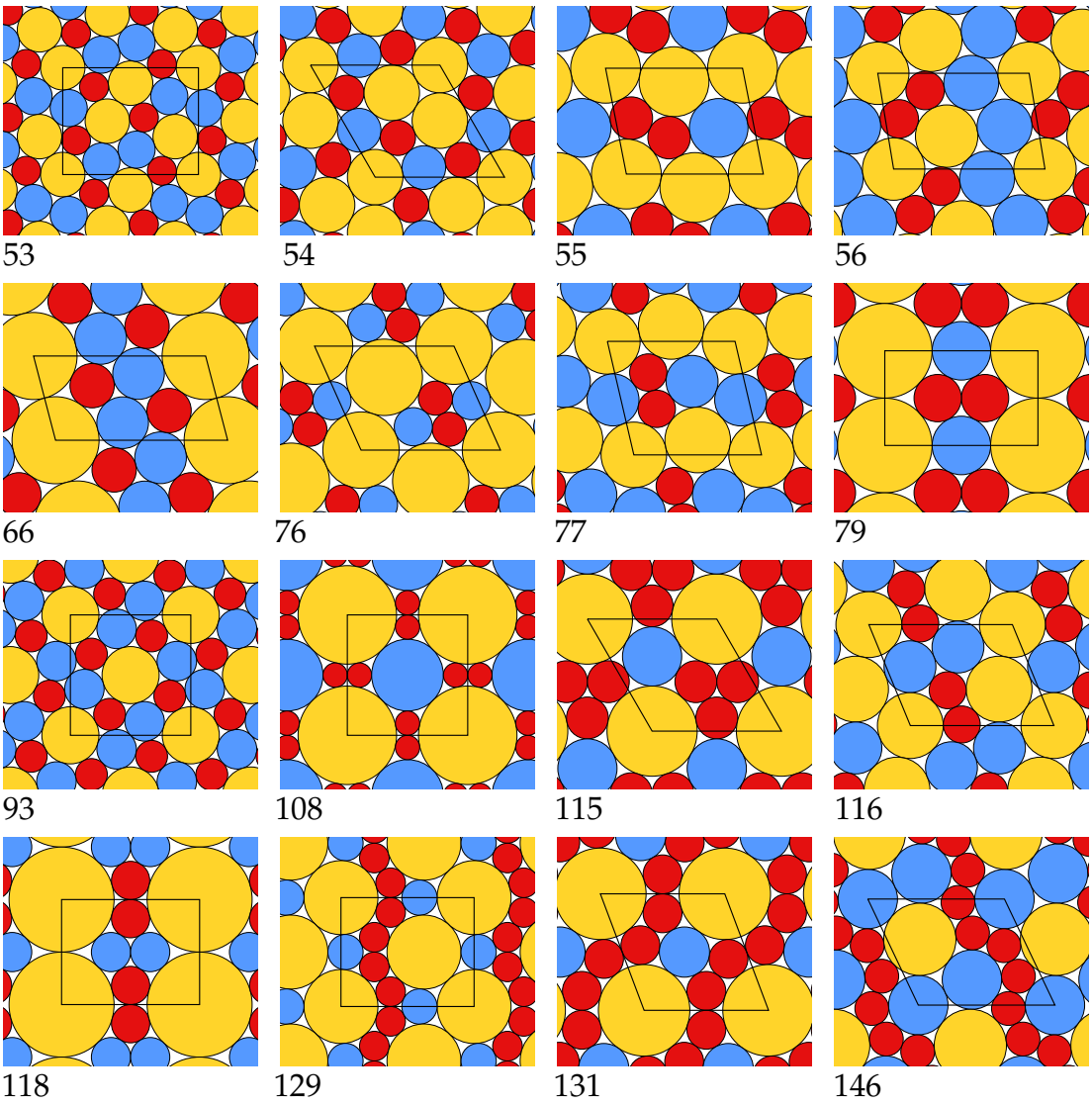

Figure 3.1: The 16 triangulated ternary packings proved to maximize the density (Theorem 3.1.(a)).

The triangulated packings maximizing the density for the cases from Th. 3.1.(a) are depicted in Fig. 3.1. For Th. 3.1.(b), 2-disc triangulated packings which maximize the density are present in Fig. 2.38 while 3-disc triangulated packings are given in Fig. 3.2. Triangulated 3-disc packings and non-triangulated denser packings for Th. 3.2 are given in Fig. 3.16 and in Appendix 3.B.

All in all, we proved the Connelly conjecture to be false and classified the 149 cases where it was applicable in several groups: 16 cases for which the conjecture holds (Th. 3.1.(a)), 16 cases where the density is maximized on a triangulated packing using only two discs out of three (Th. 3.1.(b)), 45 (periodic) counter examples to the initial conjecture (Th. 3.2), and the other cases where our proof strategy does not work. Figure 3.3 represents each case as a point with coordinates $(r, \frac{s}{r})$ and its number. The color of the point and the number corresponds to the class assigned to the case.

Sections 3.1–3.5 are dedicated to the cases where a ternary triangulated packing is proved to maximize the density. The only difference between the proof of Th. 3.1.(a)

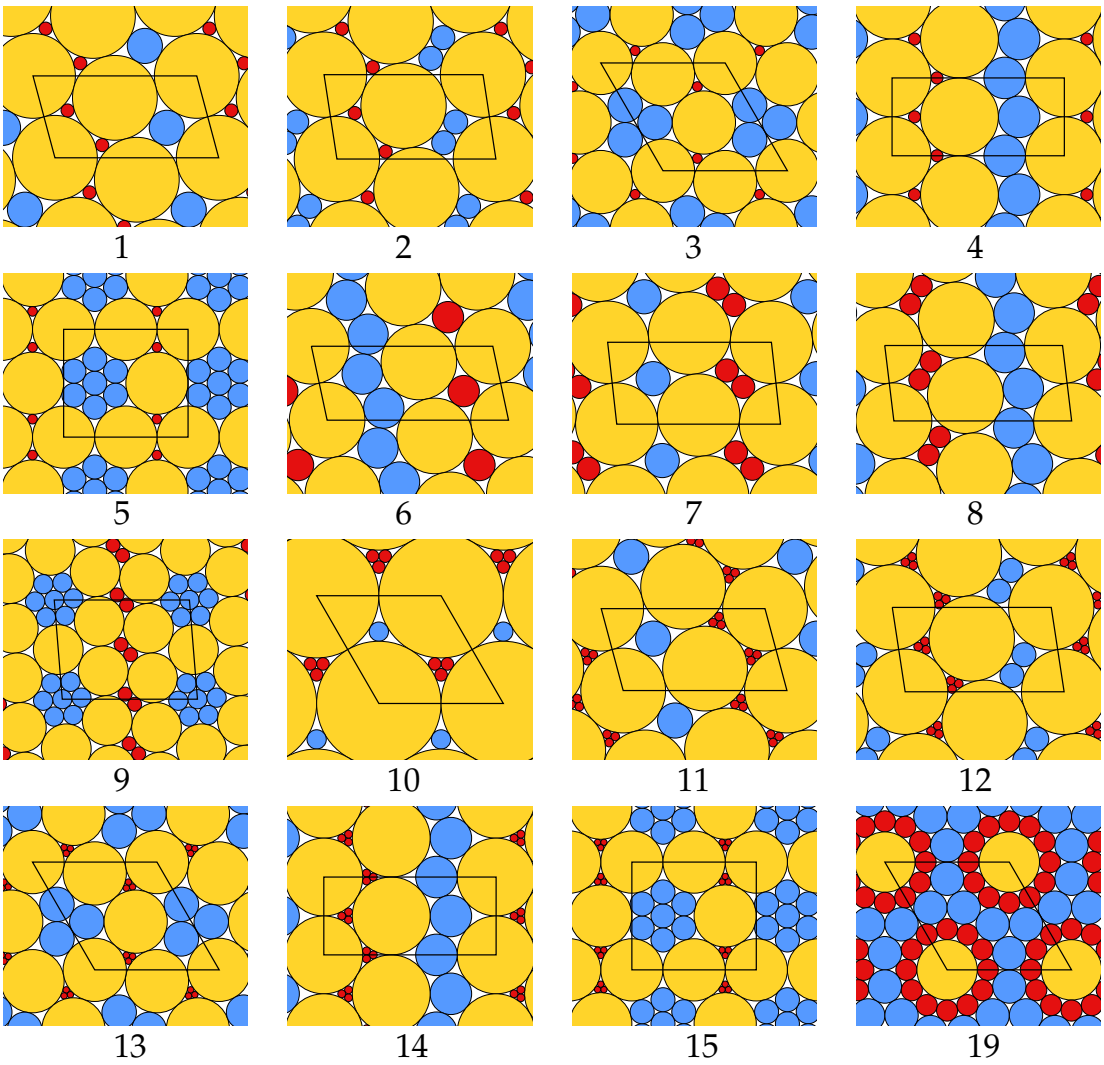

Figure 3.2: Triangulated ternary packings for cases from Theorem 3.1.(b), where triangulated *binary* packings maximize the density. For cases 1–5, it is the triangulated packing of b_8; for case 6 — b_4; for cases 7–9 — b_7; for cases 10–16 — b_9, for case 19 — b_6.

and Th. 3.1.(b) is discussed in Section 3.2.1.

In Section 3.1, we explain the approach of density localization also used in the similar proofs for binary packings [BF22,Ken05,Hep03]. Sections 3.2 and 3.3 constitute the core of the proof which resembles the one given in [BF22] (which, in turn, shares similarities with [Ken05]). However, we had to make substantial enhancements to adapt the prior techniques to our context. Firstly, some intermediate results hold for 2-disc packings but not for 3-disc packings, requiring us to address this issue. Another improvement was the generalization of the code universal to all the cases instead of treating them one by one. Lastly, we advanced by leaving a bunch of parameters as free variables instead of fixing them arbitrarily in the beginning.

Section 3.4 encloses some advanced properties of FM-triangles which were omitted in Section 2.2.1 but play a crucial role in the proof of Theorem 3.1 (notably, in Sections 3.2, 3.3).

Our proof, as quite a few recent results in the domain [Hal05,FKS23,Fer22], is based

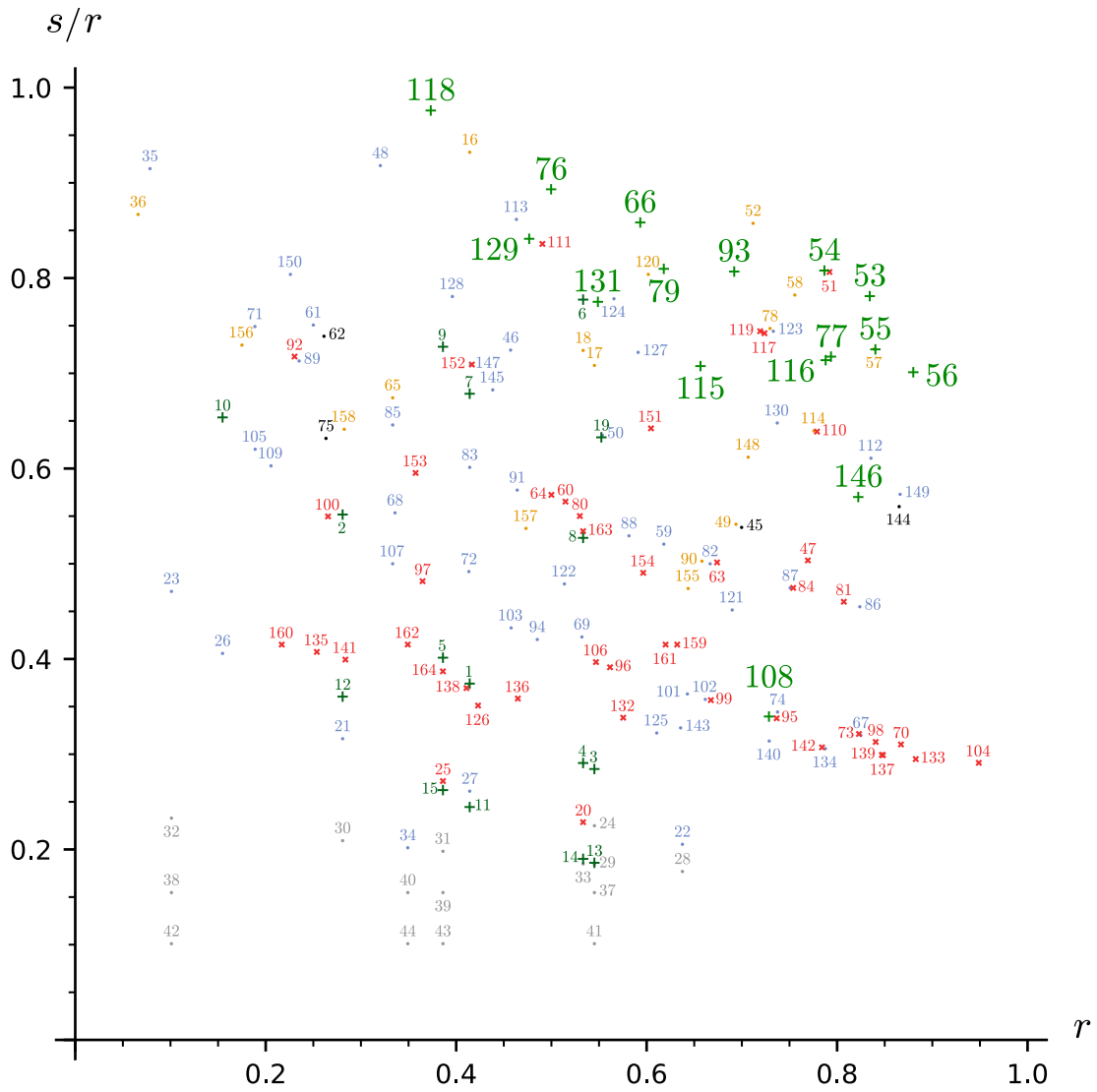

Figure 3.3: The "map" of the 164 cases with triangulated ternary packings. The cases where no triangulated packing is saturated are marked in grey. The cases with a ternary triangulated packing proved to maximize the density are marked by green + with larger case numbers. The cases where we proved a triangulated binary packing to maximize the density are marked by dark green +. The cases with counterexamples are red (✖). The cases featuring two coronas (find the details in Section 5.1.1) are orange. The cases with empty polytopes (see Section 5.1.2) are blue. The remaining cases are marked in black (Section 5.1.3).

on computer calculations. The main details of the implementation are provided in Section 3.5 (the complete code is available at `https://github.com/tooticki/ternary_triangulated_disc_packings`).

Section 3.6 is dedicated to the proof of Theorem 3.2. We obtain a counterexample for each of the cases from this theorem by applying the *flip-and-flow* method [CG21] on the triangulated binary packings with disc radii ratio close to the radii ratios of pairs of discs of this case.

The remaining 72 cases which are not covered by Theorems 3.1 and 3.2 are discussed in Chapter 5.

3.1 Localizing density, the method

Everywhere in this chapter, unless explicitly mentioned, we suppose that $1, r$, *and* s, $1 > r > s$ *are the radii of one of the cases from Theorem 3.1,* P^* *is the corresponding triangulated packing maximizing the density (Fig. 3.1, 2.38).*
Our aim is to prove that, for any saturated packing P *using the same discs, its density* $\delta(P)$ *never exceeds the density* δ^* *of* P^*.

In our proof, we follow the cell balancing approach introduced by Heppes [Hep03], discussed in Section 2.2.3. We start by partitioning the plane into small cells: triangles of the FM-triangulation introduced in Section 2.2.1. Let $\mathcal{T}$ and $\mathcal{T}^*$ respectively denote the FM-triangulations of P and P^*. Instead of working with densities, we introduce an additive function E, called *emptiness*, which, for a triangle T in $\mathcal{T}$, is defined by

$$E(T) := A(T) \cdot \delta^* - A(T \cap P)\,.$$

This function was used in [Ken05] by the name of "excess". It was inspired by "surplus area" introduced in [Hep03] defined as $A(T) - \frac{A(T\cap P)}{\delta^*}$, identical to the emptiness up to multiplication by δ^*. A similar but more complex function called "score" is used in the proof of the Kepler conjecture [HF06].

The emptiness function reflects how "empty" the triangle is compared to δ^*. Indeed, $E(T)$ is positive if the density of T is less than δ^*, negative if T is denser, and equals zero if $\delta(T) = \delta^*$. We use the emptiness rather than the density because of its additivity: the emptiness of a union of two triangles equals the sum of their emptiness values. This property does not hold for the density.

Let the *average emptiness of packing* P be defined as

$$\overline{E(P)} := \limsup_{n\to\infty} \frac{1}{A(B_n)} \sum_{T\in\mathcal{T},\, T\subset B_n} E(T).$$

Proposition 3.1. *For any packing* P*, its average emptiness equals the difference between* δ^* *and* $\delta(P)$*,*

$$\overline{E(P)} = \delta^* - \delta(P).$$

Proof. One derives that

$$\begin{aligned}\overline{E(P)} &= \limsup_{n\to\infty} \frac{1}{A(B_n)} \sum_{T\in\mathcal{T},\, T\subset B_n} (\delta^* A(T) - A(T\cap P)) \\ &= \limsup_{n\to\infty} \frac{1}{A(B_n)} \left(\delta^* A\left(\bigcup_{T\in\mathcal{T}, T\subset B_n} T \right) - A\left(\bigcup_{T\in\mathcal{T}, T\subset B_n} T\cap P \right) \right).\end{aligned}$$

Since the lengths of the edges of an FM-triangle are uniformly bounded (Lemma 3.1), analogously to the proof of Proposition 2.1 given in Appendix 2.A, the area of triangles intersecting the border of B_n is of order $O(n)$ when n tends to infinity. This implies

$$A(B_n) - A\left(\bigcup_{T\in\mathcal{T}, T\subset B_n} T \right) = A\left(\bigcup_{T\in\mathcal{T}, T\setminus B_n\neq\emptyset} T\cap B_n \right) = O(n)$$

and

$$A(B_n \cap P) - A\left(\bigcup_{T\in\mathcal{T}, T\subset B_n} T\cap P\right) = A\left(\bigcup_{T\in\mathcal{T}, T\setminus B_n\neq\emptyset} T\cap P\cap B_n\right) = O(n).$$

Therefore, since $A(B_n)=\pi n^2$, we have

$$\begin{aligned}\overline{E(P)} &= \limsup_{n\to\infty}\frac{1}{A(B_n)}\left(\delta^* A(B_n) - \delta^* O(n) + A(B_n\cap P) - O(n)\right)\\ &= \delta^* - \limsup_{n\to\infty}\frac{A(B_n\cap P)}{A(B_n)} = \delta^* - \delta(P).\end{aligned}$$

□

Proposition 3.1 implies that demonstrating $\delta(P)\leq\delta^*$ is equivalent to showing that $\overline{E(P)}\geq 0$. In simple terms, this means that if P is, on average, more empty than P^*, then it is also less dense than P^*.

Instead of working directly with the emptiness, we define a so-called *potential* which plays the role of density redistribution mentioned above. We do it since this function, constructed explicitly, is easier to manipulate than the emptiness. We will construct a potential U satisfying two constraints. First, for any triangle $T\in\mathcal{T}$, its potential shall not exceed its emptiness:

$$\forall T\in\mathcal{T},\ E(T)\geq U(T). \tag{T}$$

Second, the *average potential* of triangles in $\mathcal{T}$ is non-negative:

$$\overline{U(P)} := \limsup_{n\to\infty}\frac{1}{A(B_n)}\sum_{T\in\mathcal{T}, T\subset B_n} U(T)\geq 0. \tag{3.1}$$

If, for P^*, there exists U satisfying (T) and (3.1) for any packing P, then P^* maximizes the density among packings using the same disc radii: indeed, by Proposition 3.1,

$$(T),(3.1)\implies \overline{E(P)}\geq 0 \implies \delta^*\geq\delta(P)\,.$$

The rest of the proof consists in construction of a potential U satisfying both (T) and (3.1) for any saturated packing P using the same discs as P^*.

3.2 Choosing potentials

To construct the potential, we take the approach first used by Kennedy in [Ken05] who introduced the "localizing potential" being inspired by a statistical mechanics notion of "m-potentials". We follow almost the same steps as in [BF22], where 2-disc triangulated packings were proved optimal, and in [Fer19], which treats computationally the "simplest" case among the 3-disc triangulated packings (case 53).

We define the total potential of a triangle as a sum of potentials of "smaller" units, the *vertex potential* $\dot{U}$ and the *edge potential* $\bar{U}$:

$$U(T) := \dot{U}(T) + \bar{U}(T).$$

Emptiness redistribution takes place through vertex and edge potentials: the sum of vertex potentials around each vertex in the triangulation will be non-negative as well as the sum of two edge potentials of triangles sharing this edge.

The vertex potential of a triangle is composed of three vertex potentials associated to its vertices: if A, B, and C are the vertices of triangle T in the FM-triangulation $\mathcal{T}$ of packing P,

$$\dot{U}(T) := \dot{U}_A(T) + \dot{U}_B(T) + \dot{U}_C(T)\,.$$

We seek to choose the vertex potential in a way that the sum of vertex potentials around any vertex $v \in \mathcal{T}$ is non-negative:

$$\text{for any vertex } v \in \mathcal{T} \quad \sum_{T\in\mathcal{T}|v\in T} \dot{U}_v(T) \geq 0\,. \tag{$\bullet$}$$

The complete definition of $\dot{U}_v(T)$ is given in Section 3.2.1.

The edge potential of triangle T is equal to the sum of edge potentials corresponding to its three edges:

$$\bar{U}(T) := \bar{U}_{AB}(T) + \bar{U}_{AC}(T) + \bar{U}_{BC}(T)\,.$$

The edge potentials will be designed to ensure that their sum around any given edge $e \in \mathcal{T}$ results in a non-negative value:

$$\text{for any edge } e \in \mathcal{T} \quad \sum_{T\in\mathcal{T}|e\in T} \bar{U}_e(T) \geq 0\,. \tag{$-$}$$

The complete definition of $\bar{U}_e(T)$ is given in Section 3.2.2.

These two aforementioned local conditions on each vertex and edge guarantee us the "global" inequality (3.1) on the average potential.

Proposition 3.2. *Conditions ($\bullet$) and ($-$) imply inequality (3.1).*

Proof. First, by definition of the potential,

$$\begin{aligned}\sum_{T\in\mathcal{T},T\subset B_n} U(T) &= \sum_{T\in\mathcal{T},T\subset B_n} \dot{U}(T) + \bar{U}(T)\\ &= \sum_{T\in\mathcal{T},T\subset B_n} \left(\sum_{v\in T} \dot{U}_v(T) + \sum_{e\in T} \bar{U}_e(T)\right)\\ &= \sum_{v\in\mathcal{T}\cap B_n} \sum_{T\in\mathcal{T}|v\in T} \dot{U}_v(T) + \sum_{e\in\mathcal{T}\cap B_n} \sum_{T\in\mathcal{T}|e\in T} \bar{U}_e(T) + O(n).\end{aligned}$$

The last holds since the vertex and edge potentials are bounded by definition (see Sections 3.2.1 and 3.2.2), therefore, the sum of vertex and edge potentials of triangles intersecting the border of B_n is of order $O(n)$ (the same argument was used in the proof of Proposition 3.1). Finally, if ($\bullet$) and ($-$) hold,

$$\begin{aligned}\overline{U(P)} &= \limsup_{n\to\infty} \frac{1}{A(B_n)} \sum_{T\in\mathcal{T},T\subset B_n} U(T)\\ &= \limsup_{n\to\infty} \frac{1}{A(B_n)} \left(\sum_{v\in\mathcal{T}\cap B_n} \sum_{T\in\mathcal{T}|v\in T} \dot{U}_v(T) + \sum_{e\in\mathcal{T}\cap B_n} \sum_{T\in\mathcal{T}|e\in T} \bar{U}_e(T)\right) \geq 0.\end{aligned}$$

□

All in all, in Sections 3.2.1 and 3.2.2, we are constructing the vertex and edge potentials in a way that conditions $(\bullet)$, $(-)$ are satisfied, at the same time trying to minimize the potential of each triangle. The last step is to verify for any triangle that its potential is lower than its emptiness (i.e., (T) is satisfied), this part is discussed in Section 3.3.

3.2.1 Vertex potentials

As mentioned above, we construct the vertex potentials which are high enough around each vertex to sum up into a non-negative (to satisfy $(\bullet)$) but are low enough in each triangle so that the final version of the potential never exceeds the emptiness in a triangle (condition (T)).

We start by defining the vertex potentials V_{xyz} in tight triangles and then generalize the definition to the other triangles, obtaining $\dot{U}_v(T)$, in order to directly ensure $(\bullet)$. We then discuss special cases where densest triangulated packings use only 2 disc sizes (Th. 3.1.(b)), since the previous steps are slightly different in that setting. We conclude by introducing a *capped* version of the vertex potential $Z(\dot{U}_v(T))$ which still satisfies $(\bullet)$ but is often significally lower, which is necessary to meet the condition (T) in the end of the proof.

Vertex potentials of tight triangles

Recall that a *tight triangle* is a triangle formed by three pairwise tangent discs. By definition, all FM-triangles of a triangulated packing are tight. For each set of three distinct disc radii, there are 10 tight triangles, one for each set of three disc radii (see Fig. 3.4). Let E_{xyz} denote the emptiness of the tight triangle formed by discs of radii x, y, z (indeed the emptiness does not depend on the order or disc radii, so $E_{xyz} := E_{yxz} := E_{zyx}$). We denote by V_{xyz} the vertex potential of this triangle in the vertex corresponding to the y-disc. We set $V_{xyz} = V_{zyx}$, so there are 18 distinct constants V_{xyz}.

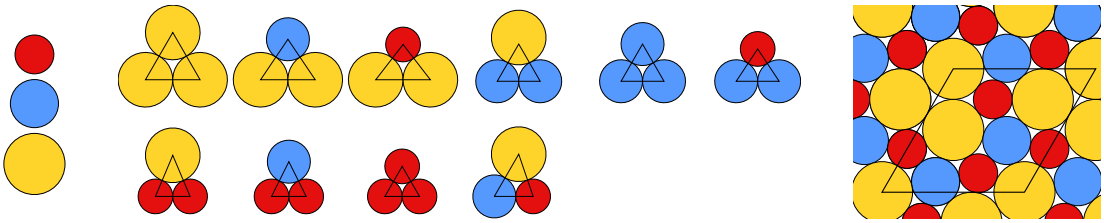

Figure 3.4: The discs of the case 54 (on the left), its tight triangles (in the middle), and its triangulated packing (on the right).

Inequalities (T) and (3.1), applied to $\mathcal{T}^*$, imply a few constraints on the vertex potentials of tight triangles appearing in $\mathcal{T}^*$. To see this, we need to note that the edge potential of tight triangles equals zero by definition (see Section 3.2.2), therefore, inequality (T) for P^*, is equivalent to satisfying

$$\dot{U}(T) \leq E(T) \text{ for all } T \in \mathcal{T}^*.$$

If there exists a triangle T' where this inequality is strict, then, for sufficiently large n,

$$\frac{1}{A(B_n)} \sum_{T \in \mathcal{T}^* \cap B_n} \dot{U}(T) - E(T) \leq \frac{n_{T'}}{A(D)} \left(\dot{U}(T') - E(T') \right) + o(1) < 0, \tag{3.2}$$

where $n_{T'}$ denotes the number of occurrences of T' in the domain D of $\mathcal{T}^*$ (recall that P^* is a periodic packing, so $\mathcal{T}^*$ is also periodic). Inequality (3.2) holds since the number of occurrences of T' in B_n is equal to $n_{T'}$ multiplied by number of the domain parallelograms inside B_n, which equals $\frac{A(D)}{A(B_n)} + o(1)$ when $n \to \infty$.

On the other hand, the average emptiness of P^* equals zero since $\delta(P^*) = \delta^*$. Therefore, by (3.1),

$$\limsup_{n\to\infty} \frac{1}{A(B_n)} \sum_{T\in\mathcal{T}^*\cap B_n} \dot{U}(T) - E(T) = \overline{U(P^*)} \geq 0.$$

which is in conflict with (3.2), hence, for each $T \in \mathcal{T}^*$,

$$\dot{U}(T) = E(T). \tag{3.3}$$

Equation (3.3) implies that

$$\overline{U(P^*)} = \overline{E(P^*)} = 0. \tag{3.4}$$

Given a disc in a packing, a sequence of its neighbors in the FM-triangulation (such that each one is tangent to the next member of the sequence) is called its *corona* (see examples in Fig. 3.5). Note that in the triangulated packings we consider (Fig. 3.1), all appearances of a disc with a given radius x have the same corona (up to rotation), called the *x-corona* of the packing (see examples in Fig. 3.5). In general, this is not always the case, for instance, in the triangulated packing of case b_5 depicted in Figure 2.38, the small disc appears with two distinct coronas; such cases of 3-disc packings are discussed in Section 5.1.1. Let C_x denote the sum of vertex potentials of the triangles of the x-corona in P^*:

$$C_x := \sum_{i=1}^{N} V_{y_i x y_{i+1}},$$

where $y_1, \ldots, y_N$ is the sequence of disc radii in the x-corona and $y_{N+1} := y_1$. For example, let us compute this sum for the 1-corona of the triangulated packing of case 54 (Fig. 3.4 depicts the triangulated packing, its coronas are given in Fig. 3.5).

$$C_1 = V_{11s} + V_{s1r} + V_{r1s} + V_{s1r} + V_{r1s} + V_{s11} + V_{111}.$$

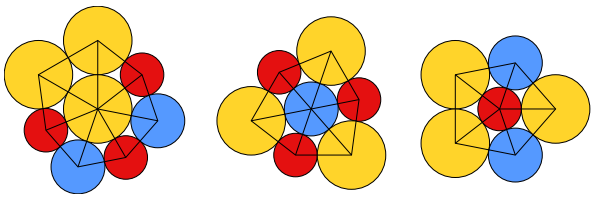

Figure 3.5: Three coronas of the triangulated packing of case 54.

Let us rewrite the average vertex potential of P^* in (3.4) using C_1, C_r, and C_s.

$$\begin{aligned} 0 = \overline{U(P^*)} &= \limsup_{n\to\infty} \frac{1}{A(B_n)} \sum_{v\in\mathcal{T}^*} \sum_{T\in T^*\cap B_n | v\in T} \dot{U}_v(T) \\ &= \sum_{v\in D | r(v)=1} C_1 + \sum_{v\in D | r(v)=r} C_r + \sum_{v\in D | r(v)=s} C_s, \end{aligned}$$

where D is the domain of T^*, $r(v)$ denotes the radius of the disc centered in v. On the other hand, by $(\bullet)$, C_1, C_r, and C_s are non-negative which implies

$$C_1 = 0,\ C_r = 0,\ C_s = 0. \tag{C}$$

Equations (3.3) and (C) establish linear constraints on the tight vertex potentials. Let us illustrate this system with the case 54 (see Fig. 3.4). There are only three types of tight triangles present in this packing, so (3.3) produces the following equations.

$$3V_{111} = E_{111}, \qquad V_{1s1} + 2V_{11s} = E_{1s1}, \qquad V_{1rs} + V_{rs1} + V_{s1r} = E_{1rs}\,.$$

The equations (C) for the three coronas given in Fig. 3.5 are respectively

$$V_{111} + 2V_{11s} + 4V_{r1s} = 0, \qquad 6V_{1rs} = 0, \qquad V_{1s1} + 4V_{1sr} = 0\,.$$

We thus have 18 variables and 6 equations with only 5 of them being independent due to periodicity of the packing: since the sum of the emptiness of tight triangles of the fundamental domain of the packing equals zero, there is a linear combination of tight triangle vertex potentials which is equal to zero.

To simplify the following computations, we set the potentials of *all* 10 tight triangles equal to their emptiness (not only the ones present in P^*). Let $\mathbb{T}^*$ denote the set of tight triangles formed by discs of radii $1, r, s$,

$$\text{for all } T^* \in \mathbb{T}^*\ \ \dot{U}(T^*) = E(T^*). \tag{$\mathbb{T}^*$}$$

Our system remains independent after adding these additional equations; we end up with 12 equations for 18 variables which leaves us with 6 free variables.

Until now our construction of vertex potentials followed the same strategy as [BF22] which does not work for the cases considered here, except the case 53 treated earlier in [Fer19]. The problem is that in [BF22, Fer19], the free variables mentioned above are all directly set to zero to simplify further computations. We, in contrast, keep these 6 variables free and fix them later, in order to satisfy all inequalities $(\bullet)$ around the vertices. The 6 tight vertex potentials left free are the vertex potentials of the isosceles (but not equilateral) tight triangles in the vertex adjacent to the two equal edges.

$$V := \{V_{xyx} \mid x, y \in \{1, r, s\}, x \neq y\}.$$

From now on, the remaining tight vertex potentials are fixed as solutions of the system of equations and only depend on the 6 variables from V.

Defining vertex potentials to ensure condition $(\bullet)$

The next step is to choose the vertex potentials of all the other (non-tight) triangles in a way to satisfy $(\bullet)$.

The *vertex potential* of triangle T in vertex $v \in R$ is defined as follows:

$$\dot{U}_v(T) := V_{xyz} + m_y|\hat{v} - \widehat{xyz}|,$$

where x, y, z are the disc radii of T, y is the radius of the disc centered in v, $\hat{v}$ is the angle of T in v, $\widehat{xyz}$ is the angle in the vertex of the y-disc in the tight triangle with discs of radii x, y, z, and m_y is a positive constant defined below. Figure 3.6 depicts and example of a triangle T and the corresponding tight triangle.

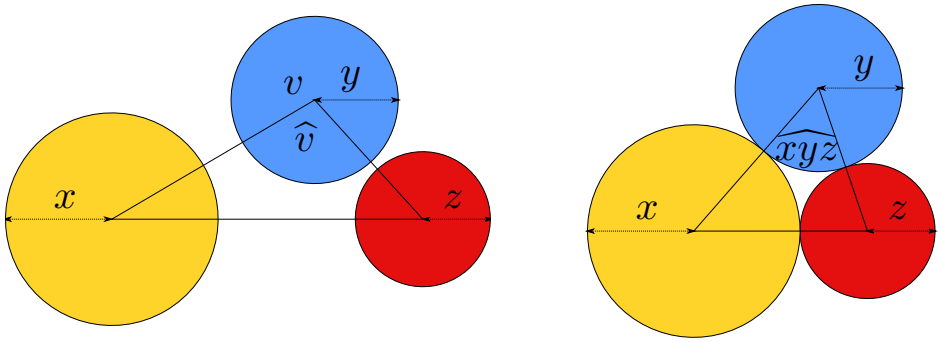

Figure 3.6: Illustration of the definition of the vertex potential in vertex v.

The difference between the vertex potential of T in v and the vertex potential of the tight triangle with the same discs is proportional to their angle difference in the corresponding vertices, or "how different triangle T in v is from the tight one". Let us choose the constants m_1, m_r, m_s reflecting the weight of this angle deviation and 6 free variables from V in a way that condition (•) holds.

Given an FM-triangle T with discs of radii x, y, z, let T^* denote the tight triangle formed by the same discs.

Proposition 3.3. *Let v be a vertex of $\mathcal{T}$ with disc of radius y, $T_1, \ldots, T_k$ be the corona of v, and $\hat{v}(T^*)$ denote the angle of T^* in the vertex corresponding to v in T.*

$$m_y \left| 2\pi - \sum_{i=1}^{k} \hat{v}(T_i^*) \right| \geq - \sum_{i=1}^{k} \dot{U}_v(T_i^*)\,. \tag{m}$$

implies inequality (•) in v.

Proof. By definition of the vertex potential,

$$\begin{aligned} \sum_{j=1}^{k} \dot{U}_v(T_j) &= \sum_{j=1}^{k} \dot{U}_v(T_j^*) + m_y \sum_{j=1}^{k} |\hat{v}(T_j) - \hat{v}(T_j^*)| \\ &\geq \sum_{j=1}^{k} \dot{U}_v(T_j^*) + m_y \left| \sum_{j=1}^{k} \left(\hat{v}(T_j) - \hat{v}(T_j^*)\right) \right| \\ &= \sum_{j=1}^{k} \dot{U}_v(T_j^*) + m_y \left| 2\pi - \sum_{j=1}^{k} \hat{v}(T_j^*) \right| \end{aligned} \tag{3.5}$$

The last equation, (3.5), holds since the sum of angles in v of all the triangles in the corona around v is equal to 2π. Therefore, (m) implies (•) in v. □

The angles of tight triangles are constant, so inequalities (m) are linear inequalities on the six variables from V and m_1, m_r, m_s.

Since the angles of FM-triangles are uniformly bounded from below by $a_s := \arcsin\left(\frac{s}{2+2s}\right) > 0$ (Corollary 3.1), the number of discs in a corona is at most $\frac{2\pi}{a_s}$. Therefore, the number of sequences of disc radii corresponding to a corona is finite. This implies that for any packing P, the system of inequalities (M) defined as

$$m_1, m_r, m_s > 0 \text{ and } \forall v \in \mathcal{T}, (m), \tag{M}$$

is finite.

The solutions of system (M), which are a subset of $\mathbb{R}^9$, are the combinations of tight vertex potentials V and m_1, m_r, m_s satisfying $(\bullet)$. We solve the system using computer and obtain an unbounded set of solutions. Before choosing a specific solution (i.e., fixing the values of V and m_1, m_r, m_s), we shall add more constraints to the system. These constraints, needed for the last step of the proof (ensuring (T)), are introduced in Section 3.3.1.

The details of the computer implementation of this part, as well as how we choose a specific solution, are described in Section 3.5.2.

Notice that the only coronas where inequality (m) does not depend on m_y are those where the angles of the corresponding tight triangles sum up to 2π. We found out by computer search that it only happens for the coronas present in the triangulated packing (C_1, C_r, and C_s) and for coronas consisting of six copies of the central disc (so all the tight triangles are equilateral).

The sum of vertex potentials of triangles in coronas C_1, C_r, and C_s equals zero by (C) which implies (m). In the remaining case, by definition of tight vertex potentials, we get

$$\sum_{j=1}^{6} \dot{U}_v(T_j^*) = 6\, V_{yyy} = 2\, E(T_{yyy}) = 2\, A(T_{yyy})(\delta^* - \delta_{\text{hex}}) > 0,$$

where T_{yyy} denotes the tight triangle formed by three y-discs (as we saw in Section 2.1, its density equals δ_{hex}). Therefore, (m) also holds in this case.

When a binary triangulated packing is denser

The triangulated packings of cases 1–18 are special: they are called "large separated" in [FHS21] because they do not contain pairs of adjacent medium and small discs. Case 19 is "small-separated": it contains no pairs of adjacent large and medium discs (Fig. 3.2 depicts cases 1–15 and 19). For each of these cases, in addition to 3-disc triangulated packings, there are triangulated packings using only two discs out of three. It happens because the radii of small and/or medium disc coincide with the radii of a small disc of a case among b_1–b_9. It is thus possible to assemble packings having the same density as the binary packings of mentioned cases using only two of three discs.

It turns out that for all these cases, the density of one of the mentioned binary packings exceeds the density of the ternary one. This means that for each of cases 1-19, the densest packing among the triangulated ones is a 2-disc packing corresponding to a case from b_1-b_9 (Fig. 2.38). Indeed, each of the 3-disc packings of cases 1–18 is formed as a "combination" of two binary packings one of which is denser than the other. Thus, the densest of the binary packings will also be denser than its combination with a less dense packing. For case 19, there is only one binary packing, b_6, whose disc sizes coincide with the ones from 19 and whose density is higher than the density of 19.

We were able to show that the denser triangulated 2-disc packing maximizes the density among all 3-disc packings (not only triangulated ones) for the cases from 1 to 15 and 19, all depicted in Figure 3.2. This is formulated in Theorem 3.1.(b). The proof is the same as for the cases from Theorem 3.1.(a) except for the part where we select which variables of tight vertex potentials to leave free.

Let $i \in \{1, \dots, 15, 19\}$ be the case number and P_3 denote its triangulated 3-disc packing. Let P_2^* denote the densest triangulated binary packing using two discs of case i. We already know that P_2^* is denser than any other *triangulated* packing, notably,

$\delta(P_2^*) > \delta(P_3)$. Our aim is to show that P_2^* maximizes the density among *all* packings by the discs of case i.

The only difference with the strategy used for cases from Theorem 3.1.(a) concerns vertex potentials. Since P_2^* has only two discs out of three, it features only two coronas instead of three. So (C) consists of two equations instead of three. These two corona equations together with the 10 equations for tight triangles, give us at most 11 independent equations instead of 12.

We now need to choose 7 free variables instead of 6. We pick 6 tight potentials of isosceles triangles as before. Let us choose the last free variable. Vertex potentials of equilateral tight triangles can not be picked because of the equations of type $3\,V_{xxx} = E_{xxx}$: they are already fixed. The remaining vertex potentials of isosceles triangles ($V_{xxy},\ x \neq y$) can not be used since they are dependent of the first 6 free variables and the equations $2V_{xxy} + V_{xyx} = E_{xyx}$. The only candidates thus are $V_{1rs}, V_{1sr}, V_{r1s}$; we add one of them. After this point, remaining reasoning applies to all the cases from Theorem 3.1.(a) and 3.1.(b).

For cases 16, 17, and 18, the densest binary packing is b_5 which features two different coronas around the small disc, so our method is not applicable to them as discussed in Section 5.1.1.

To summarize, for cases 1-19, among triangulated packings, the density is maximized by a binary packing, not a ternary one. However, whether this packing maximizes the density among all packings is still an open question for cases 16, 17 and 18.

Capping vertex potential

In the end, the potentials shall be low enough to satisfy (T). We will cap each vertex potential with a constant value depending only on the disc type of the vertex. More precisely, we are going to show that for any vertex, as soon as the vertex potential of a triangle in its corona exceeds a certain value, the remaining vertex potentials will never be "too negative" which implies inequality $(\bullet)$ in this vertex. This allows us to diminish vertex potential while still satisfying its non-negativity around each vertex $(\bullet)$. It was not needed in [Fer19] for case 53 but turns out to be necessary for all the other cases we consider.

The vertex potential of triangle T in vertex v corresponding to a y-disc will be rewritten as

$$Z(\dot{U}_v(T)) := \min\left(\dot{U}_v(T), Z_y\right).$$

Let $\mathbb{T}_y^*$ denote the set of pairs of tight triangles containing a y-disc and their vertices corresponding to the center of an y-disc:

$$\mathbb{T}_y^* := \{(T^*, v) \mid T^* \in \mathbb{T}^*,\ v \in T^*,\ r(v) = y\}.$$

The capping constants Z_y for $y = 1, r, s$ are defined as follows.

$$Z_y := -2\pi \min_{(T^*,v)\in\mathbb{T}_y^*} \frac{\dot{U}_v(T^*)}{\hat{v}(T^*)}. \tag{3.6}$$

Z_1, Z_r, and Z_s are all positive in all of our cases. For the cases from Theorem 3.1.(a), this holds since at least one of tight vertex potential corresponding to a given radius is negative by the corona inequalities (C). For the cases from Theorem 3.1.(b), the previous might not hold for the corona not present in the densest binary triangulated

packing. For the majority of cases, the constructed vertex potentials always lead to positive values of Z_1, Z_r, and Z_s. For the remaining exceptions, we do not cap the vertex potential for the radius in question. Let us show that $Z(\dot{U})$ satisfies (•).

Proposition 3.4. *If for all $y = 1, r, s$ for any tight triangle T^* with a vertex v corresponding to a y-disc,*

$$m_y \geq -\frac{\dot{U}_v(T^*)}{\hat{v}(T^*)}, \tag{3.7}$$

then the capped potential $Z(\dot{U})$ satisfies (•), i.e., for any vertex $v \in \mathcal{T}$,

$$\sum_{T \in \mathcal{T} | v \in T} Z(\dot{U}_v(T)) \geq 0.$$

Proof. Let T be an FM-triangle in a corona around vertex $v \in \mathcal{T}$, let $\hat{v}(T)$ denote the angle of T in v, let T^* denote the corresponding tight triangle, and $\hat{v}(T^*)$ the angle of T^* in the vertex corresponding to v.

First case: $\dot{U}_v(T^*) \geq 0$,

$$\frac{\dot{U}_v(T)}{\hat{v}(T)} = \frac{\dot{U}_v(T^*) + m_y|\hat{v}(T) - \hat{v}(T^*)|}{\hat{v}(T)} \geq 0.$$

Second case. $\dot{U}_v(T^*) < 0$ and $\hat{v}(T^*) \geq \hat{v}(T)$. By (3.7), $\dot{U}_v(T^*) + m_y \hat{v}(T^*)$ is non-negative, therefore,

$$\begin{aligned}\frac{\dot{U}_v(T)}{\hat{v}(T)} &= \frac{\dot{U}_v(T^*) + m_y(\hat{v}(T^*) - \hat{v}(T))}{\hat{v}(T)} = \frac{\dot{U}_v(T^*) + m_y \hat{v}(T^*)}{\hat{v}(T)} - m_y \\ &\geq \frac{\dot{U}_v(T^*) + m_y \hat{v}(T^*)}{\hat{v}(T^*)} - m_y = \frac{\dot{U}_v(T^*)}{\hat{v}(T^*)}.\end{aligned}$$

Third case: $\dot{U}_v(T^*) < 0$ and $\hat{v}(T^*) < \hat{v}(T)$, then

$$\frac{\dot{U}_v(T)}{\hat{v}(T)} = \frac{\dot{U}_v(T^*) + m_y|\hat{v}(T) - \hat{v}(T^*)|}{\hat{v}(T)} \geq \frac{\dot{U}_v(T^*)}{\hat{v}(T)} \geq \frac{\dot{U}_v(T^*)}{\hat{v}(T^*)}.$$

Three previous inequalities imply that, for any triangle T in the corona of v,

$$\frac{\dot{U}_v(T)}{\hat{v}(T)} \geq \min\left(0, \frac{\dot{U}_v(T^*)}{\hat{v}(T^*)}\right). \tag{3.8}$$

If for each triangle T in the corona of v, its potential does not exceed Z_y, then the capping is not applied: $Z(\dot{U}_v(T)) = \dot{U}_v(T)$ and inequality (•) holds in this vertex for $Z(\dot{U})$.

Suppose now that there is a triangle $T_>$ in the corona whose potential exceeds Z_y:

$$\dot{U}_v(T_>) > Z_y = -2\pi \min_{(T'^*, v) \in \mathbb{T}^*_y} \frac{\dot{U}_v(T'^*)}{\hat{v}(T'^*)}.$$

Using (3.8) and the fact that the sum of angles around a vertex equals 2π, we get

$$\begin{aligned}\sum_{T\in\mathcal{T}|v\in T} Z(\dot{U}_v(T)) &\geq \sum_{v\in T, T\neq T_>} \hat{v}(T)\min\left(0, \frac{\dot{U}_v(T^*)}{\hat{v}(T^*)}\right) + Z(\dot{U}_v(T_>)) \\ &= \sum_{v\in T, T\neq T_>} \hat{v}(T)\min\left(0, \frac{\dot{U}_v(T^*)}{\hat{v}(T^*)}\right) - 2\pi \min_{(T'^*,v)\in\mathbb{T}_y^*} \frac{\dot{U}_v(T'^*)}{\hat{v}(T'^*)} \\ &= \sum_{v\in T, T\neq T_>} \hat{v}(T)\left(\min\left(0, \frac{\dot{U}_v(T^*)}{\hat{v}(T^*)}\right) - \min_{\mathbb{T}_y^*} \frac{\dot{U}_v(T'^*)}{\hat{v}(T'^*)}\right) - \hat{v}(T_>)\min_{\mathbb{T}_y^*} \frac{\dot{U}_v(T'^*)}{\hat{v}(T'^*)} \\ &\geq 0,\end{aligned}$$

which allows us to conclude. □

Inequality (3.7) is verified for all the cases from Theorem 3.1.(a), 3.1.(b). The test can be simply done by a computer: there are only a finite number of inequalities to check [1]. Therefore, by Proposition 3.4, we can use the capped vertex potential $Z(\dot{U}_v(T))$ instead of $\dot{U}_v(T)$ for all the cases of Theorem 3.1.(a) and 3.1.(b).

3.2.2 Edge potentials

In order to keep the potential lower than the emptiness in all triangles (to satisfy (T)), we introduce the edge potential $\bar{U}$. We define the total potential $U(T)$ of a triangle T as the sum of the capped vertex potential and the edge potential:

$$U(T) := Z(\dot{U}(T)) + \bar{U}(T)\,.$$

We need $\bar{U}$ to compensate the vertex potential of triangles where one angle is too large, i.e., those which are "close" to being stretched (stretched triangles were introduced in Section 2.2.1). Such triangles feature high vertex potential and low emptiness, but they always have an "empty" neighbor; the edge potential distributes emptiness evenly among the two triangles.

Let O denote the center of the support disc of a triangle $T \in \mathcal{T}$, we define the value $d_e(T)$ as the *signed distance* from the support disc center to an edge e of T as follows:

$$d_e(T) := \begin{cases} d(O,e) & \text{if } O \text{ and } T \text{ are on the same side of } e \\ -d(O,e) & \text{otherwise,}\end{cases}$$

where $d(O,e)$ denotes the Euclidean distance from the point O to the line containing the edge e. Figure 3.7 illustrates the definition of $d_e(T)$: Fig. 3.7a depicts an example with the positive distance and Fig. 3.7b with the negative distance.

This allows us to define the edge potential.

$$\bar{U}_e(T) := \begin{cases} q_{xy} d_e(T) & \text{if } |e| > l_{xy} \\ 0 & \text{otherwise,}\end{cases}$$

where x, y are the radii of the discs centered in the endpoins of edge e; the constants q_{xy}, l_{xy} are defined below.

[1] 18, to be precise: $\mathbb{T}_y^*$ contains 6 elements for each value of y

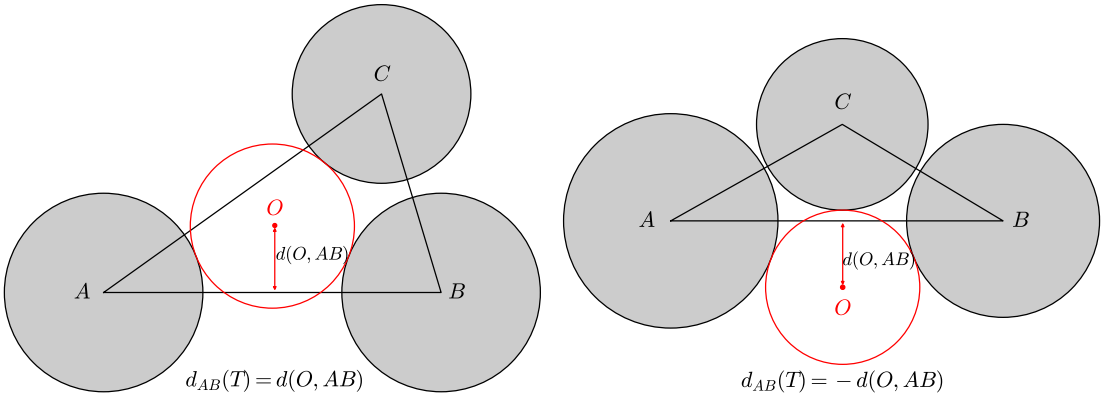

(a) (b)

Figure 3.7: The signed distance: a positive case (left) and a negative case (right).

By Lemma 3.3 proved in Section 3.4, the sum of edge potentials of two triangles sharing this edge is always non-negative which implies $(-)$. Thus, the potential U defined as the sum of the vertex and the edge potential satisfies the global inequality (3.1). Meanwhile, the edge potential affects the local distribution of potentials among adjacent triangles allowing us to satisfy (T) at the end.

We pick the pairs of constants q_{xy} and l_{xy} (there are 6 of them, one for each pair (x, y) of disc radii: $q_{xy} := q_{yx}$, $l_{xy} := l_{yx}$) in order to compensate high vertex potential of stretched triangles. To find constants allowing to do this, we compute the vertex potential and the emptiness of the most "dangerous" triangles: those with two pairs of tangent discs (see an example in Figure 3.8). We represent them as curves in function of the length of the remaining "flexible" edge.

To choose q_{xy} and l_{xy} for given (x, y), let us trace the curves as ones shown in Figure 3.8 for three triplets of discs radii: $x1y, xry, xsy$. The aim of the edge potential is not to let the capped vertex potential $Z(\dot{U}_v(T))$ (dashed red line) exceed the emptiness $E(T)$ (dark blue line). In all the cases considered here, the capped vertex potential and the emptiness have at most one intersection except the leftmost point corresponding to the tight triangle (the neighborhood of this point is a special case treated in Section 3.3.1). This intersection is the side length such that stretching the triangle even more causes vertex potential to be greater than emptiness.

Let l^*_{xqy} be the side length where this intersection occurs for a triangle formed by discs with radii x, q, y. Notice that d_e is a decreasing monotonous function on the side length $|e|$. If $d_{l^*_{xqy}} < 0$ (which is the case for all the proved cases), then we set l_{xy} equal to $l^*_{xqy} - \alpha$ with a small enough α (we used $\alpha = 10^{-5}$):

$$l_{xy} := \min_{q=1,r,s} l^*_{xqy} - \alpha.$$

For example, when choosing q_{ss} and l_{ss} for case 54 (see Fig. 3.8), the 2-contact triangle with discs of radii s, s, s has the leftmost intersection of $E(T)$ and $Z(\dot{U}_v(T))$ (* on the first graph). Therefore, $l_{ss} := l^*_{sss} - \alpha$ in this case.

Then we choose the coefficient q_{xy} in a way that $Z(\dot{U}_v(T)) + d_e q_{xy}$ stays below E starting from $l^*_{xqy} - \alpha$ for all $q = 1, r, s$ (which is always possible since d_e is negative on this segment).

These choices guarantee the total potential $U(T)$ (**bold red line** in Fig. 3.8) to be below the emptiness all the way from tight to stretched triangles. At this point though, there is no guarantee that it would be the case for all other triangles. However, this

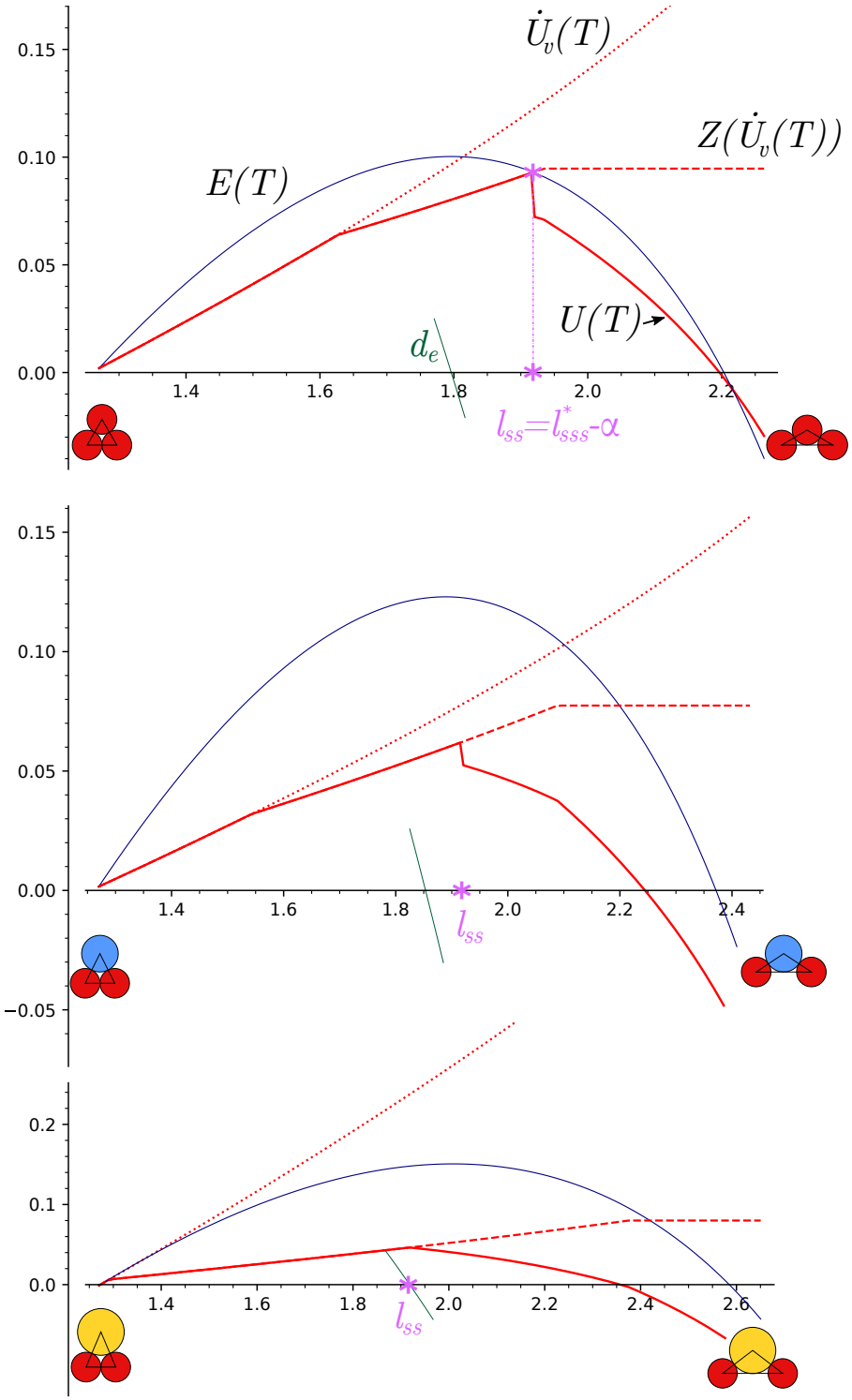

Figure 3.8: Case 54, triangles with discs sss, srs, $s1s$ with two contacts: behavior of the emptiness (in dark blue) and the potential while stretching an edge. Initial vertex potential $\dot{U}(T)$ is marked by the dotted red line, capped vertex potential $Z(\dot{U}(T))$ is the dashed red line, the total potential $U(T)$ is the **bold red line**. The dark green segment designates $d_e(T)$ around the moment it becomes negative, and the pink asterisk $*$ indicates the value of l_{ss}.

choice of the constants of the edge potential was heuristically appropriate: it allows us to carry out the last part of the proof explained in the next section.

3.3 Verifying local inequality (T)

In the previous section, we constructed the potential satisfying (3.1). Let us show that (T) holds, i.e., the potential of a triangle present in $\mathcal{T}$ never exceeds its emptiness. We first treat the triangles that are close to the tight ones, so-called *ϵ-tight triangles*, in Section 3.3.1 and then verify (T) for all the remaining triangles in Section 3.3.2.

3.3.1 Limit cases: ϵ-tight triangles

The definition of the vertex potential allows us to directly show that it does not exceed the emptiness in the triangles "close enough" to the tight ones. We do it by comparing the differentials of the two functions. We treat this specific class of FM-triangles separately since tight triangles are the limiting points where the emptiness is equal to the potential.

Let $\mathcal{T}_\epsilon$ denote the set of *ϵ-tight* triangles, those where each pair of discs is at distance at most ϵ. Given a tight triangle T^*, let $\mathcal{T}_\epsilon^*$ denote the set of ϵ-tight triangles with the same discs. We can bound the variation of emptiness between the tight triangle T^* and any ϵ-tight triangle T from $\mathcal{T}_\epsilon^*$ using the mean-value theorem:

$$E(T) - E(T^*) \geq \sum_{i=1,2,3} \min_{\mathcal{T}_\epsilon} \frac{\partial E}{\partial x_i} \Delta x_i,$$

where x_1, x_2, x_3 are the lengths of the sides.

We consider only the values of ϵ that are strictly smaller than all the constants l_{xy}, so that the edge potential does not play a role in this case. We can thus find the lower bound of the variation of the potential for all $T \in \mathcal{T}_\epsilon^*$,

$$U(T) - U(T^*) \leq \sum_{i=1,2,3} \max_{\mathcal{T}_\epsilon} \frac{\partial \dot{U}}{\partial x_i} \Delta x_i \,.$$

As the potential equals the emptiness on tight triangles, if for a given ϵ, for $i = 1, 2, 3$,

$$\min_{\mathcal{T}_\epsilon} \frac{\partial E}{\partial x_i} \Delta x_i \geq \max_{\mathcal{T}_\epsilon} \frac{\partial \dot{U}}{\partial x_i} \Delta x_i, \tag{ϵ}$$

then the local inequality (T) is satisfied by all triangles in $\mathcal{T}_\epsilon$.

However, some values of the tight vertex potentials and m_1, m_r, m_s lead to the absence of a positive value of ϵ satisfying (ϵ). Notably, if m_1, m_r, m_s are too large, so is the variation of the potential. We fix the free variables from V and m_1, m_r, m_s to ensure the existence of a positive value of ϵ such that the ϵ-tight triangles verify (T).

To guarantee a positive value of ϵ, it is necessary that (ϵ) holds for $\epsilon = 0$, i.e., that for $T^* \in \mathbb{T}^*$ for $i = 1, 2, 3$,

$$\left.\frac{\partial E}{\partial x_i}\right|_{T^*} \geq \left.\frac{\partial \dot{U}}{\partial x_i}\right|_{T^*}. \tag{ϵ_0}$$

Note that each inequality from (ϵ_0) is a linear inequality on m_1, m_r, m_s (the values of tight vertex potentials do not play a role in the derivative since they are constant for each given type of triangle). The system (ϵ_0) produces three linear inequalities on

m_1, m_r, m_s for each tight triangle; the intersection of its solutions and the solutions of (M), defined on page 59, is the polyhedron of values of V-variables and m_1, m_r, m_s guaranteeing (3.1) and (ϵ_0). We heuristically choose a point in this polytope in order to keep the potentials as small as possible, this is discussed in Section 3.5.2. From now on, the values of tight vertex potentials are all fixed, as well as m_1, m_r, m_s, so the vertex potential is completely defined for all triangles. The aforementioned constants for each case are given in Appendix 3.A.

Now that the existence of a positive value of ϵ is guaranteed, we find the greatest value of ϵ satisfying (ϵ) (maximizing the set $\mathcal{T}_\epsilon$, we minimize the set of the remaining triangles that should be treated afterwards). We use a dichotomic search, aiming to maximize ϵ: at each step of the search, we compute both parts of the inequality in interval arithmetic (explained in Section 3.5.1) and if the intervals of these values do not intersect and satisfy inequality (ϵ), the given ϵ is valid. The explicit values of ϵ are given in Appendix 3.A.

3.3.2 Remaining FM-triangles

The final step in the proof of Theorems 3.1.(a) and 3.1.(b) is to verify (T) on the set of non-ϵ-tight FM-triangles. Thanks to the properties of FM-triangulations of saturated packings, this set is compact. Indeed, by Lemma 3.1 given in Section 3.4, the length of the edge connecting centers of discs of radii x and y in a triangle is at least $x + y$ and at most $x + y + 2s$.

Working with intervals rather than precise values allows us to decompose a compact continuum set of triangles into a finite set. Given three disc radii, each side of each triangle with the discs of these radii is bounded. Therefore, to prove inequality $E(T) \geq U(T)$ for all triangles with given disc radii, it is enough to show it for the triangle with sides represented by intervals depending on these radii. More precisely, we should verify the following inequality:

$$E(I(T_{xyz})) \geq U(I(T_{xyz})),$$

where $I(T_{xyz})$ is a triangle with discs of radii x, y, z and sides represented by intervals $[y + z, y + z + 2s], [x + z, x + z + 2s], [x + y, x + y + 2s]$. If it holds (the returned value is `True`), then the inequality holds for all possible triangles with discs x, y, z. If the returned value is `False`, this means either that the inequality is false or that the intervals in question intersect (and thus are incomparable). In this case, we subdivide initial intervals to increase precision. Section 3.5.1 describes in detail how it is done in practice, using interval arithmetic tools of SageMath.

At this step we can not treat ϵ-tight triangles (as indicated in Section 3.5.1, the recursive subdivision method would never stop in the neighborhood of tight triangles), so in reality, we rather verify that inequality only for triangles from $I(T_{xyz})$ which are not in $\mathcal{T}_\epsilon$ (i.e the length of at least one of the edges shall be longer the sum of the disc radii by at least ϵ), this gives the following set of triplets of side lengths:

$$B \setminus B_\epsilon,$$

where

$$B = [y + z, y + z + 2s] \times [x + z, x + z + 2s] \times [x + y, x + y + 2s],$$
$$B_\epsilon = [y + z, y + z + \epsilon] \times [x + z, x + z + \epsilon] \times [x + y, x + y + \epsilon].$$

Dimension reduction

In order to reduce the set of triangles to verify, we turn to the dimension reduction technique seen in Section 2.2.2. As a reminder, Fejes Tóth and Mólnar in [FTM58] proved that given an FM-triangle T of uniformity q, there is an FM-triangle of uniformity at least q having at least two contacts whose density is at least $\delta(T)$ (Lemma 2.4 on page 31). This lemma allows to verify the density inequality only on a relatively small set of triangles with two contacts instead of the whole set of possible FM-triangles.

Unfortunately, we can not directly apply this lemma to reduce the set of triangles in the case of 3-disc packings: first of all, we work with the potential and the emptiness instead of the density, and moreover, we only consider packings using three disc sizes which is not equivalent to the set of packings with a given uniformity value.

We, however, can derive a similar result allowing us, in certain cases, to reduce the set of triangles to the triangles having at least one contact between discs or between a disc and an edge. To do this, we perform the first transformation of Fejes Tóth and Mólnar in [FTM58] (see page 31).

Proposition 3.5 (Dimension reduction for 3-disc packings)**.** *Let x, y, z be disc radii from $\{1, r, s\}$ such that $x \leq y \leq z$. If the sum of the edge potential coefficients $Q := q_{xy} + q_{yz} + q_{xz}$ satisfies*

$$Q \leq \frac{1}{s}\left(1 + \frac{y+z}{y+z+2s}\right)\frac{\pi x^2}{2}, \tag{3.9}$$

then for any FM-triangle T formed by discs of radii x, y, z

$$U(\lambda T) \leq E(\lambda T) \text{ implies } U(T) \leq E(T),$$

where λT denotes the image of T under homothety with ratio $\lambda \leq 1$ (applied only to the vertices of the triangle: the disc radii stay the same) such that λT is an FM-triangle with at least one contact between discs.

Proof. By definition, the emptiness of T equals

$$E(T) := A(T) \cdot \delta^* - A(T \cap P)\,.$$

Meanwhile, the emptiness of λT is equal to

$$E(\lambda T) = A(\lambda T) \cdot \delta^* - A(T \cap P) = \lambda^2\, A(T) \cdot \delta^* - A(T \cap P).$$

On the other hand, $\dot{U}(\lambda T) = \dot{U}(T)$ since the homothety preserves the angles. Therefore,

$$\begin{aligned} U(T) - E(T) &= \dot{U}(T) + \bar{U}(T) - A(T) \cdot \delta^* + A(T \cap P) \\ &= U(\lambda T) - E(\lambda T) + \bar{U}(T) - \bar{U}(\lambda T) + (\lambda^2 - 1)\,\delta^*\, A(T) \\ &\leq \bar{U}(T) - \bar{U}(\lambda T) + (\lambda^2 - 1)\,\delta^*\, A(T). \end{aligned} \tag{3.10}$$

By definition of the edge potential, for any edge e of T,

$$\bar{U}_e(T) - \bar{U}_e(\lambda T) = \begin{cases} q_{xy}(d_e(T) - d_e(\lambda T)) = (1-\lambda) q_{xy} d_e(T) & \text{if } |e| \geq \lambda|e| > l_{xy} \\ q_{xy} d_e(T) & \text{if } |e| > l_{xy} \geq \lambda|e| \\ 0 & \text{otherwise.} \end{cases}$$

Since the packing is saturated, no disc intersects an opposite edge and the support disc radius is at most s, therefore, the distance from the support disc center to any edge is at most s. Therefore, we get the following upper bound

$$\bar{U}(T) - \bar{U}(\lambda T) \leq Qs. \tag{3.11}$$

We can bound the area of T from below by the part if T covered by the discs $cov(T)$ which is at least $\frac{\pi x^2}{2}$,

$$A(T) \geq \frac{\pi x^2}{2}. \tag{3.12}$$

Applying (3.9), (3.11) and (3.12) to (3.10), we get

$$U(T) - E(T) \leq (\lambda^2 - 1)\frac{\pi x^2}{2} + Qs \leq (\lambda + 1)\frac{\pi x^2}{2} - \left(1 + \frac{y+z}{y+z+2s}\right)\frac{\pi x^2}{2}. \tag{3.13}$$

Since T and λT are FM-triangles, by Lemma 3.1, the edge of T with discs of radii y and z in its vertices is no longer than $y + z + 2s$, while the corresponding edge of λT is no shorter than $y + z$. Therefore,

$$\lambda \geq \frac{y+z}{y+z+2s},$$

which, applied to (3.13), allows us to conclude .

□

This proposition allows us to reduce the set of triangles for the disc triplets satisfying (3.9). In practice, for almost all cases we considered, it was satisfied.

3.4 Additional properties of FM-triangles

This section is dedicated to the properties of FM-triangles of multi-size packing needed in the previous sections. Section 2.2.1 provides the definition of FM-triangulations together with several properties which do not depend on the number of discs in the packing so they also hold for 3-disc packings.

Similar results for 2-disc packings are given in [BF22] and some of them were generalized for 3-disc packings in [Fer19]. Here we give alternative more detailed proofs and, to be as general as possible, state all the results for packings of a given uniformity s which indeed include 3-disc packings by discs of radii $1, r, s$, with $s \leq r \leq 1$.

In this section, T denote a triangle in an FM-triangulation of packing P of uniformity s; A, B, and C denote the vertices of T and D_A, D_B, and D_C are the discs of radii r_A, r_B, and r_C respectively centered in A, B, and C.

Lemma 3.1. *The length of AB is at least $r_A + r_B$ and at most $r_A + r_B + 2s$. (The same holds for other edges.)*

Proof. The lower bound comes from the fact that discs do not intersect:

$$|AB| \geq r_A + r_B.$$

Let O be the center of the support disc of T; by the support disc property, its radius is at most s. Applying the triangle inequality to AOB, we obtain

$$|AB| \le |OA| + |OB| \le r_A + r_B + 2s.$$

□

Lemma 3.2. *The angle $\widehat{A}$ corresponding to vertex A in T satisfies*

$$\widehat{A} \ge \arcsin\left(\min\left(\frac{r_B}{r_A + r_B + 2s}, \frac{r_C}{r_C + r_B + 2s}\right)\right).$$

(The same holds for other angles.)

Proof. We assume that $\widehat{A} < \frac{\pi}{2}$ (otherwise, the inequality directly holds).

Suppose first that $\widehat{C} \le \widehat{B}$ and, therefore, $\widehat{C} < \frac{\pi}{2}$. The altitude of B in T is at least r_B: otherwise the disc sector defined by edges BA and BC would intersect the edge AC which contradicts Property 2.3 of FM-triangles (page 28).

On the other hand, by Lemma 3.1, $|AB| \le r_A + r_B + 2s$. Therefore,

$$\sin(\widehat{A}) \ge \frac{r_B}{|AB|} \ge \frac{r_B}{r_A + r_B + 2s}.$$

If $\widehat{C} > \widehat{B}$, the same reasoning yields

$$\sin(\widehat{A}) \ge \frac{r_C}{r_C + r_A + 2s}.$$

□

Lemma 3.2 implies the following corollary.

Corollary 3.1. *Any angle of T is at least*

$$\arcsin\left(\frac{s}{2 + 2s}\right).$$

Lemma 3.3. *Let $T' = ABC'$ be the FM-triangle which shares the edge AB with T in the FM-triangulation of P. Then the sum of signed distances from the support disc centers of T and T' to AB is always non-negative:*

$$d_{AB}(T) + d_{AB}(T') \ge 0.$$

Proof. If both distances are non-negative, then the statement directly holds. Without loss of generality, assume $d_{AB}(T) \le 0$. Let L_{AB} denote the line containing AB. The points C and O lie on the different sides of L_{AB}. (see Fig. 3.9a).

Let O' denote the center of the support disc of T'. As discussed in Section 2.2.1, the set of centers of discs tangent both to D_A and D_B is a branch of hyperbola H with foci in A and B. Both O and O' lie on H. The closer the disc center (on H) to AB the smaller its radius.

Let L^+ and L^- denote the centers of discs of radius s tangent to both D_A and D_B, L^+ being on the same side of AB as C and L^- on the other side. Since the packing is saturated, the radii of D_O and $D_{O'}$ are both less than s, therefore, O and O' are both between L^- and L^+ on H.

If O' is between L^- and O (as in Fig. 3.9), than it is further than O from AB and we immediately conclude:

$$d_{AB}(T) + d_{AB}(T') = -d(AB, O) + d(AB, O') \ge 0.$$

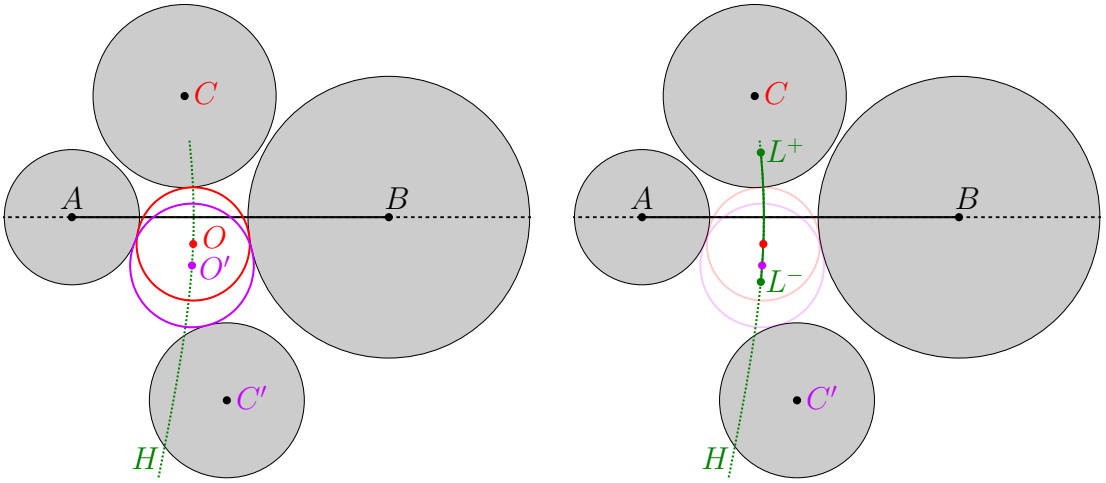

Figure 3.9: Illustration for the proof of Lemma 3.3: discs D_A, D_B, D_C, and $D_{C'}$, the support discs of T and T': D_O (in red) and $D_{O'}$ (in purple), and the hyperbola branch H (in green).

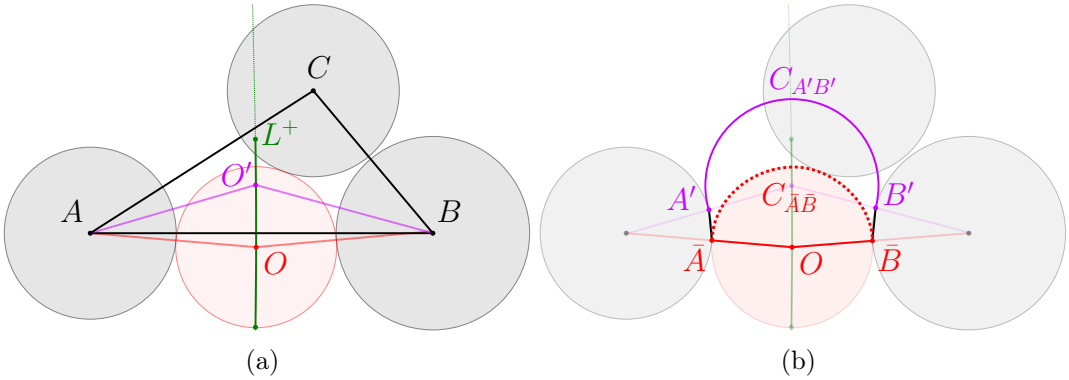

Figure 3.10: Illustration for the proof of Lemma 3.3: the case where O' is between O and L^+ on H.

We thus assume that O' is between O and L^+ on H (as depicted in Fig. 3.10a). Let A' denote the point of intersection of AO' with the border of D_A; point B' is defined analogously. Let $C_{A'B'}$ denote the uppermost arc $A'B'$ of the border circle of $D_{O'}$ (i.e., the one which is further from AB). In Figure 3.10b, $C_{A'B'}$ is traced in purple.

Let $\bar{A}$ denote the point of intersection of AO and the border of D_A; we define $\bar{B}$ by analogy. Let $C_{\bar{A}\bar{B}}$ denote the arc of the border circle of D_O tangent to D_C (dotted red line in Figure 3.10b).

Let us denote by S the set bounded by $O\bar{A} \cup \bar{A}A' \cup C_{A'B'} \cup B'\bar{B} \cup \bar{B}O$. Showing that the arc $C_{\bar{A}\bar{B}}$ entirely belongs to S allows us to conclude since this would mean that the point of contact of D_O and D_C belongs to S and, therefore, D_C intersects $D_{O'}$, D_A, or D_B which leads to contradiction. The remaining part of the proof is dedicated to demonstrating that $C_{\bar{A}\bar{B}}$ is in S.

The border circles of D_O and $D_{O'}$ have up to 2 intersection points. If they have 1 or zero intersection points, then the interiors of D_O and $D_{O'}$ do not intersect and the arc $C_{\bar{A}\bar{B}}$ lies entirely inside S (see Fig. 3.11a)

Suppose D_O and $D_{O'}$ have two intersections (see Fig. 3.11b). By Lemma 3.4 proved below, one of them is contained in triangle AOO' and another one in triangle BOO'.

Let us denote these intersection points by X_A and X_B respectively.

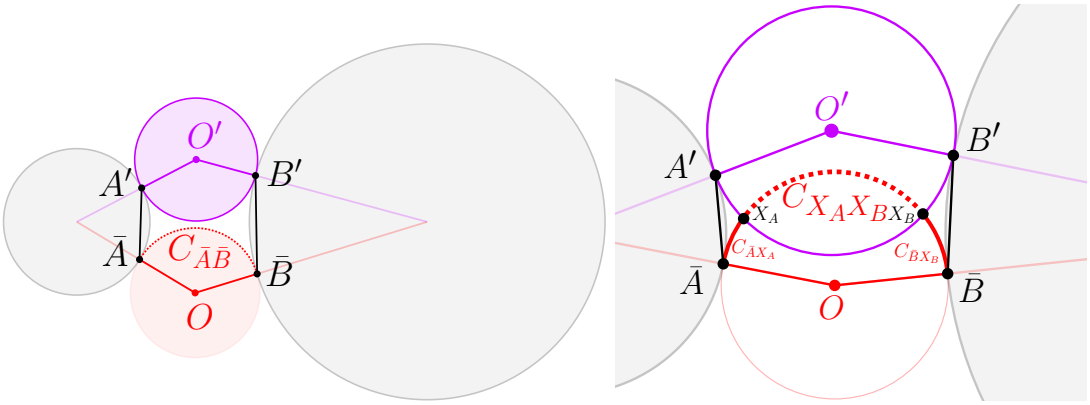

Figure 3.11: Illustration for the proof of Lemma 3.3.

Let $C_{X_AX_B}$ denote the part of the arc $C_{\bar{A}\bar{B}}$ limited by X_A and X_B, it entirely belongs to $D_{O'}$ and hence to S (in Fig. 3.11b, $C_{X_AX_B}$ is the red dotted line). Let $C_{\bar{A}X_A}$ and $C_{\bar{B}X_B}$ denote the two remaining sub-arc named according to their extremities (marked in bold red in Fig. 3.11b). Since X_A and X_B lie respectively in AOO' and BOO' and D_O does not intersect D_A nor D_B, the arcs $C_{\bar{A}X_A}$ and $C_{\bar{B}X_B}$ belong respectively to AOO' and BOO'. Therefore, $C_{\bar{A}\bar{B}}$ belongs to S which allows us to conclude. □

Lemma 3.4. *Given two circles C_O and $C_{O'}$ centered in O and O' which have two points of intersection and a disc D_A centered in A tangent to both of them whose interior is disjoint from both of them, the triangle AOO' contains at least one point of intersection of C_O and C'_O.*

Proof. Let $L_{OO'}$ denote the line containing OO', N denote its intersection with $C_{O'}$ from the other side of O in respect to O', and S denote its the intersection with C_O from the other side of O' in respect to O (see Figure 3.12a).

C_O and $C_{O'}$ are both symmetric with respect to $L_{OO'}$ and thus have one intersection at each side of $L_{OO'}$. Let h denote the half-space generated by $L_{OO'}$ which contains A (dotted half-plane in Fig. 3.12a). Let X denote the point of intersection of two circles lying in h.

Let C_{SX} denote the open arc of C_O entirely belonging to H (dotted red line in Fig. 3.12a); let C_{NX} denote the circular interval of $C_{O'}$ entirely belonging to h (dotted purple line in Fig. 3.12a). For any point $H \in C_{SX}$, points X and O' lie at the same side from the line L_{OH} (the half-plane in question is filled by transparent red in Fig. 3.12a). Similarly, for any point $H' \in C_{NX}$, points X and O lie at the same side from the line $L_{O'H'}$ (the half-plane in question is filled by transparent purple in Fig. 3.12a).

Let $\bar{A}$ denote the point of contact between D_A and C_O, let A' denote the point of contact of D_A and $C_{O'}$. Point $\bar{A}$ belongs to C_{NX} and X' belongs to C_{SX} since D_A is disjoint from the interiors of discs bounded by C_O and $C_{O'}$ (see Fig. 3.12b for illustration).

As showed above, the half-plane formed by AO' containing point O also contains X and the half-plane formed by AO containing O' also contains X. Besides that, by definition, the half-plane h formed by OO' and containing A also contains X. Therefore, X belongs to the triangle $OO'A$ which allows us to conclude.

□

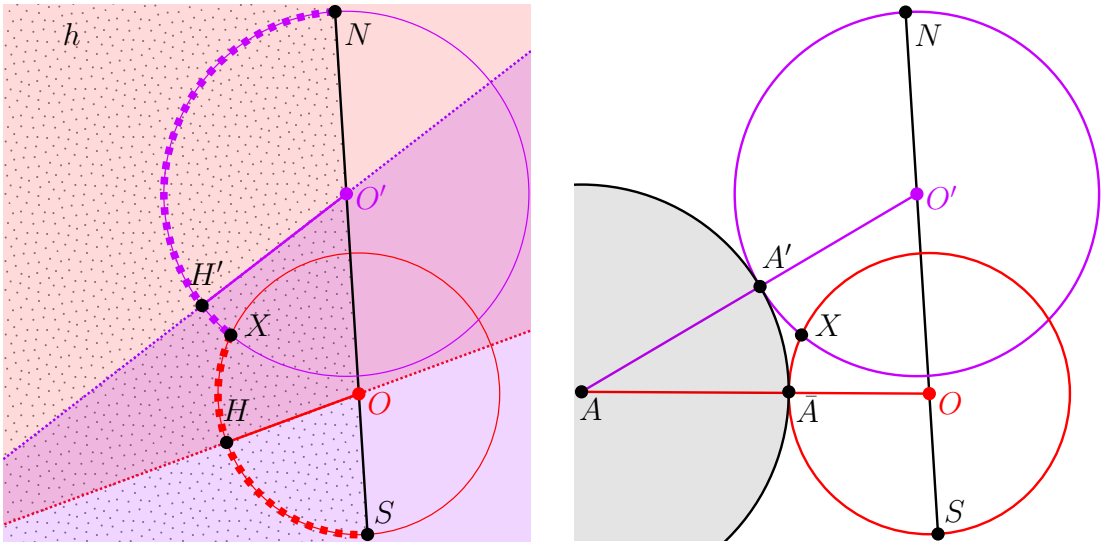

(a) (b)

Figure 3.12: Illustration for the proof of Lemma 3.4.

3.5 Implementation

As many proofs of the domain, notably the proof of the Kepler Conjecture [Hal05], the proofs of the maximal density for triangulated packings, like ours and those from [BF22, Fer19, Ken05], essentially rely on computer calculations. This section is dedicated to the implementation of the computer-aided part of the proof.

The treatment of each case consists of two steps and computer assistance is needed for two distinct purposes. First, we need to find valid (i.e., satisfying inequality (3.1)) constants from the construction of the potential (Section 3.2): tight vertex potentials V_{xyz}, constants m_y, capping values Z_y, and constants l_{xy}, q_{xy} of the edge potentials. Second, we verify that the potential never exceeds the emptiness in an FM-triangle (Section 3.3).

The following sections discuss the important issues of the implementation. Section 3.5.1 explains our usage of interval arithmetic throughout the implementation, Section 3.5.2 is dedicated to the choice of the constants V, m_1, m_r, m_s of the vertex potential. In Section 3.5.3, we explain how to find the center and the radius of the support disc of an FM-triangle.

The entirety of the code, written in SageMath [2] [3], is given at `https://github.com/tooticki/ternary_triangulated_disc_packings`. The implementation is divided into three independent parts: folder "`a`" contains the code supporting the proof of Theorem 3.1.(a), folder "`b`" – the proof of Theorem 3.1.(b), and finally, folder "`c`" houses the code that generates the counterexamples from Theorem 3.2.

In this section, we will primarily refer to folder "`a`". The differences between the implementation needed for Theorem 3.1.(a) and for Theorem 3.1.(b) are negligible (as explained in the end of Section 3.2.1), so are the differences between "`a`" and "`b`". Finally, the code corresponding to the proof of Theorem 3.2 (folder "`c`") is discussed in Section 3.6.

Here is a short description of the structure of the code in "`a`".

- Folder `input`:
  - `cases.csv`: This file is the table containing the information necessary to identify each case and its triangulated packing, i.e., the polynomials describing the radii r, s, the coronas, and the number of triangles of each type in the domain of the triangulated packing.
- Folder `library`:
  - `drawing.sage`: This module contains functions related to drawing of local configurations of discs and graphs like the one in Figure 3.8.
  - `input_ternary.sage`: This module handles input processing: among other, it computes the values of r, s as roots of polynomials, the value of the density of the target triangulated packing, and returns them as intervals (see Section 3.5.1).
  - `potentials_basic_functions.sage`: This module contains basic functions related to the potential and its derivatives.
  - `small_functions_ternary.sage`: This module includes smaller auxiliary functions needed for calculations (for instance, the ones from Section 3.5.3) and combinatorial search (as the enumeration of all possible sequences of radii in a corona around a disc to get (M)).
- `ternary_main_functions.sage`: This file links together all the tools, notably the input part, needed for the two main files `generate_polyhedron.sage` and `test_given_polyhedron.sage`.
- `generate_polyhedron.sage`: This file contains the code responsible for generating the polyhedron representing the set of valid constants necessary for the vertex potential, as well as ϵ (see Section 3.5.2). We separated it in a distinct file since this code is relatively time-consuming, so the generated polyhedron is stored as an object and we do not need to recompute it each time we make modifications in the remaining part of the code.
- `test_given_polyhedron.sage`: Given that the polyhedron was already constructed by the previous program, this code chooses a point in it, computes the values

[2] `https://www.sagemath.org/` (accessed on 15 July, 2023)

[3] This choice was driven by immediate simplicity and is not the most optimal on the long run. By chance, the computations were not excessively time-consuming; otherwise we would have used C++, as we do for the 3-dimensional density bound in Chapter 4.

needed for the edge potential, and verifies (T) using subdivision method (see Section 3.5.1).

3.5.1 Interval arithmetic

In our code, interval arithmetic appears in two completely different contexts: to work with real numbers non-representable in computer memory and, more importantly, to verify inequalities on uncountable but compact sets of values.

Originally, interval arithmetic was introduced to bound errors in numerical computations. When interval arithmetic is applied to computing, each value is represented by a closed interval containing this value and whose endpoints are exact values finitely representable in computer memory (e.x., floating-point numbers) [4]. In this manuscript, we use the following notations: a real value x is represented by an interval denoted by X; the endpoints of X are denoted by $\underline{X}$ and $\overline{X}$:

$$x \in X := [\underline{X}, \overline{X}].$$

Notice that while x is an arbitrary real number, both $\underline{X}$ and $\overline{X}$ are floating-point numbers. The length of the interval X is called its *diameter* and is denoted by $|X|$:

$$|X| := \overline{X} - \underline{X}.$$

Functions in interval arithmetic preserve both the belonging to the interval and the representativity of the endpoints. More precisely, if $X_1, \dots, X_n$ are intervals, and f is an n-ary function, the interval $f(X_1, \dots, X_n)$ must contain $f(x_1, \dots, x_n)$ for all $(x_1, \dots, x_n) \in X_1 \times \dots \times X_n$ and its endpoints, $\underline{f(X_1, \dots, X_n)}$ and $\overline{f(X_1, \dots, X_n)}$, are floating-point numbers.

Notice that in general, the interval $f(X_1, \dots, X_n)$ might be much larger than the image of f on $X_1 \times \dots \times X_n$ for two reasons. First, the set of values of a non-continuous function might simply not be an interval. Second, there is no implementation of interval arithmetic guaranteeing the resulting interval to be minimal. For more on interval arithmetic in general and its implementations, see [MKC09, Rev20].

To verify an inequality on two intervals $X < Y$, it is enough to compare the right endpoint of X with the left endpoint of Y:

$$X < Y \ := \ \overline{X} < \underline{Y},$$

the inequality holds if and only if each pair of values from these intervals satisfy the inequality.

We use intervals to represent the values of radii of discs r, s which are algebraic numbers obtained as roots of polynomials in [FHS21], as well as the value of π. However, representing algebraic values is not the main reason to use interval arithmetic: we need it to verify inequalities on compact continuum sets of triangles in Section 3.3. We use the *recursive subdivision method*, an instance of the so-called *branch-and-bound* method from optimization. Similar techniques are widely applied in the context of both disc [FKS23, BF22] and sphere packings [Hal11d].

The recursive subdivision approach is used to resolve the following class of problems.

[4] We assume that $-\infty$ and ∞ count as floating-point numbers (which is the case in IEEE 754), so infinite intervals are allowed.

Problem 3.1. *Given an n-ary continuous function f and an n-dimensional box $B = X_1 \times \cdots \times X_n$ where $X_1, \ldots, X_n$ are bounded intervals, determine if*

$$\forall x \in B, f(x) \geq 0.$$

The method of recursive subdivision consists in the following steps. If the interior of interval $f(X_1, \ldots, X_n)$ does not contain 0, this interval can be compared to 0 and the result is the result of the comparison. Otherwise, we bisect each of intervals X_i in two, X_i^0, X_i^1, and verify the inequality on each of 2^n combinations of sub-intervals

$$\{X_1^{b_1} \times \cdots \times X_n^{b_n} \mid b_1 \ldots b_n \in \{0,1\}^n\}.$$

We return `True` if it holds for each of them:

$$\forall b_1 \ldots b_n \in \{0,1\}^n \quad \underline{f(X_1^{b_1}, \ldots, X_n^{b_n})} \geq 0 \,.$$

The result is `False` if for one of the combinations $X_1^{b_1}, \ldots, X_n^{b_n}$, interval $f(X_1^{b_1}, \ldots, X_n^{b_n})$ does not contain 0 and does not satisfy the inequality, i.e.,

$$\exists b_1 \ldots b_n \in \{0,1\}^n \quad \overline{f(X_1^{b_1}, \ldots, X_n^{b_n})} < 0.$$

Otherwise, we continue the subdivision on the combinations on which the interior of f contains zero.

This algorithm always stops after a finite number of steps if f is continuous, except the case where the inequality holds and there is a point in the closure of B where it becomes an equality. Besides that, if f is never equal to 0 but is very close to 0 in some points of B, the number of subdivisions might be too huge in practice despite being finite. As a consequence, this algorithm alone is not sufficient to verify tight bounds: the neighborhoods of zeros of f shall be treated by another method. That is why, when verifying inequality (T) by recursive subdivision with $f = E - U$, we have to deal with ϵ-tight triangles separately (Section 3.3.1). In tight triangles, the emptiness coincides with the potential (inequality (T) becomes an equality: $E(T^*) - U(T^*) = 0$), we thus exclude their neighborhoods to have our algorithm halt in a reasonable time. On the other hand, the derivatives of these functions in tight triangles are, in practice, far enough, which allows us to compare them directly, without subdivision method, to verify inequality (ϵ) for a given value of ϵ.

The subdivision method is used in the Hales' proof of the Kepler conjecture [HF06], as well as in numerous results on the density of disc packings in containers [NO99, MC05, Mar21, FKS23] already mentioned in Section 1.2.1.

We use the SageMath [Dev22] implementation of interval arithmetic called Arbitrary Precision Real Intervals [5]. The interval endpoints are floating-point numbers; we work with the default precision of the library where the mantissa encoding has 53 bits. That means, the relative diameters of intervals representing real values are all equal to 2^{-53}.

However, when we verify inequality (T) on tight triangles, at the first step of subdivision, intervals representing the edge lengths are of diameter $2s - \epsilon$ which is at least 0.2. This value, indeed, increases when performing arithmetic operations and applying trigonometric functions to such intervals, so we have to subdivide a lot. The lack of accuracy notably affects the calculation of the radius of the support disc; we discuss this in detail in Section 3.5.3.

[5] `https://doc.sagemath.org/html/en/reference/rings_numerical/sage/rings/real_mpfi.html` (accessed on 15 July, 2023)

3.5.2 Linear inequalities and `Polyhedra`

Let us follow the steps of the implementation complementing Section 3.2.1. First, we solve the system of linear equations $(C, \mathbb{T}^*)$ and obtain the values of $\{V_{xyz} \mid x = y = z \text{ or } x \neq z\}_{x,y,z\in\{1,r,s\}}$ in terms of the remaining free variables V. Let us denote the set of solutions of (M) by $P_{V,m}$, it is a convex subset of $\mathbb{R}^9$ bounded by a finite set of linear inequalities.

To ensure the existence of a positive value of ϵ from Section 3.3.1, we impose inequalities (ϵ_0). In practice, we intersect $P_{V,m}$ with the polyhedron P_{ϵ_0} corresponding to (ϵ_0); let P_{V,m,ϵ_0} denote the intersection. For all the cases considered in this section, this intersection is not empty (the cases where it was empty are discussed in Section 5.1.2).

After that, we have to choose a point in P_{V,m,ϵ_0} to fix the values of variables from V and m_1, m_r, m_s. Our aim at that step is to minimize potentials of all triangles in order to eventually satisfy (T). We thus find the three vertices of the polyhedron minimizing m_1, m_r and m_s respectively, compute a linear combination of them (the weights that worked well in practice were respectively 1, 1 and 4), and take a point between this one and the center of the polyhedron in order to avoid the approximations problems on the border which are discussed in the next paragraph. The method described above is a heuristic, sufficient for all the cases we considered.

In our implementation, solutions of a system of linear inequalities are stored as a `Polyhedron` object of SageMath [6]. `Polyhedra` represent the convex subsets of the Euclidean space defined by a system of linear inequalities and equations. However, the `Polyhedron` class does not allow coefficients of constraints to be intervals, while some of the coefficients of our inequalities depend on π and the disc radii and are stored as intervals. `Polyhedra` do not support intervals as a base ring for a good reason: solutions of a system of linear inequalities with interval coefficients do not form a convex polyhedron. More precisely, all possible solutions of the system is a union of a huge number of polyhedra. For example, Figure 3.13 depicts the solutions of three linear equations $ax + by = 1$ with real coefficients together with the solutions of the same equations where the coefficients a and b are replaced by intervals $A = (a - \epsilon, a + \epsilon), B = (b - \epsilon, b + \epsilon)$ of radius $\epsilon = 0.2$. Each solution of $Ax + By = 1$ is a set bounded by four lines which correspond to the combinations of lower and upper bounds of the intervals: $\underline{A}x + \underline{B}y = 1, \underline{A}x + \overline{B}y = 1, \overline{A}x + \underline{B}y = 1, \overline{A}x + \overline{B}y = 1$. All possible solutions of the system of corresponding inequalities (i.e., $Ax + By \leq 1$) are contained in the (potentially infinite) intersection of three unions of triplets of half-planes (dotted polygon in Fig. 3.13). To compute this set for a system of n linear inequalities on m variables, we potentially have to compute all points of intersections of $2^m \times n$ hyperplanes...

In our case, the number of inequalities is already huge, so after multiplying it by 2^9, the computations become way too costly.

We choose to replace the intervals with their centers and work with an approximation $\widetilde{P}_{V,m,\epsilon_0}$ of the actual set P_{V,m,ϵ_0} of valid values for tight potential s and m_1, m_r, m_s. Our `Polyhedron` $\widetilde{P}_{V,m,\epsilon_0}$ is stored in a field of rational values, since this field is computationally quite efficient.

`Polyhedron` $\widetilde{P}_{V,m,\epsilon_0}$ and set P_{V,m,ϵ_0}, in general, have non-empty differences. That means, after choosing a point inside $\widetilde{P}_{V,m,\epsilon_0}$, we can not know if this point actually satisfies all the constraints. To make sure it does, we then rigorously verify that all

[6] `https://doc.sagemath.org/html/en/reference/discrete_geometry/sage/geometry/polyhedron/constructor.html` (accessed on 15 July, 2023)

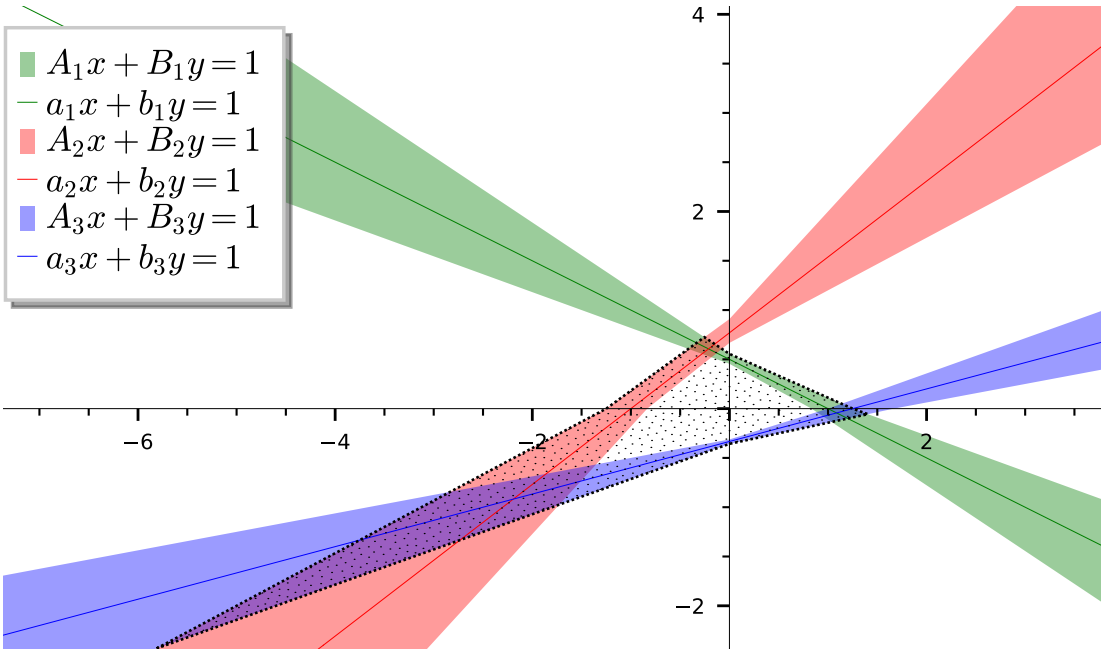

Figure 3.13: Solutions of three linear equations with real coefficients $a_1 = 1, b_1 = 2, a_2 = -1, b_2 = 1.3, a_3 = 0.8, b_3 = -3$ (green, red, and blue lines) and the sets of solutions of the same inequalities whose coefficients $A1, B1, A2, B2, A3, B3$ are intervals of radius $\epsilon = 0.2$ (green, red, and blue areas).

the inequalities with interval coefficients (M) hold in this point; inequalities (ϵ_0) are verified later when choosing the value of ϵ.

To resume, here are some functions playing important roles in the construction of the `Polyhedron` $\widetilde{P}_{V,m,\epsilon_0}$, choosing a point in it, and verifying that this point belongs to P_{V,m,ϵ_0}.

File `library/small_functions_ternary.sage` contains auxiliary functions needed to enumerate inequalities (M).

- `corona_generator(q)`: runs through all possible sequences of radii that could form a corona around a q-disc.

In `generate_polyhedron.sage`: generating the polyhedron $\widetilde{P}_{V,m,\epsilon_0}$.

- `eps_polyhedron(eps)`: computes a `Polyhedron` approximating the set of values of m_1, m_r, m_s satisfying (ϵ) for $\epsilon =$`eps`: $\widetilde{P_{\epsilon_0}} =$ `eps_polyhedron(0)`.
- `Vm_polyhedron(q)`: computes a `Polyhedron` approximating the set of V, m_1, m_r, m_s satisfying the $m_{\mathtt{q}}$-inequalities in (M): $\widetilde{P}_{V,m} = \widetilde{P}_{V,m_1} \cap \widetilde{P}_{V,m_r} \cap \widetilde{P}_{V,m_s}$ and $\widetilde{P}_{V,m_{\mathtt{q}}} =$ `Vm_polyhedron(q)`.
- `get_one_polyhedron(q, case)`: computes and saves a `Polyhedron` of a given type. The type denotes which systems of inequalities should be respected: '`e`' stands for (ϵ_0), '`1`', '`r`', and '`s`' — for the $m_{\mathtt{1}}$-, $m_{\mathtt{r}}$-, and $m_{\mathtt{s}}$- inequalities in (M) respectively. For instance, to generate $\widetilde{P}_{V,m,\epsilon_0}$ for case 54, it is enough to call `get_one_polyhedron("e1rs", 54)`.

In `test_given_polyhedron.sage`: choosing a point in $\widetilde{P}_{V,m,\epsilon_0}$ and verifying that it actually satisfies (M) and (ϵ_0).

- `choose_point(P)` returns a point from $\widetilde{P}_{V,m,\epsilon_0}$ according to the heuristic detailed above (aiming to minimize the values m_1, m_r, and m_s).
- `verify_vm(q)` checks if the chosen point satisfies the $m_{\mathtt{q}}$-inequalities in (M).
- `test_eps(m1,mr,ms,eps)` checks if (ϵ) is satisfied for m_1=`m1`, m_r=`mr`, m_s=`ms`, ϵ=`eps`.

Possible *optimization* of point choice

There might be a more clever way to fix the values of V and m_x among the points of $\widetilde{P}_{V,m,\epsilon_0}$. As explained above, we choose the point minimizing $m_1 + m_r + 4m_4$ which is not too close to the frontier of the `Polyhedron`. Our eventual goal, however, is to minimize the potentials in triangles so that (T) is satisfied. We thus considered a more direct way to choose a point through optimization methods.

Given a triangle T, inequality (T) $(E(T) \geq U(T))$ might be formulated as a system of linear inequalities on V, m_x, Z_x, q_{xy}, and l_{xy} (where $x, y \in \{1, r, s\}$). We shall just add some additional variables and inequalities to represent how constants Z_x depend on V (see (3.6)) and $\min(Z_x, \dot{U}_v(T))$ for capping. Let us denote this system by (L_T).

Here is a sketch of a possible algorithm for fixing the constants in a clever way: we start by heuristically choosing a point in $\widetilde{P}_{V,m,\epsilon_0}$ and then run the subdivision algorithm on all possible triangles. If we find a box B of triangles not satisfying (T), we intersect $\widetilde{P}_{V,m,\epsilon_0}$ with the solution of the systems $\{(L_T),\}_{T\in B}$, choose a point in this intersection and continue to iterate. There is indeed no guarantee of converging but at least we directly take into account the constraints (T) instead of blindly picking a heuristics only depending on m_x.

Unfortunately, the core of this idea is wrong: our method to choose the constants q_{xy} and l_{xy} cannot be formulated as a linear constraint. Even though this algorithm was left aside and the simple heuristic was enough for all the cases from Theorem 3.1, we might need to use it in future for one of the open problems from Chapter 5, since the potential can be defined in different ways and a minor modification might suffice to "linearize" the problem.

3.5.3 Support disc and signed distance

At the final step of the proof (Section 3.3), we perform the subdivision method on the set of triangles with bounded edge lengths to verify that inequality (T) holds on all FM-triangles.

By Property 2.2, FM-triangles have support discs of radii at most s. However, some of the triangles from the initial box are not FM-triangles, so we shall skip them in the process of subdivision. For the remaining triangles, we compare their potential and their emptiness; in order to derive the edge potential of a triangle, we need to compute the signed distance for each edge. Therefore, at each step of subdivision, we have to compute the parameters of the support disc of a triangle.

Let us first find the formulas for the radius and the coordinates of the center of the support disc. Let T be an FM-triangle with vertices A, B, C and edge lengths $a = |BC|, b = |AC|, c = |AB|$. Let r_A, r_B, and r_C denote the radii of the discs centered in A, B, and C respectively. To facilitate the calculations, without loss of generality, we place vertex A in the origin and B – on the positive part of x-axis: $A := (0, 0)$ and

$B := (c, 0)$. Let us derive the coordinates of the third vertex C.

$$x_C = \frac{b^2 + c^2 - a^2}{2c},\ y_C := \sqrt{b^2 - x_C^2}.$$

Let (x, y) denote the coordinates of the center of the support disc and R denote its radius. Then the tangency points between the support disc and the three discs of T imply the following equations.

$$\begin{aligned} x^2 + y^2 &= (R + r_A)^2 \\ (x - c)^2 + y^2 &= (R + r_B)^2 \\ (x - x_C)^2 + (y - y_C)^2 &= (R + r_C)^2. \end{aligned} \tag{3.14}$$

They allow us to find x and y as functions of R,

$$x = \frac{c^2 + 2\,Rr_A + r_A^2 - 2\,Rr_B - r_B^2}{2\,c}$$

$$y = \frac{\begin{array}{r} c^2(a^2 + b^2 - c^2) + \big(a^2 - b^2 + c^2\big)r_A^2 - \big(a^2 - b^2 - c^2\big)r_B^2 + 2c^2\,r_C^2 \\ + 2R\left(\big(a^2 - b^2 + c^2\big)r_A - \big(a^2 - b^2 - c^2\big)r_B - 2r_C\right) \end{array}}{c\sqrt{2(a^2b^2 + b^2c^2 + a^2c^2) - a^4 - b^4 - c^4}},$$

as well as a quadratic equation on R.

$$\mathcal{A}R^2 + \mathcal{B}R + \mathcal{C} = 0, \tag{3.15}$$

where

$$\begin{aligned} \mathcal{A} = {} & 4\left(r_A^2 - r_Ar_B - r_Ar_C + r_Br_C\right)a^2 \\ & -4\left(r_Ar_B - r_B^2 - r_Ar_C + r_Br_C\right)b^2 \\ & +4\left(r_Ar_B - r_Ar_C - r_Br_C + r_C^2\right)c^2 \\ & -(a{+}b{+}c)(a{+}b{-}c)(a{-}b{+}c)(-a{+}b{+}c) \end{aligned}$$

$$\begin{aligned} \mathcal{B} = {} & -2a^2\big(b^2(r_A{+}r_B) - a^2r_A - 2\,r_A^3 + r_A^2(r_C + r_B) + r_B^2(r_A - r_C) + r_C^2(r_A - r_B)\big) \\ & -2b^2\big(c^2(r_B{+}r_C) - b^2r_B - 2\,r_B^3 + r_B^2(r_A + r_C) + r_C^2(r_B - r_A) + r_A^2(r_B - r_C)\big) \\ & -2c^2\big(a^2(r_A{+}r_C) - c^2r_C - 2\,r_C^3 + r_C^2(r_A + r_B) + r_A^2(r_C - r_B) + r_B^2(r_C - r_A)\big) \end{aligned}$$

$$\begin{aligned} \mathcal{C} = {} & r_A^2\left(a^4 - a^2(b^2 + c^2)\right) + r_B^2\left(b^4 - b^2(a^2 + c^2)\right) + r_C^2\left(c^4 - c^2(a^2 + b^2)\right) \\ & +r_A^2\,r_B^2\left(c^2 - a^2 - b^2\right) + r_B^2\,r_C^2\left(a^2 - b^2 - c^2\right) + r_A^2\,r_C^2\left(b^2 - a^2 - c^2\right) \\ & +a^2r_A^4 + b^2r_B^4 + c^2r_C^4 - a^2b^2c^2. \end{aligned}$$

By Property 2.1 (page 25), there is at most one disc of radius $\le s$ satisfying equations (3.14), so the radius of the support disc is the smallest positive root of (3.15) which is equal to

$$R = \frac{-\mathcal{B} - \operatorname{sign}(\mathcal{C})\sqrt{\mathcal{B}^2 - 4\mathcal{A}\mathcal{C}}}{2\mathcal{A}}. \tag{3.16}$$

Computing the value of R at this point would be simple if a, b, and c were not intervals, and even simpler if both them and the disc radii were values representable as floating-point numbers. Unfortunately, r_A, r_B, and r_C are intervals representing algebraic numbers (i.e., relatively small), while intervals a, b, and c are, at the first step of subdivision, of width at least $2s - \epsilon$ (see Section 3.5.1).

To give you an idea of the problem we are faced with, let us consider an example for the case 54. The disc radii are represented by the following intervals.

$$r_{54} = [\underline{r_{54}}, \overline{r_{54}}] \approx [0.786662839819061, 0.786662839819062],$$
$$s_{54} = [\underline{s_{54}}, \overline{s_{54}}] \approx [0.635014533102744, 0.635014533102745].$$

We use "$\approx$" instead of "$=$" because the values given above are approximations of the actual interval endpoints. Here and later, for the sake of simplicity some values are given approximately; you can be assured though: they are always preceded by "$\approx$". In case your doubt the scale of "simplicity", here are the actual values of the endpoints of r_{54} and s_{54} (which are floating-point numbers with 53 bits of precision).

$$\underline{r_{54}} = \mathbf{0.786662839819061}59894492702733259648084640502929687 5,$$
$$\overline{r_{54}} = \mathbf{0.786662839819061}70996722948984825052320957183837890625,$$
$$\underline{s_{54}} = \mathbf{0.635014533102744}02763724310716497711837291717529296875,$$
$$\overline{s_{54}} = \mathbf{0.635014533102744}13865954556968063116073608398437 5.$$

The value of ϵ is a rational number, $\epsilon_{54} = \frac{449669}{142171195} \approx 0.00316$ (see Appendix 3.A). The intervals of edge lengths at the first step of the subdivision of the set of triangles with discs of radii $r_A = 1, r_B = r_{54}$, and $r_C = s_{54}$ are

$$a = [\underline{r_B} + \underline{r_C} + \epsilon_{54}, \overline{r_B} + \overline{r_C} + 2\,\overline{s_{54}}],$$
$$b = [\underline{r_A} + \underline{r_C} + \epsilon_{54}, \overline{r_A} + \overline{r_C} + 2\,\overline{s_{54}}],$$
$$c = [\underline{r_A} + \underline{r_B} + \epsilon_{54}, \overline{r_A} + \overline{r_B} + 2\,\overline{s_{54}}].$$

The width of each of these intervals is at least $2\overline{s_{54}} - \epsilon_{54} > 1.26686$. When we compute $\mathcal{A}, \mathcal{B}, \mathcal{C}$ with these values of a, b, c, r_A, r_B, r_C, we get the following intervals:

$$\mathcal{A} \approx [-613.97658, 3.97043]$$
$$\mathcal{B} \approx [-555.70041, 124.76024]$$
$$\mathcal{C} \approx [-258.06282, 692.81740].$$

They all, besides being extremely large, contain zero which is a problem when we try to compute R using (3.16).

After 5 steps of subdivision, the diameters of a, b, c are $2^5 = 32$ times smaller. Nevertheless, the diameters of $\mathcal{A}$, $\mathcal{B}$, $\mathcal{C}$ on some of the triplets of intervals attain 27, 35, and 68 respectively. None of the triplets give $\mathcal{A}$, $\mathcal{B}$ or $\mathcal{C}$ containing zero, but the value of R computed with (3.16) is not accurate enough... Let us explain how we resolve these issues, and what "accurate enough" means in this context.

Let us fix the disc radii r_A, r_B, and r_C. During the subdivision process, at each step, we are given a triplet of intervals representing the edge lengths a, b, and c. Let $T_{a\times b\times c}$ denote the set of triangles with edges contained in the mentioned intervals and with disc radii fixed above. Our aim is to compute an interval containing all values of radii

of support discs of triangles from $T_{a\times b\times c}$, and make this interval as small as possible (returning $[-\infty,\infty]$ would be of no help). We have the following possibilities.

If neither $\mathcal{A}$ nor $\mathcal{C}$ contain zero, then we use (3.16) to compute the value of the support disc radius.

Suppose that $0\in\mathcal{A}$ or $0\in\mathcal{C}$, i.e., $0\in\mathcal{A}\cdot\mathcal{C}$. Since the roots of an equation depend continuously on its coefficients, when $\mathcal{A}$ tends to 0, one of the roots tends to infinity, while the other, call it r_1, tends to $-\frac{\mathcal{C}}{\mathcal{B}}$.

$$r_1=\frac{-\mathcal{B}+\sqrt{\mathcal{B}^2-4\,\mathcal{A}\,\mathcal{C}}}{2\mathcal{A}}=-\frac{\mathcal{C}}{\mathcal{B}}\,f\left(\frac{4\mathcal{A}\,\mathcal{C}}{\mathcal{B}^2}\right), \tag{3.17}$$

where $f(x):=\frac{2}{x}\left(1-\sqrt{1-x}\right)$.

Let us set $f(0):=1$, then f is continuously derivable on $(-\infty,1)$. By the mean value theorem, for any $x<1$, there exists $\xi\in(0,x)$ such that $f(x)=1+xf'(\xi)$. f' is positive and increasing over $(-\infty,1)$ and $f'(0.78)<1$. If x is an interval which contains 0 and whose upper bound is at most 0.78, then

$$f(x)\subset 1+x\times f'((-\infty,0.78])\subset 1+x\times[0,1]=1+x.$$

Therefore,

$$R=-\frac{\mathcal{C}}{\mathcal{B}}\,f\left(\frac{4\,\mathcal{A}\,\mathcal{C}}{\mathcal{B}^2}\right)\subset-\frac{\mathcal{C}}{\mathcal{B}}\left(1+\frac{4\,\mathcal{A}\,\mathcal{C}}{\mathcal{B}^2}\right).$$

If $\mathcal{A}$ and $\mathcal{B}$ both contain 0, the above yields $R=[-\infty,\infty]$. Moreover if the upper bound of the interval $\frac{4\mathcal{A}\mathcal{C}}{\mathcal{B}^2}$ exceeds 0.78, we can not apply the above formula and also return $R=[-\infty,\infty]$. In practice, both cases only happen when the intervals $\mathcal{A}$, $\mathcal{B}$, $\mathcal{C}$ are rather large so we just continue subdivision when it happens.

Let us go back to our subdivision algorithm. If $T_{a\times b\times c}$ contains no FM-triangles, we do not need to check (T) on it. On the other hand, if at least one triangle in $T_{a\times b\times c}$ is an FM-triangle, we shall compare the potential with the emptiness and continue subdivision if the precision does not allow to conclude. The set $T_{a\times b\times c}$ contains no FM-triangles if the support radius of each of its triangle is greater than s. Therefore, in our algorithm, we compute the interval of the support disc radius as explained above and

- if it is strictly greater than s, we do not need to consider $T_{a\times b\times c}$,
- if it is equal to $[-\infty,\infty]$, we directly proceed to subdivision since the precision is not high enough,
- otherwise, test (T).

To resume, here are the function dedicated to the support disc parameters in our implementation. They all have arguments looking like `(a,b,c,ra,rb,rc)`. In our implementation, they are the parameters describing the triangle ABC such that $|AB|=$ `a`, $|AC|=$ `b`, $|AB|=$ `c`, $r_A=$ `ra`, $r_B=$ `rb`, $r_C=$ `rc`. Indeed, all of these arguments are intervals.

In `library/small_functions_ternary.sage`:

- `radius(a,b,c,ra,rb,rc)`: computes the constants $\mathcal{A},\mathcal{B},\mathcal{C}$ and returns the interval containing the set of radii of support discs of triangles from the box (all function arguments are intervals).

- `dist(a,b,c,ra,rb,rc,R)`: given a box of triangles and the interval `R` containing their support disc radii, returns the interval of signed distances d_e, where e corresponds to the edge of length `a`.

In `test_given_polyhedron.sage`:

- `test_triangle(a,b,c,ra,rb,rc)`: a step of the subdivision algorithm described above and in Section 3.5.1.

In all the cases treated in this chapter, the number of subdivision necessary to obtain a sufficient precision was small enough so that the time-cost of the subdivision algorithm was acceptable. Nevertheless, the precision of the interval expression strongly depends on the "size" and "complexity" of the formula. An analogous problem in 3 dimensions, for instance, yields truly gigantic formulas and we have to adapt them to optimize our code. Section 4.2.3 described the problems we encounter and our solutions in the 3-dimensional case.

3.6 Flip-and-flow method: proof of Theorem 3.2

Starting to work on the density of ternary saturated triangulated packings, we believed the Connelly conjecture to hold, i.e., that for all of the 149 cases, a triangulated packing would maximize the density. Realization that our proof strategy failed for many of them made us suspect the conjecture to be false. The density of binary triangulated packings (all of them are given in Figure 2.38 on page 42) often exceeds the density of the concerned ternary triangulated packing, this suggests us to use them in order to find counterexamples (i.e., cases having a non-triangulated packing which is denser than any triangulated one).

First, we obtained the result for case 110 [FP21]. After generalization, we ended up with 45 counterexamples (20, 25, 47, 51, 60, 63, 64, 70, 73, 80, 81, 84, 92, 95, 96, 97, 98, 99, 100, 104, 106, 110, 111, 117, 119, 126, 132, 133, 135, 136, 137, 138, 139, 141, 142, 151, 152, 153, 154, 159, 160, 161, 162, 163, 164). Each of these cases features a non-triangulated packing P' using only two discs out of three which has greater density than triangulated packings using all three discs. We obtained P' deforming a "dense" binary packing with discs whose size ratio is "close" to the one of a pair of discs in the triplet associated to the case. Tiny deformations do not dramatically lower the density and these packings are dense enough to outplay the ternary triangulated ones. The "dense" binary packings in question are the 9 triangulated packings (see Figure 2.38), as well as two non-triangulated packing corresponding to the packings with $r = r_c \approx 0.216845$ and $r = r_b \approx 0.369102$ from the r_9–1-flow in [Fer22] (Figures 7, 13) which are conjectured to be optimal. In this manuscript, we denote the packing with $r = r_c$ by b_A (Fig. 3.14) and the one with $r = r_b$ by b_B (Fig. 3.15).

Let us explain our method on an example. Recall that the pairs of discs allowing binary triangulated packings are denoted by $b_1, \ldots, b_9$ while the triplets with ternary triangulated packings are indexed by positive integers from 1 to 164. Let us consider case 73, its triangulated ternary packing is given in Figure 3.16, on the right. Notice that the radius of the small disc ($s_{73} \approx 0.264$) of case 73 is close to the radius of the small disc ($r_{b_7} \approx 0.281$) of case b_7. Let us deform the triangulated binary packing of b_7, P_{b_7} (Figure 3.16, on the left), replacing the small disc of b_7 by the smallest disc from case 73. We choose a deformation which breaks as few contacts between discs

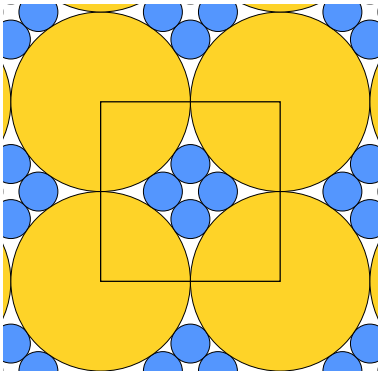

$\delta \approx 0.933122$ $r \approx 0.216845$

Figure 3.14: Packing b_A.

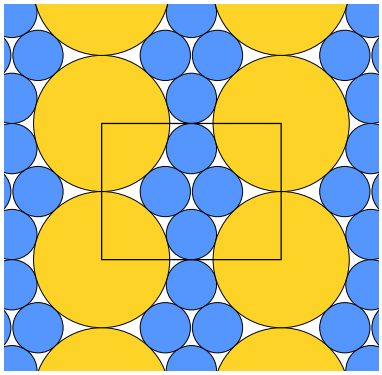

$\delta \approx 0.920350$ $r \approx 0.369102$

Figure 3.15: Packing b_B.

as possible: the one given in the center of Figure 3.16. Observe that the only broken contact is between the two small discs: they are not tangent anymore.

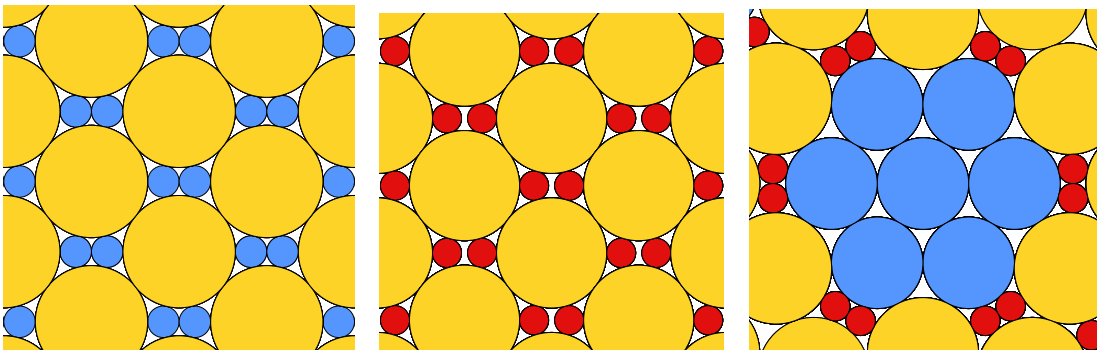

$\delta_{b_7} \approx 0.931901$ $r_{b_7} \approx 0.280776$ $\delta'_{73} \geq 0.924545$ $s_{73} \approx 0.263654$ $\delta_{73} \leq 0.920565$ $s_{73} \approx 0.263654$

Figure 3.16: Left: a triangulated binary packing of case b_7. Middle: a deformation where the small discs are replaced with the small discs of case 73. Right: a triangulated periodic packing of case 73, its fundamental domain and description are given in [FHS21].

To go further, this packing transformation, call it $P'(r)$, is defined for all $r \in (r_{b_8}, r_{b_7})$ in a way that $P'(r_{b_8}) = P_{b_8}$ and $P'(r_{b_7}) = P_{b_7}$: Figure 3.17 depicts the curve of its density when r varies from r_{b_8} to r_{b_7} and the local configurations defining the domain of $P'(r)$ for $r = r_{b_8}, s_{73}, r_{b_7}$. The density of the non-triangulated packing $P'(s_{73})$ is equal to $\delta'_{73} \approx 0.9245$, which is higher than the density of the triangulated packing of case 73 $\delta_{73} \approx 0.9206$ (Figure 3.16, on the right).

This method, introduced by Fejes Toth [FT64], is called *flip-and-flow* [CG21] and was used, e.g., in [CG21] to give a new original proof of the Koebe-Andreev-Thurston (KAT) theorem. It was also applied by Connelly and Pierre to construct, starting from a triangulated packing of case 53, a multi-disc packing strictly denser than $\frac{\pi}{2\sqrt{3}}$ of highest known uniformity ≈ 0.6585340820 [CP19], which gives a new lower bound on the critical uniformity value discussed in Section 2.2.2, page 34.

The 45 counterexamples were found by computer search. You can find the respective SageMath code in folder "`c`"[7].

[7] Of the project `https://github.com/tooticki/ternary_triangulated_disc_packings`.

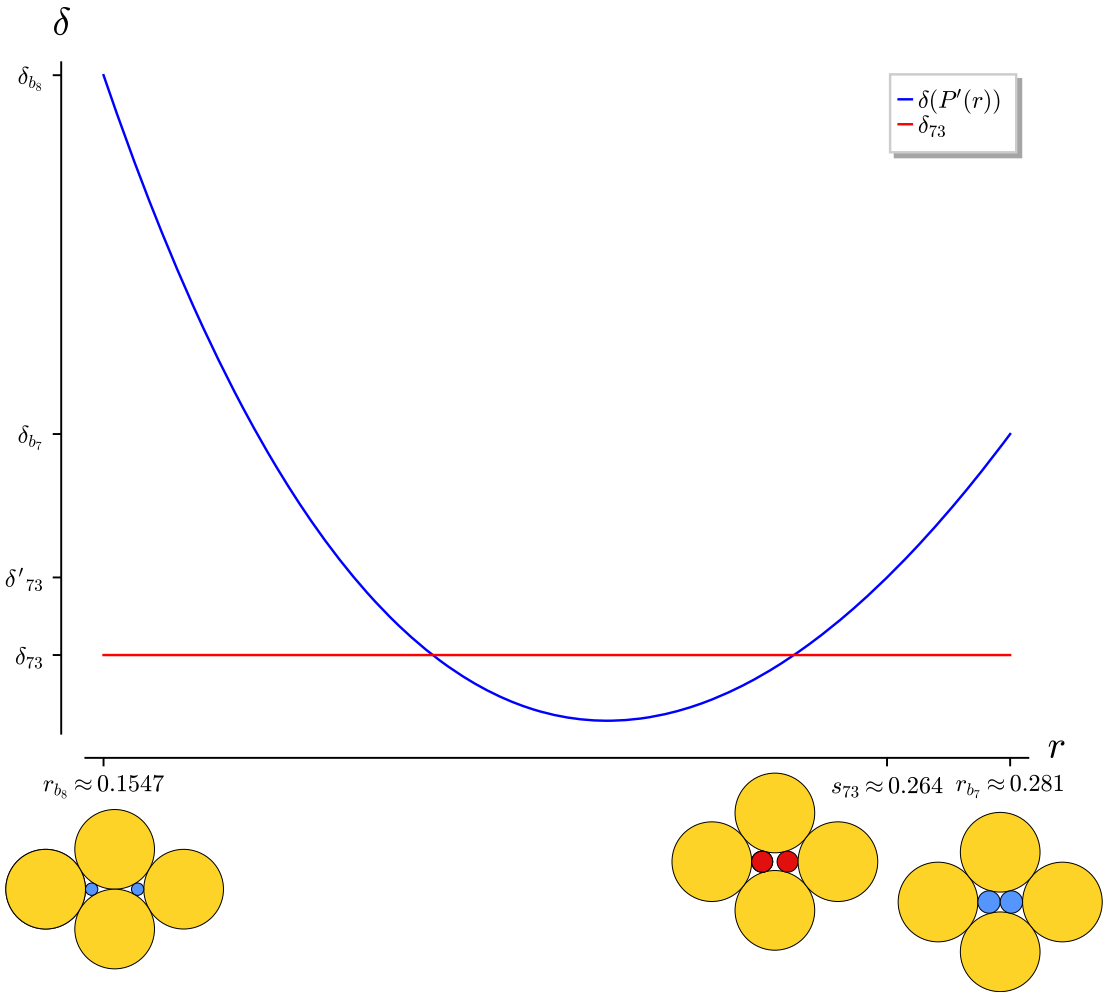

Figure 3.17: The density curve of the continuous deformation $P'(r)$ from P_{b_8} to P_{b_7} (in blue) and the density δ_{73} of the triangulated packing of case 73 (in red). The radii r_{b_8}, r_{b_7}, and s_{73} are indicated, as well as the densities of the corresponding packings, and the local configurations of their domains.

First, for each case b_i, $i \in \{1, 2, 3, 4, 5, 6, 7, 8, 9, A, B\}$, we find the set of pairs of radii from the cases 1-164 with radii ratio "close enough" (we choose the distance heuristically) to the ratio of the discs of b_i. Then we deform the triangulated packing of b_i to obtain packings with the found disc ratios. Our way to deform packings was chosen in order to minimize the number of broken contacts between discs since intuitively it is the best way to keep the density high. Finally, the densities of 45 packings obtained by our method were higher than the densities of the respective ternary triangulated packings which leaves us with the counterexamples given in Appendix 3.B.

Our method is not universal: there might be other deformations for certain cases to obtain even higher density and even more counterexamples. Besides that, there might be other cases with ternary counterexamples (notably, among the cases discussed in Sections 5.1.2).

3.A Constants to define potential

In this section, you will find the approximate values of radii r, s and the optimal density δ^* (Table 3.1), as well as the precise values of all the constants needed for construction of potentials (Section 3.2) for all the cases from Theorem 3.1.(a). The analogous constants for the cases from Theorem 3.1.(b) look the same, so we find it unnecessary to provide them here. In our code, these constants are represented as rational values (objects of the class `Rational` of SageMath [8]), so we give the rationals from our code together with their approximate values.

Table 3.2 gives the values of ϵ, m_1, m_r and m_s; Tables 3.3 – 3.7 contain the values of tight vertex potentials; Table 3.8 gives the values of Z_1, Z_r and Z_s for each of the cases; finally, Tables 3.9, 3.10 contain constants l_{xy}, q_{xy} necessary for edge potentials.

case	r	s	δ^*
53	≈ 0.834306	≈ 0.651050	≈ 0.909307
54	≈ 0.786663	≈ 0.635015	≈ 0.909751
55	≈ 0.840201	≈ 0.608673	≈ 0.910069
56	≈ 0.879994	≈ 0.616368	≈ 0.909417
66	≈ 0.593296	≈ 0.508858	≈ 0.912366
76	≈ 0.499692	≈ 0.445999	≈ 0.915933
77	≈ 0.793580	≈ 0.568863	≈ 0.909962
79	≈ 0.618034	≈ 0.500000	≈ 0.913512
93	≈ 0.691972	≈ 0.557834	≈ 0.911166
108	≈ 0.728440	≈ 0.246876	≈ 0.932968
115	≈ 0.656547	≈ 0.464102	≈ 0.915322
116	≈ 0.787963	≈ 0.561911	≈ 0.909855
118	≈ 0.373318	≈ 0.364082	≈ 0.922361
129	≈ 0.476679	≈ 0.400692	≈ 0.918324
131	≈ 0.548820	≈ 0.425011	≈ 0.917772
146	≈ 0.822210	≈ 0.468169	≈ 0.912961

Table 3.1: Values of r, s and δ^*.

[8] `https://doc.sagemath.org/html/en/reference/rings_standard/sage/rings/rational_field.html` (accessed on 15 July, 2023)

case	ϵ	m_1	m_r	m_s
53	$\frac{1176925}{68356306} \approx 0.01722$	$\frac{50009221}{140402798} \approx 0.35618$	$\frac{2723337}{120584098} \approx 0.02258$	$\frac{5778897}{86552789} \approx 0.06677$
54	$\frac{449669}{142171195} \approx 0.00316$	$\frac{16220096}{37462299} \approx 0.43297$	$\frac{1989773}{183380498} \approx 0.01085$	$\frac{4407140}{48865847} \approx 0.09019$
55	$\frac{1430441}{95953358} \approx 0.01491$	$\frac{36536515}{98111043} \approx 0.3724$	$\frac{7502427}{124941320} \approx 0.06005$	$\frac{3613575}{127342153} \approx 0.02838$
56	$\frac{3522811}{275838274} \approx 0.01277$	$\frac{35007429}{96878522} \approx 0.36135$	$\frac{8620837}{32474691} \approx 0.26546$	$\frac{2305766}{36698223} \approx 0.06283$
66	$\frac{2210033}{163362041} \approx 0.01353$	$\frac{33562513}{127939144} \approx 0.26233$	$\frac{5188877}{88290729} \approx 0.05877$	$\frac{3397775}{69036821} \approx 0.04922$
76	$\frac{362065}{57812223} \approx 0.00626$	$\frac{20087005}{71673617} \approx 0.28026$	$\frac{3440522}{65891241} \approx 0.05222$	$\frac{2108006}{61259231} \approx 0.03441$
77	$\frac{835841}{55422201} \approx 0.01508$	$\frac{13472513}{45345546} \approx 0.29711$	$\frac{32090601}{139541582} \approx 0.22997$	$\frac{5182207}{85150724} \approx 0.06086$
79	$\frac{1218999}{172212845} \approx 0.00708$	$\frac{15573983}{48806125} \approx 0.3191$	$\frac{2020488}{103164737} \approx 0.01959$	$\frac{162486112}{4004886337} \approx 0.04057$
93	$\frac{990864}{65825803} \approx 0.01505$	$\frac{21645656}{73723633} \approx 0.29361$	$\frac{2509939}{132639364} \approx 0.01892$	$\frac{6554705}{120244928} \approx 0.05451$
108	$\frac{463263}{273796114} \approx 0.00169$	$\frac{8042703}{52554113} \approx 0.15304$	$\frac{6661333}{63247809} \approx 0.10532$	$\frac{6533785}{316772726} \approx 0.02063$
115	$\frac{1485001}{190582571} \approx 0.00779$	$\frac{17140105}{55517858} \approx 0.30873$	$\frac{13760623}{87420078} \approx 0.15741$	$\frac{5828549}{570660224} \approx 0.01021$
116	$\frac{1604678}{222983443} \approx 0.0072$	$\frac{41108546}{112103317} \approx 0.3667$	$\frac{4381679}{88327076} \approx 0.04961$	$\frac{1511998}{29953323} \approx 0.05048$
118	$\frac{958156}{154157215} \approx 0.00622$	$\frac{5822445}{27531238} \approx 0.21149$	$\frac{6202654}{185006825} \approx 0.03353$	$\frac{1371904}{60754829} \approx 0.02258$
129	$\frac{206353}{98983426} \approx 0.00208$	$\frac{37104625}{133765674} \approx 0.27739$	$\frac{5171822}{60833819} \approx 0.08502$	$\frac{3476521}{100017909} \approx 0.03476$
131	$\frac{640718}{144691047} \approx 0.00443$	$\frac{17992279}{63112750} \approx 0.28508$	$\frac{5584157}{225168507} \approx 0.0248$	$\frac{1537939}{56005679} \approx 0.02746$
146	$\frac{371458}{161787115} \approx 0.0023$	$\frac{3863153}{12558197} \approx 0.30762$	$\frac{31997709}{136109947} \approx 0.23509$	$\frac{3787124}{59368599} \approx 0.06379$

Table 3.2: Values of ϵ, m_1, m_r and m_s.

case	V_{111}	V_{11r}	V_{11s}	V_{1r1}
53	$\frac{325800}{234459689} \approx 0.00139$	$\frac{8450}{14058009} \approx 0.0006$	$\frac{-44077}{55145732} \approx -0.0008$	$\frac{228442}{149065815} \approx 0.00153$
54	$\frac{221590}{134610741} \approx 0.00165$	$\frac{305261}{228284146} \approx 0.00134$	$\frac{-35117}{77201001} \approx -0.00045$	$\frac{-5542}{71941269} \approx -0.00008$
55	$\frac{285409}{155963734} \approx 0.00183$	$\frac{97329}{60319375} \approx 0.00161$	$\frac{-72382}{97528051} \approx -0.00074$	$\frac{94720}{122717157} \approx 0.00077$
56	$\frac{319653}{219975310} \approx 0.00145$	$\frac{221537}{184495490} \approx 0.0012$	$\frac{-459270}{254004089} \approx -0.00181$	$\frac{282177}{255349169} \approx 0.00111$
66	$\frac{400733}{126975027} \approx 0.00316$	$\frac{20691}{166089520} \approx 0.00012$	$\frac{-96408}{83839007} \approx -0.00115$	$\frac{32805}{101120917} \approx 0.00032$
76	$\frac{720365}{138125036} \approx 0.00522$	$\frac{89309}{205526609} \approx 0.00043$	$\frac{-183014}{294273939} \approx -0.00062$	$\frac{-30576}{89509279} \approx -0.00034$
77	$\frac{190519}{107767687} \approx 0.00177$	$\frac{45736}{157543341} \approx 0.00029$	$\frac{-259715}{162116084} \approx -0.0016$	$\frac{231709}{94151727} \approx 0.00246$
79	$\frac{109802}{28764067} \approx 0.00382$	$\frac{160296}{131495735} \approx 0.00122$	$\frac{-134122}{176626739} \approx -0.00076$	$\frac{46503}{87937561} \approx 0.00053$
93	$\frac{278266}{112961577} \approx 0.00246$	$\frac{106484}{94812843} \approx 0.00112$	$\frac{-84340}{137168963} \approx -0.00061$	$\frac{17127}{167614025} \approx 0.0001$
108	$\frac{1712470}{113781947} \approx 0.01505$	$\frac{3145159}{250664382} \approx 0.01255$	$\frac{-63946}{216987907} \approx -0.00029$	$\frac{1009093}{112353585} \approx 0.00898$
115	$\frac{430411}{88511059} \approx 0.00486$	$\frac{-248219}{335882942} \approx -0.00074$	$\frac{-271443}{205697434} \approx -0.00132$	$\frac{1243127}{150835383} \approx 0.00824$
116	$\frac{208593}{122244688} \approx 0.00171$	$\frac{257001}{203680337} \approx 0.00126$	$\frac{-16280}{11902133} \approx -0.00137$	$\frac{41498}{163939003} \approx 0.00025$
118	$\frac{508783}{56995879} \approx 0.00893$	$\frac{67074}{130886983} \approx 0.00051$	$\frac{26999}{197736313} \approx 0.00014$	$\frac{-347012}{209313319} \approx -0.00166$
129	$\frac{3713401}{562975123} \approx 0.0066$	$\frac{-23162}{139424585} \approx -0.00017$	$\frac{-127980}{126173933} \approx -0.00101$	$\frac{177478}{79231899} \approx 0.00224$
131	$\frac{1111537}{177076737} \approx 0.00628$	$\frac{161389}{96696960} \approx 0.00167$	$\frac{-90281}{126648235} \approx -0.00071$	$\frac{224340}{123990893} \approx 0.00181$
146	$\frac{356161}{101766861} \approx 0.0035$	$\frac{-79406}{104522365} \approx -0.00076$	$\frac{6173}{53897140} \approx 0.00011$	$\frac{901496}{93547789} \approx 0.00964$

Table 3.3: Values of V_{111}, V_{11r}, V_{11s}, V_{1r1}.

case	V_{1rr}	V_{1rs}	V_{1s1}	V_{1sr}
53	$\frac{2015}{461472577} \approx 0.0$	$\frac{-841}{385209367} \approx -2 \times 10^{-6}$	$\frac{29895}{117760993} \approx 0.00025$	$\frac{-9163}{144377853} \approx -0.00006$
54	$\frac{11723}{118621886} \approx 0.0001$	0	$\frac{-26122}{74203063} \approx -0.00035$	$\frac{11980}{136123221} \approx 0.00009$
55	$\frac{12997}{119896940} \approx 0.00011$	$\frac{-47360}{122717157} \approx -0.00039$	$\frac{-33871}{136659263} \approx -0.00025$	$\frac{45221}{147968582} \approx 0.00031$
56	$\frac{41924}{53103455} \approx 0.00079$	$\frac{-83848}{53103455} \approx -0.00158$	$\frac{97477}{73891281} \approx 0.00132$	$\frac{2441}{31787918} \approx 0.00008$
66	$\frac{-458671}{336688979} \approx -0.00136$	$\frac{-376887}{178071748} \approx -0.00212$	$\frac{-161987}{221779564} \approx -0.00073$	$\frac{-25935}{92158198} \approx -0.00028$
76	$\frac{11308}{124364429} \approx 0.00009$	$\frac{-66288}{161407103} \approx -0.00041$	$\frac{-90435}{79289233} \approx -0.00114$	$\frac{-437105}{1406951977} \approx -0.00031$
77	$\frac{-48674}{111111885} \approx -0.00044$	$\frac{-176579}{120382941} \approx -0.00147$	$\frac{-9689}{90618281} \approx -0.00011$	$\frac{246465}{613518902} \approx 0.0004$
79	$\frac{-168203}{172173716} \approx -0.00098$	$\frac{-206167}{223817379} \approx -0.00092$	$\frac{-51941}{80531422} \approx -0.00064$	$\frac{-13241}{69020401} \approx -0.00019$
93	$\frac{-16579}{69323586} \approx -0.00024$	$\frac{-39910}{122250733} \approx -0.00033$	$\frac{-134819}{126390553} \approx -0.00107$	$\frac{-31856}{112924549} \approx -0.00028$
108	$\frac{360391}{108743242} \approx 0.00331$	0	$\frac{-210581}{147579697} \approx -0.00143$	$\frac{45359}{169141739} \approx 0.00027$
115	$\frac{-42045}{31968808} \approx -0.00132$	0	$\frac{43766}{71667503} \approx 0.00061$	$\frac{-25909}{123189230} \approx -0.00021$
116	$\frac{20589}{105666682} \approx 0.00019$	$\frac{-31499}{93181102} \approx -0.00034$	$\frac{-100201}{103356994} \approx -0.00097$	$\frac{-8631}{91551974} \approx -0.00009$
118	$\frac{-77931}{132766843} \approx -0.00059$	$\frac{-81394}{98460005} \approx -0.00083$	$\frac{-317694}{203107049} \approx -0.00156$	$\frac{6291}{126248248} \approx 0.00005$
129	$\frac{-19019}{76340749} \approx -0.00025$	$\frac{-588290}{270898663} \approx -0.00217$	$\frac{-77871}{120358175} \approx -0.00065$	$\frac{88658}{73048147} \approx 0.00121$
131	$\frac{-36851}{95665223} \approx -0.00039$	$\frac{-29129}{24406939} \approx -0.00119$	$\frac{-29633}{100839283} \approx -0.00029$	$\frac{36758}{189517691} \approx 0.00019$
146	$\frac{97314}{68894261} \approx 0.00141$	$\frac{-16481}{77215330} \approx -0.00021$	$\frac{-481585}{105245161} \approx -0.00458$	$\frac{-62725}{138865036} \approx -0.00045$

Table 3.4: Values of V_{1rr},V_{1rs},V_{1s1},V_{1sr}.

case	V_{1ss}	V_{r1r}	V_{r1s}	V_{rrr}
53	$\frac{-35358}{161085143} \approx -0.00022$	$\frac{190076}{79041785} \approx 0.0024$	$\frac{-33953}{168461726} \approx -0.0002$	$\frac{140743}{145510097} \approx 0.00097$
54	$\frac{10922}{94983467} \approx 0.00011$	$\frac{132856}{66619687} \approx 0.00199$	$\frac{-23945}{130065379} \approx -0.00018$	$\frac{42041}{41269131} \approx 0.00102$
55	$\frac{-3533}{19445512} \approx -0.00018$	$\frac{459316}{137727463} \approx 0.00333$	$\frac{-44657}{122465127} \approx -0.00036$	$\frac{110413}{85469164} \approx 0.00129$
56	$\frac{-36476}{49533695} \approx -0.00074$	$\frac{104639}{63906459} \approx 0.00164$	$\frac{46580}{141507769} \approx 0.00033$	$\frac{293001}{260378075} \approx 0.00113$
66	$\frac{-97509}{140032160} \approx -0.0007$	$\frac{339340}{113715011} \approx 0.00298$	$\frac{177451}{154316194} \approx 0.00115$	$\frac{88543}{79702982} \approx 0.00111$
76	$\frac{-56271}{40214185} \approx -0.0014$	$\frac{-12446}{116364225} \approx -0.00011$	$\frac{-30449}{123196648} \approx -0.00025$	$\frac{662599}{508822613} \approx 0.0013$
77	$\frac{-143331}{145136567} \approx -0.00099$	$\frac{173023}{49950800} \approx 0.00346$	$\frac{-72642}{172870465} \approx -0.00042$	$\frac{156403}{140479662} \approx 0.00111$
79	$\frac{-380667}{488395735} \approx -0.00078$	$\frac{266905}{66939231} \approx 0.00399$	$\frac{130009}{171210284} \approx 0.00076$	$\frac{195307}{133947043} \approx 0.00146$
93	$\frac{-30073}{119633949} \approx -0.00025$	$\frac{379508}{168564927} \approx 0.00225$	$\frac{1}{9007199254740991} \approx 10^{-16}$	$\frac{258797}{219408033} \approx 0.00118$
108	$\frac{-45359}{169141739} \approx -0.00027$	$\frac{1409001}{67336003} \approx 0.02092$	$\frac{64269}{149285749} \approx 0.00043$	$\frac{816111}{102190966} \approx 0.00799$
115	$\frac{-10669}{34044866} \approx -0.00031$	$\frac{1034003}{135085043} \approx 0.00765$	$\frac{95638}{211445847} \approx 0.00045$	$\frac{153766}{73357269} \approx 0.0021$
116	$\frac{-31882}{191426077} \approx -0.00017$	$\frac{194292}{99227183} \approx 0.00196$	$\frac{-249115}{186512183} \approx -0.00134$	$\frac{122803}{115911904} \approx 0.00106$
118	$\frac{-36763}{161196872} \approx -0.00023$	$\frac{272131}{684308614} \approx 0.0004$	$\frac{-22952}{128564457} \approx -0.00018$	$\frac{317747}{255407287} \approx 0.00124$
129	$\frac{-71301}{71847074} \approx -0.00099$	$\frac{98909}{71816183} \approx 0.00138$	$\frac{19365}{120011999} \approx 0.00016$	$\frac{748954}{499712669} \approx 0.0015$
131	$\frac{-229951}{873803917} \approx -0.00026$	$\frac{523029}{129646253} \approx 0.00403$	$\frac{279108}{226956251} \approx 0.00123$	$\frac{116929}{61844441} \approx 0.00189$
146	$\frac{-64128}{79251067} \approx -0.00081$	$\frac{361927}{84421144} \approx 0.00429$	$\frac{-400293}{269722016} \approx -0.00148$	$\frac{303815}{128411542} \approx 0.00237$

Table 3.5: Values of V_{1ss},V_{r1r},V_{r1s}, V_{rrr}.

case	V_{rrs}	V_{rsr}	V_{rss}	V_{s1s1}
53	$\frac{12290}{202836989} \approx 0.00006$	$\frac{149873}{130786347} \approx 0.00115$	$\frac{70509}{261033953} \approx 0.00027$	$\frac{-117143}{175859932} \approx -0.00067$
54	$\frac{49927}{131454735} \approx 0.00038$	$\frac{161194}{149168351} \approx 0.00108$	$\frac{36473}{83527086} \approx 0.00044$	$\frac{-156645}{123306533} \approx -0.00127$
55	$\frac{-14997}{78345814} \approx -0.00019$	$\frac{243568}{154153245} \approx 0.00158$	$\frac{173997}{309816554} \approx 0.00056$	$\frac{-47736}{47100665} \approx -0.00101$
56	$\frac{-83313}{77623709} \approx -0.00107$	$\frac{361334}{157962623} \approx 0.00229$	$\frac{-45091}{110834336} \approx -0.00041$	$\frac{-22623}{71399158} \approx -0.00032$
66	$\frac{98197}{92792330} \approx 0.00106$	$\frac{54372}{84086939} \approx 0.00065$	$\frac{-131834}{188384931} \approx -0.0007$	$\frac{-98813}{124759400} \approx -0.00079$
76	$\frac{-260869}{174158492} \approx -0.0015$	$\frac{1101389}{168921922} \approx 0.00652$	$\frac{58003}{65840626} \approx 0.00088$	$\frac{80002}{75294417} \approx 0.00106$
77	$\frac{6169}{113536204} \approx 0.00005$	$\frac{108281}{145300834} \approx 0.00075$	$\frac{-34239}{98313617} \approx -0.00035$	$\frac{-12935}{27218102} \approx -0.00048$
79	$\frac{133633}{125651947} \approx 0.00106$	$\frac{207584}{175012059} \approx 0.00119$	$\frac{57897}{112567619} \approx 0.00051$	$\frac{-6993}{103226699} \approx -0.00007$
93	$\frac{79820}{122250733} \approx 0.00065$	$\frac{43955}{38953404} \approx 0.00113$	$\frac{52084}{97335443} \approx 0.00054$	$\frac{-399771}{321879676} \approx -0.00124$
108	$\frac{17846}{125484417} \approx 0.00014$	$\frac{789230}{256552447} \approx 0.00308$	$\frac{96765}{78641753} \approx 0.00123$	$\frac{-128538}{149285749} \approx -0.00086$
115	$\frac{29841}{37660900} \approx 0.00079$	$\frac{362267}{173635633} \approx 0.00209$	$\frac{100863}{43789414} \approx 0.0023$	$\frac{-290653}{321302044} \approx -0.0009$
116	$\frac{10390}{122364981} \approx 0.00008$	$\frac{159959}{306641349} \approx 0.00052$	$\frac{37693}{177552229} \approx 0.00021$	$\frac{-200347}{84326664} \approx -0.00238$
118	$\frac{146262}{88343789} \approx 0.00166$	$\frac{144048}{404101739} \approx 0.00036$	$\frac{118777}{131156670} \approx 0.00091$	$\frac{-63376}{94893531} \approx -0.00067$
129	$\frac{132005}{48089318} \approx 0.00274$	$\frac{-158827}{94454912} \approx -0.00168$	$\frac{172970}{98083033} \approx 0.00176$	$\frac{14775}{129686839} \approx 0.00011$
131	$\frac{114850}{86568393} \approx 0.00133$	$\frac{276603}{173111228} \approx 0.0016$	$\frac{125760}{211174267} \approx 0.0006$	$\frac{-91660}{111799787} \approx -0.00082$
146	$\frac{-34578}{77471381} \approx -0.00045$	$\frac{180797}{161268425} \approx 0.00112$	$\frac{51295}{122046411} \approx 0.00042$	$\frac{-34131}{25876985} \approx -0.00132$

Table 3.6: Values of V_{rrs}, V_{rsr}, V_{rss}, V_{s1s}.

case	V_{srs}	V_{sss}
53	$\frac{68089}{131604127} \approx 0.00052$	$\frac{77103}{130905968} \approx 0.00059$
54	$\frac{72867}{102301427} \approx 0.00071$	$\frac{93415}{140727459} \approx 0.00066$
55	$\frac{-21050}{110628619} \approx -0.00019$	$\frac{110723}{163314821} \approx 0.00068$
56	$\frac{62105}{70710634} \approx 0.00088$	$\frac{72277}{130922752} \approx 0.00055$
66	$\frac{252345}{64841051} \approx 0.00389$	$\frac{99573}{121845916} \approx 0.00082$
76	$\frac{91831}{61034786} \approx 0.0015$	$\frac{95283}{91847546} \approx 0.00104$
77	$\frac{15285}{11332879} \approx 0.00135$	$\frac{60289}{105383418} \approx 0.00057$
79	$\frac{458551}{248904245} \approx 0.00184$	$\frac{54901}{57528134} \approx 0.00095$
93	$\frac{129173}{125324272} \approx 0.00103$	$\frac{99221}{129438647} \approx 0.00077$
108	$\frac{-208886}{196064373} \approx -0.00107$	$\frac{172935}{188528048} \approx 0.00092$
115	$\frac{-154770}{90170989} \approx -0.00172$	$\frac{119516}{114107467} \approx 0.00105$
116	$\frac{14073}{148491065} \approx 0.00009$	$\frac{59837}{111062057} \approx 0.00054$
118	$\frac{206683}{115099670} \approx 0.0018$	$\frac{186437}{157559831} \approx 0.00118$
129	$\frac{-8461}{61887604} \approx -0.00014$	$\frac{93525}{88312762} \approx 0.00106$
131	$\frac{669571}{280513896} \approx 0.00239$	$\frac{30467}{26869926} \approx 0.00113$
146	$\frac{-108771}{136069163} \approx -0.0008$	$\frac{114432}{149176991} \approx 0.00077$

Table 3.7: Values of V_{srs}, V_{sss}.

case	Z_1	Z_r	Z_s
53	$\frac{5547783}{1016513968} \approx 0.00546$	$\frac{87498}{6515591413} \approx 0.00001$	$\frac{872521}{737330825} \approx 0.00118$
54	$\frac{4470609}{446813636} \approx 0.01001$	$\frac{1863088}{4573000465} \approx 0.00041$	$\frac{12392495}{7374229959} \approx 0.00168$
55	$\frac{12333423}{1503089954} \approx 0.00821$	$\frac{1649215}{677606586} \approx 0.00243$	$\frac{1270051}{1094182731} \approx 0.00116$
56	$\frac{10286053}{818253879} \approx 0.01257$	$\frac{14800809}{1453457467} \approx 0.01018$	$\frac{1915557}{488348444} \approx 0.00392$
66	$\frac{6845597}{801849216} \approx 0.00854$	$\frac{19322116}{1651817877} \approx 0.0117$	$\frac{6620199}{1642448210} \approx 0.00403$
76	$\frac{4433985}{915869126} \approx 0.00484$	$\frac{9236227}{995212354} \approx 0.00928$	$\frac{11262135}{1610483246} \approx 0.00699$
77	$\frac{11979320}{1046892327} \approx 0.01144$	$\frac{11331593}{1238106420} \approx 0.00915$	$\frac{6033870}{1166652607} \approx 0.00517$
79	$\frac{13143319}{2316930818} \approx 0.00567$	$\frac{4870315}{931660748} \approx 0.00523$	$\frac{10563769}{2655274324} \approx 0.00398$
93	$\frac{13908709}{1305432088} \approx 0.01065$	$\frac{6707496}{3527620691} \approx 0.0019$	$\frac{4100196}{852802091} \approx 0.00481$
108	$\frac{9893852}{729015949} \approx 0.01357$	$\frac{9747109}{745245698} \approx 0.01308$	$\frac{6527441}{1355138972} \approx 0.00482$
115	$\frac{11588560}{1144562923} \approx 0.01012$	$\frac{6560174}{519478339} \approx 0.01263$	$\frac{1979429}{1254838475} \approx 0.00158$
116	$\frac{11377688}{560976519} \approx 0.02028$	$\frac{3043973}{1443240895} \approx 0.00211$	$\frac{3121473}{712106975} \approx 0.00438$
118	$\frac{11854605}{1526525473} \approx 0.00777$	$\frac{1267863}{198551150} \approx 0.00639$	$\frac{6160097}{1031524625} \approx 0.00597$
129	$\frac{3417512}{415958631} \approx 0.00822$	$\frac{11256793}{973018526} \approx 0.01157$	$\frac{72283899}{7859259836} \approx 0.0092$
131	$\frac{8677771}{1020378230} \approx 0.0085$	$\frac{35765401}{5337842584} \approx 0.0067$	$\frac{3798669}{2912914612} \approx 0.0013$
146	$\frac{11256934}{881683437} \approx 0.01277$	$\frac{10169426}{1503499293} \approx 0.00676$	$\frac{16233280}{846128987} \approx 0.01919$

Table 3.8: Values of Z_1, Z_r and Z_s.

case	l_{11}	q_{11}	l_{1r}	q_{1r}	l_{1s}	q_{1s}
53	$\frac{122887477}{40707363} \approx 3.019$	$\frac{36063139}{175953552} \approx 0.205$	$\frac{153036360}{53813723} \approx 2.844$	$\frac{37151497}{201440901} \approx 0.184$	$\frac{440137099}{167091278} \approx 2.634$	$\frac{26365359}{162923057} \approx 0.162$
54	$\frac{144602498}{48435237} \approx 2.985$	$\frac{64432549}{309393877} \approx 0.208$	$\frac{161775829}{58553208} \approx 2.763$	$\frac{13893556}{76637871} \approx 0.181$	$\frac{130928785}{50604081} \approx 2.587$	$\frac{4707306}{28981111} \approx 0.162$
55	$\frac{520918957}{176285283} \approx 2.955$	$\frac{41325099}{200755723} \approx 0.206$	$\frac{264654327}{94918037} \approx 2.788$	$\frac{33139461}{178251898} \approx 0.186$	$\frac{843891525}{333844051} \approx 2.528$	$\frac{36564268}{233543255} \approx 0.157$
56	$\frac{65464642}{22195283} \approx 2.949$	$\frac{82763964}{393543307} \approx 0.21$	$\frac{110056493}{39011858} \approx 2.821$	$\frac{39028723}{198603379} \approx 0.197$	$\frac{37299106}{14743685} \approx 2.53$	$\frac{50682751}{312538746} \approx 0.162$
66	$\frac{126000004}{44823185} \approx 2.811$	$\frac{134417147}{649138259} \approx 0.207$	$\frac{129800925}{55057958} \approx 2.358$	$\frac{9764904}{60006565} \approx 0.163$	$\frac{59231467}{26062322} \approx 2.273$	$\frac{40504590}{269293583} \approx 0.15$
76	$\frac{97734709}{35836430} \approx 2.727$	$\frac{24776776}{120020051} \approx 0.206$	$\frac{77646770}{35762171} \approx 2.171$	$\frac{43760805}{319985389} \approx 0.137$	$\frac{87960415}{41646409} \approx 2.112$	$\frac{58264792}{449879835} \approx 0.13$
77	$\frac{164794171}{57121431} \approx 2.885$	$\frac{38573693}{181698045} \approx 0.212$	$\frac{36233033}{13610248} \approx 2.662$	$\frac{37614593}{199494490} \approx 0.189$	$\frac{125285793}{51976274} \approx 2.41$	$\frac{34684010}{219346553} \approx 0.158$
79	$\frac{155167258}{55275125} \approx 2.807$	$\frac{87804263}{429142895} \approx 0.205$	$\frac{71793224}{30016993} \approx 2.392$	$\frac{30562177}{185559317} \approx 0.165$	$\frac{941388757}{417028927} \approx 2.257$	$\frac{17614232}{119191337} \approx 0.148$
93	$\frac{144613219}{50326656} \approx 2.873$	$\frac{57199727}{274472355} \approx 0.208$	$\frac{218643183}{85824800} \approx 2.548$	$\frac{26090691}{151093628} \approx 0.173$	$\frac{124057339}{51967183} \approx 2.387$	$\frac{32179951}{206333241} \approx 0.156$
108	$\frac{188829973}{79254190} \approx 2.383$	$\frac{33122992}{168798743} \approx 0.196$	$\frac{39557547}{18859747} \approx 2.097$	$\frac{62400631}{338932373} \approx 0.184$	$\frac{174355673}{113087668} \approx 1.542$	$\frac{55395017}{477490923} \approx 0.116$
115	$\frac{139033605}{50619592} \approx 2.747$	$\frac{20033812}{93174913} \approx 0.215$	$\frac{73452396}{30988195} \approx 2.37$	$\frac{31926849}{179957882} \approx 0.177$	$\frac{104093996}{47984647} \approx 2.169$	$\frac{38050195}{263326192} \approx 0.144$
116	$\frac{106818504}{37489597} \approx 2.849$	$\frac{91804390}{423011039} \approx 0.217$	$\frac{223507076}{84513865} \approx 2.645$	$\frac{62579252}{337289387} \approx 0.186$	$\frac{244274543}{102677534} \approx 2.379$	$\frac{19608819}{124344491} \approx 0.158$
118	$\frac{100319327}{38614070} \approx 2.598$	$\frac{50591426}{249305625} \approx 0.203$	$\frac{1139523769}{596151925} \approx 1.911$	$\frac{66781865}{538663366} \approx 0.124$	$\frac{203027362}{106792337} \approx 1.901$	$\frac{44912349}{370316191} \approx 0.121$
129	$\frac{153840087}{58135976} \approx 2.646$	$\frac{39107195}{184538834} \approx 0.212$	$\frac{84931345}{41170823} \approx 2.063$	$\frac{32755877}{221179109} \approx 0.148$	$\frac{195434858}{98921391} \approx 1.976$	$\frac{37537039}{267782368} \approx 0.14$
131	$\frac{87969797}{32646391} \approx 2.695$	$\frac{68033951}{331880125} \approx 0.205$	$\frac{128397317}{58109788} \approx 2.21$	$\frac{20501610}{128070641} \approx 0.16$	$\frac{165624427}{79756741} \approx 2.077$	$\frac{42189726}{304773269} \approx 0.138$
146	$\frac{263421415}{97096977} \approx 2.713$	$\frac{60705780}{273915401} \approx 0.222$	$\frac{235033573}{92860644} \approx 2.531$	$\frac{62291313}{314109136} \approx 0.198$	$\frac{117747313}{56737175} \approx 2.075$	$\frac{105958602}{755404415} \approx 0.14$

Table 3.9: Values of l_{11} , q_{11} , l_{1r} , q_{1r} , l_{1s} , q_{1s}.

case	l_{rr}	q_{rr}	l_{rs}	q_{rs}	l_{ss}	q_{ss}
53	$\frac{146016811}{54690215} \approx 2.67$	$\frac{4096339}{24776437} \approx 0.165$	$\frac{782530847}{317943970} \approx 2.461$	$\frac{26773183}{185158171} \approx 0.145$	$\frac{96780371}{42971281} \approx 2.252$	$\frac{28543911}{226202021} \approx 0.126$
54	$\frac{60310108}{23719495} \approx 2.543$	$\frac{43125089}{276201258} \approx 0.156$	$\frac{170345773}{71916703} \approx 2.369$	$\frac{88238971}{634245231} \approx 0.139$	$\frac{138040269}{62907019} \approx 2.194$	$\frac{45440513}{367352490} \approx 0.124$
55	$\frac{112186724}{42776559} \approx 2.623$	$\frac{63480209}{379095202} \approx 0.167$	$\frac{14860273}{6286496} \approx 2.364$	$\frac{8173477}{58167309} \approx 0.141$	$\frac{233310341}{110792569} \approx 2.106$	$\frac{40980621}{348755996} \approx 0.118$
56	$\frac{481731067}{178868593} \approx 2.693$	$\frac{54028977}{294394229} \approx 0.184$	$\frac{163694347}{68115334} \approx 2.403$	$\frac{48141941}{318551383} \approx 0.151$	$\frac{138459840}{65423293} \approx 2.116$	$\frac{109269544}{884469033} \approx 0.124$
66	$\frac{152279521}{80078708} \approx 1.902$	$\frac{35291716}{270098819} \approx 0.131$	$\frac{135939221}{74668172} \approx 1.821$	$\frac{52132680}{442016441} \approx 0.118$	$\frac{442326973}{254105991} \approx 1.741$	$\frac{47797650}{452590531} \approx 0.106$
76	$\frac{96225987}{59783998} \approx 1.61$	$\frac{14851185}{138012272} \approx 0.108$	$\frac{509154632}{328140815} \approx 1.552$	$\frac{31097827}{308117949} \approx 0.101$	$\frac{148460861}{99352783} \approx 1.494$	$\frac{267276715}{2834456719} \approx 0.094$
77	$\frac{186052809}{76238510} \approx 2.44$	$\frac{243872900}{1457968763} \approx 0.167$	$\frac{102145359}{46637669} \approx 2.19$	$\frac{44161835}{315681436} \approx 0.14$	$\frac{595306739}{306523636} \approx 1.942$	$\frac{50651141}{435432613} \approx 0.116$
79	$\frac{210517627}{106440533} \approx 1.978$	$\frac{34227509}{264911014} \approx 0.129$	$\frac{104870234}{56865111} \approx 1.844$	$\frac{32376804}{281526583} \approx 0.115$	$\frac{331147203}{193535537} \approx 1.711$	$\frac{12114009}{118796042} \approx 0.102$
93	$\frac{122262149}{54925112} \approx 2.226$	$\frac{18215153}{130862725} \approx 0.139$	$\frac{67001293}{32411291} \approx 2.067$	$\frac{48314789}{386657713} \approx 0.125$	$\frac{301685771}{158194087} \approx 1.907$	$\frac{7454803}{66503398} \approx 0.112$
108	$\frac{164213875}{90547243} \approx 1.814$	$\frac{53574944}{313296961} \approx 0.171$	$\frac{117840011}{92867908} \approx 1.269$	$\frac{49832181}{508651126} \approx 0.098$	$\frac{15921239}{20416244} \approx 0.78$	$\frac{9489688}{170559065} \approx 0.056$
115	$\frac{238490613}{119668352} \approx 1.993$	$\frac{41251195}{279934443} \approx 0.147$	$\frac{97926977}{54528588} \approx 1.796$	$\frac{23392187}{195892195} \approx 0.119$	$\frac{68152917}{42492803} \approx 1.604$	$\frac{21790754}{229473837} \approx 0.095$
116	$\frac{144102773}{58993321} \approx 2.443$	$\frac{73380703}{468753732} \approx 0.157$	$\frac{139305755}{63804638} \approx 2.183$	$\frac{29476792}{223446385} \approx 0.132$	$\frac{110179927}{57306167} \approx 1.923$	$\frac{36531203}{328450085} \approx 0.111$
118	$\frac{69641289}{56650622} \approx 1.229$	$\frac{31120883}{445224486} \approx 0.07$	$\frac{157807226}{129393583} \approx 1.22$	$\frac{37421237}{540555844} \approx 0.069$	$\frac{81610731}{67450754} \approx 1.21$	$\frac{7614668}{111157925} \approx 0.069$
129	$\frac{695177333}{472448058} \approx 1.471$	$\frac{19863027}{176481965} \approx 0.113$	$\frac{34344403}{24795737} \approx 1.385$	$\frac{49541377}{482731705} \approx 0.103$	$\frac{310335832}{238716969} \approx 1.3$	$\frac{19813692}{212786341} \approx 0.093$
131	$\frac{168534939}{97536515} \approx 1.728$	$\frac{97729027}{820646206} \approx 0.119$	$\frac{88812143}{55564158} \approx 1.598$	$\frac{24352847}{239573736} \approx 0.102$	$\frac{128865459}{87609652} \approx 1.471$	$\frac{39095936}{455466053} \approx 0.086$
146	$\frac{77157958}{32821039} \approx 2.351$	$\frac{57771755}{331924753} \approx 0.174$	$\frac{148814280}{78220753} \approx 1.902$	$\frac{36585601}{291039079} \approx 0.126$	$\frac{93114473}{69420828} \approx 1.341$	$\frac{19407904}{159765287} \approx 0.121$

Table 3.10: Values of l_{rr}, q_{rr} , l_{rs}, q_{rs} , l_{ss}, q_{ss}.

3.B Counterexamples

In this section, we give the 45 counterexamples, discussed in Section 3.6. They are grouped according to the binary case used in their construction (the list of binary triangulated packings is given in Fig. 2.38). Each counterexample is presented as in Fig. 3.16: to the left, we give the deformed binary packing using a pair of discs whose radii ratio is close to the one of the binary triangulated packing; to the right, the triangulated ternary packings.

Counter examples derived from b1

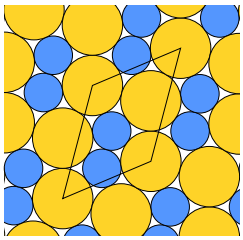

$\delta \approx 0.910683$ $r \approx 0.637556$

b1

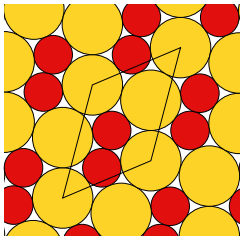

$\delta \geq 0.910497$ $s \approx 0.637945$

51 counter example

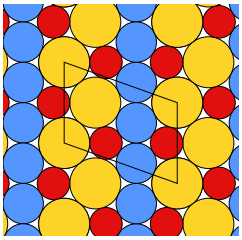

$\delta \leq 0.909503$ $s \approx 0.637945$

51 triangulated

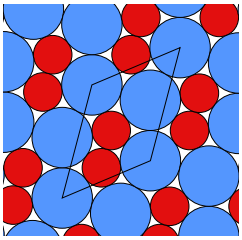

$\delta \geq 0.910537$ $\frac{s}{r} \approx 0.63786$

110 counter example

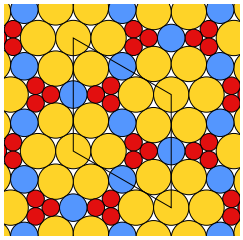

$\delta \leq 0.910448$ $s \approx 0.496826$

110 triangulated

Counter examples derived from b3

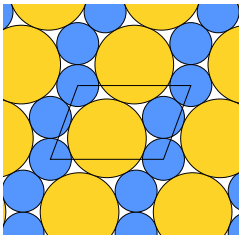

$\delta \approx 0.914180$ $r \approx 0.533296$

b3

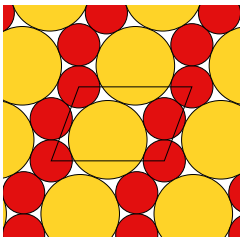

$\delta \geq 0.912306$ $s \approx 0.536428$

117 counter example

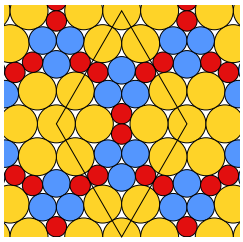

$\delta \leq 0.909801$ $s \approx 0.536428$

117 triangulated

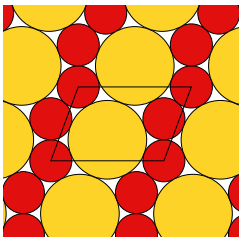

$\delta \geq 0.913415$ $s \approx 0.534565$

119 counter example

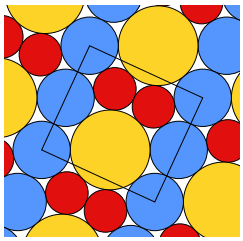

$\delta \leq 0.911230$ $s \approx 0.534565$

119 triangulated

Counter examples derived from b4

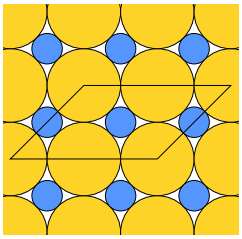

$\delta \approx 0.920151$ $r \approx 0.414214$

b4

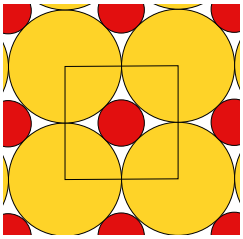

$\delta \geq 0.917188$ $s \approx 0.409604$

111 counter example

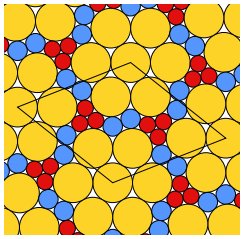

$\delta \leq 0.914148$ $s \approx 0.409604$

111 triangulated

Counter examples derived from b5

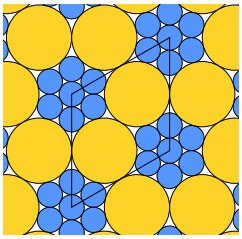

$\delta \approx 0.920063$ $r \approx 0.386106$

b5

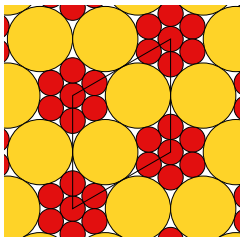

$\delta \geq 0.919703$ $s \approx 0.386662$

47 counter example

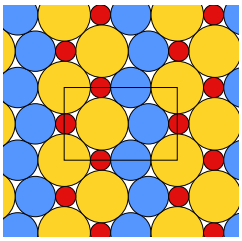

$\delta \leq 0.915670$ $s \approx 0.386662$

47 triangulated

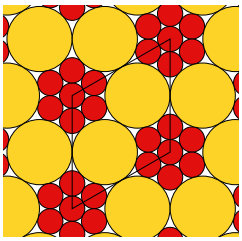

$\delta \geq 0.919027$ $s \approx 0.387709$

151 counter example

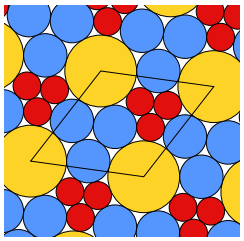

$\delta \leq 0.914455$ $s \approx 0.387709$

151 triangulated

Counter examples derived from b6

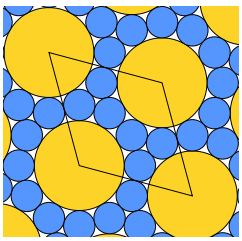

$\delta \approx 0.924649$ $r \approx 0.349198$

b6

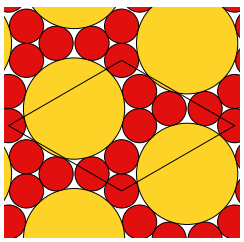

$\delta \geq 0.917953$ $s \approx 0.337336$

63 counter example

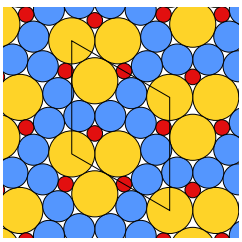

$\delta \leq 0.914301$ $s \approx 0.337336$

63 triangulated

Counter examples derived from b7

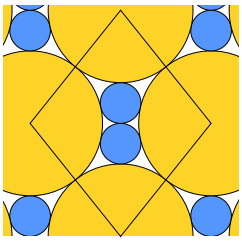

$\delta \approx 0.931901$ $r \approx 0.280776$

b7

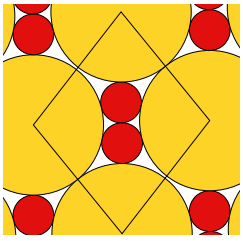

$\delta \geq 0.923787$ $s \approx 0.290478$

60 counter example

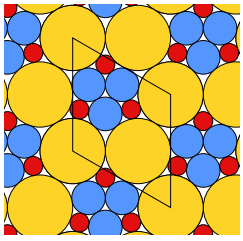

$\delta \leq 0.921391$ $s \approx 0.290478$

60 triangulated

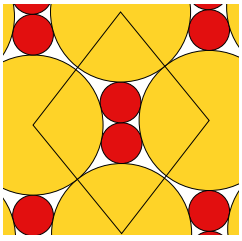

$\delta \geq 0.923374$ $s \approx 0.291004$

80 counter example

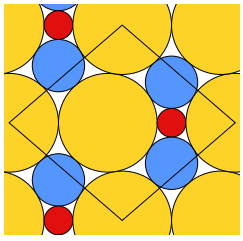

$\delta \leq 0.916939$ $s \approx 0.291004$

80 triangulated

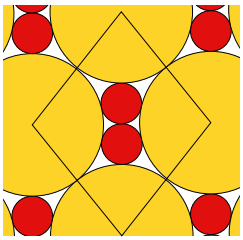

$\delta \geq 0.927652$ $s \approx 0.285714$

64 counter example

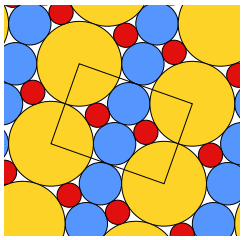

$\delta \leq 0.923712$ $s \approx 0.285714$

64 triangulated

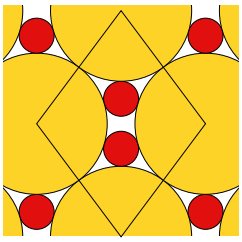

$\delta \geq 0.919930$ $s \approx 0.248062$

95 counter example

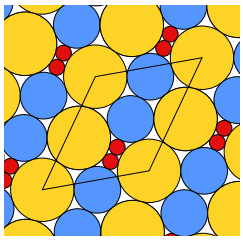

$\delta \leq 0.915309$ $s \approx 0.248062$

95 triangulated

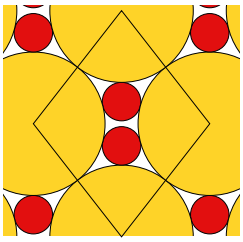

$\delta \geq 0.926300$ $s \approx 0.268266$

70 counter example

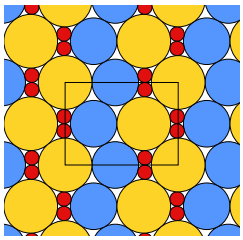

$\delta \leq 0.921134$ $s \approx 0.268266$

70 triangulated

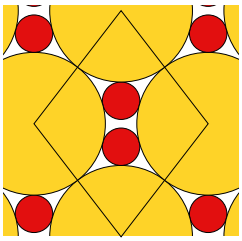

$\delta \geq 0.924033$ $s \approx 0.262214$

98 counter example

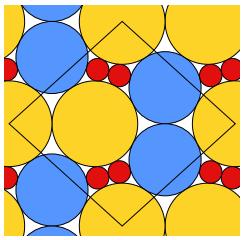

$\delta \leq 0.920708$ $s \approx 0.262214$

98 triangulated

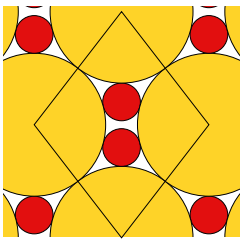

$\delta \geq 0.924545$ $s \approx 0.263654$

73 counter example

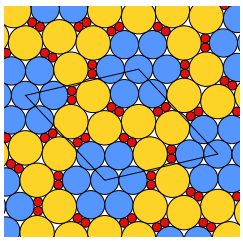

$\delta \leq 0.920565$ $s \approx 0.263654$

73 triangulated

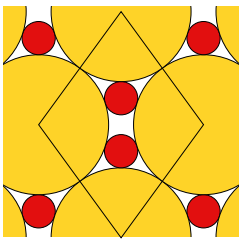

$\delta \geq 0.918039$ $s \approx 0.237538$

99 counter example

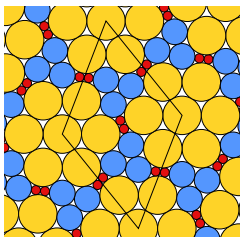

$\delta \leq 0.914656$ $s \approx 0.237538$

99 triangulated

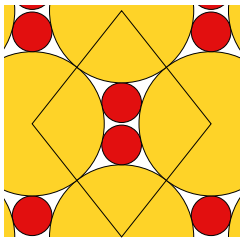

$\delta \geq 0.929245$ $s \approx 0.275178$

104 counter example

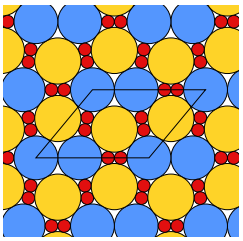

$\delta \leq 0.926316$ $s \approx 0.275178$

104 triangulated

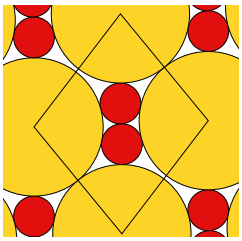

$\delta \geq 0.920311$ $s \approx 0.295016$

152 counter example

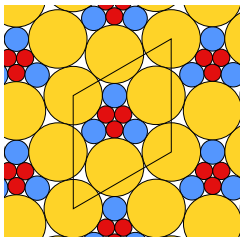

$\delta \leq 0.916740$ $s \approx 0.295016$

152 triangulated

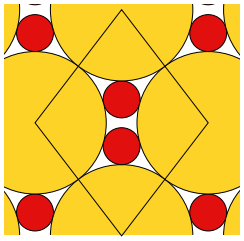

$\delta \geq 0.923104$ $s \approx 0.259471$

133 counter example

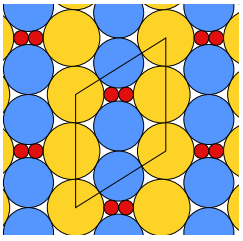

$\delta \leq 0.913852$ $s \approx 0.259471$

133 triangulated

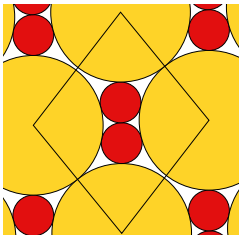

$\delta \geq 0.922609$ $s \approx 0.291987$

154 counter example

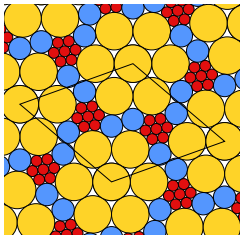

$\delta \leq 0.914322$ $s \approx 0.291987$

154 triangulated

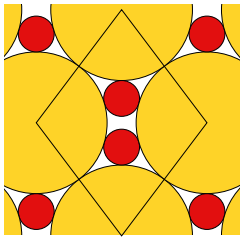

$\delta \geq 0.921135$ $s \approx 0.252889$

137 counter example

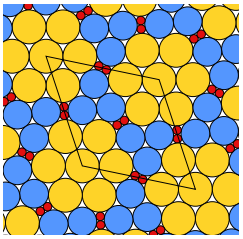

$\delta \leq 0.913256$ $s \approx 0.252889$

137 triangulated

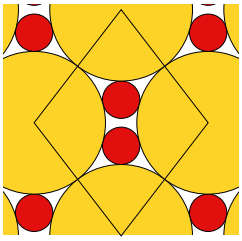

$\delta \geq 0.923895$ $s \approx 0.261820$

159 counter example

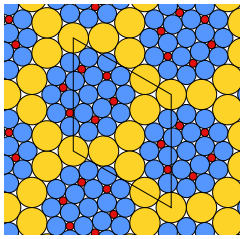

$\delta \leq 0.911735$ $s \approx 0.261820$

159 triangulated

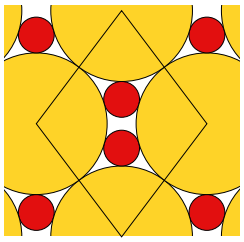

$\delta \geq 0.921070$ $s \approx 0.252651$

139 counter example

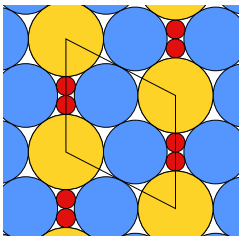

$\delta \leq 0.916585$ $s \approx 0.252651$

139 triangulated

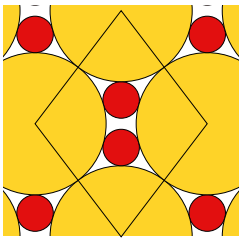

$\delta \geq 0.922253$ $s \approx 0.256777$

161 counter example

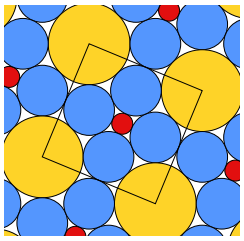

$\delta \leq 0.912783$ $s \approx 0.256777$

161 triangulated

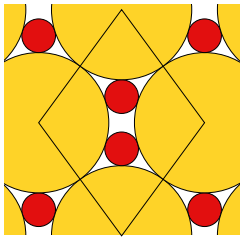

$\delta \geq 0.918420$ $s \approx 0.240205$

142 counter example

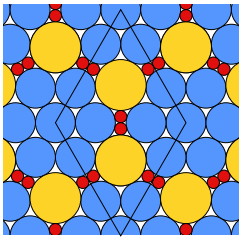

$\delta \leq 0.917352$ $s \approx 0.240205$

142 triangulated

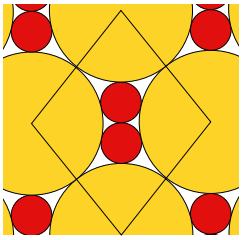

$\delta \geq 0.928754$ $s \approx 0.284405$

163 counter example

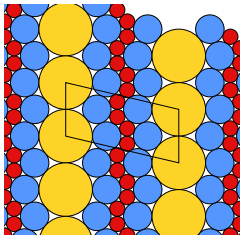

$\delta \leq 0.914180$ $s \approx 0.284405$

163 triangulated

Counter examples derived from b8

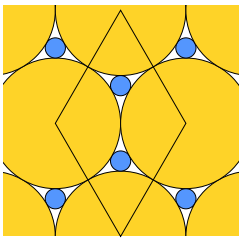

$\delta \approx 0.950308$ $r \approx 0.154701$

b8

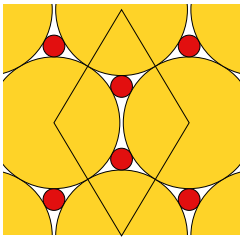

$\delta \geq 0.940262$ $s \approx 0.165044$

92 counter example

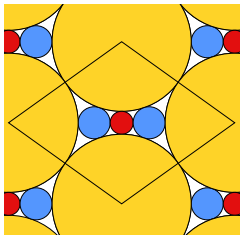

$\delta \leq 0.939949$ $s \approx 0.165044$

92 triangulated

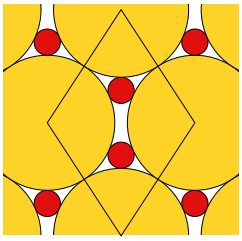

$\delta \geq 0.922660$ $s \approx 0.194146$

132 counter example

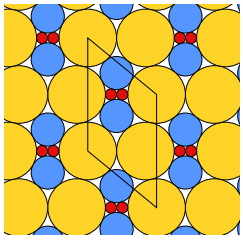

$\delta \leq 0.917705$ $s \approx 0.194146$

132 triangulated

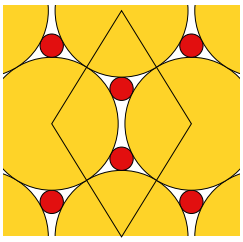

$\delta \geq 0.932390$ $s \approx 0.175341$

97 counter example

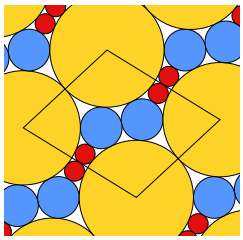

$\delta \leq 0.931017$ $s \approx 0.175341$

97 triangulated

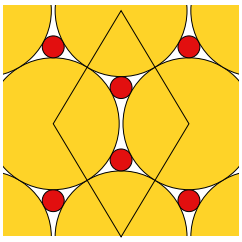

$\delta \geq 0.939305$ $s \approx 0.166169$

136 counter example

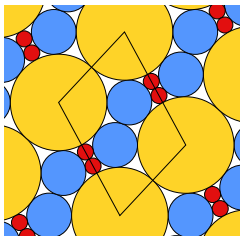

$\delta \leq 0.924522$ $s \approx 0.166169$

136 triangulated

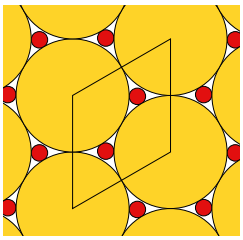

$\delta \geq 0.945389$ $s \approx 0.145672$

100 counter example

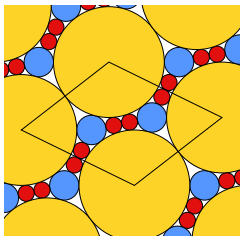

$\delta \leq 0.943442$ $s \approx 0.145672$

100 triangulated

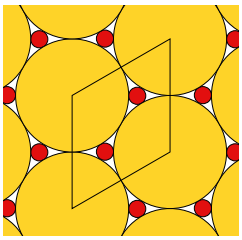

$\delta \geq 0.948474$ $s \approx 0.151397$

138 counter example

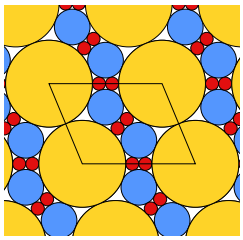

$\delta \leq 0.933093$ $s \approx 0.151397$

138 triangulated

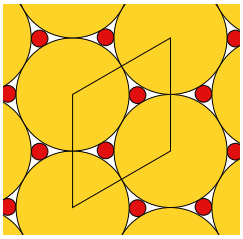

$\delta \geq 0.946696$ $s \approx 0.148125$

126 counter example

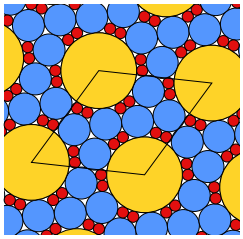

$\delta \leq 0.937034$ $s \approx 0.148125$

126 triangulated

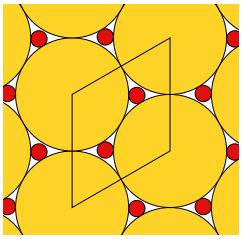

$\delta \geq 0.944847$ $s \approx 0.144643$

162 counter example

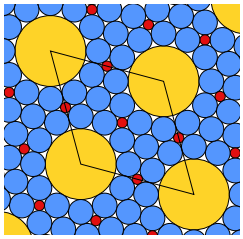

$\delta \leq 0.919990$ $s \approx 0.144643$

162 triangulated

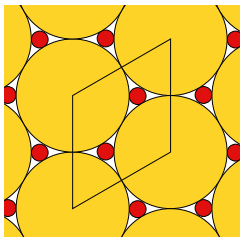

$\delta \geq 0.947210$ $s \approx 0.149078$

164 counter example

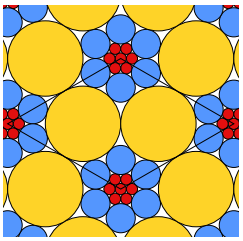

$\delta \leq 0.922026$ $s \approx 0.149078$

164 triangulated

Counter examples derived from b9

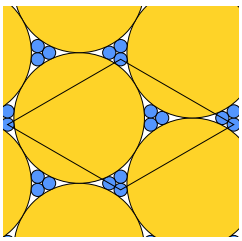

$\delta \approx 0.962430$ $r \approx 0.101021$

b9

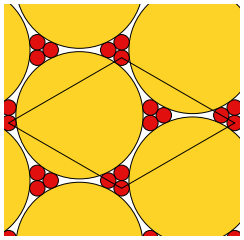

$\delta \geq 0.937371$ $s \approx 0.121445$

20 counter example

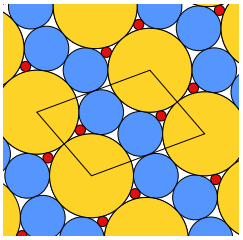

$\delta \leq 0.931369$ $s \approx 0.121445$

20 triangulated

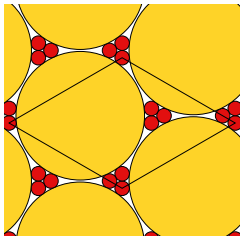

$\delta \geq 0.946934$ $s \approx 0.113037$

141 counter example

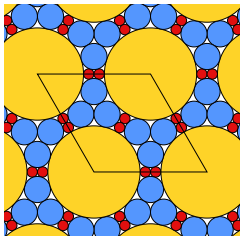

$\delta \leq 0.940871$ $s \approx 0.113037$

141 triangulated

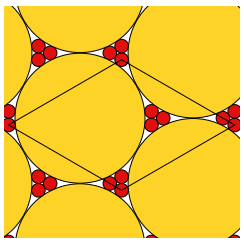

$\delta \geq 0.957603$ $s \approx 0.104582$

25 counter example

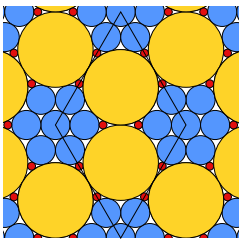

$\delta \leq 0.939902$ $s \approx 0.104582$

25 triangulated

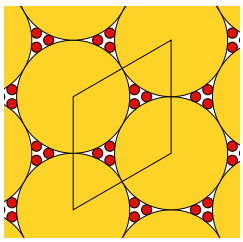

$\delta \geq 0.950799$ $s \approx 0.0898203$

160 counter example

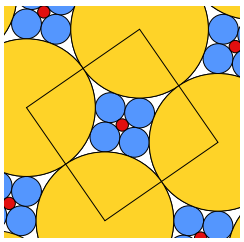

$\delta \leq 0.939458$ $s \approx 0.0898203$

160 triangulated

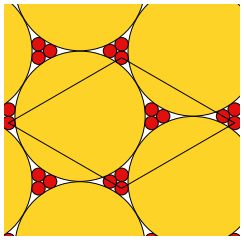

$\delta \geq 0.959548$ $s \approx 0.103129$

135 counter example

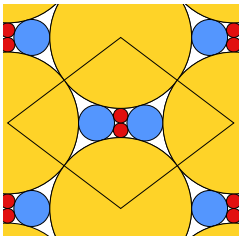

$\delta \leq 0.938718$ $s \approx 0.103129$

135 triangulated

Counter examples derived from A

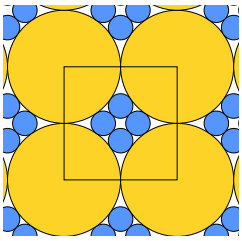

$\delta \approx 0.933122$ $r \approx 0.216845$

b10

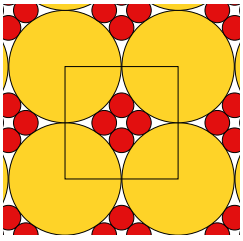

$\delta \geq 0.930656$ $s \approx 0.219224$

96 counter example

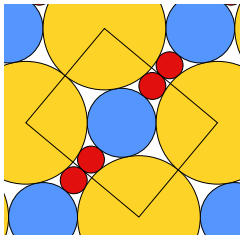

$\delta \leq 0.924297$ $s \approx 0.219224$

96 triangulated

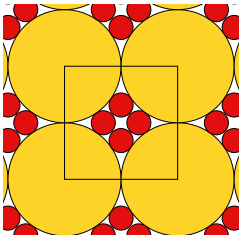

$\delta \geq 0.927208$ $s \approx 0.212461$

153 counter example

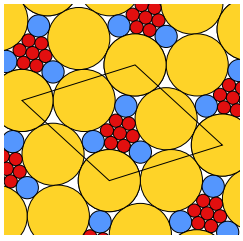

$\delta \leq 0.921582$ $s \approx 0.212461$

153 triangulated

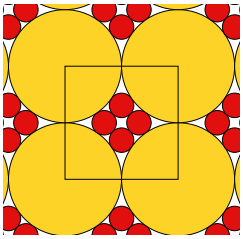

$\delta \geq 0.932559$ $s \approx 0.216432$

106 counter example

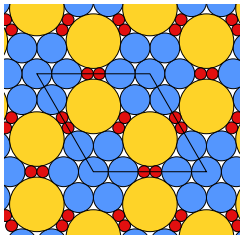

$\delta \leq 0.922828$ $s \approx 0.216432$

106 triangulated

Counter examples derived from B

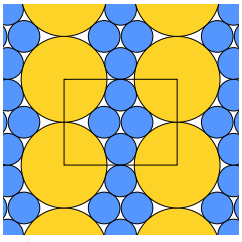

$\delta \approx 0.920350$ $r \approx 0.369102$

b11

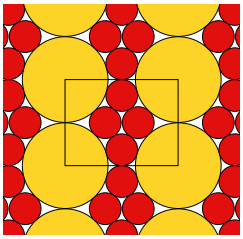

$\delta \geq 0.918451$ $s \approx 0.370614$

81 counter example

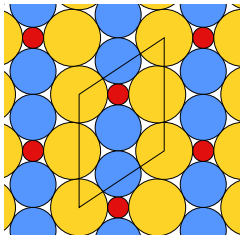

$\delta \leq 0.911339$ $s \approx 0.370614$

81 triangulated

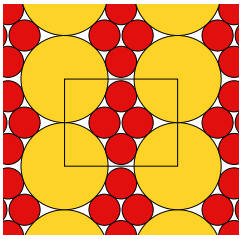

$\delta \geq 0.913644$ $s \approx 0.357117$

84 counter example

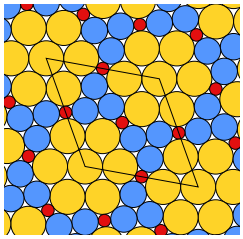

$\delta \leq 0.911064$ $s \approx 0.357117$

84 triangulated

Chapter 4



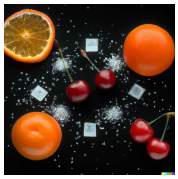
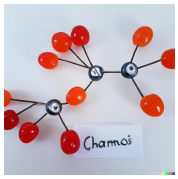

Density of sphere packings

> ... many mathematicians believe, and all physicists know, that the density cannot exceed $\frac{\pi}{\sqrt{18}} = 0.7404\ldots$, ...
>
> C. A. Rogers, 1958 [Rog58]

This chapter focuses on the sphere packings of 3-dimensional space. In Section 4.1, we talk about optimal *packings of congruent spheres* (also called *1-sphere packings*), the Kepler conjecture and its proof. Section 4.2 is dedicated to the density bounds for 2-sphere packings and contains our partial results.

4.1 Kepler conjecture

Until recently, the proof of the Kepler conjecture stood out as the most well-known result in the area of sphere packings. This conjecture dates back to 1611 when Kepler stated that the "cannonball packing" maximized the density among 1-sphere packings [Kep11]. This packing belongs to a family of *close-packings* which can be constructed by superposing layers of spheres placed as in the hexagonal packing (see Fig. 4.1–4.3) they all have the same density, $\frac{\pi}{3\sqrt{2}} \approx 0.74048$. This claim took 400 years to prove and was included in the list of Hilbert's problems as a part of the 18th problem [Hil02]. Hales and Ferguson finally resolved the Kepler conjecture in 1998. Their proof, consisting of 6 papers and tens of thousands of lines of computer code, took several years to review by the group of 12 referees, led by Gabor Fejes Tóth. After all, the reviewers expressed a "99% sure" confidence in the correctness of the proof and its complete revised version was finally published in 2006 [HF06]. Hales initiated a project called Flyspeck aiming to transform his result into a formal proof using two proof assistants, which was completed in 2017 [HAB+17].

We bring up the Kepler conjecture not only for its fame (see Section 4.1.1 for further details on it history), but rather because our proof of the optimality of triangulated disc packings shares some ideas and follows similar steps to the proof of the Kepler conjecture by Hales and Ferguson. This reassures us that we would not have to radically change our approach when studying sphere packings in 3D (the proof techniques applied to packings in high dimensions, as [Via17, DLDOFV14], are quite different from ours). On the other hand, the distinctions between our proof and the proof of the Kepler conjecture guide us in making necessary adjustments to our approach to make it work in 3D. A brief summary of the author's understanding of the proof of the Kepler conjecture is

provided in Section 4.1.2.

The dimension reduction method, introduced in Section 2.2.2 for multi-size disc packings, significantly reduces the computation time for 3-disc packings (see Section 3.3.2). This method is also extensively employed in the proof of the Kepler conjecture for the same reasons; Section 4.1.3 is dedicated to the dimension reduction in the proof of the Kepler conjecture.

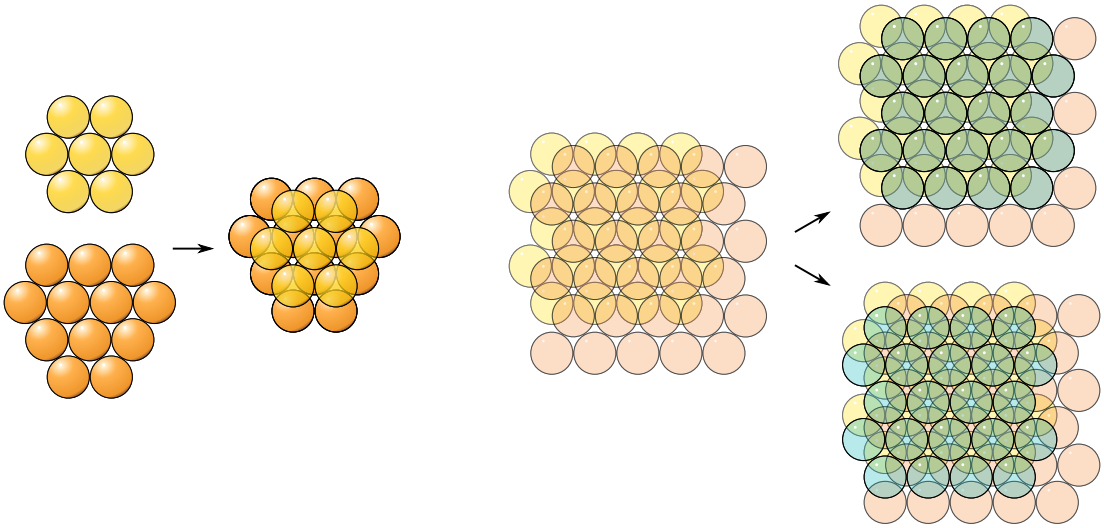

Figure 4.1: Layer-by-layer construction of close-packings of congruent spheres.

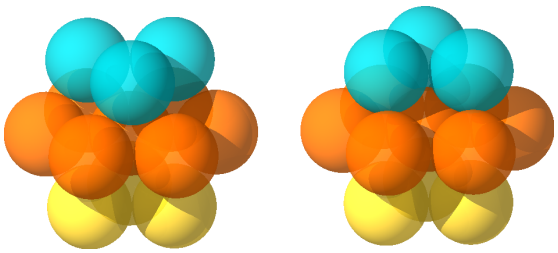

Figure 4.2: Local FCC (to the left) and HCP (to the right) configurations of spheres.

4.1.1 History

> While greengrocers reached their conclusion through experience and intuition, Hales spent 10 years developing a complex 250-page argument, which relies on three gigabytes of computer files.
>
> S. Singh, New Yorker, August 25, 1998

The "cannonball packing" described by Kepler in his manuscript [Kep11], is today known by the name of *face-centered cubic* (or *FCC*) *packing*. It is a lattice packing: the sphere centers are arranged in the vertices of the FCC lattice, which gave the name to the packing. Figure 4.2, to the left, illustrates the local FCC configuration; Figure 4.3 depicts a heap of oranges arranged on an FCC lattice. An equally dense close-packing generated by another regular lattice, the *hexagonal close-packing* (or HCP), was first mentioned by Barlow in 1883 [Bar83] (Fig. 4.2, to the right). There actually exist

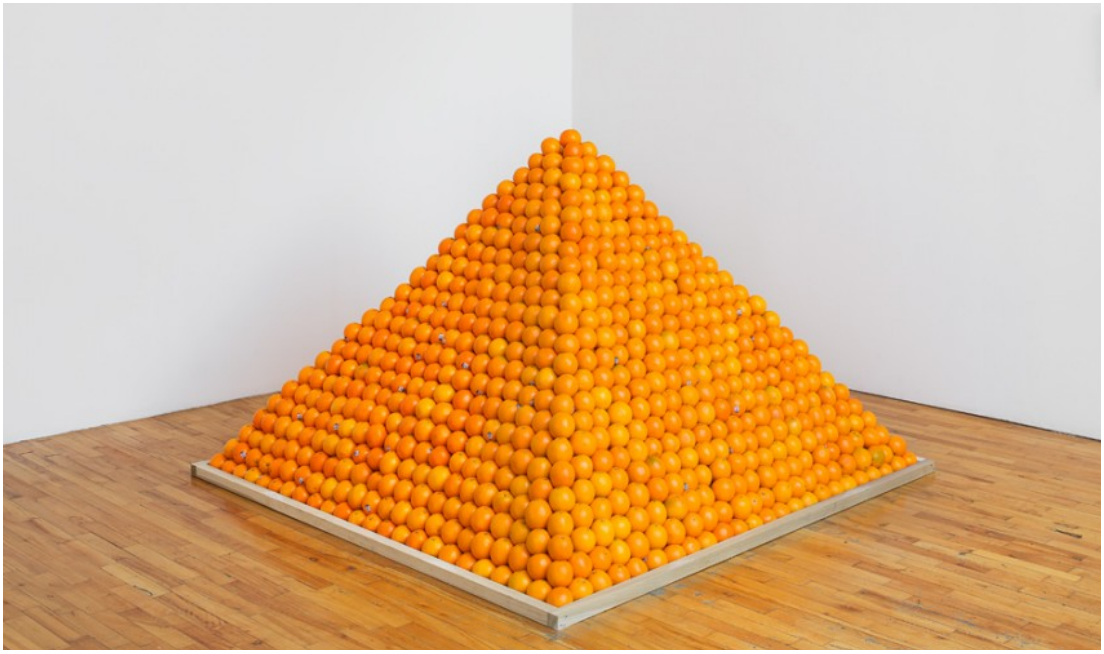

Figure 4.3: Roelof Louw, "Soul City (Pyramid of Oranges)", 1967, Tate Aspen Art Museum, 2016.

an infinite family of globally distinct close-packings, all having the same density $\frac{\pi}{3\sqrt{2}}$, they are called *close-packings*. Each close-packing is obtained by superposing the layers of spheres whose centers form an hexagonal packing; each new layer can be placed in two different ways with respect to the two previous layers (see Fig. 4.1), so we obtain an uncountable number of packings in the end. There are, however, only two local configurations around a sphere, depicted in Fig.4.2 and 4.8, that appear in close-packings; their both Voronoi cells are of density $\frac{\pi}{3\sqrt{2}}$.

Gauss in 1831 [Gau31] established a connection between quadratic forms and lattices which implies that the close-packings maximize the density among the lattice packings. The analogous implication for the 2-dimensional case is discussed in Section 2.1.1, on page 17. In 1993, this result was generalized to the class of packings of parallel strings of spheres by Bezdek, Kuperberg, and Makai [BKMJ91].

The general result turned out to be much harder. The Kepler conjecture was even included in the Hilbert's list of problems [Hil02] as the third part of the 18th problem in 1900. In the following years, researchers used various approaches to obtain increasingly tighter upper bounds on the maximal density of 1-sphere packings. Blichfeldt obtained first upper bounds (0.884 and 0.835) in 1919 and 1929 [Bli19, Bli29]. In 1958, Rogers bounded the density of a packing by the density inside the tetrahedron formed by four pairwise tangent spheres (we call such tetrahedra *tight*), equal to ≈ 0.7796, [Rog58]. The best upper bound prior to the resolution of the Kepler conjecture was given by Muder [Mud93] and equals ≈ 0.773055.

The Kepler conjecture is a continuous optimization problem (we try to maximize the function of the density over the set of all packings) with an infinite number of variables (there are an infinite number of spheres to pack). László Fejes-Tóth made a huge advancement on the way to the proof of the Kepler conjecture by proposing to use the local density approach [FT53]. This approach allows to reduce this infinitely-dimensional optimization problem to the one with a finite number of variables. Moreover, he was the

first to suggest the use of a computer; in his book on regular figures [FT64], he writes:

> In view of the intricacy of this function we are far from attempting to determine the exact minimum. But, mindful of the rapid development of our computers, it is imaginable that the minimum may be approximated with great exactitude.

The most famous unsuccessful attempt to prove the conjecture belongs to Wu-Yi Hsiang who, in 1990, submitted a proof where he applied the local density approach to the Voronoi cells. His proof received extensive media attention but it, along with subsequent revisions, contained serious flaws and experts agreed on its incompleteness. For more information, refer to Hales' survey on the question [Hal94].

Hales' initial approach to the Kepler conjecture [Hal92, Hal93] was based on the Delaunay partition of the space and did not lead to a complete proof. Consequently, he adopted a hybrid partition involving Delaunay simplices and modified Voronoi cells. In collaboration with Ferguson, Hales completed the first version of the proof in 1997. It comprised 6 preprints and tens of thousands of lines of computer code and, after several years of intensive revision by a team of experts, the improved version was published in 2006 [HF06]. In the meantime, an abridged version of this proof appeared in Annals of Mathematics [Hal05].

In 2003, Hales launched a worldwide collaborative project to obtain a formal proof of the Kepler conjecture. The project was named Flyspeck, which is an expansion of "FPK", for "the Formal Proof of the Kepler conjecture". The aim of the project was to construct a complete formal proof verifiable by proof assistants such as HOL Light and Isabelle. Flyspeck was completed in 2014; three years later, after a meticulous review by the mathematical community, the formal proof was accepted by Forum of Mathematics [HAB+17].

You can find detailed insights on the history of the Kepler conjecture and its proof up until 2003 in Szpiro's popular book [Szp03].

4.1.2 Proof ideas

In this section, δ^* denotes the density of close-packings, i.e., $\delta^* := \frac{\pi}{3\sqrt{2}} \approx 0.7405$, and P denotes an arbitrary saturated 1-sphere packing.

The stages of the proof of the Kepler conjecture and of our results on triangulated disc packings from Chapter 3 are immeasurably different in complexity bust still share same global ideas. Both our proof (the detailed strategy is given in Section 3.1, page 53) and the proof of the Kepler conjecture, as well as other results based on the local density approach, roughly consist of the following steps:

1. partitioning the space into well-defined cells,
2. choosing a convenient function to represent the density,
3. redistributing the density among the vertices of each cell,
4. showing for each possible local configuration around a vertex, that the redistributed density never exceeds the optimal density,
5. treating configurations that are close to the local maxima in terms of the redistributed density and demand particular techniques.

First step consists in choosing the space partition suitable for the density redistribution. In general, there are two natural choices of the space partition: Voronoi decomposition or Delaunay partition. In 3D, both are defined in exactly the same manner as in 2D (formal definitions are given in Section 4.2.1). The choice of partition depends on the rest of the proof: we shall avoid cells which feature especially high density in comparison with the configurations of the target packings. In the case of the Voronoi partition, the Voronoi cell, having the shape of the regular dodecahedron, of the configuration of spheres centered in the vertices of the regular icosahedron, is very dense. This configuration, depicted in Figure 4.4, actually maximizes the density among all possible Voronoi cells of a sphere in a sphere packing, and is not present in close-packings (see Section 1.2.1, page 5 for more details on the dodecahedral conjecture). Using exclusively Delaunay tetrahedra was not enough neither: the pentahedral prism configuration (see Fig.4.5) was one of the obstacles in the first Hales' proof tentative [Hal92]. Finally, to be able to flexibly combine advantages of both partitions, Hales introduced a hybrid *HF-partition* [HF11] which consists of deformed Voronoi cells and Delaunay simplices featuring special geometric properties, let $\mathcal{P}$ denote the HF-partition of the packing P.

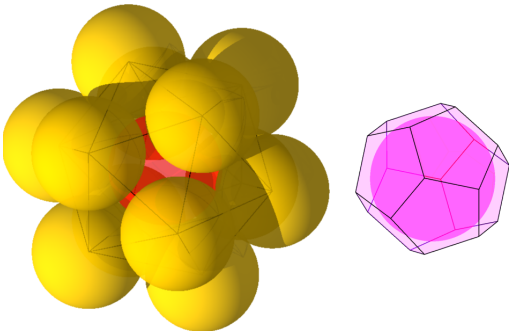

Figure 4.4: Spheres tangent to the red sphere are centered in the vertices of the regular icosahedron, the Voronoi cell of the central sphere (to the right) is a regular dodecahedron.

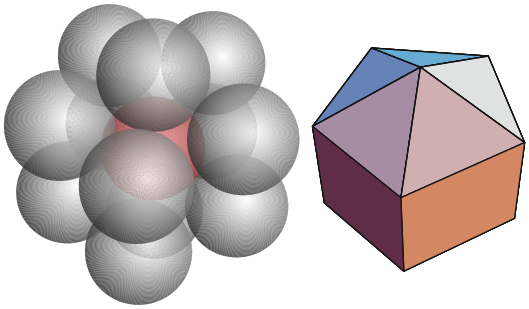

Figure 4.5: The centers of the spheres tangent to the central (red) sphere form a pentahedral prism also depicted to the right.

The second step consists in selecting a suitable function to represent the density. By "suitable", we mean additive: our aim is to prove density inequalities for small local patches and then extend them to the entire space. The density function itself is not additive, as the density of the union of two cells is generally not equal to the sum of their densities. In the context of 3-disc packings discussed in Chapter 3, we introduced the emptiness function (page 53), which reflects the density and is additive (Section 3.1, page 53). Hales used a function called *compression* which, at first glance, appears as a negative 3D version of the emptiness:

$$\Gamma(R) := V(R \cap P) - \delta_{\text{oct}} \cdot V(R),$$

$V(R)$ denote the volume of the region and δ_{oct} is the density of the tight regular octahedron.

The first glance is misleading: instead of comparing with δ^*, as in the case of the emptiness, the compression reflects whether a region is denser or not than δoct, the density inside the regular octahedron formed by tangent spheres (see Figure 4.7), which is less than δ^*. This value is not arbitrary: in the space partition defined by the contact graph of a close-packing, two types of polyhedra are present, regular tetrahedra

(Fig. 4.6) and regular octahedra (Fig. 4.7). This means that the target density is equal to the linear combination of the densities of the above:

$$\delta^* = \frac{\delta_{\text{tet}}}{3} + 2\frac{\delta_{\text{oct}}}{3},$$

where

$$\delta_{\text{tet}} := 2\sqrt{2}\arctan\left(\frac{\sqrt{2}}{5}\right) \approx 0.7796, \quad \delta_{\text{oct}} := \frac{12\arccos\left(\frac{1}{\sqrt{3}}\right) - 3\pi}{2\sqrt{2}} \approx 0.7209.$$

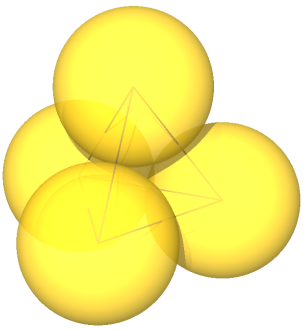

Figure 4.6: Regular tetrahedron, its density $\delta_{\text{tet}} \approx 0.7796$.

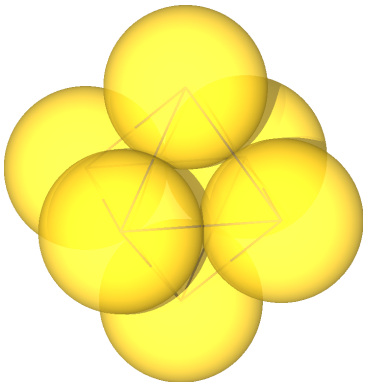

Figure 4.7: Regular octahedron, its density $\delta_{\text{oct}} \approx 0.7209$.

The compression of a region is positive if the region is denser than δ_{oct} and negative otherwise, so Hales' proof consists in redistributing the compression inside the cells and showing that the result is "low enough" on each local configuration.

The redistribution of the compression among the vertices of the cells is called *score* (step 3). The score of a cell R in a given vertex v is denoted by $\sigma(R, v)$. The definition of $\sigma(R, v)$ depends on the type of the cell: if R is a Voronoi cell and v is its center ($R = Vor(v)$), then $\sigma(R, v) := 4\,\Gamma(R)$ and $\sigma(R, w) = 0$ for $w \neq v$. In other words, the score of a Voronoi cell is concentrated in its center. The score of a simplex varies in function of its properties and depends on Γ. By definition, the overall score of a region always equals to 4 times its compression [HF11].

This is the main difference between the Hales' method and the method of localizing potentials that we use in Chapter 3. In our proof for 3-disc packings, to redistribute the emptiness, we use the potential function which is a lower bound of the emptiness in each triangle and which is nonnegative if summing up on all triangles of a packing. We choose the potential function which is easy to manipulate and construct it in order to satisfy both conditions (for more information, see Section 3.2 on page 54). On the other hand, in the proof of the Kepler conjecture, the distributed compression (i.e., the score) always equals the compression itself in each cell (instead of being a lower bound of it). As a result, the score is a non-trivial function in contrast to the potential which was linear in the value of the angle of the triangle in the vertex. The advantage of Hales' method is that there is no need to verify the inequality between the score and the compression on each cell: they are equal by definition, while in our proof, we had to run through all possible triangles to verify the local inequality (see Section 3.3.2).

At step 4, all possible local configurations around a vertex are analyzed in order to show that that the emptiness is non-negative (for 3-disc packings) and that the compression is $\leq 8pt$ (for 1-sphere packings), where pt is a constant defined below. In 2D, these

local configurations around a disc were coronas of its neighbor discs surrounding it. In the proof of the Kepler conjecture, each local configuration, called *decomposition star*, is the set of the cells of the neighbor spheres (the spheres whose centers are connected by an edge with the central vertex in the graph of the HF-partition) around a given sphere, they form a graph in 3D that can be embedded on a sphere. Hales reduced the global density inequality to a compact set of local problems [HF11] by proving that $\delta(P) \leq \delta^*$ holds as soon as for each $v \in \mathcal{P}$,

$$\sum_{R \in D_v} \sigma(R, v) \leq 8\, pt, \tag{4.1}$$

where D_v is the decomposition star around v and the constant pt is defined as follows:

$$pt = 4 \arctan\left(\frac{\sqrt{2}}{5}\right) - \frac{\pi}{3} = \sqrt{2}\,\delta_{\text{tet}} - \frac{\pi}{3} = -2\left(\sqrt{2}\,\delta_{\text{oct}} - \frac{\pi}{3}\right).$$

The combinatorics of a decomposition star D_v can be represented by the graph $G(D_v)$ which is the FH-partition graph reduced to the neighbors of v. To verify (4.1), Hales starts by treating the decomposition stars whose graphs do not belong to the class of so-called *tame* graphs. The tame graphs are potential counter-examples of (4.1) while the non-tame graphs are those whose geometry relatively easily implies (4.1). The non-tame graphs are treated in [Hal11c] with the use of interval arithmetic.

The class of tame graphs has restricted geometry (they are planar, connected, have no loops and multiple joints, each face has between 3 and 8 edges, each vertex is of degree between 2 and 6 and so on) is finite and relatively small (a few thousands). The classification of all tame graphs is a crucial component of the Hales' proof of the Kepler conjecture. They are treated one by one by computer, and for each of them, an upper bound on the score of the attached decomposition star is computed. This is done by solving a linear relaxation of the nonlinear optimization problem of maximizing the score over all decomposition stars with the aid of recursive subdivision [Hal11d].

At this point, one particular tame graph turned out to be problematic: to prove (4.1) on the graph corresponding to the pentahedral prism depicted in Figure 4.5, Hales and Ferguson had to employ more delicate methods, including dimension reduction discussed in the next section and careful analysis of function behavior [Fer11].

Finally, step 5 is dedicated to the extremal cases: the local configurations present in the optimal packing. The two optimal local configurations in the proof oh the Kepler conjecture are the FCC (Voronoi cell is a Rhombic Dodecahedron) and the HCP (Voronoi cell is a Trapezoidal Dodecahedron) local configurations given in Fig. 4.8 together with the corresponding graphs. By definition, they are local maxima of the score, so recursive subdivision can not be applied to the set of "close enough" decomposition stars having the same graph (find more information about this issue in Section 3.5.1, page 75). Hales and Ferguson [Hal11b] used differential geometry and interval arithmetic in order to prove that the FCC and HCP configurations are local maxima of the score; we applied similar methods in Chapter 3 to treat ϵ-tight triangles (see Section 3.3.1).

4.1.3 Dimension reduction for 1-sphere packings

In the Hales' and Ferguson's proof, the scoring bound for decomposition stars often relies on six-dimensional relations, as they are formulated in terms of the edge lengths of a tetrahedron. Other types of regions can lead to even higher-dimensional problems.

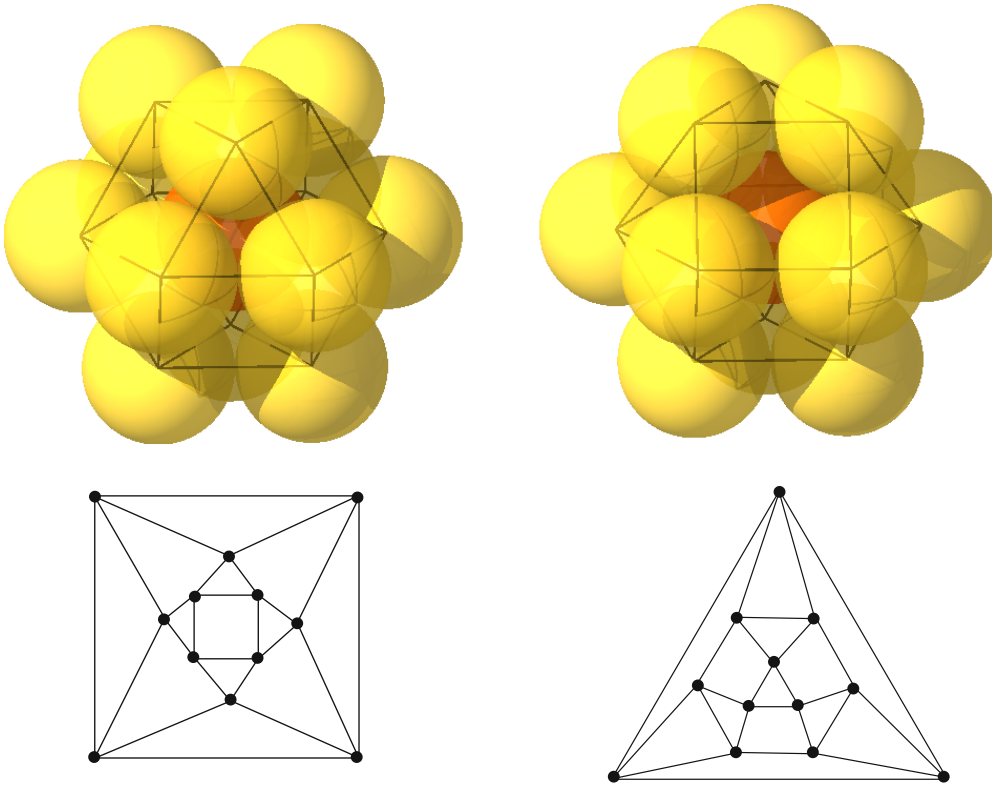

Figure 4.8: FCC (to the left) and HCP (to the right) local configurations of close-packings together with the corresponding contact graphs.

Resolving high-dimensional relations with the subdivision method can be very expensive from the computational point of view. The dimension reduction for the compression function, introduced in [Hal11a], is used to reduce the computational expense during the treatment of the pentahedral prism in [Fer11], where it was also generalized for alternative scoring functions.

In this section, we discuss the detailed proof of the dimension reduction in terms of the compression function for 1-sphere packings, initially given by Hales in [Hal11a]. The result resembles one particular step of the dimension reduction for multi-size disc packings [FTM58], discussed in Section 2.2.2 , where using several deformations we transformed any FM-triangle into an FM-triangle with at least 2 contacts without decreasing the density . We also used a simplified dimension reduction in the case of 3-disc packings in Section 3.3.2 to obtain one contact without breaking the inequality between the emptiness and the potential. In 2-dimensional case (see Section 2.2.2, page 30), one of the transformations consisted in sliding a disc along an edge until a contact was created. It turns out that applying the same kind of transformation for 1-sphere packings does not diminish the compression. This potentially reduces the dimension of the problem from six to four (or even three in certain cases) by reducing the set of tetrahedra to the tetrahedra with two (or three) contacts.

The original version of the result presented below is given by Proposition 8.7.1 in [Hal11a].

Definition 4.1. *A **Delaunay simplex** of a point set S is any simplex formed by points in S whose circumscribing sphere contains no other point of S.*

Let us adapt the above definition from the literature to the case of sphere packings. To

avoid confusion, we will use the term "tetrahedron" instead of "simplex" when speaking of sphere packings in 3D.

Definition 4.2. *A **Delaunay tetrahedron** is a Delaunay simplex of the set of sphere centers of a 3-dimensional packing of the unit spheres.*

Section 2.1.2 (page 20) contains more information on the Delaunay simplices in 2-dimensional case. For more details on the simplicial partition of a sphere packing, see Section 4.2.1, the Delaunay partition being a particular case of an FM-partition of a 2-sphere packing.

Since the volume of the part of the Delaunay tetrahedron covered by its spheres can be computed using its solid angles, the compression of the Delaunay tetrahedron T with vertices A, B, C, D can be written as

$$\Gamma(T) = V(T \cap P) - \delta_{oct} V(T) = \frac{\widehat{A}_T + \widehat{B}_T + \widehat{C}_T + \widehat{D}_T}{3} - \delta_{oct} V(T),$$

where $\widehat{X}_T$ denotes the solid angle in the vertex X of the tetrahedron T.

Proposition 4.1 (Corresponds to Proposition 8.7.1 [Hal11a])**.** *Let $T = ABCD$ be a Delaunay tetrahedron such that the side lengths $|AB|, |AC|, |AD|$ are greater than 2. Let us take $A' \in AD$ such that $|AA'|$ is "small" and $|A'B|, |A'C|, |A'D|$ are still greater than 2 and the circumradius of $T' = A'BCD$ is at most 2 (so it is a Delaunay tetrahedron). Then*

$$\Gamma(T') > \Gamma(T).$$

Notice that [Hal11a] gives no lower bound on how "small" $|AA'|$ is required to be. Such bound can likely be derived from a careful analysis of undermentioned Claim 4.1 and of the remainders of the Taylor approximations figuring in inequalities (4.5) on page 109. Since this was not done in the source nor by the author, Proposition 4.1 does not guarantee a successful dimension reduction. Indeed, consequently reducing edge AD by a small value could never result in a new contact if this value decreased too fast at each step.

Let $\widehat{X}_{YZW}$ (and $\widehat{X}_T$) denote the solid angle in X of the tetrahedron $T = XYZW$ (in the same manner, $\widehat{X}_{Y_1 \cdots Y_n}$ denotes the solid angle in X of the pyramid $XY_1 \cdots Y_n$). Let $\widehat{XY}_{ZW}$ (and $\widehat{XY}_T$) denote the dihedral angle of the edge XY in the tetrahedron $T = XYZW$. Let $\widehat{XYZ}$ denote the angle in Y of the triangle XYZ.

Let dT denote the tetrahedron $A'ABC$, it represents the "difference" between T and T', we have $T = T' \cup dT$. Let $d\hat{A} := \widehat{A'}_{T'} - \widehat{A}_T$ and $d\hat{X} := \widehat{X}_{T'} - \widehat{X}_T$ for $X \in \{B, C\}$; the remaining solid angle remains unchanged: $\widehat{D}_T = \widehat{D}_{T'}$.

Notice that by definition, $d\hat{C}$ and $d\hat{B}$ are negative, we also have $\widehat{DA}_{CB} = \widehat{DA'}_{CB}$, $\widehat{CAD} < \widehat{CA'D}$, and $\widehat{BAD} < \widehat{BA'D}$. Let B' (and C') denote respectively the intersection of BD (CD) with the plane parallel to ABC passing through A', as illustrated in Figure 4.9. Notice that $A'C' || AC$ and $A'B' || AB$, so angle $d\hat{A}$ is equal to $\widehat{A'}_{BCC'B'}$ and is positive being an area of quadrilateral region of a sphere.

Let us write the difference of the compressions of T' and T.

$$\Gamma(T') - \Gamma(T) = \frac{d\hat{A}}{3} + \frac{d\hat{B}}{3} + \frac{d\hat{C}}{3} + \delta_{oct} V(dT),$$

Since $d\hat{A} \geq 0$, to conclude the proof of Proposition 4.1, it is enough show the following lemma.

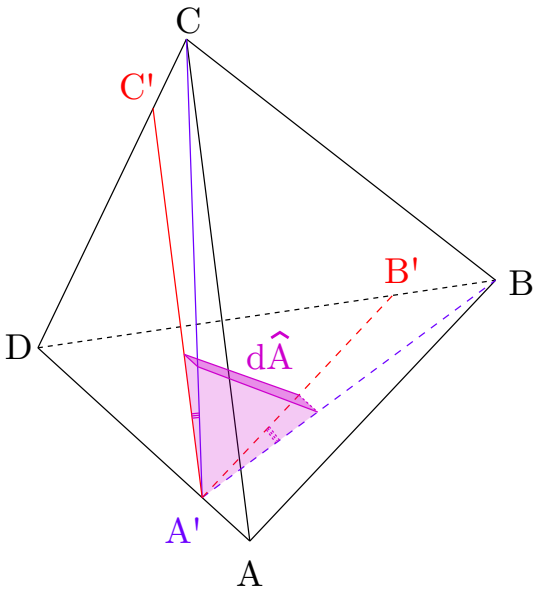

Figure 4.9: Positivity of $d\hat{A}$.

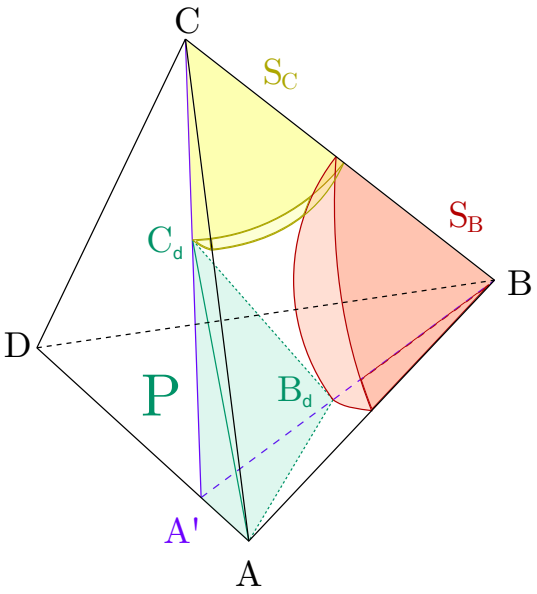

Figure 4.10: P and ball segments S_B, S_C.

Lemma 4.1.

$$\delta_{oct}\, V(dT) > -\frac{d\hat{B}}{3} - \frac{d\hat{C}}{3}$$

Proof. Let h be the distance from A to the plane $A'BC$. We define $T'(h)$ as the tetrahedron $A'BCD$ where $h < 0.15$ is the mentioned distance; this function maps positive real numbers to the set of tetrahedra with fixed lengths of BC, BD, and CD, as well as the direction of DA'.

Let B_d (C_d) denote the point on $A'B$ ($A'C$) which is at distance $d = 1.15$ from B (C). Let P be the tetrahedron AB_dC_dA'. Additionally, let S_B (S_C) denote the intersection of dT with a ball of radius d centered in B (C) (see Fig. 4.10).

Claim 4.1. *For h sufficiently small, P is (essentially) disjoint from S_B and S_C.*

Claim 4.1 is given in [Hal11a] without a proof. The author did not succeed to provide a complete and accurate proof, so this can be considered as a flaw in the whole argument. Nevertheless, the claim likely holds, since all the results from [Hal11a] were meticulously verified by the experts.

First, let us prove that $V(P) > V(S_B \cap S_C)$. We start by deriving a lower bound on $V(P)$,

$$V(P) = \frac{h \cdot A(A'B_dC_d)}{3} = \frac{h}{6} \sin\left(\widehat{BA'C}\right) |A'B_d|\, |A'C_d|. \tag{4.2}$$

Since T' is a Delaunay tetrahedron, its circumscribed sphere is of radius at most 2, this implies that the radius of the circumcircle of any of its faces is at most 2. Let us use the same argument as in Lemma 2.1 (page 22): by the law of sines,

$$\frac{|BC|}{\sin\left(\widehat{BA'C}\right)} \le 4.$$

Therefore, since $|BC| \ge 2$, we have

$$\sin\left(\widehat{BA'C}\right) \ge \frac{1}{2}.$$

Applying this to (4.2), we obtain the lower bound on the volume of P:

$$V(P) \geq \frac{h}{12}(2-d)^2 = \frac{0.7225\,h}{12} > 0.06\,h. \tag{4.3}$$

Let us now compute an upper bound of $V(S_B \cap S_C)$. If this intersection is empty, we conclude. If the intersection is not empty, $|BC| < 2d$.

The intersection of two spheres is the union of two spherical caps. Therefore, to compute $V(S_B \cap S_C)$, we use the formula of the volume of a spherical cap, $V = \frac{\pi x^2}{3}(3d - x)$, of a sphere of radius d with x being the height of the cap.

$$V(S_B \cap S_C) = 2V \times \frac{\widehat{BC}_{AA'}}{2\pi} = \frac{x^2\,(3d-x)\,\widehat{BC}_{AA'}}{3}. \tag{4.4}$$

Since the heights of both caps equal $x := d - \frac{|BC|}{2}$, we have

$$V(S_B \cap S_C) = \frac{\left(d - \frac{|BC|}{2}\right)^2 \left(2d + \frac{|BC|}{2}\right) \widehat{BC}_{AA'}}{3} < (d-1)^2\, d\, \widehat{BC}_{AA'}.$$

Let H be the base of the height from A to the plane $A'BC$ ($AH \perp A'BC$) and H'

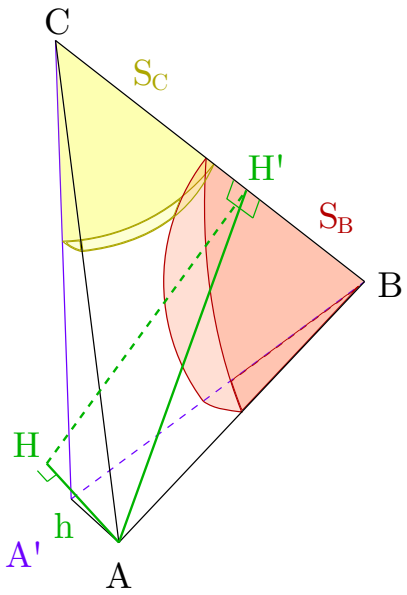

Figure 4.11: $S_B \cap S_C$.

be the height from A to BC ($AH' \perp BC$) (see Fig. 4.11). Then the plane AHH' is perpendicular to CB, which implies that $\widehat{BC}_{AA'} = \widehat{AH'H}$. Note that $|AH| = h$ and without loss of generality, $|H'B| < |H'C|$, so we have

$$|AH'| = \sqrt{|AB|^2 - |H'B|^2} \geq \sqrt{4 - d^2} > 1.$$

Therefore, $\sin\left(\widehat{AH'H}\right) = \frac{|AH|}{|AH'|} < h$. Thus, $\tan\left(\widehat{AH'H}\right) < h + o(h^2)$ and for sufficiently small h,

$$\widehat{BC}_{AA'} < \tan\left(\widehat{BC}_{AA'}\right) = \tan\left(\widehat{AH'H}\right) \leq h + O(h^2) \tag{4.5}$$

.

Using (4.4),(4.5), and (4.3), we have

$$V(S_B \cap S_C) < d\,(d-1)^2\,(1+O(h))\,h < 0.026\,(1+O(h))\,h < 0.03\,h < V(P)$$

for small h.

Therefore, for sufficiently small h, we can write

$$V(dT) \geq V(P) + V(S_B) + V(S_C) - V(S_B \cap S_C) > d^3\left(-\frac{d\hat{B}}{3} - \frac{d\hat{C}}{3}\right).$$

Since $\delta_{oct}\,d^3 > 1$, multiplying both sides by δ_{oct}, we conclude:

$$\delta_{oct} V(dT) > -\frac{d\hat{B}}{3} - \frac{d\hat{C}}{3}.$$

Notice that this proof applies to other definitions of the compression where δ_{oct} is replaced by any value superior to $\frac{1}{d^3} \approx 0.6575$.

□

4.2 Density bounds for 2-sphere packings

Throughout this section, we work with 2-sphere packings by spheres of radii 1 and $r < 1$.

The density of multi-size sphere packings in three dimensions has mostly been explored by researchers in experimental sciences as chemistry and materials sciences [OH11, HST12]. One specific focus of research in these areas are binary sphere packings (*2-sphere packings*), which have received significant attention due to their connection to crystallization at atomic and nanoparticle scales [Sch00]. Researchers from these areas are motivated to find sphere packings with densities greater than the close-packed arrangement of 1-spheres ($\frac{\pi}{3\sqrt{2}}$) seen in the previous chapter. In certain cases, self-assembly processes can result in phase separation, where spherical particles are separated into distinct clusters of close-packed spheres. As higher-density packings are often favorable for self-assembly [OH11], the existence of a packing that is strictly denser than the one obtained through phase separation increases the likelihood of creating new materials. Overall, most results on multi-size sphere packings in 3D focus on identifying particularly dense packings, thereby establishing lower bounds on the optimal density.

In analogy to the density bounds of disc packings (see Section 2.2.2, page 29), when the radius r of the small sphere is too close to 1, the close-packings (i.e. phase separation) seems to maximize the density. On the other hand, in 2010, Marshall and Hudson showed that for any value of r up to ≈ 0.623, there exist a 2-sphere packing denser than $\frac{\pi}{3\sqrt{2}}$ [MH10]. In 2011, O'Toole and Hudson presented two new high-density binary sphere arrangements obtained using Monte Carlo [OH11]. They were the first to find a 2-sphere packings with $r > 0.623$ denser than the close-packings. Their result expanded the interval of values of r with dense binary packing up to ≈ 0.659786. A year later, Hopkins, Stillinger, and Torquato revealed numerous densest binary sphere packings exhibiting unique number ratios (i.e., concentration of spheres of a given size) using the Torquato-Jiao sphere-packing algorithm which employs a combination of local and global optimization techniques to find dense packings of spheres [HST12].

The only known upper bound on the density of 2-sphere packings is given by de Laat, de Oliveira Filho, and Vallentin in [DLDOFV14]. Their method, based on semidefinite

programming and harmonic analysis, is applicable to any dimension. They provide some numerical results for dimensions $2, \ldots, 5$. In 3-dimensional case, the bound is equal to 0.813 for $r = \sqrt{2} - 1$ (the case we consider in Sections 4.2.2, 4.2.3). This section is dedicated to our partial results that might lead to an improvement of this bound.

The Florian upper bound on the density of multi-size disc packings is the density of a triangle formed by two small and one big disc, all pairwise tangent [Flo60]; basically, he proved this triangle to maximize the density among all possible triangles which might appear in a triangulation of a packing (the complete proof is given in Section 2.2.2). By analogy, we aim to obtain a better upper bound on the maximal density of 2-sphere packings providing a tetrahedron which maximizes the density for a given value of r.

Section 4.2.1 explains how to generalize the notion of FM-triangulation to 3D. Section 4.2.2 describes the 3D-version of the class of triangulated packings. In Section 4.2.3, we use the recursive subdivision method in order to provide an upper bound on the density of the subclass of tetrahedra appearing in the partition of 2-sphere packings for $r = \sqrt{2} - 1$. Even though this technique is not sufficient to obtain the bound on the density of any packing due to the time cost of the computations, it might be completed by the dimension reduction method, this is discussed in Section 4.2.4. Some openings of this research are given in the next chapter (Section 5.4.2).

4.2.1 FM-simplicial partition

In 2D, we used FM-triangulation to partition the plane. The generalization to 3D is the *FM-simplicial partition*, or, shortly, *FM-partition* (it could also be called "FM-tetrahedralization" in parallel to FM-triangulation). As in the 2-dimensional case considered in Section 2.2.1, to define it, we first consider the Voronoi partition of a sphere packing. For a packing of congruent spheres, the Voronoi cells are just convex polyhedra. A face of a Voronoi cell of a multi-size sphere packing is a region bounded by sheets of *elliptic hyperboloids of two sheets*. An elliptic hyperboloids of two sheets is a surface obtained by rotating a hyperbola around the axes which cuts it. See Figure. 4.12 for an example of configuration of spheres with their Voronoi boundaries; Figure. 4.13 depicts the intersection of this configuration with the plane passing through the centers of the spheres, it corresponds to the Voronoi partition in 2D.

In analogy with the 2-dimensional case, some degenerate configurations can produce a Voronoi partition whose dual is not a simplicial graph. More precisely, this happens when more than 4 Voronoi cells share a common vertex. In this case, we have to choose an arbitrary partition of the convex polyhedron formed by the dual of these cells into simplices (this operation is also called *simplication*). Such partition always exists, as proved in [Edm70]. As a consequence, certain sphere packings may have more than one valid FM-tetrahedralization. Figure 4.14 depicts eight spheres centered in the vertices of a cube, the dual graph of their Voronoi partition is a cube (not a simplex); an arbitrary simplication of the dual is given on the right.

For the sake of simplicity, given an FM-simplicial partition of a packing, by *tetrahedron* we mean a simplex of the partition together with the spheres centered in its vertices. The main property of the FM-partition of a sphere packing is the three-dimensional version of the support disc property of the FM-triangulation given by Claim 2.2.

Definition 4.3. *Given an FM-tetrahedron, its* ***support sphere*** *is a smallest sphere tangent to the four spheres in its vertices without intersecting any of them.*

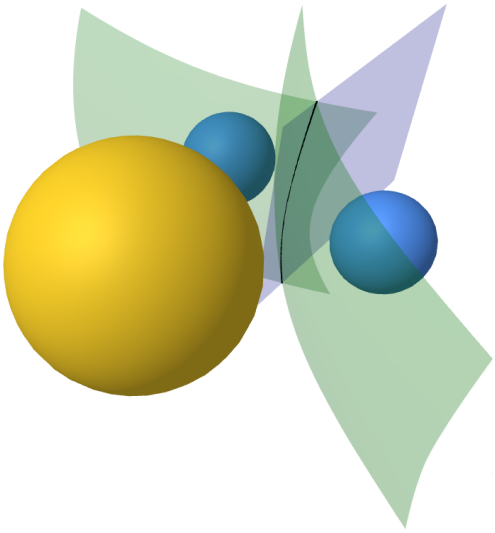

Figure 4.12: Boundaries of Voronoi cells of a configuration of three spheres.

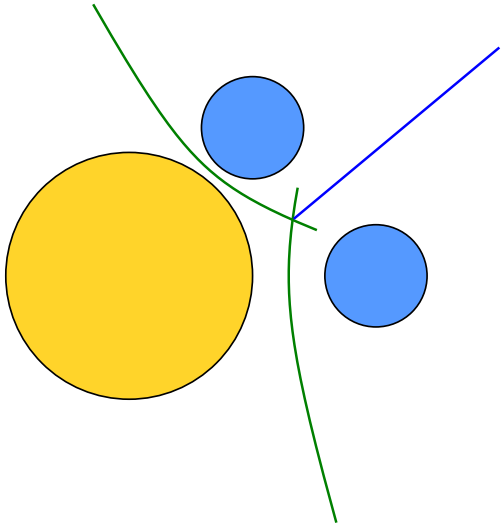

Figure 4.13: Intersection of this configuration with the plane passing through the sphere centers.

Claim 4.2 (Support sphere property)**.** *The support sphere of an FM-tetrahedron in a packing does not intersect other spheres of the packing.*

The proof of this claim is a 3-dimensional version of the proof of the support disc property, initially given in [FTM58].

Notice that, as in 2D, given a saturated sphere packing, the support sphere property implies that the support sphere radii of its FM-partition do not exceed the radius of the smallest sphere r.

A tetrahedron together with the spheres in its vertices is called *FM-tetrahedron* if it appears in an FM-partition of a saturated sphere packing. Analogously to the 2-dimensional case (Lemma 3.1 on page 69), the edge lengths of an FM-tetrahedron in a saturated packing are bounded:

Lemma 4.2. *Let T be an FM-tetrahedron in a 2-sphere packings with spheres of radii 1 and $r < 1$, let A, B, C, D be its vertices and r_A, r_B be the radii of the spheres centered in A and B respectively. Then*

$$r_A + r_B \leq |AB| \leq r_A + r_B + 2r.$$

Proof. The lower bound comes from the fact that the spheres do not intersect. Let O be the center of the support sphere of T; the support sphere property implies that $|OA| < r + r_A$ and $|OB| < r + r_B$. By the triangle inequality,

$$|AB| \leq |OA| + |OB| \leq r_A + r_B + 2r.$$

□

4.2.2 Rock salt packings

In 2D, the only tight bounds on the density of multi-size disc packings were obtained for the cases where triangulated packings maximize the density. Indeed, having a relatively

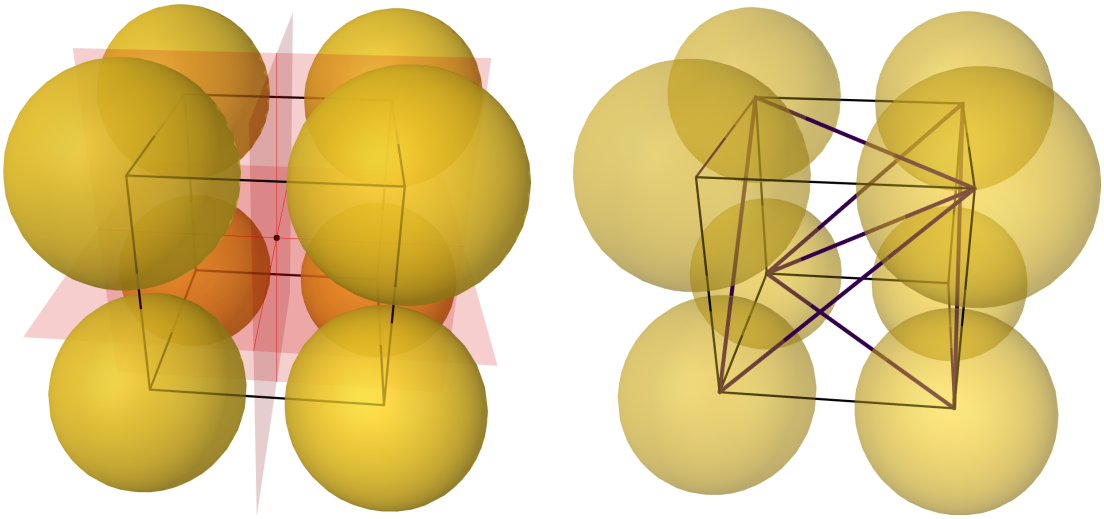

Figure 4.14: Configuration of 8 spheres centered in the vertices of a cube. On the left: their Voronoi cells (in red) sharing a common vertex, so the dual graph is a cube. On the right: an arbitrary partition of the dual graph into 6 simplices.

simple combinatorial structure of the contact graph of the target packing simplifies the problem. The 3-dimensional analogue of triangulated packings are *simplicial packings*, i.e., those whose contact graphs are pure 3-simplicial complexes.

The study of simplicial (or "compact") packings in higher dimenstions is given in [KM23] by Kikianty and Messerschmidt, generalizing the 2-dimensional result in [Mes23] to other dimensions. They show that for any dimension $d > 0$ and number $n > 0$, the set of n-tuples $r_1, \dots r_n$ such that $r_1 < \cdots < r_n = 1$ for which there exists a simplicial packing of $\mathbb{R}^d$ by spheres of radii $r_1, \dots, r_n$ (where spheres of each of n sizes are present), is finite.

Close-packings are not simplicial: the contact graphs of both local configurations around a sphere, depicted in Figure 4.8, feature quadrilateral faces. Therefore, non-triangular faces are present in the contact graph of any close-packing. In contrast with disc-packings, there are no simplicial 1-sphere packing in 3D.

Fernique showed that the only value of r allowing simplicial 2-sphere packings is $\sqrt{2}-1$ [Fer21]. The simplicial packings by spheres of radii 1 and $\sqrt{2}-1$, which we call *rock salt packings*, are constructed by taking a close-packing and filling its octahedral holes with small spheres (an example is given in Fig. 4.15). Let us call the pair of spheres of radii 1 and $\sqrt{2}-1$, the ones forming rock salt packings, *rock salt spheres*.

The name chosen for this class of packings comes from chemistry: rock salt (also known as halite) is the mineral form of sodium chloride and its crystallographic structure corresponds to a face-centered-cubic packing of chloride ions whose octahedral holes are filled with sodium ions. This structure is common among the two-element crystals [Sei40].

The rock salt packings all have the same density, denoted δ_{RS}, which can be easily computed using the density of the close-packings seen in Section 4.1.2.

$$\frac{\pi}{3\sqrt{2}} = \frac{\delta_{\text{tet}}}{3} + 2\frac{\delta_{\text{oct}}}{3} \quad \Rightarrow \quad \delta_{RS} = \frac{\delta_{\text{tet}}}{3} + 2\frac{\delta'_{\text{oct}}}{3}$$

where δ'_{oct} denotes the density of the octahedral hole filled with the sphere of radius $\sqrt{2}-1$. Let us find its value:

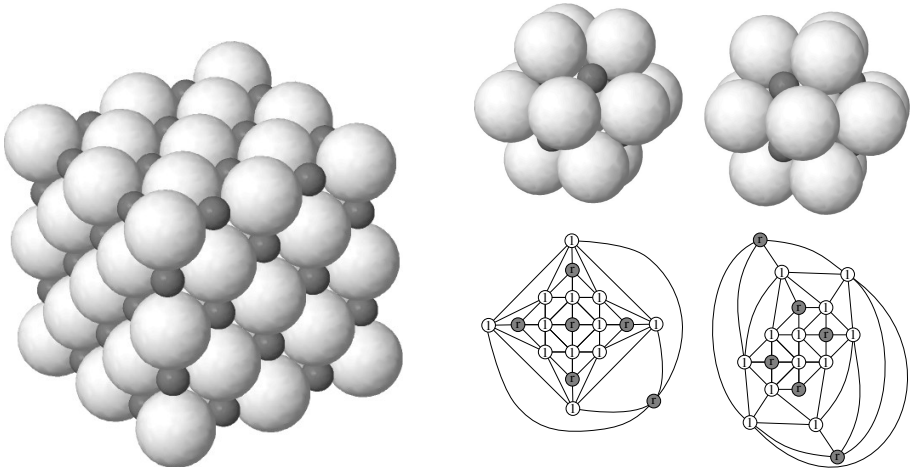

Figure 4.15: An example of a rock salt packing, two local configurations around a unit sphere present in rock salt packings, and their contact graphs.

$$\delta'_{\text{oct}} = \frac{4\left(4\arccos\left(-\frac{1}{\sqrt{3}}\right)-\pi\right)+\frac{4}{3}\pi\ \left(\sqrt{2}-1\right)^3}{\frac{8\sqrt{2}}{3}} = \delta_{\text{oct}} + \frac{\pi}{4}\left(10-7\sqrt{2}\right).$$

Therefore, the density of rock salt packings can be written as

$$\delta_{RS} = \frac{\pi}{3\sqrt{2}} + \frac{\pi}{6}\left(10-7\sqrt{2}\right) = \frac{\pi}{3\sqrt{2}}\left(5\sqrt{2}-6\right) \approx 1.071 \cdot \frac{\pi}{3\sqrt{2}} \approx 0.7931048.$$

We conjecture this density to be optimal.

Conjecture 4.1. *The rock salt packings maximize the density among packings by spheres of radii* 1 *and* $\sqrt{2}-1$.

This conjecture is discussed in detail in the next chapter, in Section 5.4.1.

4.2.3 Recursive subdivision to bound the density of star tetrahedra

In this section, we consider the case of the rock salt spheres, i.e., $r := \sqrt{2}-1 \approx 0.4142$.

As explained in Section 2.2.2, to obtain an upper bound on the density of multi-size disc packings, Florian provided a tight upper bound on the density inside an FM-triangle [Flo60]. To get this bound, he used the dimension reduction result from [FTM58] that for any FM-triangle T, there is an FM-triangle T_2 with at least two contacts (tangencies between discs) which is denser than T. This allows us to drastically reduce the set of FM-triangles whose densities shall be bounded. Finally, the densest triangle with two contacts (the tight triangle formed by one small and two big discs) can be found using computations and function analysis.

By analogy, an upper bound on the density of an FM-tetrahedron in a packing is also an upper bound on the density of the whole packing. In order to find the maximal density of an FM-tetrahedron, we aim to follow the same steps. The dimension reduction (to 3 contacts) is a work in progress which is discussed in Section 4.2.4. This section is dedicated to the density bound for a subclass of FM-tetrahedra with three contacts

(tangencies between spheres). Notice that instead of working on all packings of a given uniformity, as Florian did [Flo60], we only consider 2-sphere packings with the fixed value of r. To bound the density over this class of tetrahedra, we use the recursive subdivision method, already discussed in Section 3.5.1 for 3-disc packings.

Similarly to the 2-dimensional case, an FM-tetrahedron whose spheres are all pairwise tangent is called *tight* . Let $T^t_{r_1r_2r_3r_4}$ denote the tight tetrahedron formed by spheres of radii r_1, r_2, r_3, r_4. There are 5 tight tetrahedra, one for each collection of four disc radii; they are depicted in Figure 4.16.

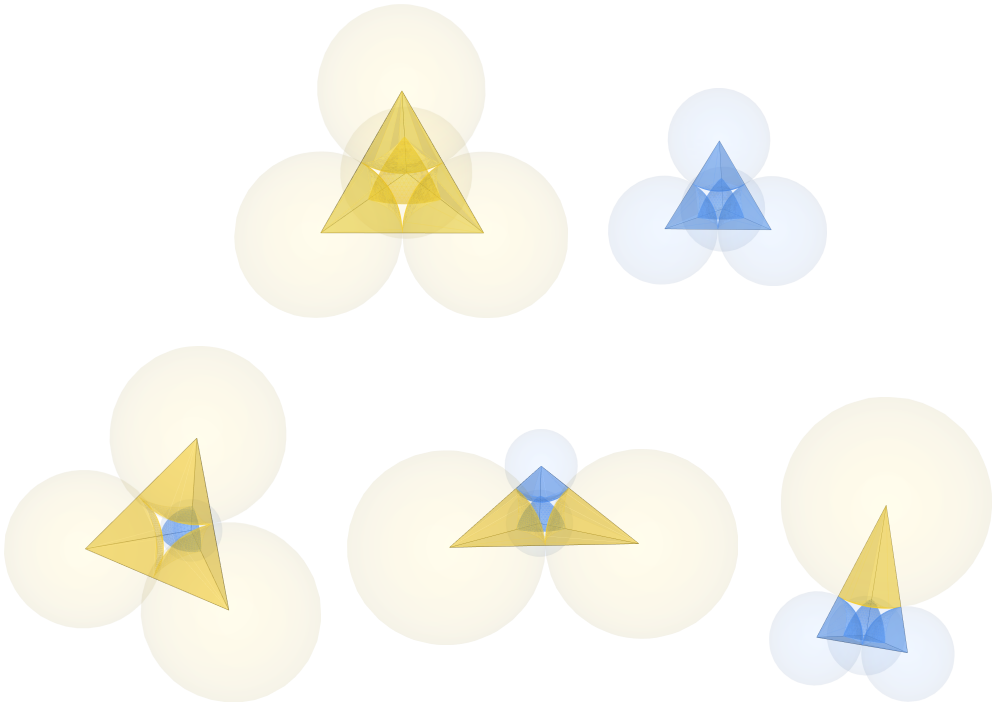

Figure 4.16: Tight tetrahedra for $r = \sqrt{2} - 1$: $T^t_{1111}, T^t_{rrrr}, T^t_{111r}, T^t_{11rr}$, and T^t_{1rrr}.

An FM-tetrahedron is called *1-stretched* if it has 5 contacts (i.e., all spheres except *one* pair are pairwise tangent) and its support sphere is of radius r. Let $T^1_{r_1r_2r_3r_4}$ denote the 1-stretched tetrahedron formed by spheres of radii r_1, r_2, r_3, r_4 such that only the r_3-sphere and the r_4-sphere are not tangent. There are 9 different 1-stretched tetrahedra: T^1_{1111}, T^1_{111r}, T^1_{1r11}, T^1_{11rr}, $T^1_{1r1r}, T^1_{rr11}, T^1_{1rrr}$, T^1_{rr1r}, and T^1_{rrrr} (some of them are depicted in Figures 4.17 and 4.18). Table 4.1 provides the symbolic formula of the lengths of the edges of 1-stretched tetrahedra.

An FM-tetrahedron is called *2-stretched* if the overall number of contacts is equal to 4, and its support sphere is of radius r. In this manuscript, we are only interested in the 2-stretched tetrahedron formed by four spheres of radii r such that one of its spheres has 3 contacts and the two stretched edges are of equal lengths. It is unique and we denote it by T^2_{rrrr} (see Figure 4.19). The lengths of the edges of T^2_{rrrr} are the following:

$$|AB| = |AC| = |AD| = |BC| = 2\sqrt{2}-2, \quad |BD| = |CD| = \left(\sqrt{2}-1\right)\sqrt{2\sqrt{6}+6} \approx 1.37,$$

and its density equals

$$\delta(T^2_{rrrr}) \approx 0.7847.$$

$r_A\, r_B\, r_C\, r_D$	$\lvert AB\rvert$	$\lvert AC\rvert$	$\lvert\mathbf{AD}\rvert$	$\lvert BC\rvert$	$\lvert BD\rvert$	$\lvert CD\rvert$
1111	2	2	$2\sqrt{2} \approx 2.83$	2	2	2
$111r$	2	2	$\sqrt{8\sqrt{5\sqrt{2}-7}+14-8\sqrt{2}} \approx 2.2$	2	$\sqrt{2}$	$\sqrt{2}$
$1r11$	2	$\sqrt{2}$	$\frac{4}{7}\sqrt{14(3-\sqrt{2})} \approx 2.69$	$\sqrt{2}$	2	$\sqrt{2}$
$11rr$	2	$\sqrt{2}$	$\sqrt{\frac{2}{7}(8\sqrt{2}-3+4\sqrt{205-143\sqrt{2}})} \approx 2.07$	$\sqrt{2}$	$\sqrt{2}$	$2\sqrt{2}-2$
$1rr1$	$\sqrt{2}$	$\sqrt{2}$	$\frac{2}{3}\sqrt{6(4\sqrt{2}-3)} \approx 2.66$	$2\sqrt{2}-2$	$\sqrt{2}$	$\sqrt{2}$
$r11r$	$\sqrt{2}$	$\sqrt{2}$	$4\sqrt{10\sqrt{2}-14} \approx 1.51$	2	$\sqrt{2}$	$\sqrt{2}$
$1rrr$	$\sqrt{2}$	$\sqrt{2}$	$\frac{4-2\sqrt{2}+\sqrt{8\sqrt{2}-6}}{\sqrt{3}} \approx 2.01$	$2\sqrt{2}-2$	$2\sqrt{2}-2$	$2\sqrt{2}-2$
$r1rr$	$\sqrt{2}$	$2\sqrt{2}-2$	$2\sqrt{2}\sqrt{\frac{104\sqrt{2}-147}{8\sqrt{2}-11}} \approx 1.41$	$\sqrt{2}$	$\sqrt{2}$	$2\sqrt{2}-2$
$rrrr$	$2\sqrt{2}-2$	$2\sqrt{2}-2$	$\frac{4(2-\sqrt{2})}{\sqrt{3}} \approx 1.35$	$2\sqrt{2}-2$	$2\sqrt{2}-2$	$2\sqrt{2}-2$

Table 4.1: Edge lengths of 1-stretched tetrahedra $T^1_{r_A r_B r_C r_D}$.

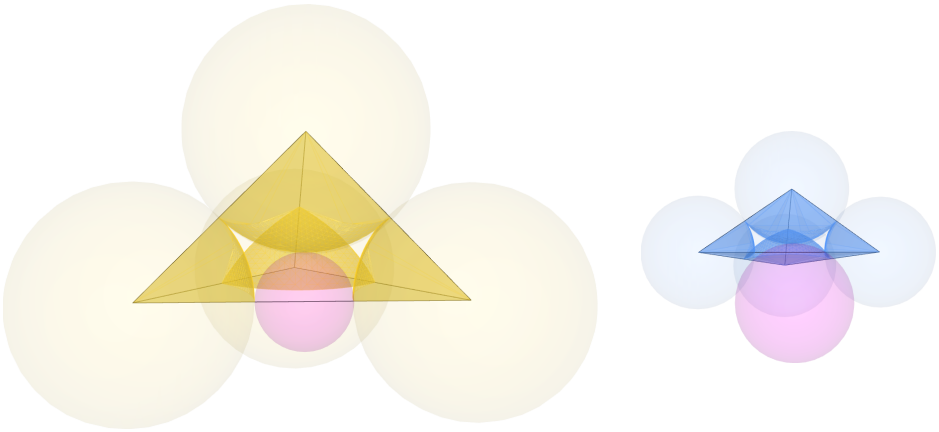

Figure 4.17: 1-stretched tetrahedra T^1_{1111} and T^1_{rrrr}.

Notice that, as stretched triangles in 2D, 1-stretched and 2-stretched tetrahedra are not FM-tetrahedra but are on the border of the set of FM-tetrahedra.

In this section, we only consider the FM-tetrahedra where one sphere is tangent to three others (so at least 3 contacts are present), we call them *star tetrahedra*. We separate the star tetrahedra into different classes according to the present sphere radii and their contacts: let $r_{1 r_2\, r_3\, r_4}$ denote the set of star tetrahedra where an r_1-sphere is tangent to the r_2-, r_3-, and r_4- spheres, we call them $r_{1 r_2\, r_3\, r_4}$-*stars*. We thus have 8 classes: 1_{111}, 1_{11r}, r_{111}, 1_{1rr}, r_{11r}, 1_{rrr}, r_{1rr}, and r_{rrr}. Some of these classes have non-empty intersections, for instance, the tight tetrahedron T^t_{111r} belongs both to 1_{11r} and to r_{111}.

Table 4.2 gives the approximate values of densities of tight and 1-stretched tetrahedra. It turns out that for each class of star tetrahedra, the optimal density is reached by one of the tetrahedra from this table or the 2-stretched $rrrr$-tetrahedron mentioned above. The 1-stretched tetrahedron T^1_{1r11} is the densest of all (its density is marked in bold), it is depicted in the middle of Figure 4.18, and it is the densest among *all* star tetrahedra.

	1111	$111r$	$1r11$	$11rr$	$1r1r$	$rr11$	$1rrr$	$rrr1$	$rrrr$
tight	≈ 0.7796	≈ 0.7998		≈ 0.8105			≈ 0.8065		≈ 0.7796
1-stretched	≈ 0.7209	≈ 0.7547	$\approx \mathbf{0.8125}$	≈ 0.7842	≈ 0.808	0.8065	≈ 0.8048	≈ 0.7974	≈ 0.7796

Table 4.2: Approximate density values of tight and 1-stretched tetrahedra.

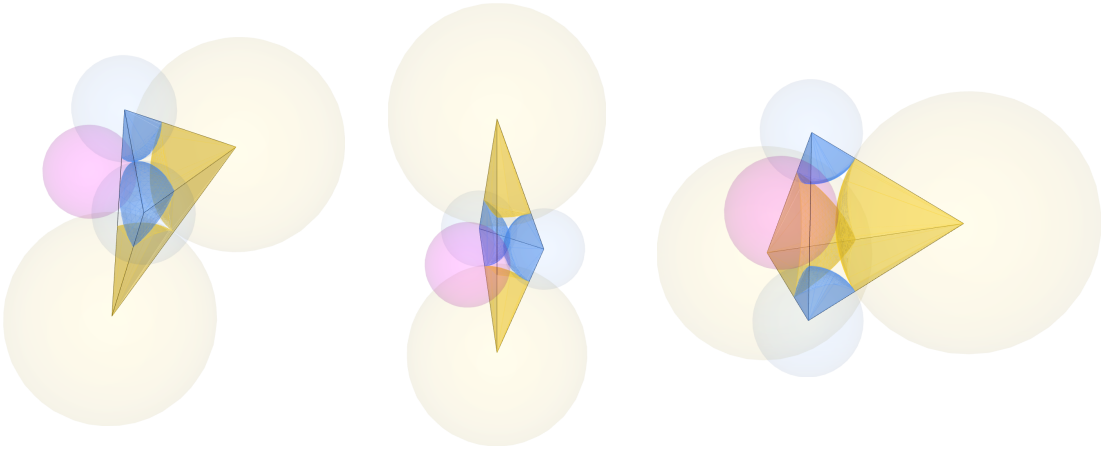

Figure 4.18: 1-stretched tetrahedra T^1_{1r1r}, T^1_{rr11}, and T^1_{11rr} (from left to right).

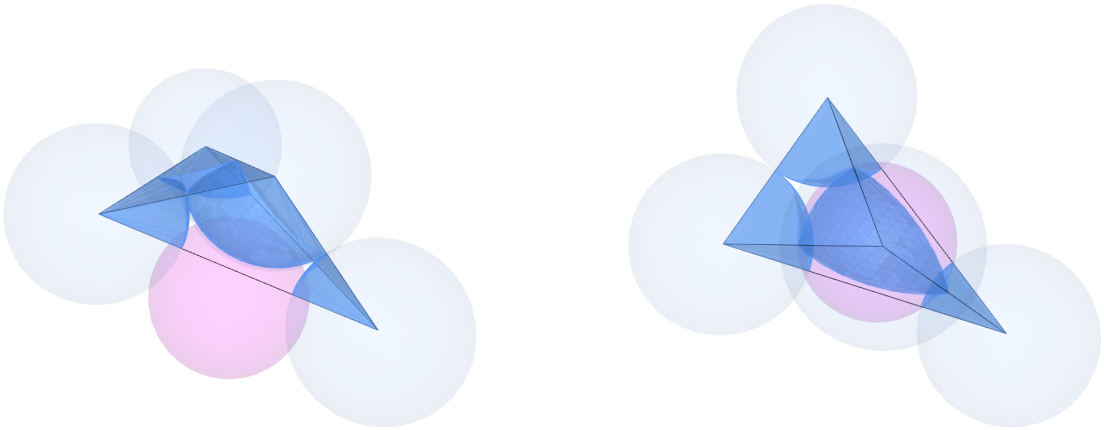

Figure 4.19: 2-stretched tetrahedron T^2_{rrrr} from two different angles.

Theorem 4.1. *The following table gives the maximal values of the density for each class of the star tetrahedra.*

$r_1r_2r_3r_4$	1_{111}	1_{11r} r_{111}	1_{1rr} r_{11r}	1_{rrr} r_{1rr}	r_{rrr}
$\delta^*_{r_1r_2r_3r_4}$	$\delta(T^t_{1111}) \approx 0.7209$	$\delta(\mathbf{T^1_{1r11}}) \approx \mathbf{0.8125}$	$\delta(T^t_{11rr}) \approx 0.8105$	$\delta(T^t_{1rrr}) \approx 0.8065$	$\delta(T^2_{rrrr}) \approx 0.7847$

The maxima are attained by tight tetrahedra, except for classes 1_{11r} and r_{111} where the optimum is the 1-stretched tetrahedron T^1_{1r11} and class r_{rrr} whose optimum is the 2-stretched tetrahedron T^2_{rrrr}.
The densest tetrahedra for each class are depicted in Figure 4.20. Theorem 4.1 directly implies that T^1_{1r11} is the optimum of the density among all star tetrahedra.

Corollary 4.1. *The density of a star tetrahedron is at most the density of the 1-stretched tetrahedron T^1_{1r11} which is equal to*

$$\begin{aligned}\delta(T^1_{1r11}) =& \sqrt{\frac{23}{8}+\frac{17}{4\sqrt{2}}}\left(\arctan\left(\sqrt{\frac{106\sqrt{2}}{289}-\frac{146}{289}}\right)\right.\\ &+(5\sqrt{2}-7)\arctan\left(2\sqrt{1+\sqrt{2}}\right)\\ &\left.+2\arctan\left(\sqrt{-5+6\sqrt{2}-4\sqrt{5-3\sqrt{2}}}\right)\right) \approx 0.8125420278108348669436.\end{aligned}$$

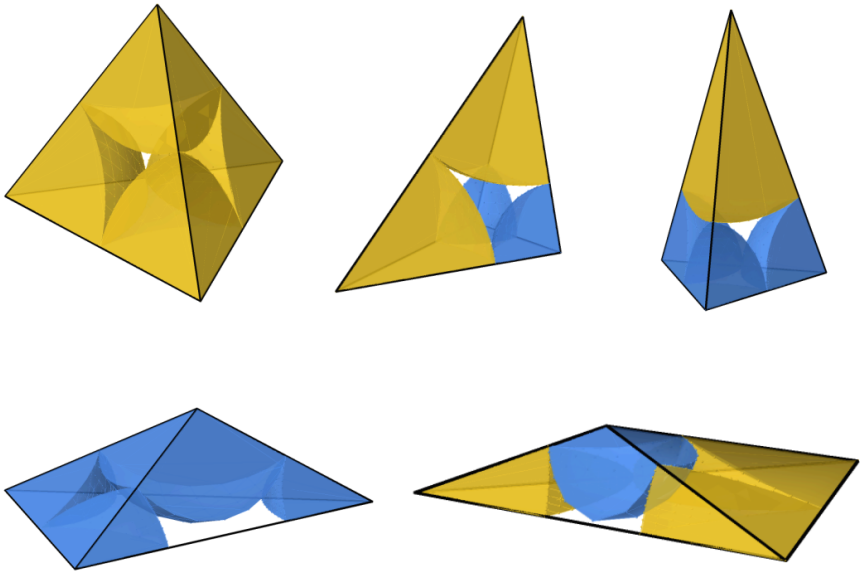

Figure 4.20: The densest tetrahedra for each class of star tetrahedra from Theorem 4.1. At the top: T^t_{1111}, T^t_{11rr}, T^t_{1rrr}. At the bottom: T^2_{rrrr} and T^1_{1r11}.

This value is quite close to the bound proposed by de Laat et al. [DLDOFV14] (0.813); nevertheless, due to the low precision of the bound given in his paper, we do not know if our bound is strictly lower. Even if it is not, a strictly better bound can be obtained by enhancing our techniques (see Section 5.4).

To prove Theorem 4.1, the most straightforward approach is computer verification. By Lemma 4.2, the edge lengths of FM-tetrahedra are bounded, so the star tetrahedra of each type form a compact subset of $\mathbb{R}^3$ (a tetrahedron is defined by the lengths of its edges and three edges of a star-tetrahedron are of fixed lengths). We, therefore, can apply the subdivision method described in Section 3.5.1 (page 76), i.e., verify the density bound for all mentioned FM-tetrahedra by representing the length of each edge as an interval and subdividing when the precision does not allow to conclude.

The supporting code can be found at `https://github.com/tooticki/rock_salt_tetrahedra`.

Let us fix the sphere radii r_1, r_2, r_3, r_4, let $T^*_{r_1r_2r_3r_4}$ denote the tetrahedron with the maximal density assigned to the class $r_{1r_2r_3r_4}$ by Theorem 4.1 and let $\delta^*_{r_1r_2r_3r_4} := \delta(T^*_{r_1r_2r_3r_4})$ denote its density. Let us describe an algorithm to verify that

$$\forall T \in r_{1r_2r_3r_4}, \quad \delta(T) < \delta^*_{r_1r_2r_3r_4}. \tag{4.6}$$

In other words, we should verify that the inequality holds for all FM-tetrahedra T such that $|AB| = r_1 + r_2$, $|AC| = r_1 + r_3$, $|AD| = r_1 + r_4$, where A, B, C, and D denote the vertices of T respectively corresponding to the r_1-, r_2-, r_3-, and r_4-spheres.

Let e, f, and g denote positive intervals, let $T_{e\times f\times g}$ denote the set of tetrahedra such that the length of their edges BC, BD and CD are respectively contained in e, f, and g, while the remaining edges are as described above.

$$T_{e\times f\times g} := \{T_{ABCD} \mid |AB| = r_1 + r_2,\ |AC| = r_1 + r_3,\ |AD| = r_1 + r_4,\\ |BC| \in e, \qquad |BD| \in f, \qquad |CD| \in g\}.$$

At the initial step of the algorithm, $e = e_0,\ g = g_0,\ f = f_0$ are the intervals formed but the lower and upper bounds for the corresponding edges given in Lemma 4.2. By definition, the described set of tetrahedra contain all tetrahedra from $r_{1r_2r_3r_4}$. Nevertheless, it also potentially contain tetrahedra which are not FM-tetrahedra, so $r_{1r_2r_3r_4} \subseteq T_{e_0 \times f_0 \times g_0}$.

At each step of the algorithm, we are given a box $e \times f \times g$ and shall verify that all FM-tetrahedra from $T_{e \times f \times g}$ satisfy (4.6).

First, we verify if there are FM-tetrahedra in the box. This does not hold if the radius of the support sphere of any tetrahedron from the box is at least r. This verification is even more complex than in the 2-dimensional case and is discussed in Section 4.2.3. If there are no FM-tetrahedra, we consider that the inequality holds on the box since any inequality holds on an empty set.

If there are potentially FM-tetrahedra in the box, we compute the interval of the density $\delta(T_{e \times f \times g})$. If it is strictly smaller than $\delta^*_{r_1r_2r_3r_4}$, then (4.6) holds in the box; if it is strictly greater, then (4.6) does not hold; otherwise, we subdivide e, f, g and treat each combination of the subintervals.

Notice that our upper bound is tight: it equals to the density of the tetrahedron $T^*_{r_1r_2r_3r_4}$ which lies on the border of the set $r_{1r_2r_3r_4}$ and, as mentioned on page 76, this means the subdivision algorithm would never stop in the neighborhood of $T^*_{r_1r_2r_3r_4}$. In the case of disc packings, we solved the analogous problem by treating ϵ-neighborhoods of tight triangles by another method: we computed partial derivatives to verify that tight triangles were indeed local maxima of $U - E$ (Section 3.3.1, page 66).

We apply a similar method for tetrahedra. We use elementary differential geometry and, after studying the shape of the set of star tetrahedra in the neighborhood of $T^*_{r_1r_2r_3r_4}$, we manage to show for a certain value of ϵ that $T^*_{r_1r_2r_3r_4}$ maximizes the density in its ϵ-neighborhood of star tetrahedra. More details are given in the following subsection.

Extremal cases

In this part, we treat the neighborhoods of extremal cases: tetrahedra which are "close enough" to an optimal one. Here, we should show that the optimal tetrahedron is a local maximum of the density in a small neighborhood.

The way to show it depends on how the optimal tetrahedron is placed in the set of star tetrahedra of a given type. The simplest case is when the optimal tetrahedron is tight, since it is situated in the "corner" of the set of star tetrahedra: all three free edges are of minimal possible lengths. To show that it maximizes the density, as in the 2-dimensional case of ϵ-triangles, it is enough to show that all three partial derivatives of the density are negative in the ϵ-neighborhood of the tight tetrahedron. Computing the partial derivatives of the density function in interval arithmetic, we found the values of ϵ for classes $1_{111}, 1_{1rr}, r_{11r}, 1_{rrr}$, and r_{1rr} which allowed the recursive subdivision algorithm described above to verify the density inequality in a short time from several seconds to a few minutes. Table 4.3 indicates the values of ϵ and the time of execution for all classes.

The classes where a stretched tetrahedron maximizes the density are more tricky. Let us give you the detail of how we treat the 1_{11r} and r_{111} classes, the optimal tetrahedron for both of them is the 1-stretched tetrahedron T^1_{1r11} which also maximizes the density among all start tetrahedra. The remaining class r_{rrrr} whose optimum is a 2-stretched tetrahedron is treated by a similar approach.

Let us first define the distance between two tetrahedra represented by ordered lists of edge lengths. We adopt the L_∞ distance: i.e., the distance is the maximal difference between the lengths of corresponding edges. More formally, let T be a tetrahedron with edges of lengths $\{x_i\}_{i=1}^6$ and T' a tetrahedron with edges of lengths $\{x'_i\}_{i=1}^6$,

$$d_\infty(T, T') := \max_{i=1,\dots,6}(|x_i - x'_i|).$$

We define an ϵ-neighborhood of the tetrahedron T as

$$B_\epsilon^\infty(T) := \{T' \mid d_\infty(T, T') < \epsilon\}.$$

Let us show that the 1-stretched tetrahedron T^1_{1r11} maximizes the density in its neighborhood of r_{111} and of 1_{11r}. We start with the class r_{111}, which is the simplest case.

Lemma 4.3. *For $\epsilon_r = 0.0005$, T^1_{1r11} maximizes the density among the r_{111}-star tetrahedra in its ϵ_r-neighborhood,*

$$\forall T \in B^\infty_{\epsilon_r}(T^1_{1r11}) \cap r_{111}, \quad \delta(T) < \delta(T^1_{1r11}). \tag{4.7}$$

Proof. Let T be a tetrahedron in r_{111} and A, B, C, D be its vertices, let A denote its vertex corresponding to the star-center ($r_A = r$), B, C and D denote the centers of the other spheres. The tetrahedron T is completely defined by the triplet of edge lengths $|BC|, |BD|$, and $|CD|$ (since the remaining ones are fixed: $|AB| = |AC| = |AD| = 1+r$). Let us use variables x, y, z instead of respectively $|BC|, |BD|, |CD|$ and if $t = (x, y, z) \in \mathbb{R}^3$, let T_t denote the tetrahedron $ABCD$ defined as above. Let S_r denote the subset of the Euclidean 3-dimensional space corresponding to the triplets of edges lengths of the r_{111}-star tetrahedra:

$$S_r := \{t \in \mathbb{R}^3 \mid T_t \in r_{111}\}.$$

Since the lengths of the eges of the FM-tetrahedra are uniformly bounded and the support sphere radius never exceeds r, we get

$$S_r \subseteq (2, 2 + 2r)^3 \cap \{t \in \mathbb{R}^3 \mid r_s(t) < r\},$$

where $r_s(t)$ denotes the radius of the support sphere of T_t. Therefore, S_r is contained in an intersection of a box and a set bounded by a surface implicitly defined as $r_s(t) = r$. The box and the surface are depicted in Figure 4.21, to the left.

Let $\delta(t)$ denote the density of the tetrahedron T_t:

$$\begin{aligned}
\delta(x,y,z) = \quad & \frac{8\left(7-5\sqrt{2}\right)}{\sqrt{4\,x^2y^2+4\,x^2z^2+4\,y^2z^2-x^2y^2z^2-2\,x^4-2\,y^4-2\,z^4}} \\
& \left(-\arctan\left(\frac{\sqrt{-2\,x^4+4\,x^2y^2-2\,y^4-2\,z^4-((x^2-4)y^2-4\,x^2)z^2}}{\left(x+\sqrt{2}\right)y^2+\sqrt{2}x^2-\sqrt{2}z^2+\left(x^2+2\,\sqrt{2}x\right)y}\right)\right. \\
& \quad -\arctan\left(\frac{\sqrt{-2\,x^4+4\,x^2y^2-2\,y^4-2\,z^4-((x^2-4)y^2-4\,x^2)z^2}}{\left(x+\sqrt{2}\right)z^2+\sqrt{2}x^2-\sqrt{2}y^2+\left(x^2+2\,\sqrt{2}x\right)z}\right) \\
& \quad -\arctan\left(\frac{\sqrt{-2\,x^4+4\,x^2y^2-2\,y^4-2\,z^4-((x^2-4)y^2-4\,x^2)z^2}}{\left(y+\sqrt{2}\right)z^2-\sqrt{2}x^2+\sqrt{2}y^2+\left(y^2+2\,\sqrt{2}y\right)z}\right) \\
& \quad \left. +\arctan\left(\frac{\sqrt{-2\,x^4+4\,x^2y^2-2\,y^4-2\,z^4-((x^2-4)y^2-4\,x^2)z^2}}{\sqrt{2}x^2+\sqrt{2}y^2+\sqrt{2}z^2-16\,\sqrt{2}}\right)\right).
\end{aligned}$$

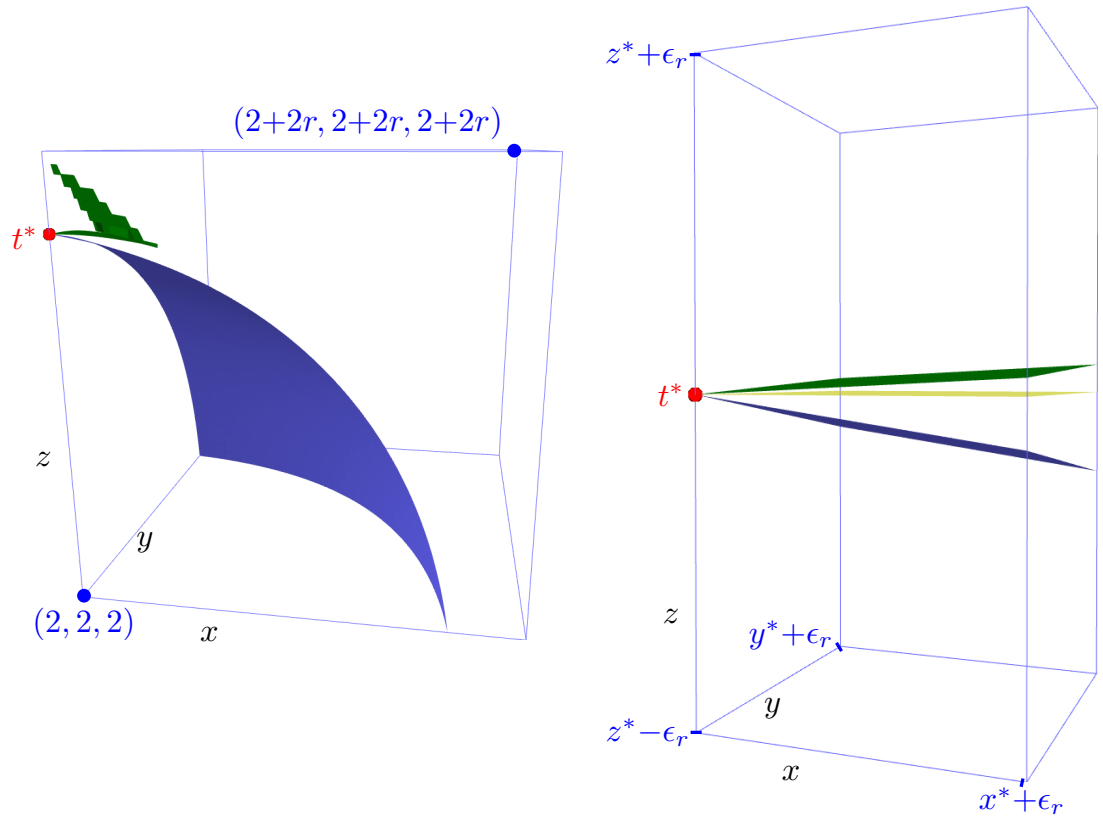

Figure 4.21: To the left, the border of S_r in blue and the surface $\delta(x, y, z) = \delta^*$ in green. To the right, the same in the ϵ_r-neighborhood of t^*, the plane $z = z^*$ is marked in yellow.

By symmetry, w.l.o.g, we assume that $|CD| \geq \max(|BC|, |BD|)$, so we will only treat one point of the local maximum out of the three symmetrical ones. Let $t^* = (2, 2, 4\sqrt{2}\sqrt{\frac{r}{2r+1}})$ denote the point corresponding to T^1_{1r11}, it is on the border of S_r. We shall prove that t^* maximizes δ in its ϵ-neighborhood intersected with S_r (see Fig. 4.21).

Since δ is smooth on S_r, using the mean value theorem, we get that for any $t \in S_r$ there exists $c \in (0, 1)$ such that

$$\delta(t) - \delta(t^*) = \nabla\delta\,(c\,t + (1-c)\,t^*) \cdot (t - t^*). \tag{4.8}$$

Using interval arithmetic, we get the following bounds on the partial derivatives of δ for any $t \in S_r \cap B^\infty_{\epsilon_r}(t^*)$:

$$\frac{\partial\delta}{\partial x}(t) < a_x := -0.006, \qquad \frac{\partial\delta}{\partial y}(t) < a_y := -0.006, \qquad \frac{\partial\delta}{\partial z}(t) > a_z := 0.6. \tag{4.9}$$

On the other hand, the surface corresponding to $r_s(t) = r$ can be expressed explicitly as $z_{r_s}(x, y)$ which is the value of z in function of x, y inside $(2, 2 + 2\,r)^3$ (the formulas of the support sphere radius are discussed in the next section on page 124):

$$\forall (x, y, z) \in (2, 2 + 2r)^3, \;\; r_s(x, y, z) = r \Leftrightarrow z = z_{r_s}(x, y).$$

In Figure 4.21, z_{r_s} is marked in blue. We can now rewrite S_r as follows:

$$S_r \subseteq \{(x, y, z) \mid x \in (2, 2 + 2r),\; y \in (2, 2 + 2r),\; z \in (2, z_{r_s}(x, y))\}. \tag{4.10}$$

Using interval arithmetic, we get that for all x, y such that $x \in (x^*, x^* + \epsilon_r)$ and $y \in (y^*, y^* + \epsilon_r)$,

$$\frac{\partial z_{r_s}}{\partial x}(x, y) < -0.127, \qquad \frac{\partial z_{r_s}}{\partial x}(x, y) < -0.127.$$

This implies that for all (x, y), $x \in (x^*, x^* + \epsilon_r)$ and $y \in (y^*, y^* + \epsilon_r)$

$$z_{r_s}(x, y) < z_{r_s}(x^*, y^*) = z^*. \tag{4.11}$$

Inequality (4.11) implies that if (x, y, z) is in $B^\infty_{\epsilon_r}(t^*) \cap S_r$, then $z < z^*$. Let us rewrite (4.8) using (4.9) and the fact that for all $(x, y, z) \in B^\infty_{\epsilon_r}(t^*) \cap S_r$, we have $x > x^*$, $y > y^*$, $z < z^*$. For all $t = (x, y, z) \in B^\infty_{\epsilon_r}(t^*)$, for some $t' \in B^\infty_{\epsilon_r}(t^*) \cap S'_r$:

$$\begin{aligned}\delta(t) - \delta(t^*) &= \frac{\partial \delta}{\partial x}(t')\,(x - x^*) + \frac{\partial \delta}{\partial y}(t')\,(y - y^*) + \frac{\partial \delta}{\partial x}(t')\,(z - z^*) \\ &< \underbrace{a_x}_{<0}\underbrace{(x - x^*)}_{>0} + \underbrace{a_y}_{<0}\underbrace{(y - y^*)}_{>0} + \underbrace{a_z}_{>0}\underbrace{(z - z^*)}_{<0} < 0.\end{aligned}$$

□

The case of 1_{11r} is harder to treat but consists of the similar steps.

Lemma 4.4. *For $\epsilon_1 = 0.0008$, T^1_{1r11} maximizes the density among the 1_{11r}-star tetrahedra in its ϵ_1-neighborhood:*

$$\forall T \in B^\infty_{\epsilon_1}(T^1_{1r11}) \cap 1_{11r}, \quad \delta(T) < \delta(T^1_{1r11}).$$

Proof. Let $T \in 1_{11r}$ and A, B, C, D be its vertices, let A denote its vertex corresponding to the star-center, B and D denote the centers of other 1-spheres, and C denote the center of the r-sphere: $r_A = r_B = r_D = 1$, $r_C = r$. The tetrahedron T is completely defined by the triplet of edge lengths $|BC|$, $|BD|$, and $|CD|$ (since the remaining ones are fixed: $|AB| = 2$, $|AC| = 1 + r$, $|AD| = 2$). Let us use variables x, y, z instead of respectively $|BC|$, $|CD|$, $|BD|$ and if $t = (x, y, z) \in \mathbb{R}^3$, let T_t denote the tetrahedron $ABCD$ defined as above and let

$$S_1 := \{t \in \mathbb{R}^3 \mid T_t \in 1_{11r}\}.$$

Since the edges lengths of the FM-tetrahedra are bounded and the support sphere radius never exceeds r, we get

$$S_1 \subseteq (1 + r, 1 + 3r) \times (1 + r, 1 + 3r) \times (2, 2 + 2r) \cap \{t \mid r_s(t) < r\},$$

where $r_s(t)$ denotes the radius of the support sphere of T_t. This set is depicted in Figure 4.22, to the left.

Let $\delta(t)$ denote the density of the tetrahedron T_t. As in the previous case, δ is smooth on S_1. We do not give the formula: it resembles the one of the previous case. Let $t^* = (1 + r,\, 1 + r,\, 4\sqrt{2}\sqrt{\frac{r}{2r+1}})$ denote the point corresponding to T^1_{1r11}, it is on the border of S_1. As in the previous case, by the mean value theorem, for any $t \in S_1$, there exists $c \in (0, 1)$ such that

$$\delta(t) - \delta(t^*) = \nabla\delta\,(c\,t + (1 - c)\,t^*) \cdot (t - t^*). \tag{4.12}$$

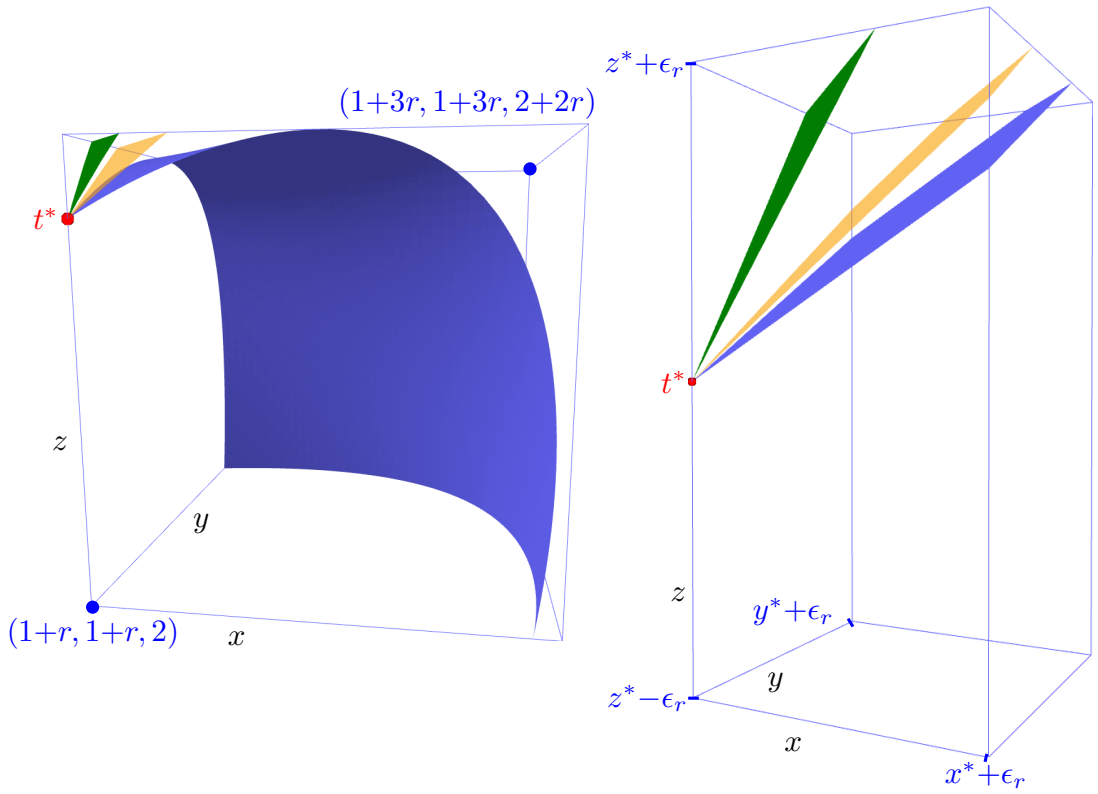

Figure 4.22: To the left, the border of S_1 in blue and the surface $\delta(x, y, z) = \delta^*$ in green, the plane $z = z^* + b_x\,(x - x^*) + b_y\,(y - y^*)$ is marked in orange. To the right, the same in the ϵ_1-neighborhood of t^*.

Using interval arithmetic, we prove that for any $t \in B^\infty_{\epsilon_1}(t^*) \cap S'_1$,

$$\frac{\partial \delta}{\partial x}(t) < a_x := -0.88, \qquad \frac{\partial \delta}{\partial y}(t) < a_y := -0.88, \qquad 0 < \frac{\partial \delta}{\partial z}(t) < a_z := 1.1. \tag{4.13}$$

As in the previous case, the surface corresponding to $r_s(t) = r$ can be expressed explicitly as $z_{r_s}(x, y)$:

$$\forall (x, y, z) \in (1 + r, 1 + 3r) \times (1 + r, 1 + 3r) \times (2, 2 + 2r),\ \ r_s(x, y, z) = r \Leftrightarrow z = z_{r_s}(x, y).$$

In Figure 4.22, z_{r_s} is marked in blue. We can now rewrite S_1 as follows:

$$S_1 \subseteq \{(x, y, z) \mid x \in (1 + r, 1 + 3r),\ y \in (1 + r, 1 + 3r),\ z \in (2, z_{r_s}(x, y))\}.$$

Using interval arithmetic, we bound the partial derivatives of z_{r_s} for $(x, y) \in (x^*, x^* + \epsilon_1) \times (y^*, y^* + \epsilon_1)$,

$$\frac{\partial z_{r_s}}{\partial x}(x, y) < b_x := 0.6, \qquad \frac{\partial z_{r_s}}{\partial y}(x, y) < b_y := 0.6.$$

Let us apply the previous inequalities together with the mean value theorem to z_{r_s} (which is smooth in $(x^*, x^* + \epsilon_r) \times (y^*, y^* + \epsilon_r)$). We get, for all $(x, y) \in (x^*, x^* + \epsilon_r) \times (y^*, y^* + \epsilon_r)$,

$$\begin{aligned} z_{r_s}(x, y) &< z_{r_s}(x^*, y^*) + b_x\,(x - x^*) + b_y\,(y - y^*) \\ &= z^* + b_x\,(x - x^*) + b_y\,(y - y^*). \end{aligned} \tag{4.14}$$

star class	ϵ	execution time (in seconds)	number of boxes
1_{111}	0.03	1	52176
1_{1rr}	0.005	18	826632
1_{rrr}	0.006	22	1181736
r_{11r}	0.009	840	46629199
r_{1rr}	0.006	300	12215213
1_{11r}	0.0008	22	1039782
r_{111}	0.0005	562	28703078
r_{rrr}	0.0009	2700	120923613

Table 4.3: The value of ϵ, executions time, and the overall number of boxes considered by the subdivision algorithm for each star class.

The last inequality, combined with (4.12) and (4.13), implies that for all $t = (x, y, z) \in B^\infty_{\epsilon_1}(t^*) \cap S_1$ for some $t' \in B^\infty_{\epsilon_1}(t^*) \cap S_1$:

$$\begin{aligned}\delta(t) - \delta(t^*) &= \frac{\partial\delta}{\partial x}(t')\,(x - x^*) + \frac{\partial\delta}{\partial y}(t')\,(y - y^*) + \frac{\partial\delta}{\partial x}(t')\,(z - z^*) \\ &\leq \underbrace{a_x}_{<0}\underbrace{(x - x^*)}_{>0} + \underbrace{a_y}_{<0}\underbrace{(y - y^*)}_{>0} + \underbrace{\frac{\partial\delta}{\partial x}(t')}_{>0}(z - z^*) \qquad (4.15)\end{aligned}$$

For t with $z < z^*$, (4.13) gives us the signs of the coefficients, as in the proof of the previous lemma, so we directly get $\delta(t) - \delta(t^*) < 0$. Suppose $z \geq z^*$, then (4.14) implies

$$\begin{aligned}\delta(t) - \delta(t^*) &\leq a_x\,(x - x^*) + a_y\,(y - y^*) + \underbrace{a_z}_{>0}\,(z - z^*) \\ &\leq a_x\,(x - x^*) + a_y\,(y - y^*) + a_z\,(b_x\,(x - x^*) + b_y\,(y - y^*)) \\ &= (a_x + a_z\,b_x)(x - x^*) + (a_y + a_z\,b_y)(y - y^*) \\ &= -0.022\ \underbrace{(x - x^*)}_{>0} - 0.022\ \underbrace{(y - y^*)}_{>0} < 0.\end{aligned}$$

This allows us to conclude. □

Table 4.3 gives the value of ϵ for each class of star tetrahedra, as well as the time of execution of the dimension reduction algorithm, and the overall number of boxes that was considered during subdivision.

Implementation issues

The supporting code is given at `https://github.com/tooticki/rock_salt_tetrahedra`.

Interval arithmetic's major inconvenience is that even though the resulting interval is guaranteed to contain all actual values of an expression, there are no guarantuees on its size. Different representation of the same expression will give different intervals. The problem comes from the fact that multiple apparitions of the same variable in a formula are not "synchronized" in interval arithmetic. So, without reformulation of the expression, $x - x$ with $x = (0, 1)$ will

be computed as $(-1, 1)$ instead of 0. This does not particularly affect our computations in the case of 3-disc packings but it does play an important role in our study of 2-sphere packings. This section focuses on the problems we encountered and the solutions we devised.

Due to higher computational volume, we implemented supporting code in C++ rather than in SageMath, using boost interval arithmetic library [1].

Let X, Y, Z, W be the vertices of tetrahedron T, S_X, S_Y, S_Z, and S_W be the spheres centered in these vertices, and let r_X, r_Y, r_Z, and r_W denote the radii of these spheres. Let the edge lengths of T be denoted by $a = |XY|$, $b = |XZ|$, $c = |XW|$, $d = |YZ|$, $e = |YW|$, $f = |ZW|$. In our implementation, we have to recurrently compute two functions: the density of a tetrahedron and the radius of its support sphere. The density of T can be expressed as follows:

$$\begin{aligned}\delta(T) &= \frac{V(T \cap S_X) + V(T \cap S_Y) + V(T \cap S_Z) + V(T \cap S_W)}{V(T)} \\ &= \frac{r_X^3\, \widehat{X}_{YZW} + r_Y^3\, \widehat{Y}_{XZW} + r_Z^3\, \widehat{Z}_{XYW} + r_W^3\, \widehat{W}_{XYZ}}{3\, V(T)}.\end{aligned}$$

There are at least two ways to compute the solid angle in a vertex of a tetrahedron.
First way: to use dihedral angles:

$$\widehat{X}_{YZW} = \widehat{XY}_{ZW} + \widehat{XZ}_{YW} + \widehat{XW}_{YZ} - \pi.$$

To find the value of each dihedral angle, we use the law of cosine for tetrahedra together with the Herones formula. We get

$$\widehat{XY}_{ZW} = \arccos\left(-\frac{\begin{array}{c}(a+c+e)(a+c-e)(a-c+e)(a-c-e) \\ +(a+d+f)(a+d-f)(a-d+f)(a-d-f) + 4\,a^2b^2 - \left(c^2-d^2-e^2+f^2\right)^2\end{array}}{2\sqrt{\begin{array}{c}(a+c+e)(a+c-e)(a-c+e)(a-c-e) \\ (a+d+f)(a+d-f)(a-d+f)(a-d-f)\end{array}}} \right).$$

In this case, the solid angle is the sum of expressions of the same form: an arccosine of a fraction of a polynomial and a square root of a polynomial.
Second way: to compute the solid angle $\widehat{X}_{YZW}$, we can also use the following formula:

$$\widehat{X}_{YZW} = 2\,\arctan\left(\frac{\vec{a}\cdot(\vec{b}\times\vec{c})}{abc + (\vec{a}\cdot\vec{b})c + (\vec{a}\cdot\vec{c})b + (\vec{b}\cdot\vec{c})a}\right)$$

where $\vec{a} = \overrightarrow{XY}$, $\vec{b} = \overrightarrow{XZ}$, $\vec{c} = \overrightarrow{XW}$, $\vec{a}\cdot\vec{b}$ denotes the scalar product and $\vec{a}\cdot(\vec{b}\times\vec{c})$ the scalar triple product. This formula is "simpler": it is an arctangent of a fraction of two polynomials.

To illustrate the difference in precision of the two aforementioned methods, let us compute a solid angle of a tetrahedron whose edges are all intervals $(2-\epsilon, 2+\epsilon)$. For $\epsilon = 0.01$, the first method returns the interval of diameter ≈ 0.5128 while the second gives ≈ 0.2137. When we increase the precision, the difference stays of the same order: we get intervals of diameters respectively ≈ 0.0509, ≈ 0.0212 for $\epsilon = 0.001$ and ≈ 0.0051, ≈ 0.0021 for $\epsilon = 0.001$.

Another difficulty comes from the formula of the support sphere radius. Similarly to the 2-dimensional case, this value can be found as a root of a quadratic equation whose coefficients $\mathcal{A}, \mathcal{B}, \mathcal{C}$ depends on the sphere radii and the tetrahedron edge lengths. The formulas are enormous: they contain a high number of variable occurrences which considerably lower the precision of the interval computations. In order to overcome this difficulty, we precompute the formulas of the coefficients $\mathcal{A}, \mathcal{B}, \mathcal{C}$ for each different case of tetrahedra, which allows us to fix the disc radii and 3 edge lengths in the symbolic expressions and simplify them. After all, we get simpler formulas depending on three variables. For example, for the 1111-tetrahedra, fixing

[1] `https://www.boost.org/doc/libs/1_66_0/libs/numeric/interval/doc/interval.htm` (accessed on 15 July, 2023)

$r_X = r_Y = r_Z = r_W = 1$ and $|XY| = |XZ| = |XW| = 2$ (i.e., $a = b = c = 2$), we get:

$$\begin{aligned}
\mathcal{A}_{1111} &= 4\,\left(d^2 - e^2\right)^2 + 4\,f^4 + \left(\left(d^2 - 8\right)e^2 - 8\,d^2\right)f^2 \\
\mathcal{B}_{1111} &= 8\,\left(d^2 - e^2\right)^2 + 8\,f^4 + 2\,\left(\left(d^2 - 8\right)e^2 - 8\,d^2\right)f^2 \\
\mathcal{C}_{1111} &= d^2e^2f^2
\end{aligned}$$

$$\delta_{1111} = \frac{8\left(\begin{array}{r}\arctan\left(\frac{\sqrt{-4\,(d^2-e^2)^2-4\,f^4-((d^2-8)e^2-8\,d^2)f^2}}{(d+2)e^2+2\,d^2+(d^2+4\,d)e-2\,f^2}\right) \\ +\arctan\left(\frac{\sqrt{-4\,(d^2-e^2)^2-4\,f^4-((d^2-8)e^2-8\,d^2)f^2}}{(d+2)f^2+2\,d^2-2\,e^2+(d^2+4\,d)f}\right) \\ +\arctan\left(\frac{\sqrt{-4\,(d^2-e^2)^2-4\,f^4-((d^2-8)e^2-8\,d^2)f^2}}{(e+2)f^2-2\,d^2+2\,e^2+(e^2+4\,e)f}\right) \\ -\arctan\left(\frac{\sqrt{-4\,(d^2-e^2)^2-4\,f^4-((d^2-8)e^2-8\,d^2)f^2}}{2\,(d^2+e^2+f^2-32)}\right)\end{array}\right)}{\sqrt{-4\,\left(d^2 - e^2\right)^2 - 4\,f^4 - \left(\left(d^2 - 8\right)e^2 - 8\,d^2\right)f^2}}.$$

Let `A`, `B`, `C`, `delta`, denote the symbolic expressions on 10 variables r_X, r_Y, r_Z, r_W, a, b, c, d, e, f corresponding respectively to the values of $\mathcal{A}$, $\mathcal{B}$, $\mathcal{C}$, and δ for the tetrahedron with sphere radii r_X, r_Y, r_z, r_W and edges lengths a, b, c, d, e, f. Let `A1111`, `B1111`, `C1111`, `delta1111` denote the simplified expressions on 3 variables e, d, f corresponding to the respective values for the tetrahedron with radii $r_X = r_Y = r_Z = r_W = 1$ and edges of lengths $a = b = c = 2$ and d, e, f (they are given above).

Indeed, in theory, if d, e, f are real numbers, both expressions always yield the same value:

$$\begin{aligned}
&\texttt{A}(1,1,1,1,2,2,2,d,e,f) = \texttt{A1111}(d,e,f) \\
&\texttt{B}(1,1,1,1,2,2,2,d,e,f) = \texttt{B1111}(d,e,f) \\
&\texttt{C}(1,1,1,1,2,2,2,d,e,f) = \texttt{C1111}(d,e,f) \\
&\texttt{delta}(1,1,1,1,2,2,2,d,e,f) = \texttt{delta1111}(d,e,f).
\end{aligned}$$

The computer calculations, though, may lead to slightly different results if d, e, f are floating-point numbers. Finally, when they are intervals, the difference is striking. Let us compare the diameters of the resulting intervals when d, e, and f are all equal to $I := [2, 2 + \epsilon]$ for $\epsilon = 0.1$:

$$\begin{aligned}
&|\texttt{A}(1,1,1,1,2,2,2,I,I,I)| \approx 117 && |\texttt{A1111}(I,I,I)| \approx 33 \\
&|\texttt{B}(1,1,1,1,2,2,2,I,I,I)| \approx 417 && |\texttt{B1111}(I,I,I)| \approx 234 \\
&|\texttt{C}(1,1,1,1,2,2,2,I,I,I)| \approx 287 && |\texttt{C1111}(I,I,I)| \approx 22 \\
&|\texttt{delta}(1,1,1,1,2,2,2,I,I,I)| \approx 0.91 && |\texttt{delta1111}(I,I,I)| \approx 0.79
\end{aligned}$$

Recall that $|X|$ denote the diameter of the interval X. Indeed, these values may vary in function of the expressions we choose. We suspect, however, that even if `A`, `B`, `C`, and `delta` are extremely "well" simplified, they would almost never overrun `A1111`, `B1111`, `C1111`, `delta1111` (simplified by the same method).

4.2.4 Dimension reduction for 2-sphere packings

The results obtained in the previous section alone are not sufficient to derive an upper bound for all packings of rock salt spheres. Indeed, due to the computational constraints, the recursive subdivision method only allowed us to bound the density of star FM-tetrahedra with 3 contacts.

Potentially, there might exist non-star tetrahedra denser than any star tetrahedron. Nevertheless, after running a bunch of numerical experiments, we believe that, analogously to disc packings (see Section 2.2.2), any tetrahedron can be deformed into a star tetrahedron in a way that the density increases. Our experimental method consisted in randomly picking an FM-tetrahedron and then repeatedly slightly contracting one of its edges in a way to augment the density. All our tries resulted in a star tetrahedron.

Even though we do not have a proof of the above statement for two-sphere packings, we conjecture that it can be obtained using dimension reduction approach. This method consists in showing that by performing specific transformations on a tetrahedron, its density does not augment, and then using those transformation to increase the number of contacts. Our aim is to find a way to start with any tetrahedron, potentially with 0 contacts (and thus, 6 free variables of edge lengths, i.e., in dimension 6), apply a series of transformation, and obtain a star tetrahedron having 3 contacts.

In the proof of the dimension reduction by Fejes Tóth and Mólnar [FTM58] in the case of disc packings (Section 2.4, page 31), the first step consisted in deflating the triangle (keeping its disc sizes constant) until a tangency between two discs or a disc and an edge occurs, this transformation is called *deflation*. We might apply the same approach for FM-tetrahedra of 2-sphere packings to decrease the dimension by one. Nevertheless, more work is required in the case when this transformation produces a contact between a sphere and a disc. The adaptation of the Fejes Tóth and Mólnar's reasoning to 3D seems possible but not straightforward. In any case, this method alone would only allow to reduce the dimension from 6 to 5 which is not enough.

Another transformation potentially reducing the dimension is the *edge reduction*, i.e., sliding one sphere along an edge until it is tangent to another sphere, discussed in Section 4.1.3 for 1-sphere packings. Even though, the author did not succeed to fully formalize the Hales' result (given by Proposition 4.1), one might be able to partially generalize it to the case of 2-sphere packings. Unfortunately, even obtaining a complete analogical result would not be enough...

Let T denote a non-star FM-tetrahedron with vertices A, B, C, D. If it has no contacts, we apply any of two aforementioned dimension reduction methods to T and obtain a one-contact tetrahedron. If T has two contacts corresponding to two adjacent edges, we apply the edge reduction to the sphere with no contacts and reduce the dimension. However, if T has two contacts corresponding to two non-adjacent edges, then there is no way to apply deflation nor edge reduction. Other techniques are needed to reduce this and some other types of tetrahedra to a lower dimension.

Chapter 5

Open problems on disc and sphere packings

> "I checked it very thoroughly," said the computer, "and that quite definitely is the answer. I think the problem, to be quite honest with you, is that you've never actually known what the question is."
>
> Douglas Adams, The Hitchhiker's Guide to the Galaxy

This chapter is dedicated to some open problems more or less directly following the results presented in the two previous chapters. All of them together form my research project.

Section 5.1 is dedicated to the triangulated cases which remained unclassified in Chapter 3. These cases resisted to our methods for different reasons discussed in detail. Other possible approaches to obtain more density bounds for multi-size disc packings are discussed in Section 5.2. Section 5.3 proposes to study aperiodicity and decidability properties of disc packings by analogy with tilings. Finally, in Section 5.4 we discuss open problems on 2-sphere packings which are natural prolongations of the results presented in Chapter 4.

5.1 Tight density bound for 3-disc triangulated cases

In this section, we discuss the triangulated cases which were not covered by the results from Chapter 3. We separate these remaining cases in three groups depending on the "reasons why" our techniques did not work on them.

Section 5.1.1 presents the 18 cases where one of the discs appears with at least two different neighborhoods in the triangulated packing. These cases are analogous to the binary case b_5 (see Fig. 2.38 on page 42) where a small disc is either surrounded by 6 small discs or by two small discs and two big ones. Our proof technique is not sufficient to treat such cases: handling them requires a less local approach, such as the one used in [BF22] for b_5.

Section 5.1.2 treats the 50 cases where we did not find a set of constants satisfying all required inequalities needed in our proof. Even though after several attempts with higher and higher precision, we concluded that the existence of valid constants is quite unlikely, it cannot be rigorously proved for the moment.

Finally, Section 5.1.3 is dedicated to the 4 cases where the existence of such set of constants is more probable since we could find the parameters satisfying the majority of constraints, but a few of them were still not satisfied.

5.1.1 2 coronas

One of necessary conditions on vertex potentials in tight triangles, given in Section 3.2.1, is that the sum of potentials in the corona around any vertex of triangulated packing T^* must be equal to zero (C). In all the cases where our approach succeeded, each disc has only one possible corona in T^*. However, among the cases where T^* is saturated, and for which we did not find counterexamples, there are 18 cases where one of the discs appears with at least two different coronas in T^*: 16, 17, 18, 36, 49, 52, 57, 58, 65, 78, 90, 114, 120, 148, 155, 156, 157, 158. Each of these cases features a supplementary corona consisting of 6 discs of the same size as the central one. We thus have to add a supplementary condition $6V_{xxx} = 0$, where x is the radius of the disc with two coronas. This would contradict the condition $3V_{xxx} = E_{xxx} > 0$ in all of these cases.

Our density redistribution would need to be less local to solve this problem. In the context of binary triangulated packings, such a case (b_5, see Figure 2.38) is treated in detail in Section 5.3 of [BF22]. The main idea consists in distinguishing occurrences of the same disc with different coronas. More precisely, for case b_5, the vertex potential of triangles featuring the disc in question actually depends on the remaining corona of the disc in [BF22].

5.1.2 Empty polyhedra

In Section 3.2.1, we construct the set P_{V,m,ϵ_0} of solutions of systems (M, ϵ_0) which contains all valid values of tight vertex potentials and m_1, m_r, m_s derived in Section 3.2.1. In this Section, we talk about the 50 cases where the `Polyhedron` $\widetilde{P}_{V,m,\epsilon_0}$ associated to the set of solutions (see Section 3.5.2) obtained by our computations is empty: 21, 22, 23, 26, 27, 34, 35, 46, 48, 50, 59, 61, 67, 68, 69, 71, 72, 74, 82, 83, 85, 86, 87, 88, 89, 91, 94, 101, 102, 103, 105, 107, 109, 112, 113, 121, 122, 123, 124, 125, 127, 128, 130, 134, 140, 143, 145, 147, 149, 150.

The set P_{V,m,ϵ_0} represents all the values satisfying (M) featuring a non-negative valid ϵ. These constraints are necessary for our proof to be correct. If P_{V,m,ϵ_0} is empty, then there are no valid definition of the vertex potential, and thus our strategy of proof is not applicable.

Nevertheless our computations are limited by computer memory which can represent only certain values. Normally, we avoid this problem by using interval arithmetic (Section 3.5.1). However, this solution cannot be applied with `Polyhedra`. First, as mentioned in Section 3.5.2, in SageMath, the `Polyhedra` module does not support the interval field as a base ring. Implementing another way to represent "interval polyhedra" would be unreasonable due to memory and time constraints of calculations: the polyhedra are constructed from thousands of inequalities, and performing computations in interval field significantly increases time and memory costs. Instead, we use the ring of rationals to store the inequalities coefficients. Therefore, the `Polyhedron` $\widetilde{P}_{V,m,\epsilon_0}$ constructed this way is an approximation of the actual set of solutions P_{V,m,ϵ_0} and may not contain all the valid sets of values.

Yet, computing the `Polyhedra` with much higher precision still resulted into empty sets, so we believe that the actual set of solutions in question are probably empty in these cases. All in all, some of the cases from this section might actually maximize the density, but an essentially different approach would be needed to prove it. Looking forward, further attempts to treat these cases would likely use a less local density distribution.

5.1.3 The 4 mysterious cases

In the four remaining cases (45, 62, 75, and 144), the polyhedron $\widetilde{P}_{V,m,\epsilon_0}$ is not empty, like for the cases from the previous section. Nevertheless, we could not find a point in it to guarantee the local inequality (T) in all triangles. The problematic triangles are always those close to one of the tight ones, minimizing m_q and the tight potentials would thus be an obvious strategy to minimize the potentials and eventually satisfy (T) but the capping constants Z_q also dramatically affect potentials.

Trying to find appropriate values of V_{xyz}, m_q, and z_q, we represented them with all the constraints coming from (3.1) as a linear optimization problem, this approach is discussed

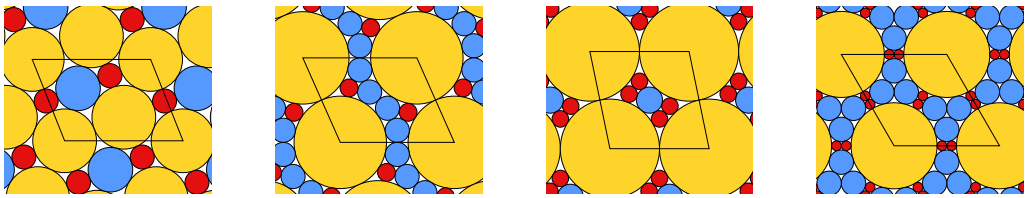

Figure 5.1: Triangulated ternary packings of the four *mysterious* cases.

in Section 3.5.2 on page 79. This allowed us to encode problematic triangles violating (T) as constraints and add them to the system, one by one, each time one appears during local verification, in hope to finally "converge" to a solution which would satisfy (T) on all triangles. However, since the constraints on the constants l_{xy}, q_x of the edge potential could not be represented by a linear program, this method failed.

The fact that we could not choose appropriate values of constants does not prove that they do not exist due to the precision issues already discussed in Section 3.5.2. We, however, believe that these cases, as well as those from the previous section, can not be treated by our proof methods; they most likely require a less local emptiness redistribution than the one we use.

5.2 Density bounds for other disc packings

Combining the methods we developed to work with 3-disc triangulated packings from Chapter 3 with the results from [Fer22], we hope to obtain other bounds on the density of multi-size disc packings.

5.2.1 Tight bounds for 2-disc packings

As mentioned in Section 2.2.3 on page 43, Fernique in [Fer22] obtained several intervals $I_1, I_2, I_3,$ and I_4 of values of r for which the optimal density of 2-disc packings is δ_{hex}, the density of the 1-disc hexagonal packing (see Fig. 2.39 on page 44). This result significantly improves the previous bounds [Bli69, Flo60] in the case of 2-disc packings, but it still leaves a few gaps, both figuratively and literally. For instance, in the gap between I_1 and I_2, $[0.4532, 0.4917]$, the lower bound is conjectured to be tight, although the obtained upper bound is much higher. The reason for this difference is the locality of the method used in [Fer22] to obtain the upper bound. Notice that this is essentially the same method as the one we use to obtain the tight density bound for 3-disc packings (in Chapter 3) and the one used for 2-disc packings in [BF22]. As explained in Section 3.1 (page 53), the density is redistributed between neighboring discs and is then bounded from above on local configurations around each disc. Therefore, the presence of extremely dense local configurations that cannot be "well" combined on a global scale, leads to excessive value of the upper density bound. To obtain a tight bound for such values of r, one needs to find a way to redistribute the density on a larger scale.

Another conjecture coming from the same article is the optimality of packings b_A and b_B (see Fig. 3.14 and 3.15). As above, our method is too local to treat them: since the target packings are non-triangulated, there are some especially dense coronas not present in them, which, at a larger scale, can not be completed into denser packings... Once again, a less-local approach is needed to handle these cases.

5.2.2 Lower density bounds with flip-and-flow method

The only tight bounds on maximal density of multi-disc packings are those obtained with triangulated packings: the 1-disc case [Thu10], the 9 cases of 2-disc packings [BF22], some values of r where the hexagonal 1-disc packing is denser than any 2-disc packing [Fer22], and, finally, the 32 cases of 3-disc packings from Chapter 3. Nevertheless, as seen in Section 2.2.2,

there are numerous lower and upper bounds on the maximal density of 2-disc packings [Flo60, Bli69, Fer22].

Combining the techniques from these results together with the methods we developed in our research on triangulated cases, it might be possible to obtain non-tight density bounds density for the remaining disc triplets.

To get a lower bound on the maximal density of a packings with given triplet of discs, it is enough to construct a "very dense" packing. One can find a general bound depending on disc sizes which would require an advanced technique of dense packing generation by the flip-and-flow method, introduced in [CG21], which consists in continuously deflating or inflating certain discs in a densest triangulated packing; this process modifies the structure of a packing keeping the density high. We used this approach on 2-disc packings to generate counterexamples to the Connelly conjecture (Section 3.6); the same method is applied to find a fine lower bound on the maximal density of 2-disc packings in [Fer22].

There are two methods to find an upper density bound. The first one is to use geometrical properties of packings, as in [Flo60, Bli69]. However, better bounds are provided by the computer-assisted method introduced in [Fer22] for 2-disc packings. To adapt this approach to 3-disc packings, it is enough to adapt the proof of maximal density for triangulated packings. The greatest challenge seems to be purely computational since we need to treat a two-dimensional set of pairs of radii (r, s) instead of a one-dimensional interval of values of r, as in [Fer22].

5.3 Triangulated packings and non-periodic tilings

The class of triangulated packings is the most "discrete" among disc packings which are generally of continuous nature. More precisely, triangulated packings can be viewed as tilings. The contact graph of a triangulated packing is a triangulation (see Fig. 5.2). Cutting the triangles out of this triangulation, we get a finite set of triangular tiles with decorations (i.e., local rules); an example of such tile set is given in Fig. 5.3. Therefore, each triangulated packing corresponds to a tiling by such tiles respecting the local rules. The density of a packing can be expressed as a weighted proportion of tiles.

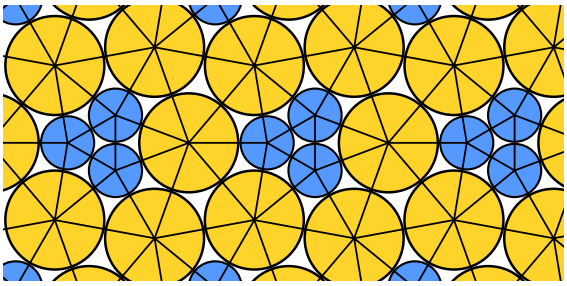

Figure 5.2: Triangulated packing with its contact graph.

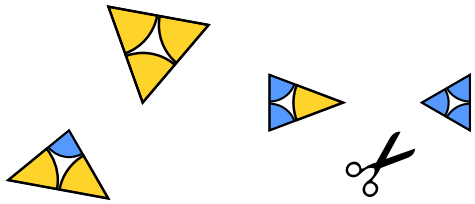

Figure 5.3: Tiles corresponding to a triangulated packing.

Viewing triangulated packings as tilings provides us with tools to study them from the computational point of view. The *domino problem* is the most known computational problem in the area of tilings. It consists in determining for a given set of unit square tiles with local rules (called *Wang tiles*) if they can tile the plane or not. Wang conjectured that every tile set that tiles the plane also tiles it periodically; he derived an algorithm solving the domino problem in that case [Wan61]. However, his conjecture was false: there exist tile sets, called *aperiodic*, whose tilings of the plane are all non-periodic. In 1966, Berger proved the domino problem to be undecidable by encoding the halting problem into the domino problem [Ber66].

Let us consider the *triangulated packing problem*: given a finite number of disc radii, determine whether there exists a triangulated packing using discs of these radii (each at least once to exclude the hexagonal 1-disc packing).

As for the domino problem, if there is no aperiodic set of discs then the problem is decidable: it is enough to use a generalization of the Wang algorithm running through all finite configurations in search of a period. On the other hand, if there is an aperiodic set of discs, its pure existence is not sufficient to show that the triangulated packing problem is undecidable: a generalized version of the Berger proof would be needed. If it can be completed, this would reinforce the intuition of a strong connection between aperiodicity and undecidability (see [Jea10] for more details on this topic).

So far, no aperiodic set of discs is found. When such a set is found or proven not to exist, the next step is to find out if the triangulated packing problem is decidable or not.

There exists no aperiodic pair nor triplet of discs. There are those allowing non-periodic packings, like the pair of radii whose packings correspond to square-triangle tilings [Ken06], but they also feature periodic ones. A possible approach to finding aperiodic set of discs is to enumerate n-disc tuples allowing triangulated packings, like it was done for triplets in [FHS21], in hope of finding an aperiodic set for $n \geq 4$. This approach is strongly based on computer brute force and the full enumeration would probably not be possible on a modern processor starting from 6-disc tuples. Nevertheless, finding an aperiodic set, if there is one, does not necessarily require full enumeration. Although it does require lots of luck.

The first aperiodic Wang tile set was introduced by Berger and consisted of 20426 tiles [Ber66]. However, with time, much smaller tile sets were discovered up till Jeandel and Rao introduced their aperiodic set of 11 tiles and proved that no smaller one exists [JR15]. For geometric tiles, Penrose tilings can be generated from two tiles, with several rotations. That allows us to hope that a relatively small aperiodic set of discs might exist, if one exists at all.

The majority of the known aperiodic tile sets produce hierarchical (self-similar) tilings, the most famous being Penrose tilings. Another approach of finding an aperiodic set of discs is to start from a non periodic structure, e.g., a Penrose tiling, and reproduce it as a triangulated disc packing. Using a Penrose-like structure here seems sensible: such structures are used to describe quasicrystals, a rare example of an non-periodic structure self-assembled in real life. The chemical experiences mentioned previously [PDKM15] indicate that the limiting configurations of self-assembly of nanoparticles often correspond to densest and/or triangulated packings. The density of sphere packings with quasicrystalline structure has already been studied before [Wil90,Hen86], and one of the densest packings of regular tetrahedra was constructed using physical simulations which converged to quasicrystalline structures [HAEK$^+$09]. All in all, if an aperiodic set of discs exists, it seems appropriate to search it among the structures that can appear in real life.

The first step would be to construct a triangulated graph corresponding to a non-periodic tiling. Then, one could use the KAT theorem (also known as the circle packing theorem) which states that for any planar graph, there is a disc packing whose contact graph is isomorphic to it. In particular, the constructive proof of the KAT theorem by Connelly and Gortler [CG21], might be of use. However, a triangulated packing obtained from a tiling triangulation graph with these methods might feature an infinite number of disc sizes and the most challenging part seems to be reducing this number to a finite one.

Another aperiodicity question of interest is to find a set of discs whose *densest* packings are all non-periodic. This question is closely related to the previous one: a triangulated non-periodic packing we aim to construct might maximize the density or, at least, give an insight on another construction maximizing it. However, using the KAT theorem on different graphs, we might also discover a *non-triangulated* non-periodic packing maximizing the density, which would be an independent result.

There are no triangulated non-periodic packings among 2-,3-, and 4-disc packings, so high number of discs might be required to get one. In contrast, even for 2-disc packings, there might exist values of r such that the densest packings are all non-periodic. This is quite unlikely due to the rather fine bounds provided by Fernique [Fer22] (see Section 2.2.3, page 43) which are tight for several intervals of values of r, but this possibility can not be completely excluded.

5.4 Sphere packings

Applying the techniques developed for triangulated disc packings (Chapters 2 and 3) to sphere packings, we propose a few ideas of how to prove the analogy of the Kepler conjecture for rock salt sphere packings (Conjecture 4.1) and discuss how to finalize our partial results on the density bound for 2-sphere packings from Section 4.2.3.

5.4.1 Rock salt packings

To show that rock salt packings maximize the density among packings by rock-salt spheres, we propose to adopt the step-by-step strategy described in Section 4.1.2 (page 102).

Step 1 in our proof scheme is dedicated to space partition. As for triangulated disc packings, the natural choice for simplicial sphere packings is the weighted Delaunay simplicial partition. This is the reason why this result seems to be more accessible than the Kepler conjecture where the optimal packings are not simplicial (see Figure 4.8 on page 106): in the proof of Hales and Ferguson, the space partition is a complex mixture of Delaunay simplices and modified Voronoi cells [HF11].

At step 3, we redistribute the density inside each tetrahedron of the simplicial partition. In 2D, we distributed it among the vertices of each triangle. In 3D, there are two natural choices of distribution: either among the vertices or among the edges of a tetrahedron.

At step 4, we shall study all possible local configurations around a vertex or an edge in order to show that the redistributed density never exceeds the optimal density. In 2D, these local configurations around a disc were "coronas" of its neighbor discs surrounded it. In 3D, that depends on our choice of density distribution unit. If the unit is a vertex, then each local configuration is the set of neighbor spheres around the given sphere, they form a sphere triangulation from the point of view of the simplicial partition (a graph we associate with a configuration is a subgraph of the simplicial graph of the packing which consists of the neighbors of the central sphere). The same kinds of local configurations were considered in the proof of the Kepler conjecture which led to a massive study of a particular family of graphs [Hal11c, Hal11d]. The enumeration of the local configurations is also particularly challenging in this case: each local configuration corresponds to a bi-colored sphere triangulation (two colors for two sphere sizes); similar problem for non-colored graphs was already treated in the context of the strong thirteen spheres problem in [MT12]. If we choose edges as units of redistribution then a configuration is a sequence of spheres surrounding a pair of spheres in the extremities of the edge. Such structures could be much simpler to enumerate and study, they resembles the coronas from the 2-dimensional case.

After the previous step, some especially dense local configurations might remain problematic, as the pentagonal prism in the proof of the Kepler conjecture [Fer11]. These arrangements require the usage of special techniques, including dimension reduction and careful analysis of function behavior. Such configurations shall be detected in the beginning of the study since they affect the whole structure of the proof. We found a few graphs which might correspond to dense configurations in the case of rock salt packings but we did not yet analyzed them in details, one of them is depicted in Fig. 5.4.

Finally, step 5 is dedicated to the extremal cases: the local configurations present in the optimal packings. We need to prove that they are local maxima of the density in a small neighborhood. Two such optimal configurations in the proof oh the Kepler conjecture are given in Fig. 4.8. The techniques used by Hales and Ferguson [Hal11b], as well as in our work on disc packings, are based on derivations and interval arithmetic. These methods shall be thus applied in the 2-sphere case. The two local configurations around a unit sphere in a rock salt packing are given in Fig. 4.15.

5.4.2 More density bounds

In Section 4.2.3, we obtained a tight upper bound on the density of star FM-tetrahedra of a packing by rock salt spheres (i.e, sphere of radii 1 and $r = \sqrt{2} - 1$). The first natural

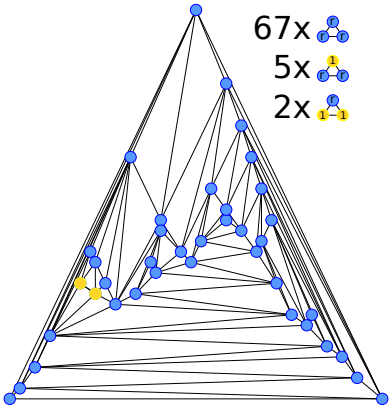

Figure 5.4: A graph which is a candidate to correspond to an specially dense local configuration around a unit sphere.

extension of this result is to derive an upper bound on the density of *any* FM-tetrahedron of such packings which directly implies the upper bound on the density of packings by rock salt spheres. We conjecture that this bound will remain the same: more precisely, that for any FM-tetrahedron with spheres of fixed radii, there is a denser star FM-tetrahedron with the same spheres. Since the computer assistance fails due to the high dimension of the set of tetrahedra, we propose to use two techniques of dimension reduction to prove this, which are both discussed in Section 3.3.2.

This result can be also generalized for other values of r. More interesting opening would be to generalize this bound on all the possible values of $r < 1$ (or, at least, on certain intervals), by analogy with the Florian bound. In order to have a clearer image of possible approaches to this task, we computed the densities of the tetrahedra maximizing the density of the classes of star tetrahedra for $r = \sqrt{2} - 1$ (i.e., (T^t_{1111}, T^1_{1r11}, T^t_{11rr}, T^t_{1rrr}, T^2_{rrrr}) for all values of r between 0 and 1. The resulting density graphs are depicted in Figure 5.5: the red curve corresponds to the density of the T^t_{11rr} tetrahedron, the dark blue curve – to the T^t_{11rr} tetrahedron, the cyan curve – to the T^1_{1r11} tetrahedron (the one that maximizes the density in the case of $r = \sqrt{2}-1 \approx 0.4142$), and the green curve – to the T^2_{rrrr} tetrahedron. This graph gives only a partial analysis, but at least, it is clear that in contrast with the Forian upper bound which was reached by the same type of triangle independently on the value of r, the structure of the optimal FM-tetrahedron for 2-sphere packings will likely depend on r.

The methods we used in Section 4.2.3 were inspired by the Florian bound on the density of disc packings: our aim is to find the maximal density in an FM-tetrahedron to obtain the upper bound on the density of a packing. Although, the Blind's approach [Bli69] gave a better result. His proof consisted in bounding the density by analyzing the properties of the power diagram of a packing and bounding the density inside its cells (for more details, see Section 2.2.2, page 34). It would be interesting to transfer this method to the case of sphere packings and compare the obtained bound with the previous one.

Notice that the Theorem 4.1 is stronger than Corollary 4.1. It can be used to construct a finer density bound of packings by rock-salt spheres.

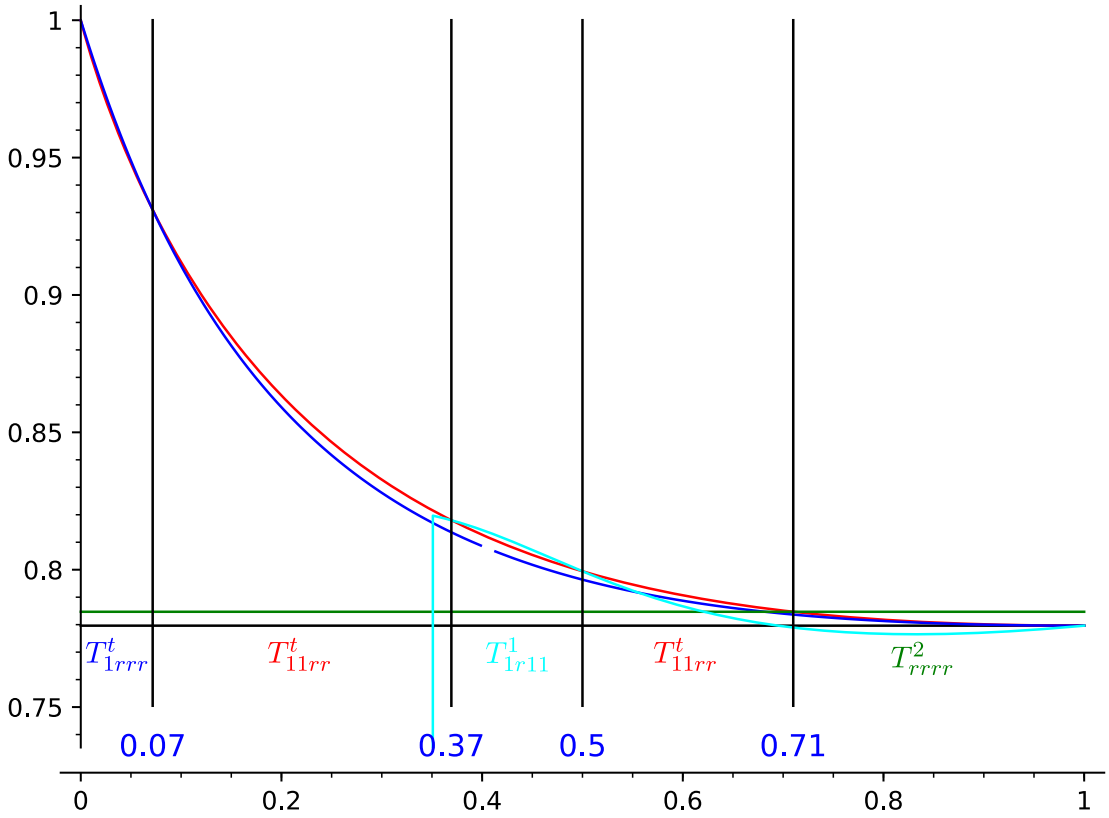

Figure 5.5: The red curve corresponds to the density of the tetrahedron T^t_{11rr} in function of the value of $r \in (0,1)$, the dark blue curve – to T^t_{1rrr}, the cyan curve – to T^1_{1r11}, and the green curve – to T^2_{rrrr}. Interval $(0,1)$ is divided into 5 intervals, in function of which tetrahedron is the densest among T^t_{1111}, T^t_{11rr}, T^t_{1rrr}, T^1_{1r11}, T^2_{rrrr}.

Index

Bibliography

[AH89] K. I. Appel and W. Haken. *Every Planar Map is Four Colorable*. Contemporary mathematics - American Mathematical Society. American Mathematical Society, 1989.

[ALS08] B. Addis, M. Locatelli, and F. Schoen. Efficiently packing unequal disks in a circle. *Operations Research Letters*, 36(1):37–42, 2008.

[Ans04] K. M. Anstreicher. The thirteen spheres: A new proof. *Discrete and Computational Geometry*, 31(4):613–625, 2004.

[Bar83] W. Barlow. Probable nature of the internal symmetry of crystals. *Nature*, 29:186–188, 1883.

[Ben10] W. Bentz. Optimal packings of 13 and 46 unit squares in a square. *The Electronic Journal of Combinatorics*, pages R126–R126, 2010.

[Ber66] R. Berger. *The Undecidability of the Domino Problem*. Memoirs ; No 1/66. American Mathematical Society, 1966.

[BF22] N. Bedaride and T. Fernique. Density of binary disc packings: The nine compact packings. *Discrete & Computational Geometry*, 67:1–24, 2022.

[BG84] U. Betke and P. Gritzmann. Über L. Fejes Tóth's Wurstvermutung in kleinen Dimensionen. *Acta Mathematica Hungarica*, 43(3):299–307, 1984.

[BH98] U. Betke and M. Henk. Finite packings of spheres. *Discrete & Computational Geometry*, 19:197–227, 1998.

[BHW94] U. Betke, M. Henk, and J. M. Wills. Finite and infinite packings. *J. Reine Angew. Math.*, 453:165–191, 1994.

[BJ93] K. Böröczky Jr. About four-ball packings. *Mathematika*, 40(2):226–232, 1993.

[BJ04] K. Böröczky Jr. *Finite Packing and Covering*. Cambridge Tracts in Mathematics. Cambridge University Press, 2004.

[BKMJ91] A. Bezdek, W. Kuperberg, and E. Makai Jr. Maximum density space packing with parallel strings of balls. *Discrete & Computational Geometry*, 6:227–283, 1991.

[Bli19] H. F. Blichfeldt. Report on the theory of the geometry of numbers. *Bulletin of the American Mathematical Society*, 25(10):449 – 453, 1919.

[Bli29] H. F. Blichfeldt. The minimum value of quadratic forms, and the closest packing of spheres. *Mathematische Annalen*, 101:605 – 607, 1929.

[Bli35] H. F. Blichfeldt. The minimum values of positive quadratic forms in six, seven and eight variables. *Mathematische Zeitschrift*, 39(1):1–15, 1935.

[Bli69] G. Blind. Über Unterdeckungen der Ebene durch Kreise. *Journal für die Reine Angewandte Mathematik*, pages 145–173, 1969.

[CE03] H. Cohn and N. Elkies. New upper bounds on sphere packings I. *Annals of Mathematics*, 157(2):689–714, 2003.

[CEG10] E. R. Chen, M. Engel, and S. C. Glotzerm. Dense crystalline dimer packings of regular tetrahedra. *Discrete & Computational Geometry*, 44:253–280, 2010.

[CG21] R. Connelly and S. J. Gortler. Packing disks by flipping and flowing. *Discrete & Computational Geometry*, 66:1262–1285, 2021.

[CGSY18] R. Connelly, S. Gortler, E. Solomonides, and M. Yampolskaya. Circle packings, triangulations, and rigidity. *Oral presentation at the conference for the 60th birthday of Thomas C. Hales*, 2018.

[Che08] E. R. Chen. A dense packing of regular tetrahedra. *Discrete & Computational Geometry*, 40:214–240, 2008.

[Chu23] J. H. Chun. On the sausage catastrophe in 4 dimensions. *https://arxiv.org/abs/2302.11555*, 2023.

[CKM+17] H. Cohn, A. Kumar, S. Miller, D. Radchenko, and M. Viazovska. The sphere packing problem in dimension 24. *Annals of Mathematics*, 185(3), 2017.

[CP19] R. Connelly and M. Pierre. Maximally dense disc packings on the plane. *https://arxiv.org/abs/1907.03652*, 2019.

[CS98] J. Conway and N. J. A. Sloane. *Sphere Packings, Lattices and Groups*. Grundlehren der mathematischen Wissenschaften. Springer New York, 1998.

[CW10] H. Chang and L. Wang. A simple proof of thue's theorem on circle packing. *https://arxiv.org/abs/1009.4322*, 2010.

[Dan63] L. Danzer. Endliche Punktmengen auf der 2-Sphäre mit möglichst grossen Minimalabstand. *Habilitationsschrift, Univ. of Göttingen, Göttingen*, 1963.

[Del34] B. Delaunay. Sur la sphere vide. *Izv. Akad. Nauk SSSR, Otdelenie Matematicheskii i Estestvennyka Nauk*, 7(793-800):1–2, 1934.

[Dev22] The Sage Developers. *SageMath, the Sage Mathematics Software System (Version 9.6)*, 2022. `http://www.sagemath.org`.

[dGvRD11] J. de Graaf, R. van Roij, and M. Dijkstra. Dense regular packings of irregular nonconvex particles. *Physical Review Letters*, 107(15):155501, 2011.

[DLDOFV14] D. De Laat, F. M. De Oliveira Filho, and F. Vallentin. Upper bounds for packings of spheres of several radii. *Forum of Mathematics, Sigma*, 2:e23, 2014.

[Dow44] C. H. Dowker. On minimum circumscribed polygons. *Bulletin of the American Mathematical Society*, 50(2):120 – 122, 1944.

[Edm70] A. L. Edmonds. Simplicial Decompositions of Convex Polytopes. *Pi Mu Epsilon Journal*, 5(3):124–128, 1970.

[ERS98] Y. Edel, E. M. Rains, and N. J. A. Sloane. On kissing numbers in dimensions 32 to 128. *The Electronic Journal of Combinatorics*, 5(1):Research paper R22, 5 p., 1998.

[Fer11] S. P. Ferguson. Sphere packings, V. Pentahedral prisms. In J. C. Lagarias, editor, *The Kepler Conjecture: The Hales-Ferguson Proof*, pages 235–274. Springer New York, New York, 2011.

[Fer19] T. Fernique. A densest ternary circle packing in the plane. *https://arxiv.org/abs/1912.02297*, 2019.

[Fer21] T. Fernique. Compact packings of space with two sizes of spheres. *Discrete & Computational Geometry*, 65(4):1287–1295, 2021.

[Fer22] T. Fernique. Density of binary disc packings: Lower and upper bounds. *Experimental Mathematics*, pages 1–12, 2022.

[FGJ+21] S. P. Fekete, V. Gurunathan, K. Juneja, P. Keldenich, L. Kleist, and C. Scheffer. Packing squares into a disk with optimal worst-case density. In *37th International Symposium on Computational Geometry (SoCG 2021)*, volume 189 of *Leibniz International Proceedings in Informatics (LIPIcs)*, pages 36:1–36:16, Dagstuhl, Germany, 2021.

[FHS21] T. Fernique, A. Hashemi, and O. Sizova. Compact packings of the plane with three sizes of discs. *Discrete & Computational Geometry*, 66(2):613–635, 2021.

[FKS23] S. P. Fekete, P Keldenich, and C. Scheffer. Packing disks into disks with optimal worst-case density. *Discrete & Computational Geometry*, 69:51–90, 2023.

[Flo60] A. Florian. Ausfüllung der Ebene durch Kreise. *Rendiconti del Circolo Matematico di Palermo*, 9:300–312, 1960.

[Flo63] A. Florian. Dichteste Packung inkongruenter Kreise. *Monatshefte für Mathematik*, 67(3):229–242, 1963.

[FMS17] S. P. Fekete, S. Morr, and C. Scheffer. Split packing: Packing circles into triangles with optimal worst-case density. In *Algorithms and Data Structures*, pages 373–384. Springer International Publishing, 2017.

[Fod99] F. Fodor. The densest packing of 19 congruent circles in a circle. *Geometriae Dedicata*, 74(2):139–145, 1999.

[Fod03] F. Fodor. The densest packing of 13 congruent circles in a circle. *Beiträge zur Algebra und Geometrie*, 44, 2003.

[FP21] T. Fernique and D. Pchelina. Compact packings are not always the densest. *https://arxiv.org/abs/2104.12458*, 2021.

[FP23a] T. Fernique and D. Pchelina. Density of triangulated ternary disc packings. *Computational Geometry*, 115:102032, 2023.

[FP23b] T. Fernique and D. Pchelina. When Ternary Triangulated Disc Packings Are Densest: Examples, Counter-Examples and Techniques. In *39th International Symposium on Computational Geometry (SoCG 2023)*, volume 258 of *Leibniz International Proceedings in Informatics (LIPIcs)*, pages 32:1–32:17, Dagstuhl, Germany, 2023.

[Fri09] E. Friedman. Packing unit squares in squares: A survey and new results. *The Electronic Journal of Combinatorics*, 2009.

[FT42] L. Fejes Tóth. Über die dichteste Kugellagerung. *Math. Z.*, 48:676–684, 1942.

[FT43] L. Fejes Tóth. Über die Abschätzung des kürzesten Abstandes zweier Punkte eines auf einer Kugelfläche liegenden punktsystems. *Jber. Deutch. Math. Verein.*, 53:66–68, 1943.

[FT53] L. Fejes Tóth. *Lagerungen in der Ebene, auf der Kugel und im Raum.* Springer, Berlin, Heidelberg, 1953.

[FT64] L. Fejes Tóth. *Regular Figures*, volume 48 of *International Series of Monographs on Pure and Applied Mathematics.* Macmillan, 1st edition, 1964.

[FT75] L. Fejes Tóth. Research problem. *Period. Math. Hungar*, 6:197 – 199, 1975.

[FT84] L. Fejes Tóth. Compact packing of circles. *Studia Sci. Math. Hungar.*, 19:103–107, 1984.

[FTM58] L. Fejes Tóth and J. Molnár. Unterdeckung und Überdeckung der Ebene durch Kreise. *Mathematische Nachrichten*, 18:235–243, 1958.

[Gar95] M. Gardner. *New mathematical diversions*. Washington, D.C. : Mathematical Association of America, 1995.

[Gau31] C. F. Gauss. Untersuchungen über die Eigenschaften der positiven ternären quadratischen Formen von Ludwig August Seber. *Göttingische gelehrte Anzeigen*, 1831.

[GDJJ98] R. L. Graham, Lubachevsky B. D., Nurmela K. J., and Ostergard P. R. J. Dense packings of congruent circles in a circle. *Discrete Mathematics*, 181(1):139–154, 1998.

[GEK10] S. Gravel, V. Elser, and Y. Kallus. Upper bound on the packing density of regular tetrahedra and octahedra. *Discrete & Computational Geometry*, 46:799–818, 2010.

[Gen05] P. Gensane, T.and Ryckelynck. Improved dense packings of congruent squares in a square. *Discrete & Computational Geometry*, 34(1):97–109, 2005.

[GO04] J. E. Goodman and J. O'Rourke, editors. *Handbook of Discrete and Computational Geometry, Second Edition*. Chapman and Hall/CRC, Boca Raton, 2nd edition edition, 2004.

[Gro63] H. Groemer. Existenzsätze für Lagerungen im Euklidischen Raum. *Mathematische Zeitschrift*, 81:260–278, 1963.

[GW92] P. M. Gandini and J. Wills. On finite sphere packings. 3(1):19–29, 1992.

[GZ92] P. M. Gandini and A. Zucco. On the sausage catastrophe in 4-space. *Mathematika*, 39(2):274–278, 1992.

[HAB+17] T. C. Hales, M. Adams, G. Bauer, D. T. Dang, J. Harrison, T. L. Hoang, C. Kaliszyk, V. Magron, S. McLaughlin, T. T. Nguyen, T. Q. Nguyen, T. Nipkow, S. Obua, J. Pleso, J. Rute, A. Solovyev, A. H. T. Ta, T. N. Tran, D. T. Trieu, J. Urban, K. K. Vu, and R. Zumkeller. A formal proof of the Kepler conjecture. *Forum of Mathematics, Pi*, 5:e2, 2017.

[HAEK+09] A. Haji-Akbari, M. Engel, A. S. Keys, X. Zheng, R. G. Petschek, P. Palffy-Muhoray, and S. C. Glotzer. Disordered, quasicrystalline and crystalline phases of densely packed tetrahedra. *Nature*, 462(7274):773—777, 2009.

[Hal92] T. C. Hales. The sphere packing problem. *Journal of Computational and Applied Math*, 44:41–76, 1992.

[Hal93] T. C. Hales. Remarks on the density of sphere packings in three dimensions. *Combinatorica*, 13(2):181–197, 1993.

[Hal94] T. C. Hales. The status of the Kepler conjecture. *The Mathematical Intelligencer*, 16(3):47–58, 1994.

[Hal05] T. C. Hales. A proof of the Kepler conjecture. *Annals of Mathematics*, 162(3):1065–1185, 2005.

[Hal11a] T. C. Hales. Sphere packings, I. In J. C. Lagarias, editor, *The Kepler Conjecture: The Hales-Ferguson Proof*, pages 379–431. Springer New York, New York, 2011.

[Hal11b] T. C. Hales. Sphere packings, III. Extremal cases. In J. C. Lagarias, editor, *The Kepler Conjecture: The Hales-Ferguson Proof*, pages 135–176. Springer New York, New York, 2011.

[Hal11c] T. C. Hales. Sphere packings, IV. Detailed bounds. In J. C. Lagarias, editor, *The Kepler Conjecture: The Hales-Ferguson Proof*, pages 177–234. Springer New York, New York, 2011.

[Hal11d] T. C. Hales. Sphere packings, VI. Tame graphs and linear programs. In J. C. Lagarias, editor, *The Kepler Conjecture: The Hales-Ferguson Proof*, pages 275–337. Springer New York, New York, 2011.

[Hen86] C. L. Henley. Sphere packings and local environments in penrose tilings. *Phys. Rev. B*, 34:797–816, 1986.

[Hep92] A. Heppes. Solid circle-packings in the Euclidean plane. *Discrete & Computational Geometry*, 7(1):29–43, 1992.

[Hep00] A. Heppes. On the densest packing of discs of radius 1 and $\sqrt{2}-1$. *Studia Scientiarum Mathematicarum Hungarica*, 36:433–454, 2000.

[Hep03] A. Heppes. Some densest two-size disc packings in the plane. *Discrete & Computational Geometry*, 30:241–262, 2003.

[HF06] T. C. Hales and S. P. Ferguson. The Kepler conjecture. *Discrete & Computational Geometry*, 36(1):1–269, 2006.

[HF11] T. C. Hales and S. P. Ferguson. A formulation of the Kepler conjecture. In J. C. Lagarias, editor, *The Kepler Conjecture: The Hales-Ferguson Proof*, pages 83–133. Springer New York, New York, 2011.

[Hil02] D. Hilbert. Mathematical problems. *Bulletin of the American Mathematical Society*, 8(10):437 – 479, 1902.

[HM10] T. Hales and S. McLaughlin. The dodecahedral conjecture. *Journal of the American Mathematical Society*, 23(2):299–344, 2010.

[HST12] A. B. Hopkins, F. H. Stillinger, and S. Torquato. Densest binary sphere packings. *Phys. Rev. E*, 85:021130, 2012.

[HW21] M. Henk and J. M. Wills. Packings, sausages and catastrophes. *Beitr. Algebra Geom.*, 62:265 – 280, 2021.

[Jea10] E. Jeandel. The periodic domino problem revisited. *Theoretical Computer Science*, 411(44):4010–4016, 2010.

[Joó09] A. Joós. On the packing of fourteen congruent Spheres in a cube. *Geometriae Dedicata*, 140(1):49–80, 2009.

[JR15] E. Jeandel and M. Rao. An aperiodic set of 11 wang tiles. *Advances in Combinatorics*, 2015.

[Kal14] Y. Kallus. The 3-ball is a local pessimum for packing. *Advances in Mathematics*, 264:355–370, 2014.

[Ken05] T. Kennedy. A densest compact planar packing with two sizes of discs. *https://arxiv.org/abs/math/0412418*, 2005.

[Ken06] T. Kennedy. Compact packings of the plane with two sizes of discs. *Discrete & Computational Geometry*, 35(2):255–267, 2006.

[Kep11] J Kepler. *Strena Seu de Niue Sexangula*. 1611. Translated by Hardie, C. in J. Kepler, *The Six-Cornered Snowflake*, Oxford University Press, 1966.

[KKW17] K. Kallal, T. Kan, and E. Wang. Improved lower bounds for kissing numbers in dimensions 25 through 31. *SIAM Journal on Discrete Mathematics*, 31(3):1895–1908, 2017.

[KM23] E. Kikianty and M. Messerschmidt. On compact packings of Euclidean space with spheres of finitely many sizes. *https://arxiv.org/abs/2305.00758*, 2023.

[KZ77] A. Korkine and G. Zolotareff. Sur les formes quadratiques positives. *Mathematische Annalen*, 11(2):242–292, 1877.

[Lag75] J. L. Lagrange. Recherches d'arithmétiques. *Nouveaux mémoires de l'Académie royale des sciences et des belles–lettres de Berlin*, pages 695–795, 1773 et 1775.

[LB13] C. O. López and J. E. Beasley. Packing unequal circles using formulation space search. *Computers & Operations Research*, 40(5):1276–1288, 2013.

[LdL23] N. Leijenhorst and D. de Laat. Solving clustered low-rank semidefinite programs arising from polynomial optimization. *https://arxiv.org/abs/2202.12077*, 2023.

[Lev79] V. I. Levenshtein. On bounds for packing in n-dimensional euclidean space. *Soviet Mathematics - Doklady*, 2:417–421, 1979.

[LHY+21] X. Lai, J.-K. Hao, D. Yue, Z. Lü, and Z.-H. Fu. Iterated dynamic thresholding search for packing equal circles into a circular container. *European Journal of Operational Research*, 299, 2021.

[Mar21] M. C. Markót. Improved interval methods for solving circle packing problems in the unit square. *Journal of Global Optimization*, 81(3):773–803, 2021.

[MC05] M. C. Markót and T. Csendes. A new verified optimization technique for the "packing circles in a unit square" problems. *SIAM Journal on Optimization*, 16:193–219, 2005.

[Mel94] H. Melissen. Densest packings of eleven congruent circles in a circle. *Geometriae Dedicata*, 50(1):15–25, 1994.

[Mes23] M. Messerschmidt. The number of configurations of radii that can occur in compact packings of the plane with discs of n sizes is finite. *Discrete & Computational Geometry*, 2023.

[MH10] G. Marshall and T. Hudson. Dense binary sphere packings. *Beiträge zur Algebra und Geometrie*, 51, 2010.

[Min04] H. Minkowski. Dichteste gitterförmige Lagerung kongruenter Körper. *Nachrichten von der Gesellschaft der Wissenschaften zu Göttingen, Mathematisch-Physikalische Klasse*, 1904:311–355, 1904.

[MKC09] R. E. Moore, R. B. Kearfott, and M. J. Cloud. *Introduction to Interval Analysis*. Other Titles in Applied Mathematics. Society for Industrial and Applied Mathematics, 2009.

[MM67] J. W. Moon and L. Moser. Some packing and covering theorems. *Colloquium Mathematicae*, 17(1):103–110, 1967.

[MNMD19] T. Montanher, A. Neumaier, Csaba M. M., and H. Domes, F.and Schichl. Rigorous packing of unit squares into a circle. *Journal of Global Optimization*, 73(3):547–565, 2019.

[Mor17] S. Morr. Split packing: An algorithm for packing circles with optimal worst-case density. SODA '17, pages 99–109, USA, 2017. Society for Industrial and Applied Mathematics.

[MSS09] A. Müller, J. J. Schneider, and E. Schömer. Packing a multidisperse system of hard disks in a circular environment. *Physical Review. E, Statistical, Nonlinear, and Soft Matter Physics*, 79(2 Pt 1):021102, 2009.

[MT12] O. Musin and A. Tarasov. The strong thirteen spheres problem. *Discrete & Computational Geometry*, 48(1):128–141, 2012.

[MT14] O. Musin and A. Tarasov. The tammes problem for n = 14. *Experimental Mathematics*, 24, 2014.

[Mud93] D. J. Muder. A new bound on the local density of sphere packings. *Discrete & Computational Geometry*, 10(4):351–375, 1993.

[Mus03] O. R. Musin. The problem of the twenty-five spheres. *Russian Mathematical Surveys*, 58(4):794, 2003.

[Nag05] H. Nagamochi. Packing unit squares in a rectangle. *The Electronic Journal of Combinatorics*, pages R37–R37, 2005.

[NO99] K. J. Nurmela and P. R. J. Ostergård. More Optimal Packings of Equal Circles in a Square. *Discrete & Computational Geometry*, 22(3):439–457, 1999.

[OH11] P. I. O'Toole and T. S. Hudson. New high-density packings of similarly sized binary spheres. *The Journal of Physical Chemistry C*, 115(39):19037–19040, 2011.

[OS79] A. M Odlyzko and N. J. A Sloane. New bounds on the number of unit spheres that can touch a unit sphere in n dimensions. *Journal of Combinatorial Theory, Series A*, 26(2):210–214, 1979.

[PDKM15] T. Paik, B. T. Diroll, C. R. Kagan, and C. B. Murray. Binary and ternary superlattices self-assembled from colloidal nanodisks and nanorods. *Journal of the American Chemical Society*, 137(20):6662–6669, 2015.

[Pir69] U. Pirl. Der Mindestabstand von n in der Einheitskreisscheibe gelegenen Punkten. *Mathematische Nachrichten*, 40:111–124, 1969.

[PWMG92] R. Peikert, D. Würtz, M. Monagan, and C. Groot. Packing circles in a square: A review and new results. *System Modelling and Optimization, Proceedings of the Fifteenth IFIP Conference*, 180:45–52, 1992.

[Rei34] K. Reinhardt. Über die dichteste gitterf örmige lagerung kongruenter Bereiche in der Ebene und eine besondere art konvexer Kurven. *Abhandlungen aus dem Mathematischen Seminar der Universität Hamburg*, 10(1):216–230, 1934.

[Rev20] N. Revol. Influence of the condition number on interval computations: Illustration on some examples. In Olga Kosheleva, Sergey P. Shary, Gang Xiang, and Roman Zapatrin, editors, *Beyond Traditional Probabilistic Data Processing Techniques: Interval, Fuzzy etc. Methods and Their Applications*, pages 359–373. Springer International Publishing, 2020.

[Rob61] R. M. Robinson. Arrangement of 24 points on a sphere. *Mathematische Annalen*, 144(1):17–48, 1961.

[Rog58] C. A. Rogers. The packing of equal spheres. *Proceedings of the London Mathematical Society*, s3-8(4):609–620, 1958.

[Sch65] J. Schaer. The densest packing of 9 circles in a square. *Canadian Mathematical Bulletin*, 8(3):273–277, 1965.

[Sch66] J. Schaer. On the Densest Packing of Spheres in a Cube. *Canadian Mathematical Bulletin*, 9(3):265–270, 1966.

[Sch94] J. Schaer. The densest packing of ten congruent spheres in a cube. In K. Böröczky and G. Fejes Tóth, editors, *Intuitive geometry (Szeged, 1991)*, volume 63 of *Colloq. Math. Soc. János Bolyai*, pages 403–424. North-Holland Pub., 1994.

[Sch00] U. Schnell. Dense sphere packings and the wulff-shape of crystals and quasicrystals. *Materials Science and Engineering A-structural Materials Properties Microstructure and Processing*, 294:221–223, 12 2000.

[Sei40] F. Seitz. *The Modern Theory Of Solids*. International Series in Physics. New York McGraw-Hill Book Co., Inc., 1940.

[SM65] J. Schaer and A. Meir. On a geometric extremum problem. *Canadian Mathematical Bulletin*, 8(1):21–27, 1965.

[Str03] W. Stromquist. Packing 10 or 11 Unit Squares in a Square. *The Electronic Journal of Combinatorics*, pages R8–R8, 2003.

[SvdW51] K. Schutte and B. L. van der Waerden. Auf welcher Kugel haben 5, 6, 7, 8 oder 9 Punkte mit Mindestabstand Eins Platz? *Math. Ann.*, 123:113–123, 1951.

[SYR+20] Y. Stoyan, G. Yaskov, T. Romanova, I. Litvinchev, S. Yakovlev, and José M. Velarde C. Optimized packing multidimensional hyperspheres: a unified approach. *Mathematical biosciences and engineering: MBE*, 17(6):6601–6630, 2020.

[Szp03] G. G. Szpiro. *Kepler's Conjecture: How Some of the Greatest Minds in History Helped Solve One of the Oldest Math Problems in the World.* Wiley, 2003.

[Tam30] P. M. L. Tammes. On the origin of number and arrangement of the places of exit on the surface of pollen-grains. *Recueil des travaux botaniques néerlandais*, 27(1):1–84, 1930.

[Tat15] M. Tatarevic. On limits of dense packing of equal spheres in a cube. *The Electronic Journal of Combinatorics*, 22(1), 2015.

[Thu92] A. Thue. On new geometric, number theoretic theorems. *Naturforskermöde*, 259:352–353, 1892.

[Thu10] A. Thue. Über die dichteste Zusammenstellung von kongruenten Kreisen in einer Ebene. *Christiania Videnskabs-Selskabets Skrifter*, I. Math.-Naturv. Klasse, 1:1–9, 1910.

[vdWS52] B. L. van der Waerden and K. Schütte. Das Problem der 13 Kugeln. *Mathematische Annalen*, 125:325–334, 1952.

[Via17] M. Viazovska. The sphere packing problem in dimension 8. *Annals of Mathematics*, 185(3), 2017.

[Vor08] G. Voronoi. Nouvelles applications des paramètres continus à la théorie des formes quadratiques. Premier mémoire. Sur quelques propriétés des formes quadratiques positives parfaites. *Journal für die reine und angewandte Mathematik (Crelles Journal)*, 1908(133):97–102, 1908.

[Wan61] H. Wang. Proving theorems by pattern recognition — II. *The Bell System Technical Journal*, 40(1):1–41, 1961.

[Wil83] J. M. Wills. Research problem 35. *Periodica Mathematica Hungarica*, 14(3–4):309–314, 1983.

[Wil90] J. M. Wills. A quasi-crystalline sphere-packing with unexpected high density. *Journal de Physique*, 51(11):1061–1064, 1990.

[Zon14] C. Zong. On the translative packing densities of tetrahedra and cuboctahedra. *Advances in Mathematics*, 260:130–190, 2014.

[Zon22] C. Zong. A computer approach to determine the densest translative tetrahedron packings. *Experimental Mathematics*, 31(1):21–41, 2022.

[ZRH+23] J. Zhou, S. Ren, K. He, Y. Liu, and Li C.-M. An efficient solution space exploring and descent method for packing equal spheres in a sphere. *https://arxiv.org/abs/2305.10023*, 2023.